UNIVERSITY OF LIVERPOOL

Phenotyping of a new conditional mouse model of alkaptonuria and investigation of nitisinone-induced tyrosinaemia

Thesis submitted in accordance with the requirements of the University of Liverpool for the degree of Doctor in Philosophy by:

Juliette Holly Hughes

June 2020

Acknowledgements

This thesis could not have been possible without my three supervisors Prof James Gallagher, Prof George Bou-Gharios and Prof Lakshminarayan Ranganath, who have taught me many, many skills and have pushed, motivated me and supported me to produce the best work that I can. George, your knowledge of mouse models was incredibly important and you have taught me so much about transgenic models which was a huge part of my project. Ranga, the clinical expertise and knowledge that you brought to my scientific research was incredibly important, reminding me that AKU patients are the ultimate reason why we do our research. Jim, I thank you for all your wise advice and guidance - you have always been positive and boosted my confidence, and have supported me the whole way through my PhD to conduct research in a professional manner. I also had the chance to be part of your lab group (and will always be part of I hope no matter where I go!), without whom my PhD would not have been the same or possible.

Huge thank you to all of my lab group, you have guided and supported me through my PhD, and more than that, been great friends. Dr Hazel Sutherland, you have taught me everything I need to know about how to work with the mice and I am thankful to have learnt the BSU ways under your wing, and had your help with numerous mouse and lab experiments. Dr Peter Wilson; you have taught me the ways of the lab, answered my many questions about my lab work, assisted me with many experiments and have always had great advice about non-work-related topics too. Hazel and Pete, you have both been very important in my PhD and I can't thank you enough! Jane Dillon, you have been wonderful to work with, always taking the time to listen and give advice, and help me with anything I needed; usually with a cup of tea involved! Eman Alawadhi, working with you has been a joy; you are a caring and generous friend and have introduced my taste buds to many new Kuwaiti snacks! Dr Brendan Norman, you have looked out for me, especially at conferences – I was very glad to see you when I eventually made it to Valencia!! You are always willing to help, whether that be with mass spec or metabolomics or something else completely different. Dr Craig Keenan, thank you for your help, particularly with histology and staining in the lab, and for bringing much laughter to our lab group.

Thank you to Andy Hughes, Dr Anna Milan, Dr Andrew Davison, Shirley Judd and Ella Shweihdi in the Royal Liverpool Hospital for any help and advice you have given me over my PhD. Andy and Anna in particular, thank you for introducing me to the world of mass spec, and for letting me loose on the QQQ and helping me to analyse my samples. Shirley, thank you for your help particularly with my dietary restriction work and NAC observational data.

There are so many other people to acknowledge over the 3 and half years I have spent doing my PhD. I have to thank the other members of George's lab group, particularly Dr Ke Liu for his help with mouse work and generation of the mouse model, Dr Steph Frost for all your help with molecular biology and Mohammed Alhashmi; both Prof Jonathan Jarvis and Prof George Bou-Gharios for their project licence supervision; Dr Antonius Plagge for culturing the ES cells to make the mouse model; Dr Takao Sakai for providing MxCre and expertise on the liver; Mandie Prior, Gemma Charlesworth and Cath Sperinck for their advice with histology; Joni Roachdown for assistance with the microscopes; all the BSU staff who took care of the mice and gave advice; all the joint lab meeting members that listened to and critiqued my work; numerous IACD staff and all the PhD students, post-docs and PI's who gave any advice or stopped for a chat. I also would like to thank Prof Nathan Jeffery for giving me the opportunity to demonstrate anatomy during my PhD, and everyone in HARC, particularly Neil Thomas, Dr Tom Butts, Dr Alistair Bond, Dr Claire Tierney and Paul Rothwell.

I of course have to thank the AKU Society for funding my PhD and giving me the opportunity to be part of this amazing group of people dedicated to this ultra-rare disease, and being an inspiration to do research. I could not have done a PhD without the AKU Society, and would never have ran a half-marathon either!

Finally, I have to thank my family and friends. I may not see you all anywhere near as often as I would like, but you are always there for me. To my Dad and Kelly, I hope that you are proud that I have conquered this alien world of research to finish a PhD, and more importantly, that I have not yet become a scouser, despite my 7½ years in Liverpool (disclaimer: I absolutely love this city). To my best friends, Amy and Amber, thank you for always being there since Year 9, you are the best of friends no matter which corner of the UK we all live in. Huge thanks to Ruby and Emma for being amazing friends since our anatomy degree days, who are now both amazing NHS A&E frontline workers, very relevant in this current covid-19 pandemic in which I am submitting; I hope you can spot an AKU patient if you ever meet one from my many years of rambling about my work. And to Jess, my literal other half, thanks for always being there by side, initially here in Liverpool when I started my PhD, and then when you moved to Manchester and then back home to Suffolk, and of course our whole lives. Your support through my PhD has been the best and I miss you all the time here in Liverpool. And last but not least Rob. You have put up with me through my whole PhD, through the ups and the downs, the stress and the joy, the end of nights out, the disaster of my travel to conferences (namely Valencia and Sienna) and my constant natter about my work (I think you could have written a good chunk of this thesis by now!), and you have supported me in every other aspect of life outside of work.

Abstract

Alkaptonuria (AKU) is an ultra-rare, autosomal recessive metabolic bone disease characterised by increased urinary and circulating homogentisic acid (HGA) caused by homogentisate 1,2-dioxygenase (HGD) enzyme deficiency. The deposition of a dark, HGA-derived ochronotic pigment in cartilage and other connective tissues causes a severe and early-onset osteoarthropathy, due to ochronotic tissue being stiff and brittle. In addition to joint manifestations in AKU, eye pigmentation, tendon rupture, kidney and prostate stones, and heart valve stenosis are common features. An existing mutagenesis AKU mouse model has previously been used to investigate initial pigmentation of cartilage and to evaluate the effectiveness of the HGA-lowering drug nitisinone. Nitisinone therapy was proven to halt ochronosis in this mouse model and has been the subject of human clinical trials (DevelopAKUre), where it has been shown to reduce HGA and slow disease progression in AKU patients. Nitisinone-induced tyrosinaemia however is an upstream effect of 4-hydroxyphenylpyruvate dioxygenase inhibition that can cause keratopathy.

The major aims of this thesis were to phenotype a new *Hgd*-targeted AKU mouse model, obtained from the KOMP repository, to use the *LacZ* gene which is expressed as a fusion transcript with the *Hgd* gene to determine the tissue expression of *Hgd* via *ex vivo LacZ* staining, to explore the effect of conditional liver-specific *Hgd* deletion on the AKU phenotype using double transgenic *Hgd tm1d (fl/fl) MxCre* mice, and finally to explore the effectiveness of dietary restriction and the potential application of an exogenous tyrosine-degrading enzyme at reducing tyrosine.

The level of HGA and the tissue distribution of ochronotic pigmentation were evaluated using the knockout-first *Hgd tm1a -/-* model. HGA was shown to be increased in the plasma and urine, with the first signs of knee joint pigmentation found at 9 weeks in the knee joint, increasing linearly with age. Pigmentation was only found associated with chondrocytes within the calcified articular cartilage of joints, the calcified endplates of vertebrae, and the calcified knee joint meniscus. *Hgd tm1a -/-* mice exhibit the early stages of human ochronosis, with pigmentation confined to calcified tissues. Positive *LacZ* staining was identified in the cytoplasm of hepatocytes and kidney proximal convoluted tubule cells, beginning at E12.5 and E15.5 respectively, in addition to the developing male germ cells within the testis and epididymis, with qPCR showing liver *Hgd* mRNA expression to be approximately 2000-7,500-fold greater than the *Hgd* mRNA expression in the testis and epididymis. Germ cell expression was deemed insignificant and unlikely to contribute towards HGA metabolism. Liver-specific *Hgd* deletion via polyinosinic: polycytidylic acid induction of *MxCre* in *Hgd tm1d (fl/fl) MxCre +/-* mice demonstrated that 20% residual liver *Hgd* mRNA does not reduce circulating HGA leading to joint pigmentation and that kidney *Hgd* mRNA cannot rescue AKU. It was determined that the minimum level of liver *Hgd* mRNA required is 26-43% to reduce circulating HGA. The detection of downstream metabolites of intravenously injected $^{13}C_6$-HGA in *Hgd tm1a -/+* plasma revealed that hepatocytes can take up and metabolise HGA. The liver should therefore be the target of future gene therapy in AKU.

Nitisinone was shown to reduce HGA and increase tyrosine, phenylalanine, 4-hydroxyphenylpyruvic acid and 4-hydroxyphenyllactic acid in the plasma of AKU mice. Dietary restriction of tyrosine/phenylalanine significantly reduced nitisinone-induced tyrosinaemia, with phenylalanine-only restriction not effective. Evidence of AKU patients reducing tyrosine was observed, although the reductions were not comparable with that of mice. Due to the proof-of-principle provided by the dietary studies, preliminary experiments then demonstrated tyrosine degradation by the bacterial enzyme tyrosine ammonia lyase, which has the potential to be developed into an oral therapeutic for reducing nitisinone-induced tyrosinaemia.

Table of contents

List of figures

Chapter 1

Chapter 2

Chapter 3

Chapter 4

Chapter 5

Chapter 8

List of tables

Chapter 1

Chapter 2

Chapter 4

Chapter 5

Chapter 8

Abbreviations

AKU	alkaptonuria
AKUSSI	AKU severity score index
β-gal	β-galactosidase
BCA	bicinchoninic acid
BH_4	tetrahydrobiopterin
DCT	distal convoluted tubule
ECM	extracellular matrix
EDTA	ethylenediaminetetraacetic acid
EGTA	ethylene glycol-bis(β-aminoethyl ether)-N, N, N', N'-tetraacetic acid (egtazic acid)
EMA	European Medicines Agency
ENU	ethylnitrosourea
EST	enzyme substitution therapy
ES cells	embryonic stem cells
FAA	fumarylacetoacetic acid
FAH	fumarylacetoacetate hydroxylase
FDA	Food and Drug Administration
GA	glutaraldehyde
GC/MS	gas chromatography/mass spectrometry
H&E	haematoxylin and eosin
HGA	homogentisic acid
HGD	homogentisate 1,2-dioxygenase
HPA	hyper-phenylalaninaemia
HPPA	4-hydroxyphenylpyruvic acid
HPLA	4-hydroxyphenyllactic acid
HPPD	4-hydroxyphenylpyruvic acid dioxygenase
HPLC	high performance liquid chromatography
HT-1	hereditary tyrosinaemia type I
HT-2	hereditary tyrosinaemia type II
HT-3	hereditary tyrosinaemia type III
IEM	inborn errors of metabolism
IP	intra-peritoneal
IPTG	isopropyl β-D-1-thiogalactopyranoside

IVD	intervertebral disc
KOMP	Knockout Mouse Project
LC/MS	liquid chromatography/mass spectrometry
MMA	maleylacetoacetic acid
NAC	National Alkaptonuria Centre
NIH	National Institutes of Health
Ni-NTA	nickel-nitrilotriacetic acid
NTBC	2-(2-nitro-4-trifluoromethylbenzoyl)-1,3-cyclohexanedione; nitisinone
PAH	phenylalanine hydroxylase
PAL	phenylalanine ammonia lyase
PAS/H	periodic acid Schiff/haematoxylin
PBS	phosphate buffered saline
PCT	proximal convoluted tubule
pIpC	polyinosinic: polycytidylic acid
PEG	polyethene glycol
PKU	phenylketonuria
QTOF	quadrupole time-of-flight
SDS-PAGE	sodium dodecyl sulfate – polyacrylamide gel electrophoresis
SOFIA	Subclinical Ochronotic Features In Alkaptonuria
SONIA-1	Suitability Of Nitisinone In Alkaptonuria 1
SONIA-2	Suitability Of Nitisinone In Alkaptonuria 2
TAE	tris-acetic acid EDTA
TAL	tyrosine ammonia lyase
TAT	tyrosine aminotransferase
TCA	tricarboxylic acid
WT	wildtype

Experiment contributions

Chapter 3

Establishment of the new AKU mouse lines documented in this thesis was carried out prior to JHH beginning her PhD programme by Prof George Bou-Gharios (GBG), Dr Ke Liu (KL), Dr Antonius Plagge (AP) and the biomedical services unit (BSU). The *Hgd tm1a -/-* line had been bred to homozygosity when JHH commenced her studies, however it had not yet been phenotyped. The *Hgd tm1c +/+* line has also been established before JHH commenced her PhD studies. JHH was involved in the breeding of the *Hgd tm1c +/+* mice with the *MxCre* line (obtained from Dr Takao Sakai's lab) to obtain the *Hgd tm1d* line. JHH carried out all genotyping of the *Hgd* mouse lines (*tm1a, tm1c, tm1d, MxCre*) throughout her PhD and was responsible for colony management with guidance from GBG and the BSU team. The BALB/c $Hgd^{-/-}$ colony was managed by Dr Hazel Sutherland (HS), and genotyping carried out by JHH.

Metabolic phenotyping was carried out by JHH; homogentisic acid and other metabolites were analysed via mass spectrometry in Clinical Chemistry Department at the Royal Liverpool University Hospital Trust under the supervision of Andrew Hughes (AH) and Dr Anna Milan (AM). Blood and urine samples collected for mass spec analysis were collected by JHH, with assistance from HS and Peter Wilson (PW).

Identification of ochronotic pigmentation by histology was carried out by JHH, including all tissue harvesting, tissue preparation, histology and staining. Pigment quantification was carried out in the knee joint by JHH and also scored by Dr Craig Keenan (CK). For OARSI scoring, joints were sectioned by CK, stained by JHH, and then OARSI scored by both JHH and CK.

Chapter 4

Whole tissue and embryo LacZ staining, tissue imaging and subsequent histology was carried out by JHH. Time-mated embryos were harvested by JHH. LacZ stained brains sections were imaged and stitched to get whole section images by Dr Joni Roachdown. For frozen section LacZ staining, JHH cryosectioned liver and kidney and HS cryosectioned embryos. Frozen section LacZ staining and section imaging was carried out by JHH. For *Hgd* mRNA analysis in different tissues, JHH and PW harvested tissues from the mice; PW then performed the RNA extraction, cDNA synthesis and qPCR. JHH collected the liver, testis and epididymis from adult

mice, and the livers from embryos for mRNA analysis, performing the RNA extraction, cDNA synthesis and qPCR.

For the *Hgd tm1d* conditional knockout experiments, KL injected the majority of mice with pIpC, with a small number of injections performed by JHH and HS. Blood, urine and tissue harvesting in these pIpC experiments was carried out by JHH, with assistance from HS and PW. JHH analysed all blood and urine samples using mass spectrometry, supervised by AT and AM. *Hgd* mRNA analysis in these experiments was performed by JHH, including the RNA extraction, cDNA synthesis and qPCR.

Injection of labelled HGA into the tail vein was performed by HS with BSU assistance. Blood samples were collected by HS, assisted by JHH and PW. Dr Brendan Norman (BN) performed the mass spectrometry flux analysis for this experiment.

Chapter 5

Dietary restriction experiments were carried out by JHH and HS, with assistance from PW. All blood samples were analysed by JHH for tyrosine pathway metabolites. JHH and PW carried out the experiment monitoring food and water intake. NAC patient data was provided to JHH by Prof Lakshminarayan Ranganath (LR) and Shirley Judd (SJ), and analysed by JHH with advice from SJ.

In vitro PAL experiments were carried out once by CK (prior to JHH's PhD), and then once by JHH. JHH analysed tyrosine and phenylalanine using the mass spectrometer under AH's supervision. A preliminary *in vitro* TAL experiment was carried out by PW before JHH's PhD. Bacterial expression of TAL and purification was then carried out by PW, with JHH observing and occasionally assisting. *In vitro* TAL experiments were then carried out by PW, and then tyrosine analysed by JHH using mass spectrometry.

1 Introduction

1.1 Inborn errors of metabolism

Inborn errors of metabolism (IEMs) make up a large group of rare genetic inherited disorders. These disorders are caused by a deficiency or absence of proteins that have important roles in cellular biochemical function, such as enzymes which are the most common, carriers, receptors or structural proteins [1]. With defective enzymes making up the majority of IEMs, in most of these diseases, symptoms arise due to increased upstream substances, reduced downstream substances, or a switch to an abnormal substrate metabolism [2]. IEM's are traditionally characterized into groups of disorders that include carbohydrate metabolism, amino acid metabolism, organic acid metabolism or lysosomal storage diseases [3].

An online database, the Online Mendelian Inheritance in Man (OMIM), is a continuously updated, freely available database of human genes and their associated genetic traits/disorders. On 21st January 2020, there were 16,254 gene descriptions, with 4,209 genes with a phenotype causing mutation entered, with 6,577 phenotypes with a known molecular basis (Online Mendelian Inheritance in Man, OMIM®. McKusick-Nathans Institute of Genetic Medicine, Johns Hopkins University (Baltimore, MD), {23/01/2020}. World Wide Web URL: https://omim.org/).

Of the amino acid metabolism disorders, alkaptonuria (OMIM #203500), which is often described as the world's first genetic disease due to it being the first disorder described to conform to Mendelian inheritance, is the subject of study in this thesis.

1.2 Alkaptonuria

Alkaptonuria (AKU) is an ultra-rare, autosomal recessive, multisystem disease in which homogentisate 1,2-dioxygenase enzyme activity (HGD; EC 1.13.11.5) is deficient [4]. The HGD enzyme converts homogentisic acid (HGA) into maleylacetoacetic acid in the tyrosine metabolism pathway, see Figure 1.1. HGD deficiency leads to increased HGA in the urine, blood and tissues. Over time, this increased HGA accumulates and deposits as a dark brown, melanin-like pigment into connective tissues, termed ochronosis. Tissue ochronosis, which primarily affects articular cartilage, eventually leads to the manifestation of an early-onset and severe osteoarthropathy. AKU patients experience a decreased quality of life due to this highly debilitating and painful osteoarthropathy.

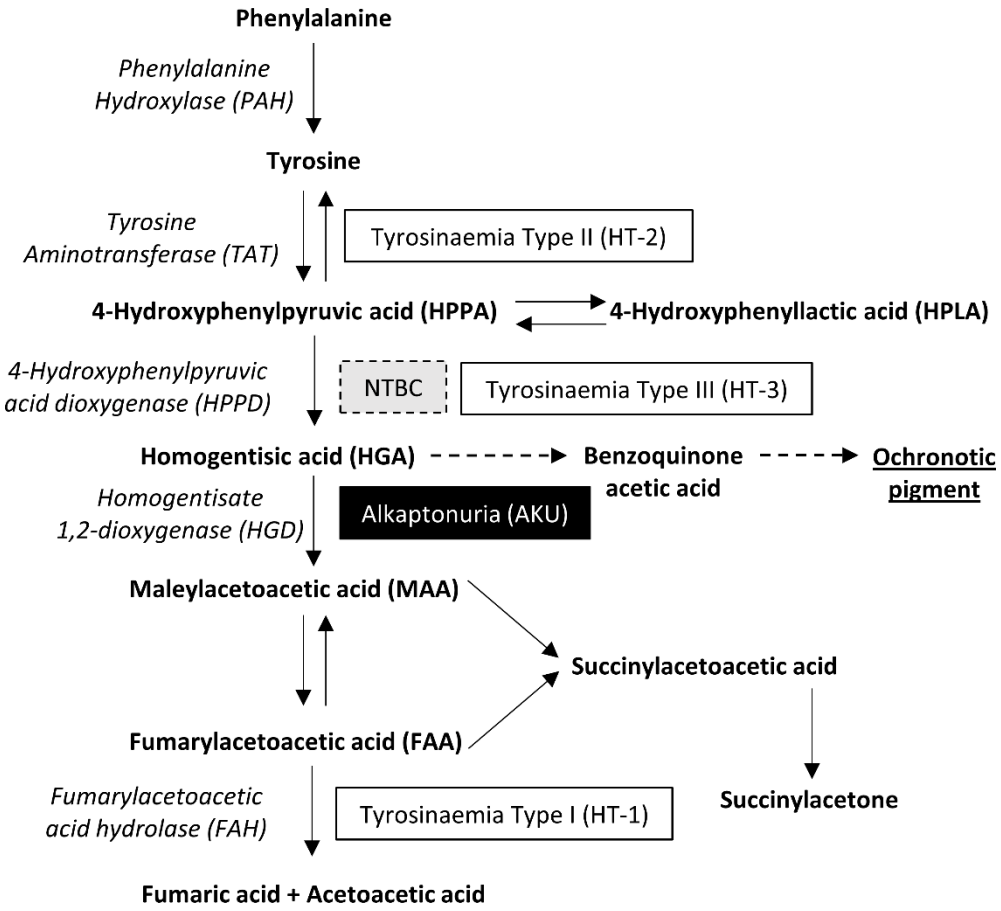

Figure 1.1. Tyrosine metabolism pathway.
Phenylalanine and tyrosine metabolites are broken down by a series of enzymes (italics). Genetic disorders associated with this pathway are shown in boxes, all of which are caused by an enzyme deficiency. Alkaptonuria is caused by a deficiency of the enzyme homogentisate 1,2-dioxygenase, leading to an increase of its substrate homogentisic acid (HGA), which is a biochemical marker of alkaptonuria. Alkaptonuria is characterised by the presence of a HGA-derived ochronotic pigment within connective tissues, which is thought to involve benzoquinone acetic acid as an intermediate compound (dashed arrows). NTBC (nitisinone) is a drug that can inhibit the 4-hydroxyphenylpyruvic acid dioxygenase enzyme, reducing HGA production.

1.2.1 History

The earliest evidence of AKU was documented in an Egyptian mummy, *Harwa*, dating to 1500BC. Radiological and biochemical analysis demonstrated that the mummy had narrowed and calcified joints with ochronotic articular surfaces that contained a pigment that was extracted and described as being identical to an air-oxidised HGA polymer [5,6]. In 1584, Scribonius described the urine of a boy that turned as "black as ink" [7,8]. In 1859, Boedeker then reported urine from a man with back pain that contained a substance that took up oxygen and caused the urine to turn black upon standing, accelerated by the addition of alkali, that he named "alcapton" [9]. In 1866, Virchow described the term ochronosis, after performing an autopsy on a 67-year old man, where he found "black as ink" cartilage all over the body [10]. On closer inspection, he found that not all the pigment was black, but a brown-yellow "ochre" colour under microscopic examination and called it "ochronosis". In addition,

Virchow also reported ochronosis in ligament, tendon, periosteum and arteries, in addition to deep ulcerations of knee joint articular cartilage down to the bony surface. In 1888, Kirk reported alcaptonuria urine containing an acid (that he named incorrectly) that was able to reduce both Fehling's solution and ferric chloride, and that upon alkalinisation darkened the urine [11]. In 1891, Wolkow and Baumann identified alkapton as 2,5-dihydroxyphenylacetic acid, and due its close structural relationship to gentisic acid, named it homogentisic acid (HGA) [12]. They also demonstrated that feeding extra tyrosine to an "alcaptonuria" patient resulted in increased excretion of HGA. It wasn't until 1902 however that Albrecht recognised the association between "alcaptonuria", ochronosis and ochronotic arthritis in a patient who passed dark urine, and at autopsy presented with both ochronosis and arthritis [13]. In 1904, Osler was the first to clinically diagnose AKU in two living brothers [14].

Approximately 50 years before the discovery of DNA [15], AKU became renowned as the world's first identified genetic disease. In 1902, Sir Archibald Garrod described the incidence of AKU, particularly the incidence within families and its relation to consanguineous marriage, concluding that AKU was somehow inheritable [16]. With advice from Bateson, he suggested that AKU is inherited by the Mendelian theories of recessive inheritance. He also reported the consistency of HGA found within urine from different individuals as uniform, suggesting that only one degree of alkaptonuria exists, either with several grammes of HGA in the urine or none at all [17]. In 1908, Garrod presented his work at the Croonian lectures, where he showed that AKU, along with other genetic disorders that included albinism and cystinuria, conformed to the laws of Mendelian inheritance [18]. Here he unveiled the term *inborn error of metabolism*, proposing that the cause of AKU was lack of an enzyme that in normal individuals split the aromatic ring of HGA. A year later, Neubauer provided the first map of the tyrosine degradation pathway [19]. Garrod's enzyme defect theory preceded the work of Beadle and Tatum, who in 1941 published their conclusions that a single defective gene can be correlated with a metabolic block in one enzymatic reaction. It wasn't until 1958 that biochemical evidence of the defect in AKU was provided by La Du, where he demonstrated the absence of HGD activity in a liver homogenate prepared from an AKU patient, establishing that failure to synthesize active enzyme was the sole cause of AKU [4].

1.2.2 Epidemiology

AKU is an ultra-rare disease; the worldwide incidence is approximately 1:250,000 to 1:1,000,000 [20]. There are however specific areas where the incidence is much higher, such as

in Slovakia and the Dominican Republic where the incidence is estimated to be 1:19,000 [21,22]. The high incidence in the Dominican Republic can be attributed to classical founder effect, where 87% of the tested AKU chromosomes had the same mutation, with C120W identified as the founder mutation in this population [23]. It is not known if the mutation originated in the Dominican Republic or if it was introduced through immigration. In Slovakia on the other hand, the incidence of AKU is difficult to explain by a founder affect, as high allelic heterogeneity has been found in this relatively small country, with little contribution from the most common European mutations. This suggests that several other independent founders may have contributed to the gene pool in Slovakia, combined with a greater mutation rate, as 7 of 12 mutations that most likely originated in Slovakia are associated with regions of hyper-mutation within the *HGD* gene, and have been traced to a small isolated area in the north-west of the country [22]. Although the incidence has not been calculated, Jordan has been recently identified as a hotspot for AKU, where 40 cases were identified in one village, with 9 cases occurring in one family [24,25]. This greater incidence is thought to have occurred due to consanguineous marriage which is common in Jordanian culture; a recent study by the Jordan Population and Family Health Surveys reports that 35% of all marriages were consanguineous in 2012, reduced from 57% in 1990 [26].

1.2.3 Clinical presentation

1.2.3.1 Tyrosine and phenylalanine

AKU is a disorder of tyrosine/phenylalanine metabolism. Phenylalanine is an essential amino acid obtained only from the diet whereas tyrosine is a non-essential amino acid, produced by the hydroxylation of phenylalanine within the body [27], although it can become an essential amino acid if phenylalanine intake is insufficient. Both of these amino acids can also be obtained from endogenous protein turnover. Tyrosine and phenylalanine are used for synthesis of hormones, melanin and other new proteins, however this only accounts for about 5% of dietary tyrosine intake, with the majority of tyrosine being metabolised to maleylacetoacetic acid and fumarylacetotacetic acid in the tyrosine metabolism pathway, via HGA (see Figure 1.1) [28]. Metabolism of phenylalanine and tyrosine produces metabolites that enter intermediate metabolism, namely ketogenesis by the production of acetoacetic acid which enters the TCA (tricarboxylic acid) cycle for the production of ATP, and for the production of fumaric acid which too can enter the TCA cycle, in addition to gluconeogenesis for the production of glucose. Tyrosine and phenylalanine are therefore both ketogenic and

glucogenic amino acids. Disruption of this metabolic pathway in AKU leads to a complete metabolic block, characterised by increased HGA in the urine and blood.

1.2.3.2 Homogentisic acid

It is not uncommon for individuals with AKU to reach adolescence/adulthood without a diagnosis, as children are usually asymptomatic with the exception of homogentisic aciduria. Dark staining of nappies/urine from babies is often observed, due to the presence of HGA, which becomes oxidised, turning the urine black [29–31]. AKU urine that is left to stand turns dark after several hours [8,20]. To further confirm the diagnosis, a fresh urine sample can be alkalinised to accelerate the oxidation of HGA, resulting in black/dark urine [32–34]. Various methods to assess HGA levels in urine have been reported and are used to diagnose AKU, some of which include an oxidation/alkalinisation step, such as spectrophotometric analysis of alkalinised urine [35], urine spots on filter paper followed by capillary electrophoresis [36,37], and colorimetric analysis of alkalinised dried urine spots [38].

Whilst filter paper methods that do not require complex laboratory equipment may be useful for screening or diagnosis where specialist services are not available, the gold standard for clinical diagnosis of AKU is quantitation of HGA in urine using methods such as spectrophotometric analysis [20,39,40], gas chromatography [41], high performance liquid chromatography (HPLC) [42], gas chromatography/mass spectrometry (GC/MS) [43–45] and liquid chromatography/mass spectrometry (LC/MS) [46]. Quantitation of HGA in serum is also used to monitor AKU and the effectiveness of therapeutic intervention [47–49].

Various studies have reported HGA levels in the plasma and urine of AKU patients. HGA is excreted in millimolar concentrations in the urine of AKU patients, see Table 1.1 for the reported urinary HGA excretion in the literature, which equates to several grams per day. The daily excretion of HGA has been investigated in 22 healthy individuals; in 15 of these, HGA excretion was below the lower limit of quantitation <1.0 µmol/L (LC/MS assay) and could not be determined, with the remaining 7 excreting HGA above this value, with a maximum excretion of 2.91 µmol/24hr which equates to approximately 0.49 mg/day [50]. Circulating HGA (either plasma or serum) is reported to be on average 30-50 µmol/L in AKU patients, see HGA in healthy individuals (n=22) [50]: <1.0 µmol/L (n=15), maximum 0.00291 mmol/24hr or 0.00049 g/24hr in remaining 7 individuals.

Tyrosine in healthy individuals (n=22) [50]: 14-147 µmol/24hr.

Table 1.2 for values from the literature. Within the 22 healthy individuals aforementioned, serum HGA was not detected as it was below the lower limit of quantitation (LC/MS assay) and therefore reported as <3.1 µmol/L [50]. A more sensitive method (GC/MS) was used to quantitate HGA in 9 healthy individuals, and determined to be 2.4-12.0 ng/ml, which is approximately 0.05 µmol/L [49]. Tyrosine in both the urine and serum/plasma is often reported in AKU patients, see Table 1.1 and HGA in healthy individuals (n=22) [50]: <1.0 µmol/L (n=15), maximum 0.00291 mmol/24hr or 0.00049 g/24hr in remaining 7 individuals.

Tyrosine in healthy individuals (n=22) [50]: 14-147 µmol/24hr.

Table 1.2 respectively, and are comparable with healthy adult reference ranges. In these AKU patients, tyrosine is about 40-80 µmol/L in plasma/serum and 100 µmol/24hr in the urine. In the 22 healthy individuals already mentioned, serum tyrosine was 30-87 µmol/L, and urinary tyrosine was reported to be 14-147 µmol/24hr [50].

Table 1.1. Mean urine concentrations of HGA and tyrosine in AKU patients from the literature.

	Urine concentration					
	n	**mmol/mmol creatinine [range]**	**g/24hr [range]**	**mmol/L [range]**	**mmol/24hr [range]**	**Reference**
HGA	3	2.51	-	-	-	Hughes et al. 2014 [46]
	58	3.12	-	-	-	Phornphutkul et al. 2002 [20]
	1	1.22	-	-	-	Wolff et al. 2015 [51]
	40	-	5.68 [0.84-9.60]	-	-	Introne et al. 2011 [40]
	17	-	0.95 [0.46-1.5]	-	-	Al-Sarayreh et al. 2014 [44]
	1	-	-	5.78	-	Öztekin et al.2018 [37]
	40	2.7 [1.9-4.3]	[2.43-11.7]	-	32.1 [14.4-69.5]	Ranganath et al. 2014 [52]
	28	2.26	-	-	20.56	Milan et al. 2017 [53]
Tyrosine	3	0.017	-	-	-	Hughes et al. 2014 [46]
	28	0.011	-	-	0.103	Milan et al. 2017 [53]

HGA in healthy individuals (n=22) [50]: <1.0 µmol/L (n=15), maximum 0.00291 mmol/24hr or 0.00049 g/24hr in remaining 7 individuals.
Tyrosine in healthy individuals (n=22) [50]: 14-147 µmol/24hr.

Table 1.2. Mean serum/plasma concentrations of HGA and tyrosine in AKU patients from the literature.

	Serum/plasma concentration			
	n	**µmol/L [range]**	**µg/ml [range]**	**Reference**
HGA	40	29.2 [5.8-45.5]	-	Ranganath et al. 2014 [52]
	58	-	6.6 [3.0-27.8]	Phornphutkul et al. 2002 [20]
	3	49.3 [30.2-75.2]	-	Hughes et al. 2015 [47]
	38	-	5.74 [3.15-10.5]	Introne et al. 2011 [40]
	28	30	-	Milan et al. 2017 [53]

Tyrosine	40	60 [39-113]	-	Ranganath et al. 2014 [52]
	58	79	-	Phornphutkul et al. 2002 [20]
	38	59.8 [41-108]	-	Introne et al. 2011 [40]
	3	51 [31-82]	-	Hughes et al. 2015 [47]
	28	42 [20-82]	-	Milan et al. 2017 [53]

HGA in healthy individuals (n=22) [50]: <3.1 µmol/L.
Tyrosine in healthy individuals (n=22) [50]: 30-87 µmol/L.

1.2.3.3 Ochronosis

The consequence of increased HGA in the circulation and extracellular fluid for decades, is the presence of a dark brown, HGA-related pigment found within connective tissues all over the body, termed ochronosis [8]. Ochronosis affects a variety of connective tissues, most commonly the weight-bearing joints and spine but also the cardiovascular system [54], eyes, and skin [55,56]. In addition to the change in appearance, pigmented tissues become stiff and brittle [57]. Articular cartilage is particularly affected by pigmentation and degenerates prematurely, manifesting clinically first as lower back and joint pain, progressing to a severe and debilitating early-onset osteoarthropathy.

1.2.3.3.1 Spinal and joint arthropathy

Other than increased HGA causing dark urine, most patients are asymptomatic until adulthood. The onset of symptoms usually begins with the onset of lower back pain (usually lumbar and then thoracic), before the age of 30 years, preceding the involvement of the cervical spine [20]. Intervertebral discs, in both the nucleus pulposus and annulus fibrosis, and ligaments become heavily pigmented and calcified over time [58]. The spinal degeneration observed in AKU is progressive and can be seen with radiographs; initially the disc space becomes narrowed, followed by disc calcification and then fusion. In addition, kyphosis, reduced lumbar spinal flexion and loss of height is observed in AKU patients [20]. AKU can be differentiated from ankylosing spondylitis, a form of inflammatory arthritis, by the lack of sacro-iliac joint involvement.

In addition to severe spinal degeneration, ochronosis causes early-onset and severe joint disease (osteoarthropathy) in AKU, involving at first the larger joints such as the knee, hip and shoulder where a reduced range of motion is observed [59], before progressing to involve most joints of the body, including the smaller joints of the hands and wrists. A study involving 58 AKU patients found that by the age of 55 years, half of patients had undergone at least one joint replacement due to osteoarthritis, with many patients requiring multiple joint replacements [20]. This study also observed a roughly linear increase in joint disease severity

after 30 years of age, with men showing a more rapid increase in severity than women. Many case reports in the literature report ochronotic joint arthroplasty of the shoulder, hip and knee, where heavily pigmented cartilage was observed at surgery/autopsy [55,60–64].

1.2.3.3.2 Connective tissue ochronosis

In addition to osteoarthritic cartilage degeneration, other musculoskeletal tissues are affected by ochronosis. Tears and ruptures have been reported in the Achilles, patellar and shoulder rotator cuff tendons [43,65]. One report documents a 57% prevalence of tendon-related symptoms, such as a thickened Achilles tendon, a 40% incidence of joint effusion (increased intra-articular fluid), and less common affects such as muscle tears after minor trauma, synovitis and ligament tears in load bearing joints [20]. Pigmentation of the synovial membrane has been reported [43]. Pigmentation of the trachea and primary bronchi cartilage has also been observed by bronchoscopy, that led to the diagnosis of AKU in a patient [66].

Ochronosis of joints is usually only ever seen at the end stage of disease, either at joint replacement or at post-mortem. Ochronosis however is visible macroscopically in the sclera and conjunctiva of the eye, the cartilage of the ear and also in the skin, where its intensity can drastically vary between individuals [20,43,56,58,59]. Perspiration may also be blue or brown [59].

At post-mortem, pigmentation can be found in areas that were not visible in life, unless observed during surgery. In addition to pigmented articular cartilage of the knee, hip and shoulder, pigmentation has also been identified in the costal cartilages, periosteum of bone (although not bone itself), cartilages of the larynx, trachea and bronchi, tendons, ligaments, epidermis of the skin, the dura of the brain, and within the cardiovascular system (see section 1.2.3.3.3)[58,59,67]. Pigmented lymph nodes have also been reported in the hilar region of lung in the thorax [58].

Ochronotic pigmentation is not seen within the pancreas, hepatobiliary system, or lung (excluding bronchial tree), gastrointestinal tract or spleen [55,58]. Similarly, ochronosis of kidney tissue has not been reported, although a macroscopically grey proteinaceous tubular cast of the medullae has been described [55].

1.2.3.3.3 Cardiac ochronosis

Within the cardiovascular system, pigmentation has been identified in both the aortic and mitral heart valves, chordae tendinae, endocardium, pericardium, atheromatous plaques and roots and walls of major arteries such as the aorta and coronary arteries, where pigmentation was present within the intima and adventitia of the arterial wall [55,58–60,67–72]. Pigmentation has also been described in the basilar and internal carotid arteries [58]. Monckeberg arteries, which are vessels that have calcification, have also been reported in the extremities of an AKU patient [56].

Aortic stenosis is the most commonly reported cardiac abnormality in AKU patients, with many patients requiring valve replacement [73]. In a group of 58 AKU patients, 3 individuals >50 years had undergone a valve replacement, presenting at a mean age of 54 years, and 50% had evidence of coronary artery calcification by 59 years [20]. A larger study investigating cardiac involvement in a group of 76 AKU patients found that overall, there was a 17% prevalence of significant aortic valve disease with a high prevalence of aortic vascular calcifications that begin to manifest in the 6th and 7th decade of life, that did not correlate with standard cardiovascular risk factors [73]. More specifically, 8% had undergone valve replacement, 16% had aortic sclerosis and 9% had aortic stenosis. Over 65 years, 50% had aortic stenosis or had undergone valve replacement. Within this group of 76 patients, 17 patients with a mean age of 55 ± 7 years had CT scans that allowed evaluation of coronary and valve calcification; 18% had significant coronary calcification, 47% had valve calcification (18% severe), 65% had significant vascular calcifications, with calcifications predominately seen in the aortic root, descending aorta and iliac arteries, and by 60 years of age, there was a 100% prevalence of intra-cardiac calcification.

1.2.3.3.4 Urogenital calculi

In addition to the connective tissue pigmentation and degeneration described above, increased HGA is also thought to exhibit adverse effects in other tissues, such as urogenital complications. Kidney stones are common in AKU, with a prevalence of 28% found in a survey of 58 AKU patients, and are thought to be related to the very high level of HGA being excreted by the kidney [20]. In the same group of patients, prostate stones were documented in 30% of men aged 31-60 years, with no apparent link to the prevalence of kidney stones [20]. Prostate stones have been reported elsewhere, and upon prostatectomy, black calculi have been observed [43,51,58,59,74–76]. Bladder stones have also been reported in AKU [74–76].

Wolff et al. in a case report investigated dark/black kidney and prostate stones (at different times) found from one AKU patient who had normal renal function, using X-ray diffraction and infrared spectroscopy techniques respectively [51]. Analysis revealed that the kidney stones were 100% calcium phosphate, although the authors acknowledged the technique may be limited in its detection of certain structures. Prostate stone analysis revealed the composition to be protein, carbapatite (carbonated calcium phosphate), and small amounts of weddellite (calcium oxalate dihydrate). This agrees with earlier reports analysing prostatic calculi composition [74–76], all of which were reported to be the standard components of non-AKU prostatic calculi [51,77]. The black substance within the black prostate stones was not identified in these reports; its absence from X-ray diffraction analysis suggest the pigment is amorphous, and was therefore undetectable with diffraction techniques that are limited to crystalline structure detection. The reported composition of the kidney and prostate stones from the AKU patient would suggest that the patient was suffering from proteinuria, hypercalciuria and hypophosphaturia, however this was not observed by Wolff et al. [51]. They postulated instead that active bone resorption due to ochronosis in the joints may have been releasing calcium and phosphate into the blood stream, which when combined with HGA, lead to the formation of black stones. In addition, the alkali secretions of the prostate may accelerate HGA oxidation to pigment and therefore increase the likelihood of prostate stones.

1.2.4 Pathophysiology of ochronosis

Ochronotic pigment is found within connective tissues all over the body, with cartilage appearing to be the most susceptible tissue. In addition to the large weight bearing joints such as the hip, knee, shoulder and elbow, pigmentation is found within many other hyaline cartilages, including the costal cartilages, larynx, trachea and bronchi, sternoclavicular joints and sacroiliac joints [20,55,58,59,66]. Pigmentation is also seen within fibrocartilaginous tissues such as the annulus fibrosis of intervertebral discs (IVDs) and pubic symphysis [55,58], and within elastic cartilage of the external ear and epiglottis [20,55]. Pigmentation is also found within non-cartilaginous tissue such as ligaments, tendons, synovial membrane, periosteum (although not the bone itself), perichondrium, sclera and conjunctiva of the eye, skin and dura of the brain [20,43,55,56,58,67]. Within the cardiovascular system, pigmentation has been identified in heart valves, chordae tendinae and roots and walls of major arteries such as the aorta, where pigmentation was present within the intima and adventitia of the arterial wall [55,58,59,67].

Although the exact mechanism of pigment deposition/formation is currently unknown, the pattern and order of pigmentation within human cartilage has been elucidated, using AKU joints obtained at joint replacement surgery. Histological analysis of human AKU cartilage with varying pigment intensities revealed that pigmentation initiates as pericellular and intracellular pigmentation of individual chondrocytes within calcified articular cartilage, close to the subchondral bone [57]. Initially, pigmentation was not found in the calcified articular cartilage inter-territorial matrix between cells, nor within the non-calcified hyaline cartilage. Pigmentation then advanced to the deep and middle hyaline cartilage zones as a blanket pigmentation covering both the territorial and inter-territorial matrix, despite the calcified articular cartilage showing only territorial matrix pigmentation. Within heavily pigmented samples, pigmentation of superficial articular cartilage and the inter-territorial matrix of calcified cartilage was observed [57]. Furthermore, a complete absence of the calcified articular cartilage and subchondral bone was observed in severely affected cartilage, hypothesized to be due to stress shielding from the heavily pigmented and subsequently stiffer hyaline cartilage zones above, that causes osteoclast resorption of the unloaded calcified cartilage and subchondral bone. Elevated urinary collagen N-telopeptide, a marker of bone resorption, has been reported in AKU patients [20].

It has been shown that ochronotic pigment has an affinity for fibrillary collagen surrounded by glycosaminoglycan-rich ground substance, particularly in hyaline cartilage [67]. Analysis of pigmented collagen fibres from the ligamentous capsule of an AKU hip joint revealed intracellular (fibroblasts) and extracellular granular pigmentation associated with collagen fibres, in addition to a homogenous pigmentation that encrusted collagen fibres [78]. The granular pigment associated with collagen fibres varied in position, distribution and intensity, with a periodic banding pattern of pigment observed on individual collagen fibres. In addition to granules, shards of pigment were observed that often bridged between collagen fibres. Taylor et al. suggest that the extracellular matrix (ECM) is normally resistant to pigmentation, and may become susceptible after biochemical or mechanical damage [57]. They showed that pigmented cartilage is much stiffer than non-pigmented cartilage, and suggest that focal pigmentation of individual chondrocytes and their associated collagen is likely to make the ECM prone to damage through normal loading, leading to further damage in an inevitable downward spiral. This work led to a theory, termed the exposed collagen hypothesis, that small granule pigmentation on collagen fibres, similar to the pattern of proteoglycan binding, occurs due to proteoglycan and glycosaminoglycan loss, acting as a nucleation point for pigment polymerization, see Figure 1.2 [79]. Solid state nuclear magnetic resonance studies

have shown nanoscale collagen disorder and proteoglycan loss in AKU cartilage, supporting the theory that loss of proteoglycans and other molecules, due to damage, may allow HGA binding [80].

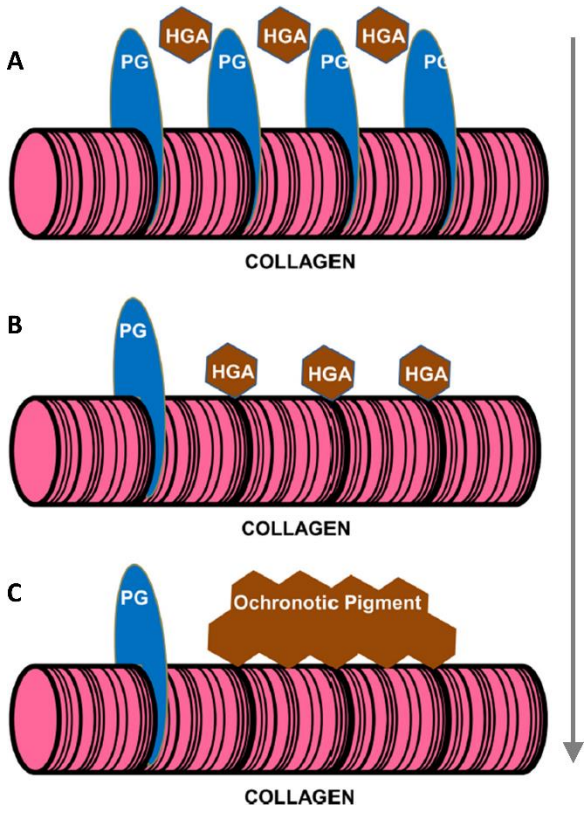

Figure 1.2. Schematic representation of the exposed collagen hypothesis of pigment deposition and progression in AKU.
A shows homogentisic acid (HGA) is present in the extracellular environment, but cannot bind to undamaged collagen fibrils, which are decorated with protective molecules including proteoglycans (PGs). As a result of repetitive mechanical loading, chemical attack or ageing and degeneration, protective molecules including PGs are lost from the collagen fibrils (B). The exposed collagen fibrils are then susceptible to attack from small molecules such as HGA. The initial binding of HGA functions as a nucleation event and is followed by further rapid deposition of HGA as a pigmented polymer (C). Binding of HGA-derived pigment to the collagen fibrils makes them stiffer and susceptible to more mechanical damage. This leads to further ultra-structural changes in collagen, increased exposure to HGA and a downward spiral of increasing pigmentation and severe ochronosis. Adapted from Gallagher et al., 2016 [79].

Experiments conducted in an *in vitro* cell model of ochronosis, where osteosarcoma cell lines that can secrete ECM are incubated with HGA, have also shown pigment deposition to be intracellular and extracellular, with the latter associated with fibrillary structures in the matrix [81]. Culture media incubated with HGA took weeks to darken in the absence of cells, compared to a few days in the presence of cells, highlighting that cellular activity accelerates pigment deposition. *In vivo,* pigment deposition is thought to take many years; pigment

deposition was observed within a few days *in vitro*. The authors suggest that the ECM *in vivo* is protective, inhibiting ochronosis; the ECM formed *in vitro* is not assembled correctly into a highly organised and complex matrix, with no periodicity observed in fibres, and may explain the rapid pigment deposition by a lack of protective factors. This would support the exposed collagen hypothesis that was later published, that the protective molecules shielding collagen could be proteoglycans and glycosaminoglycans [79]. Interestingly, of these cell lines incubated with HGA, SaOS-2 cells were the most pigmented, but synthesised the least amount of collagen (the opposite was true for TE85 cells), suggesting that the amount of collagen is not a key factor associated with pigmentation [81]. This supports an earlier comment by Taylor et al. that pigmentation appears to be of established matrix, and not newly formed matrix [57].

HGA is a reducing agent, and especially under alkaline conditions, is rapidly oxidised to benzoquinone acetic acid, turning solutions and tissues black [59,82]. Ferric chloride has been shown to cause AKU urine to turn an evanescent blue colour when added dropwise [59]. A modified Schmorl's stain, which incorporates ferric chloride in the incubating solution, has been used both in cells and in human tissue sections to enhance ochronotic pigment from a yellow-brown to an intense blue-green colour, whereby ferricyanide is reduced to ferrocyanide by the presence of ochronotic pigment, supporting that it is indeed a HGA-derived pigment [81]. Furthermore, Schmorl's reagent is usually used to stain melanin pigments which may suggest that ochronotic pigment could be structurally similar to melanin. The structure and mechanism for ochronotic pigment deposition/formation remains to be elucidated; it is not known whether ochronosis occurs by initial binding of HGA, an oxidised intermediate, or as ochronotic pigment [83]. For a more detailed review regarding the potential structure of ochronotic pigment, refer to Ranganath et al. [83].

1.2.5 HGD

Since the early 1900's, AKU has been described as a disorder of tyrosine metabolism, with the assumption that there was an abnormality in the HGD enzyme (often referred to as HGO in older literature) that caused the excretion of HGA into the urine, however the nature of the defect had not been determined. In 1958, it was La Du et al. who determined that there was no detectable HGD activity in a liver homogenate obtained from a liver biopsy from an AKU patient, concluding that AKU was caused by a failure to synthesize active HGD enzyme, creating a complete metabolic block in the tyrosine catabolism pathway [4]. They also determined that tyrosine catabolism followed the same series of reactions as other

mammals, with the conversion of tyrosine to 4-hydroxyphenylpyruvic acid (HPPA), HGA, maleylacetoacetic acid (MAA), fumarylacetoacetic acid (FAA) and acetoacetic acid, as shown in Figure 1.1, with the activity of enzymes in the AKU liver homogenate, other than HGD, shown to be comparable to those isolated from a non-AKU liver homogenate. It is now known that HGD cleaves the aromatic ring of HGA [84].

1.2.5.1 *HGD* gene

After the work by La Du in the 1950's, it was generally accepted that AKU was caused by a defect in HGD that resulted in failure to synthesize active enzyme. It was not known whether the AKU defect was a result of a regulatory or structural gene mutation. No further progress was made on the molecular characterisation of the defect causing AKU until the 1990's, when the *HGD* gene was cloned, allowing the identification of mutations (see section 1.2.5.3 for more detail on *HGD* mutations).

The human *HGD* gene was mapped to chromosome 3q2 in 1993 via a homozygosity study [85]. In 1994, a homologous murine mutation was discovered in chromosome 16 [86]. Inter-species linkage studies using conserved genetic linkage groups then confirmed this human chromosome 3q2 location [87]. Schmidt et al. in 1995 purified murine liver HGD, as a 49 kDa protein [88]. The first HGD enzyme, *hmgA*, was then cloned and characterized in 1995 in a fungus model (*Aspergillus nidulans*) that was being used to study inborn errors of phenylalanine metabolism, as a 448-residue polypeptide that was 50 kDa in size [89]. From the cloned cDNA, the amino acid sequence was deduced and used to identify expressed tag sequence clones that corresponded to human (from liver cDNA libraries) and plant *HGD* homologues [89]. They also showed that disruption of the *hmgA* resulted in HGA secretion and absence of the HGD enzyme.

In 1996, human *HGD*, determined to be a single copy gene, was then further mapped to chromosome 3q13.33 (http://www.ncbi.nlm.nih.gov/gene/3081), and shown to comprise of 14 exons encoding a 445-mer protein [90]. In addition, the authors reported the first described mutations in the *HGD* gene, see below in section 1.2.5.3. The *HG*D exons range from 35 to 360 bp in size, with the introns ranging from 605 to 17,687 bp and the 5'- and 3'- untranslated regions (UTRs) being 167 and 210 nucleotides, respectively [91]. The full *HGD* nucleotide sequence, including both exons and introns is 54,363 bp, with 3% of this sequence representing coding regions [91], see Figure 1.3.

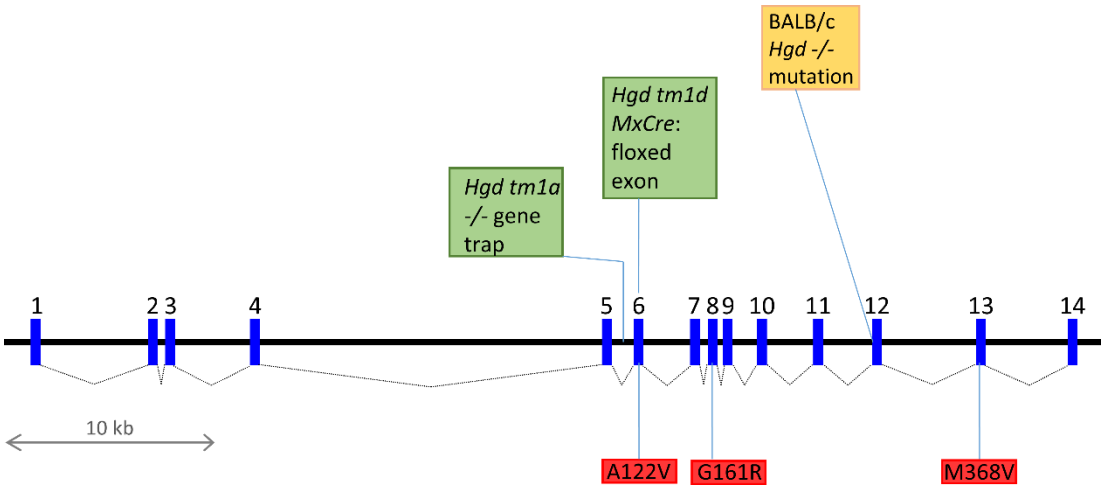

Figure 1.3. Schematic representation of the *HGD* gene exons and introns.
The gene spans 54,363 bp split into 14 exons (blue boxes) and intronic sequences (solid black line). *HGD* exons range from 35 – 360 bp in length, with introns ranging from 605 – 17,687 bp in length [91]. Mutations have been found in every exon and within most of the introns. Exons 6, 8, 10 and 13 show the highest prevalence of mutations [92]. Amongst all mutations, missense mutations are the most common with a prevalence of approximately 67% [92]. Across 172 AKU patients, the 3 most common mutations are shown in red boxes, all of which are missense. The most common mutation is G161R in exon 8 found in 68 AKU chromosomes, followed by A122V in exon 6 found in 27 AKU chromosomes and M368V in exon 13 found in 24 AKU chromosomes [93]. The mutation found within the ENU AKU mouse model BALB/c *Hgd*$^{-/-}$ is shown in a yellow box which is a splice mutation at the start of exon 12 (see section 1.3.2.3 for more information on this mouse model). This thesis reports a new AKU mouse model in chapters 3 & 4 that includes a knockout line (*Hgd tm1a -/-*) with a gene trap inserted into intron 5 and a conditional line (*Hgd tm1d*) that has exon 6 targeted for deletion (green boxes).

1.2.5.1.1 Conservation of the *HGD* gene

The *HGD* gene is a very well conserved gene across a variety of species, as can be observed using the Ensembl (Ensembl release 99, January 2020 ©) gene/protein tree tool, see Appendix, section 8.1, Figure 8.1. Shown in Figure 1.4 is a direct comparison of the human *HGD* and mouse *Hgd* from the Ensemble gene/protein tree. A comparison of the nucleotide sequences (CCDS; consensus CDS sequence) of human *HGD* (NCBI gene ID: 3081) and mouse *Hgd* (NCBI gene ID: 15233) using the NCBI nucleotide BLAST (basic local alignment search tool) alignment search was carried out. Both the mouse and human sequences contain 1338 nt, with 88.42% of nucleotides being identical (1183/1338 nt identical). The aligned sequences can be found in the Appendix, section 8.1.1.

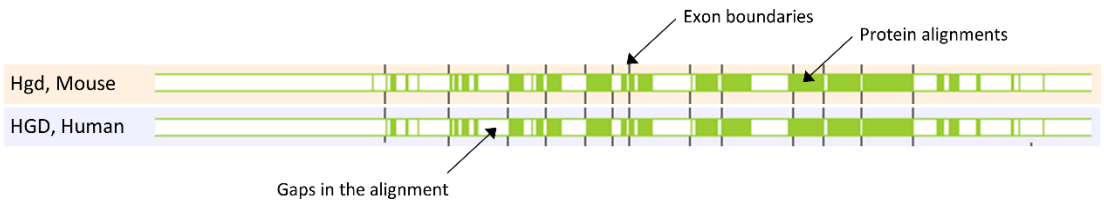

Figure 1.4. Protein tree alignment of human and mouse HGD.
Across most species, the *HGD* gene is very well conserved. A direct comparison of human *HGD* and mouse (*Mus musculus*) *Hgd* is shown, generated using the Ensemble gene tree tool (https://www.ensembl.org/index.html).

1.2.5.2 HGD protein

Murine liver HGD enzyme was purified in 1995, and its molecular mass was determined to be approximately 49 kDa. The *in vitro* pH optimum for the activity of the purified enzyme was 6.1. Schmidt et al. also determined that the presence of Fe^{2+} is an important co-factor for activity [88]. Titus et al. then determined the crystal structure of the active form of HGD to be a highly complex and dynamic hexamer, arranged as a dimer of two disk-like trimers, see Figure 1.5 stacked base-to-base [84]. The N-terminal domain of one protomer interacts with the C-terminal domain of the adjacent protomer in the trimeric structure [94]. The HGD protein can be divided into 4 general structural sections: core, active site, surface and homohexamer interfaces [93]. Each subunit (or protomer) has a single iron (Fe^{2+}) co-factor, required for the binding of HGA. A very intricate network of non-covalent interactions that includes hydrogen, salt and hydrophobic bonds are required to maintain the structure of the HGD protomer, dimer and the hexamer, with the active site conformation appearing to be highly dependent on inter-subunit hydrogen bonding and hydrophobic interactions [84].

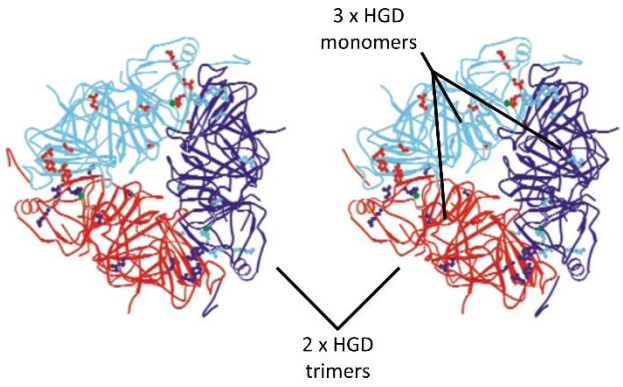

Figure 1.5. Structure of the HGD protein.
The HGD protein is a dimer of two disk-like trimers that stack base-to-base to form a hexamer. The foreground surface in this image forms the interface between the trimers in the HGD hexamer. Individual subunits are coloured light blue with red side chains, dark blue with light blue side chains and red with dark blue side chains. The iron cofactor in each subunit is drawn as a green sphere. Image adapted from Titus et al. 2000 [84].

1.2.5.3 Mutations in *HGD*

Many different *HGD* mutations have been identified in AKU, with patients carrying either homozygous or compound heterozygous variants of the *HGD* gene, which is a single copy-gene. At the same time as the cloning of the human *HGD* gene, Fernández-Cañón et al. showed that the *HGD* gene was mutated in AKU patients, describing the first reported *HGD* mutations in 1996 [90]. PCR-amplification was used to amplify the 14 *HGD* exons for members of two different Spanish AKU families, which were then directly sequenced. The heterozygous parents of one family both had a missense mutation where 1 nucleotide change caused

proline to be substituted by serine in exon 10 at amino acid position 230 (P230S), which is a conserved residue between fungal and human *HGD* [90]. The two AKU children of these heterozygous parents were homozygous for the P230S mutation, and a healthy third child was heterozygous for this mutation. This P230S mutation was also found in the second family. One parent was heterozygous with the P230S mutation, whilst the other was heterozygous for a different missense mutation, whereby valine is substituted to glycine due to a single nucleotide change in exon 12 at amino acid position 300 (V300G), which is also a conserved amino acid in fungal *HGD* [90]. Analysis of the children from this family revealed three AKU children who were compound heterozygotes for the P230S and V300G mutations, with two healthy heterozygous children (1 with the P230S and 1 with the V300G mutation) and two healthy children carrying no *HGD* mutations. This suggested that these mutations produce non-functioning alleles as they follow the recessive mode of inheritance pattern. The authors confirmed that the P230S mutation was non-functional, by expressing *HGD* with the P230S mutation in *Escherichia coli* and proving that the protein extract had no HGD activity, ultimately confirming that defects in the *HGD* gene cause AKU [90].

Since the first reported *HGD* mutations in 1996, many AKU-causing mutations have been described in AKU patients. By 2011, 115 known mutations had been identified in the human *HGD* gene, with exons 6, 8, 10 and 13 showing the highest prevalence of mutations [92]. These mutations range from missense mutations (66.4%), small deletions (12.2%) and insertions (12.2%), causing frameshift and splice mutations, and nonsense mutations (6%). To date, 203 different human *HGD* variants have been identified [93,95] which can all be found in the *HGD* mutation database; http://hgddatabase.cvtisr.sk [95]. In 2011, there were about 30 AKU chromosomes (both chromosomes must be studied as patients can have 2 different mutations) where no *HGD* mutation had been identified, and the authors suggested that the mutations may be deep within introns that have not yet been analysed, or within the promotor region or other regulatory sequences that have not yet been detected [92]. Triplets of CCC together with CpG dinucleotides are considered to be mutational hotspots in the *HGD* gene [92,96].

It has been shown that the delicate structure of HGD is easily disrupted by mutations, mainly the missense variants that represent 68% of all known AKU variants, compromising enzyme function [92,97]. In 2000 when the crystal structure of HGD was determined, more than half of the AKU associated mutations were predicted to affect residues located close to the inter-subunit interfaces, affecting the non-covalent contacts between the subunits of HGD [84]. Other mutations were predicted to affect co-factor binding, hydrophobic core structure and

electrostatic interactions. Therefore rather than AKU mutations having a direct effect on the catalytic activity of the enzyme, the majority of AKU mutations are expected to disrupt substrate binding and/or catalysis through indirect structural effects and/or misfolding [84]. A more recent paper in 2016 predicts that missense variants affect enzyme activity by 3 molecular mechanisms; decreased stability of individual protomers, disruption of protomer-protomer interactions or by modification of residues in the active site region [97]. Ascher et al. in 2019 showed that missense variants affecting function were generally associated with highly conserved residues [93].

1.2.5.4 Expression of HGD

It has been known for many years that HGD is expressed in the liver and kidney. La Du et al. in 1958 and Zannoni et al. in 1962 were the first to demonstrate the location of HGD activity, reporting that HGD activity was not detected in tissue homogenates from the liver and kidneys of AKU patients, but was detectable in non-AKU liver and kidney homogenates [4,98]. Murine HGD was then purified in 1995 from the liver [88]. In 1996, Fernández-Cañón et al. used northern blot hybridisation using a human cDNA clone as a probe for *HGD*, and confirmed that *HGD* mRNA was present in the liver and kidney, and also reporting expression in small intestine, colon and prostate tissue [90]. No *HGD* expression was found within the spleen, thymus, testis, ovary, peripheral blood lymphocytes, heart, brain, placenta, skeletal muscle, lung and pancreas [90]. More recently, reports also suggest that HGD is expressed in brain tissue from both mice and humans using western blotting [99]. In addition, further reports suggest that HGD is expressed within osteoarticular cells including chondrocytes, synoviocytes and osteoblasts, analysed via qPCR and western blotting [100]. These reports have not been verified by *in situ* hybridisation or HGD-labelling.

1.2.6 Therapy for alkaptonuria

Despite AKU being an iconic Mendelian disease first described over a century ago by Sir Archibald Garrod, no effective therapy for AKU has emerged until very recently in the past decade. A pharmacological therapy has now emerged and has been the subject of a series of mouse and human clinical trials, and will be discussed below.

1.2.6.1 Past and current therapy options

Until very recently, only palliative treatment such as analgesics and arthroplasty [28] were available for AKU, with low-protein diets, ascorbic acid and physiotherapy proven clinically ineffective [20,101,102]. None of these treatment options tackle the intrinsic cause of the disease.

Ascorbic acid (vitamin C) has been tried as a therapy for AKU, as the formation of ochronotic pigment is thought to involve the oxidation of HGA to benzoquinone acetic acid (BQA), see Figure 1.1. Reports showed that vitamin C was able to reduce urinary BQA excretion, but with no effect on HGA excretion [101]. Another report found no association between vitamin C and urinary excretion of HGA [20]. There have been no credible studies suggesting that vitamin C is clinically effective. Protein restriction, to remove excess tyrosine and phenylalanine from the diet, decreasing the flux down the metabolic pathway via HGA, would be difficult to comply with long-term and would also require specialist supervision from a dietician to ensure adequate growth and nutrition. There has been no systematic study investigating the effectiveness of protein restriction in AKU. One study investigated protein restriction in 16 patients (from medical records) aged 3-27 years, with poor dietary compliance observed, which got progressively worse with age [102]. Protein restriction in 12 of these patients resulted in reduced urinary HGA in children <12 years, with much less effect in adolescents and adults, suggesting that protein restriction was beneficial for AKU children and not adults, with the regime being questionable and impractical [102]. Phornphutkul et al. also reported no association between protein restriction and urinary HGA excretion in AKU patients [20].

Data is lacking with regards to lifestyle counselling in AKU; lifestyle factors such as hobbies, activities and occupation that affect joint loading are likely to be important but have not yet been addressed [28]. Ranganath et al. report that pain control, which is only a palliative treatment, is tackled by a variety of drugs as well as physical modalities such as acupuncture and nerve blocks, but state that pain for many patients is constant and disabling, and is therefore not completely effective [28]. Palliative surgery is used to treat at the end stage of the disease with regards to the musculoskeletal system, proving to be effective but invasive, expensive and not universally available [28]. Finally, organ replacement of the liver due to cirrhosis [103] or the kidney due to diabetic renal failure [104] has been shown to fully or partially improve the metabolic symptoms of AKU in two case studies. Organ transplantation however is perhaps unjustified in a disease with a relatively normal lifespan and is therefore not used to treat AKU. Gene or enzyme replacement therapy has not yet been investigated in AKU.

Most likely due to lack of effective treatment options, many AKU patients reach adulthood before the disease is diagnosed, either as it was missed or ignored at an earlier age. Most descriptions of the disease until recently were qualitative, with no methodology existing to measure disease severity [28]. To address this issue within the AKU field, a disease severity scoring system has been developed, allowing disease progression to be tracked and patients to be compared with one another. This scoring system is termed the 'AKU Severity Score Index' (AKUSSI), and is based on a quantitative and validated multidisciplinary assessment system [105,106].

Recently, a very promising disease modifying treatment for AKU has emerged, using a drug called nitisinone that can block the enzyme responsible for the conversion of 4-HPPA into HGA. This is discussed in detail below in section 1.2.6.2.

1.2.6.2 Nitisinone

Recently there have been trials of 2-(2-nitro-4-trifluoromethylbenzoyl)-1,3-cyclohexanedione (NTBC), more commonly referred to as nitisinone, in the treatment of AKU [52]. Nitisinone is a triketone herbicide that inhibits the 4-hydroxyphenylpyruvic acid dioxygenase (HPPD; E.C 1.13.11.27) enzyme that converts HPPA into HGA (Figure 1.1). It was not through drug screening that nitisinone was shown to inhibit HPPA, but through herbicide testing, as tyrosine metabolism is important for quinone synthesis in plants required for photosynthesis [107]. In the early 1990's, nitisinone was shown to be a potent, reversible inhibitor of rat and human liver HPPD [107–109]. Hereditary tyrosinaemia type I (HT-1; OMIM #276700), is a fatal inborn error of metabolism where fumarylacetoacetate hydroxylase (FAH; E.C. 3.7.1.2) deficiency results in liver failure, hepatocellular carcinoma and renal tubular dysfunction due to accumulation of FAA [110]. With the realisation that tyrosine metabolism could be blocked, nitisinone soon became the first effective treatment for HT-1, and has been licensed for the treatment of HT-1 since 2002 [108,111,112].

In 1998, Anikster et al. suggested that oral administration of nitisinone in combination with some dietary restriction of tyrosine and phenylalanine could be a potential therapy for AKU, as it would prevent the production of HGA [113]. They suggested the addition of dietary restriction as there had been one documented case of a nitisinone-treated HT-1 child presenting with corneal crystals, which was resolved with a tyrosine-restricted diet. A mouse study the following year reported the use of nitisinone in an AKU mouse model, where a

single oral dose of 100 µg of nitisinone resulted in reduced urinary HGA excretion to <2% of the pre-treatment level [45]. They also demonstrated a dose-responsive reduction in HGA in these mice, with nitisinone doses ranging from 1.25-100 µg. They also reported no side effects in the liver and kidney after histological assessment. In 2002, the first reported AKU patients were treated with nitisinone (0.35-1.4 mg/day, taken orally twice a day) for either 9 or 10 days, at doses less than half of that given to HT-1 children which is approximately 1 mg/kg/day [20]. They were able to show that nitisinone reduced HGA by 69% or more, providing proof-of-principle that HGA production could be reduced [20]. Low-dose nitisinone was then trialled in 9 AKU patients, starting with 0.35 mg/day (approximately 0.01 mg/kg/day), taken orally twice a day for 8 days, which was then increased to 1.05 mg/day (approximately 0.03 mg/kg/day), taken orally twice a day for 3 months [114]. Urinary HGA was effectively reduced from an average of 4 g/day to 0.2 g/day, with 1.05 mg/day nitisinone reducing urinary HGA by 94%.

Following these reports of short term use of nitisinone in AKU patients, a 3 year randomized, clinical trial of nitisinone was carried in 40 AKU patients (20 nitisinone treated; 20 control) over 36 months at the National Institutes of Health (NIH), designed to confirm the biochemical efficacy, investigate clinical outcome and to further evaluate safety of nitisinone [40]. Biochemically, this study showed a consistent 95% reduction of HGA in the urine and plasma over the course of 3 years with an oral dose of 2 mg nitisinone daily. The primary outcome of this study however was not met; no improvement was seen in the total range of motion in the hip joint. Although not statistically different, hip rotation was decreased by 0.31°/year more in the control group than the nitisinone group. In addition, no differences were observed in secondary outcome parameters that assessed the musculoskeletal system and included spinal flexion, functional reach and 6-minute walk tests. The authors suggested that due to the age of the patients in this trial (38-68 years), substantial hip degeneration was already present that could not be halted by the reduction in HGA as the damage and subsequent degeneration of the joint has already begun. They did however suggest that nitisinone needs to be trialled early in life, before the onset of joint changes.

Although the NIH trial demonstrated that nitisinone could reduce HGA, it was deemed inconclusive and ineffective due to the lack of clinical joint improvement. Following this work, nitisinone was trialled in an AKU mouse model, where it was shown to reduce HGA and completely prevent knee joint ochronosis when given from birth [115,116], see section 1.3.2.4 for more details. Furthermore, they also showed that ochronosis progression was halted, but

not reversed, when nitisinone was given mid-life to AKU mice, and that there was a clear dose-response between plasma HGA and the dose of nitisinone [116]. This work led to the off-label use of nitisinone at the National Alkaptonuria Centre (NAC, Liverpool, UK; http://www.akusociety.org/aku-national-aku-centre.html)[53,117] and to a series of human clinical trials (DevelopAKure; http://www.developakure.eu/) investigating the use of nitisinone in AKU [52,118], where its use has proven safe and effective.

The SONIA-1 (Suitability Of Nitisinone In Alkaptonuria 1) trial was a 4 week dose-response trial encompassing 5 groups of 8 patients at different nitisinone doses of 0 mg, 1 mg, 2 mg, 4 mg and 8 mg daily [52]. As with the mouse study, a clear dose-response relationship was observed between nitisinone and urinary HGA excretion. An 8 mg daily dose of nitisinone reduced urinary HGA by 98.8% and reduced serum HGA to <3.1 µmol/L in human AKU patients, concluding that nitisinone effectively reduced HGA to a level that is likely to prevent ochronosis, with no serious adverse events reported [52]. A longer-term 4-year trial then followed called SONIA-2, with a group on 10 mg daily nitisinone (n=69) and a group with no treatment (n=69) for 4 years, which finished in early 2019. The trial aimed to show whether or not nitisinone could not only reduce HGA, but also slow down the progression of AKU, and to ensure that it is safe to use. Some preliminary 1-year results have been included on the DevelopAKUre website for SONIA-2 and state that after 1-year, urinary HGA levels had been decreased on average by 99.5% and serum HGA by 97.5% (http://www.developakure.eu/Results [accessed 08/10/2019]). The results of the trial have not yet been published, however the trial is deemed to have been successful as SOBI (Swedish Orphan Biovitrum) have announced that they are applying to the European Medicines Agency (EMA) to obtain market authorisation approval for nitisinone to be used to treat AKU.

Also included in the DevelopAKUre series of clinical trial is the SOFIA (Subclinical Ochronotic Features In Alkaptonuria) trial. The SOFIA trial studied 30 AKU patients of different ages to identify the earliest age at which ochronosis can be detected in patients, and to identify an appropriate age at which nitisinone treatment could begin [119]. Ear cartilage biopsies revealed that ochronosis, which increases with age, was found in a 20-year-old AKU patient microscopically, therefore ochronosis can begin before this age. Macroscopically, eye ochronosis was first detected at 22 years from photos, with ear ochronosis not being identified until 34 years in photos. Although MRI showed lack of spine and joints changes before 30 years, gait however was found to be abnormal early on in the younger AKU

patients. Overall, it was concluded that ochronosis starts at an early age before adulthood, with the SOFIA trial unable to assess the earliest age, highlighting that a paediatric study is required to establish when ochronosis first initiates [119].

Alongside the DevelopAKUre clinical trials, nitisinone has been used off-licence at the National Alkaptonuria Centre (Liverpool, UK; opened in June 2012), where patients aged 16 years or more receive free specialist care, assessment and off-licence prescription of nitisinone in a hospital setting. At the NAC, patients began taking 2 mg nitisinone on alternate days for 3 months, followed by daily 2 mg dosing thereafter [53]. Patients are initially assessed at baseline, day 4, 3 months, 6 months and 1 year after commencing nitisinone, and then after 1 year, they are assessed annually. Urinary HGA was shown to decrease by 95.4% by 6 months, 94.8% after 1 year and 94.1% after 2 years, accompanied by an 83.2% reduction in serum HGA, in 28 patients that attended the NAC for 2 years [53].

An evaluation of 39 AKU patients attending the NAC for 3 years has recently been published, using the AKU Severity Score Index (AKUSSI) to assess the severity of AKU and compare the rate of progression of the disease between the pre-nitisinone and nitisinone treatment phases [117]. Biochemically over the 3 years of nitisinone treatment, urinary HGA was decreased by 80.2-93.9% and serum HGA by 80.2-89.3% at all follow up visits. Due to some patients attending the NAC twice before commencing nitisinone treatment, it was possible to assess disease progression over approximately 3 years, without nitisinone treatment (pre-nitisinone), where a consistent increase in all categories of the AKUSSI score was observed. Disease progression was then assessed over the 3-year duration of nitisinone treatment, with the rate of progression calculated for 1-year, 2 years and 3 years of nitisinone treatment. The sum of clinical, joint and spine AKUSSI features shows that the rate of change of score/patient/month was significantly lower for the 3 years post-nitisinone treatment phase compared to pre-nitisinone phase (in addition to the 1-year and 2 years treatment phases). The data suggests that nitisinone can slow down disease progression in AKU. Furthermore, the ear and eye pigment changes were stabilised with nitisinone treatment, suggesting that nitisinone, by lowering HGA, can reduce ochronotic pigment formation [117].

Nitisinone appears to be very effective at reducing both the urinary excretion and circulating levels of HGA in AKU patients. Although no serious adverse events have been associated with the use of nitisinone in AKU patients in the above reports, plasma tyrosine, which is within the normal physiological range in untreated AKU patients [118], has been shown to significantly elevate in all nitisinone-treated AKU patients. For example, plasma tyrosine increased from

an average of 68 µmol/L pre-nitisinone to 760 µmol/L post-nitisinone with a regular diet in 9 AKU patients [114]. In the SONIA-1 trial, nitisinone treatment for 4 weeks at 1 mg increased serum tyrosine from an average of 68 µmol/L to 653 µmol/L, and at 8 mg increased serum tyrosine from an average of 55 µmol/L to 813 µmol/L [52]. At the NAC after 2 years of 2 mg nitisinone treatment, serum tyrosine increased from an average of 42 µmol/L to 594 µmol/L [53]. In addition to increased circulating levels, tyrosine is also increased in the urine, for example from 103 µmol/24h to 1071 µmol/24h after 2 years of daily 2 mg nitisinone [53]. The elevated tyrosine caused by nitisinone, often referred to as nitisinone-induced tyrosinaemia or just tyrosinaemia, is discussed below in the next section.

1.2.6.3 Nitisinone-induced tyrosinaemia

Tyrosinaemia (elevated tyrosine) can cause eye keratopathy and sometimes an eczema-like skin rash to occur. In relation to the eye, tyrosinaemia results in corneal lesions (also referred to as corneal keratopathy), that results in symptoms such as itching, burning, photophobia, corneal erosion and corneal clouding [112]. Patients may complain of pain and/or blurred vision.

1.2.6.3.1 Nitisinone-induced tyrosinaemia in animals

The effect of nitisinone induced-tyrosinaemia has been researched in experimental animals in some depth. In all of these experimental animals (mouse, rat, rabbit, beagle dog and rhesus monkey), nitisinone has been shown to produce a marked and sustained tyrosinaemia in the plasma, which was reversible upon withdrawal of nitisinone [120–122]. In the rat, daily nitisinone administration was shown to increase plasma tyrosine about 10-fold and to cause corneal lesions, described as corneal opacities, with an occurrence of about 75% at 6 weeks of treatment with 30 µmol/kg/day, with corneal lesions still observed at a lower doses of 0.3 µmol/kg/day [120]. No differences were observed in plasma tyrosine between rats that developed lesions and those who didn't. Maximum tyrosine levels in these rats were about 2500 µmol/L in the plasma and about 3500-4000 µmol/L in the aqueous humour of the eye (which is 7-fold greater than plasma levels in untreated rats).

Interestingly in the mouse, despite marked tyrosinaemia, no corneal lesions or opacities were observed with nitisinone for 6 weeks at the same dose given to rats [121]. Daily dosing up to 160 mg/kg/day nitisinone produced a maximal tyrosinaemia level of 600-700 µmol/L in the plasma, which was about 50% lower than a single 10 mg/kg/day dose that resulted in 1200 µmol/L tyrosine in the plasma and 2200 µmol/L tyrosine in the aqueous humour of the eye.

The authors suggest that the difference between the mouse and rat may be that the mouse is able to clear or metabolise tyrosine more efficiently than the rat. This however could not be through HPPD if it is blocked by nitisinone; perhaps tyrosine is excreted more efficiently by the kidney or perhaps metabolised via a different pathway.

After the rat and mouse studies, further nitisinone experiments were carried out in the rabbit, beagle dog and rhesus monkey [122]. As with the rodents, these animals all experienced tyrosinaemia that was sustained. A 34% occurrence of corneal lesions were observed with daily nitisinone dosing between 0.1-5 mg/kg/day in the dogs for 18 weeks, which is a lower occurrence than the rat. The lesions were present in either one eye or both eyes, and were often transient, with lesions shown to be reversible with withdrawal of nitisinone. Interestingly in the dog, tyrosine in the plasma was elevated to about 1800 µmol/L and to about 1400 µmol/L in the ocular fluid, which is lower than the plasma. In contrast to the dog, no corneal lesions were observed in the rabbit with plasma tyrosine about 1500 µmol/L or rhesus monkey with plasma tyrosine about 1700 µmol/L with daily dosing of 10 mg/kg/day nitisinone for 6 or 12 weeks, respectively. In the rabbit tyrosine was increased to 1500 µmol/L in the plasma and in the ocular fluid to 1250 µmol/L (in controls it was about 90 µmol/L).

These animal studies highlight that the presence of corneal lesions due to nitisinone-induced tyrosinaemia, is not simply related to the concentration of tyrosine with the ocular fluid or blood tyrosine levels, see Figure 1.6 for a comparison between the plasma and ocular tyrosine levels in the experimental animals described, excluding the rhesus monkey. Firstly, not all of these animals developed corneal lesions despite tyrosinaemia being present in them all. The mouse for example had greater ocular tyrosine levels than that of the dog but did not develop corneal lesions. Secondly, of those species that did exhibit corneal lesions, the lesions were not present in all the animals, nor were they even present in both eyes, for unknown reasons. In addition, of the two species that did develop lesions, the rat had greater tyrosine levels in the eye than in the plasma, whereas the dog had lower levels of ocular tyrosine than the plasma. This data suggests that there must be other unknown factors involved in the presentation of corneal lesions.

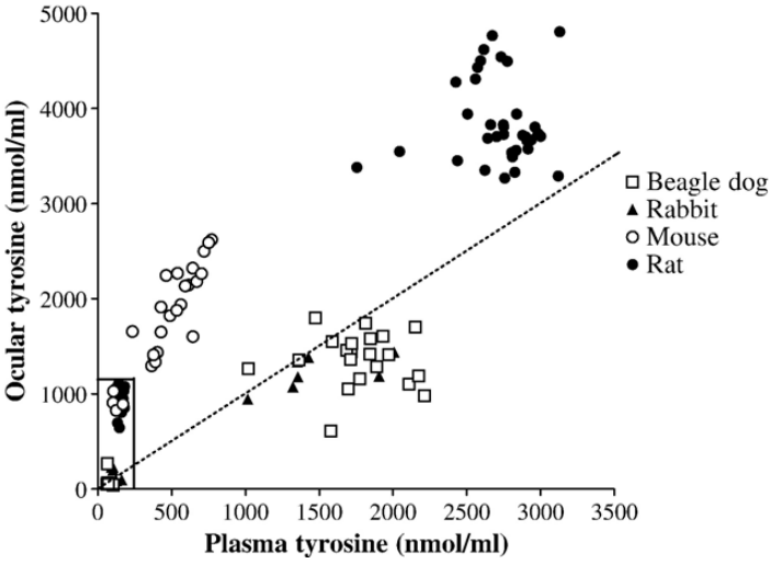

Figure 1.6. Relationship between plasma tyrosine and ocular tyrosine associated with nitisinone treatment in experimental animals.
The box in the bottom left hand corner of the graph represents untreated control animals. The beagle dog and rat experience corneal lesions associated with elevated tyrosine, whereas the rabbit and mouse do not experience corneal lesions. Graph from [122], that includes data from [120,121].

1.2.6.3.2 Nitisinone-induced tyrosinaemia in patients

Tyrosinaemia is known to cause keratopathy in nitisinone-treated HT-1 patients [40,53,123] which resembles the dermal and ocular symptoms seen in hereditary tyrosinaemia type II (HT-2; OMIM #276600), refer to Figure 1.1 [124–126]. Ocular and skin keratopathy linked to nitisinone-induced tyrosinaemia has also been reported in AKU patients whose symptoms all resolved upon lowering the dose of nitisinone, stricter protein restriction or upon the cessation of treatment [40,127–130]. Most AKU patients treated with nitisinone, including those with doses up to 8 mg daily in the SONIA-1 trial [52] and up to 10 mg daily in the SONIA-2 trial, tolerate nitisinone very well, including patients with plasma tyrosine levels >1000 µmol/L [40,129]. The same finding is also reported in HT-1 patients, that some patients with extremely high tyrosine >1000 µmol/L do not present with keratopathy [112,131]. The reason why some patients experience keratopathy whilst others do not despite having similar tyrosine concentrations remains to be elucidated.

The recommended dose of 1 mg/kg/day nitisinone for HT-1 patients [132] is much higher than the doses used in AKU patients, therefore it's reasonable to expect that more cases of keratopathy would be observed in HT-1. Low-dose nitisinone of 0.5 mg daily in an AKU patient however has been shown to induce ocular irritation and photophobia that presented before the presence of corneal crystal deposition [129]. More worryingly, a recent study has

reported the presence of mild corneal keratopathy in an AKU patient on 2 mg nitisinone daily that had not reported any ocular symptoms or pain [130]. This is an added cause for concern as untreated keratopathy could be sight-threatening and may not be detected if patients are not having regular ophthalmological assessments.

In addition to eye and skin keratopathy, it's important to consider the potential effect of nitisinone-induced tyrosinaemia on neural cognition as tyrosine is a precursor to neurotransmitters such as dopamine, adrenaline and noradrenaline. Metabolites of these neurotransmitters have previously been shown to significantly alter with nitisinone treatment in AKU patients (no psychometric data reported)[133], although a more recent study concluded that alterations in neurotransmitter metabolism due to nitisinone did not cause depression in adult AKU patients [134]. Long before these neurotransmitter changes in adult AKU patients were reported, the potential negative impact of nitisinone on the neurodevelopment of children however had arisen from the treatment of HT-1. Since the introduction of nitisinone as a treatment for children with HT-1 in 1992 [108], numerous reports and studies have documented impaired cognitive function (lower IQ, learning difficulties, impaired executive functioning, impaired social cognition and decreased motor function and speech) associated with nitisinone treatment and the subsequent elevated tyrosine, even with protein restricted diets [123,135–139]. These neurodevelopmental effects in HT-1 however could be due to either nitisinone-induced tyrosinaemia or severe liver failure experienced before diagnosis/treatment. With the cause of impaired cognition in HT-1 remaining to be elucidated, the off-licence use of nitisinone has been restricted to ≥16 years of age in AKU, therefore no data is available in AKU children.

Neurological symptoms have also been reported in HT-2 and hereditary tyrosinaemia type III (HT-3; OMIM #276710) patients where tyrosine is increased [140]. HT-2, caused by a deficiency of the tyrosine aminotransferase (TAT; EC 2.6.1.5) enzyme (see Figure 1.1)[141] is characterised by eye and skin lesions that typically develop during the first year of life [126] and has also been associated with neurological symptoms however these do not present consistently across all patients. HT-3, the rarest form of tyrosinaemia, is caused by HPPD deficiency causing neurological impairment and ataxia, with no signs of liver damage, eye or skin symptoms [142]. Neurological symptoms can include developmental delay, attention deficit and behavioural problems, neurological motor issues, and learning difficulties [143]. About 75% of cases report long term intellectual impairment in HT-3 patients [143]. These neurological symptoms have the potential to be replicated in nitisinone-treated AKU children due to the HPPD inhibition, similar to the metabolic block seen in HT-3 patients. A study comparing HT-1 mice with

wildtype mice treated with nitisinone however concludes that the slower learning and cognitive differences are caused by HT-1 itself and not nitisinone treatment [144].

Protein/tyrosine restriction is implemented in conjunction with nitisinone treatment in HT-1 patients, with <400 µM considered a target for plasma tyrosine levels [132,145]. A lack of compliance to a protein restricted diet however is commonly associated with the development of nitisinone-induced tyrosinaemia and the resulting corneal keratopathy events mentioned above, in both AKU and HT-1 patients. The ineffectiveness of protein restriction alone in treating AKU was attributed to a lack of dietary compliance as HGA differences were seen in younger children with restricted diets in comparison to older children who have more input into their diet [102]. Phornphutkul et al. suggested that a protein restricted diet should be considered as a way of preventing tyrosinaemia, but recognised that compliance would be extremely difficult in adult patients [20]. Sustaining a protein restricted diet can be difficult, expensive, has the possibility of health complications and may alter quality of life. Poor adherence to protein supplements coupled with an inadequate low protein diet can lead to essential amino acid and micronutrient deficiency [146,147]. Developing strategies other than a low-protein diet that can reduce elevated tyrosine, minimising the risk of eye, skin and neurological complications, would allow nitisinone-treated patients to eat a normal-protein diet. Although advised, no clinical study has investigated the effectiveness of dietary restriction at reducing nitisinone-induced tyrosinaemia in AKU.

Until gene/enzyme replacement therapy becomes an option for AKU, treatment with nitisinone to reduce elevated HGA that eventually causes severe joint disease, will be the choice for most, if not all AKU patients. As well as preventing eye and skin keratopathy, finding a strategy to lower tyrosine levels to avoid the possible neurological issues associated with tyrosinaemia will be a vital step that may allow the prescription of nitisinone to AKU children.

One possible strategy that could be applied to nitisinone-treated AKU patients is lowering the consumption of protein in the diet to decrease tyrosine and phenylalanine intake in order to reduce circulating tyrosine. As already mentioned above however, a low tyrosine/phenylalanine diet would most likely be ineffective in AKU patients due to compliance difficulties in adults [20,102], and would require expert dietetic intervention in adults and particularly in children in order to balance the nutritional requirements of growth and development with the possibly damaging effects of tyrosinaemia. An intervention that allows a normal protein diet to be consumed but prevents tyrosine/phenylalanine intake would be

much more desirable for both adults and children. Here in chapter 5, the effectiveness of decreasing dietary tyrosine/phenylalanine is investigated in mice by removing tyrosine and phenylalanine from the diet. If restriction of dietary tyrosine is effective, strategies that prevent the absorption of tyrosine from the intestine into the bloodstream could allow a normal protein diet to be consumed with nitisinone treatment. Potential strategies could involve the consumption of a therapeutic product that binds dietary tyrosine preventing its absorption into the circulation or a tyrosine-degrading enzyme (such as TAL discussed in the next section) that could break tyrosine down within the intestinal lumen. Although phenylalanine levels are not a concern with nitisinone treatment, phenylalanine restriction is also investigated in mice here to evaluate its effectiveness at reducing tyrosinaemia, as extensive research into a phenylalanine-reducing therapeutic enzyme called PAL exists for the treatment of phenylketonuria (PKU; OMIM #262600). If phenylalanine restriction is effective at reducing tyrosine, this PAL enzyme could potentially be applied to nitisinone-induce tyrosinaemia in AKU. This PAL enzyme, along with its tyrosine analogue TAL, are introduced and discussed in the next section.

1.2.6.4 Exogenous enzyme therapy: PAL/TAL

A potential solution to nitisinone-induced tyrosinaemia in AKU, and also HT-1, is to prevent tyrosine from accumulating by removing or breaking down tyrosine within the body, by using an exogenous tyrosine-degrading enzyme. This concept of using an exogenous enzyme to breakdown a metabolite that is increased above normal physiological levels, in this case using an enzyme called tyrosine ammonia lyase (TAL; EC 4.3.1.23) to break down tyrosine, has arisen from research investigating the breakdown of phenylalanine in the metabolic disease PKU. A bacterial enzyme called phenylalanine ammonia lyase (PAL; EC 4.3.1.24) has been developed into a therapeutic that decreases phenylalanine in the blood, which is abnormally high in PKU. The PAL and TAL enzymes are both members of the aromatic amino acid ammonia lyase family, and are discussed below.

1.2.6.4.1 Aromatic amino acid ammonia lyases

Tyrosine ammonia lyase (TAL) catalyses the deamination of tyrosine to p-coumaric acid and phenylalanine ammonia lyase (PAL) catalyses the deamination of phenylalanine to trans-cinnamic acid. TAL and PAL are part of a small group of enzymes called the aromatic amino acid ammonia-lyase family, which also includes histidine ammonia lyase (HAL; EC 4.3.1.3),

which all deaminate aromatic amino acids, with other classes of ammonia-lyases also existing [148]. A characteristic feature of the PAL/TAL/HAL enzyme family is the presence of a highly electrophilic co-factor named 4-methlidene-imidazole-5-one (MIO), produced by the post-translational condensation of a Ala-Ser-Gly amino acid group within the enzyme [149]. TAL is quite rare in nature when compared to PALs. PALs from bacteria and plants are responsible for the production of cinnamic acid which is further metabolised to molecules such as coumarins and flavonoids in plants through the phenylpropanoid pathway (phenylpropanoids are a diverse group of compounds derived from the carbon skeleton of phenylalanine), and antibiotic compounds in bacteria [150]. In plants, phenylalanine and cinnamic acid are important precursors for the production of lignin and other secondary plant metabolites, and it was in 1961 that PAL was first isolated [151]. PAL has since been researched quite extensively for its use in both commercial and therapeutic settings, as a biocatalyst for chemical production and its use as an enzyme substitution therapy (EST) in PKU.

TALs may be less common due to the specialised role of p-coumaric acid as a co-factor for photoactive yellow protein in *Rhodobacter* bacteria [152] and the role that coumaric acid plays as a precursor to caffeic acid in the synthesis of saccharomicin antibiotics [153]. A TAL enzyme was first discovered in 2001 by Kyndt et al. [154] in the bacterium *Rhodobacter capsulatus*. Understanding the journey of PAL to be used as an EST for PKU is important when considering the use of TAL for tyrosine breakdown in nitisinone-treated AKU patients, and possibly even HT-1 patients, due the synonymous nature of phenylalanine breakdown by PAL that will have worked through challenges and issues likely to be experienced during the application and development of a therapeutic TAL enzyme.

1.2.6.4.2 PKU

PKU is an autosomal recessive, inborn error of metabolism, caused by deficiency of phenylalanine hydroxylase (PAH; EC 1.14.16.1) that is responsible for the breakdown of phenylalanine to tyrosine [155]. PKU is characterised by increased blood phenylalanine levels, with classical PKU classed as phenylalanine >1200 µmol/L, and is associated with cognitive dysfunction, memory impairment and behavioural and psychiatric problems [156,157]. PKU is mainly treated with strict dietary restriction of phenylalanine, starting as early in life as possible to minimise neurocognitive abnormalities developing and continued throughout life, usually by consuming a low protein diet with phenylalanine-free amino acid supplements. As described for HT-1 and AKU, compliance with a low protein diet is a problem

in PKU patients, with phenylalanine levels often rising beyond optimal target ranges [158]. Other treatment options have therefore been investigated for PKU. PAH activity requires the BH_4 (tetrahydrobiopterin) co-factor; an orally active, synthetic form of BH_4 has been trialled in PKU patients that respond to a BH_4 loading test, which is estimated to be a potential treatment option for 30-50% of PKU patients, although these patients tend to have a more mild form of PKU [159]. For BH_4 non-responders, which is proposed to be due to lack of residual PAH activity caused by different PAH mutations, enzyme replacement therapy is a potential treatment option [155]. Enzyme replacement therapy with PAH, which is mainly found in the liver, has been challenging and so far, not successful. PAH requires its co-factor BH_4, oxygen and Fe^{2+} in order to convert phenylalanine to tyrosine. EST with the phenylalanine-degrading, prokaryotic enzyme PAL has proved to be a more promising therapy for PKU, as PAL can be produced using a bacterial expression system on a large scale, does not require a co-factor and its phenylalanine-degradation product is not toxic.

1.2.6.4.3 Development of PAL as a therapy for PKU

The first attempt to treat PKU with PAL occurred in 1980; PAL extracted from yeast was loaded into a semi-permeable gel capsule and administered orally to healthy volunteers after a protein meal, and to an untreated PKU patient where it reduced blood phenylalanine by a quarter in the patient [160]. If oral PAL administration was to succeed, the need to protect PAL from proteolytic degradation by digestive enzymes was recognised [161,162], in addition to the pH of the intestine typically being 6.0-7.4, with PAL having an optimal pH of 8-9 [163]. It was demonstrated in humans that cinnamic acid, the product of phenylalanine deamination, was eliminated as hippuric acid in the urine with benzoic acid as an intermediate compound, and that cinnamic acid had very low toxicity and no embryo-toxicity in laboratory animals [164,165]. It was concluded that the conversion of phenylalanine by PAL to cinnamic acid (and ammonia) was harmless and paved the way for more research into PAL as an EST for PKU.

Work in the 1970's then investigated non-oral PAL administration in order to directly reduce circulating phenylalanine in PKU. The first challenge was the highly immunogenic nature of non-mammalian PAL protein; the biological half-life of *Rhodotorula glutinis* (yeast) PAL was approximately 21 hours in several mammalian species such as the mouse, rat and monkey after a single injection, with repeated administration shortening the biological half-life, likely due to clearance/inactivation by the immune system [166]. A new administration method was subsequently tested; PAL was immobilised into a multi-tubular enzyme reactor within a

porous shell, and used as an extra-corporeal device in which blood could be shunted through [167]. This resulted in an 82% reduction in circulating phenylalanine in dogs with experimental hyper-phenylalaninaemia (HPA). Hollow-fibre enzyme reactors with immobilised PAL were then designed and tested *in vitro* [168,169], followed by *in vivo* studies in dogs and monkeys with experimental HPA [170]. After 2 hours, an 84% phenylalanine reduction was observed, with no increase in blood urea nitrogen from ammonia generation, no cinnamic acid toxicity and no immune response with repeated application of PAL-reactors *in vivo*. It was suggested that immobilised PAL enzymes in extracorporeal shunts could be used temporarily in PKU patients struggling to control excess phenylalanine, in situations such as fever, infection or pregnancy [170]. The PAL enzyme reactor was subsequently applied to a PKU patient, with three rounds over 5.5 hours reducing phenylalanine by 30% from 1820 µM to 1270 µM, but was considered too invasive for patient use [167].

Oral PAL administration was re-visited, with an attempt to protect PAL from proteolysis by immobilising PAL into "artificial cells" with a semi-permeable micro-encapsulation technique [171], however activity was only 20% of the free PAL enzyme [172]. The goal was to use this encapsulated PAL to reduce phenylalanine in the gastrointestinal tract, therefore its activity was tested at a range of pH levels *in vitro* to assess the feasibility of oral dosing, through which varying pH levels would be encountered [173]. The optimum pH for both free and encapsulated PAL was 8.5, with encapsulated PAL being more active at lower pH levels than free PAL. Daily oral dosing of 5U encapsulated PAL in rats with experimental HPA reduced blood phenylalanine by 65% at day 2, and was not significantly different to normal rats by 7 days of dosing [173]. Similar artificial cell experiments then found comparable results, with 5U PAL reducing phenylalanine to normal levels with a 75% reduction in 6 days [174], in addition to a reduction in intestinal phenylalanine [175]. This PKU model however reported fluctuations in phenylalanine levels in control and treated rats [174]. When tested in a true genetic PKU mouse model ($Pah^{ENU2/ENU2}$)[176] with naturally high rather than artificially elevated phenylalanine levels, no significant decrease in phenylalanine was observed [177].

At this point, PAL was not available in sufficient quantities and at reasonable cost. Sarkissian et al. therefore used a "recombinant" PAL gene from *Rhodosporidium toruloides* (red yeast; RtPAL) [178] and used an *E. coli* [179] expression system to obtain large amounts of RtPAL enzyme, and tested it in PKU mice [180]. Intra-peritoneal (IP) injections of RtPAL (2, 20 and 200U) showed reductions in phenylalanine and a dose response, but with high variability. They then showed that PAL activity was abolished by proteolytic digestive enzymes but could be protected by retaining PAL within the expression *E. coli*, which could *in vitro* reduce phenylalanine by 76%

in vitro. With the addition of chymotrypsin and intestinal fluid to PAL retained in *E. coli in vitro*, phenylalanine was still reduced by 72% and 66%, respectively. Proof of pharmacological principle was then shown, with a single IP PAL injection in PKU mice significantly reducing plasma phenylalanine, persisting for 24 hours. Proof of physiological principle was then demonstrated by oral gavage of 25U PAL retained in *E. coli*, combined with inactivation of gastric acidity by sodium bicarbonate, which lowered plasma phenylalanine by 31% in 1 hour and 44% in 2 hours. To achieve similar phenylalanine reductions with unprotected PAL, 8-fold more PAL (200U) was required, combined with aprotinin which is a protease inhibitor, highlighting the importance of protease protection [180].

The aim then shifted to developing an injectable EST for PKU. In order to protect PAL from immune recognition and to increase its circulating half-life, chemical modification of PAL was investigated, attaching polyethene glycol (PEG) molecules to the PAL protein, in addition to creating and testing mutant PALs [181–185]. PEGylation of RtPAL (*R. glutinis* PAL PEGylation was not successful) improved its effectiveness *in vitro*, with no antibody binding at greater PAL:PEG ratios when exposed to mouse antiserum [181]. *In* vivo, unmodified PAL had reduced effectiveness with repeat subcutaneous injection into PKU mice ($Pah^{ENU2/ENU2}$), whereas highly PEGylated PAL showed prolonged phenylalanine reduction, with low antibody production in PAL:PEG 1:16 at 42 days, indicating suppression of the immune response [181]. PEG-PAL conjugates were generated with different formulations and the most promising screened for immuno-reactivity against PAL-antibodies, with *in vitro* data demonstrating that PEGylation abolishes immunogenicity [182]. The best formulations were then tested in the PKU mouse, including PEG-PAL conjugates with varying degrees of linear 5- and 20-kDa PEGylation. The 20 kDa linear PEG:PAL 1:16 formulation was the most effective at reducing phenylalanine, with all PEG-PAL conjugates being as active as the unmodified enzyme, with minimal loss of catalytic efficiency with repeated injections [182].

Screening of wildtype and mutant PAL proteins from different organisms (*Anabaena variabilis* (Av), *Nostic punctiforme*, *Petroselinum crispum* and *Rhodosporidium toruloides* (Rt)) in the PKU mouse model found that subcutaneously delivered PEGylated forms of AvPAL displayed a higher efficiency and slower clearance rate than PEGylated RtPAL, and was superior over other species for other characteristics such as greater thermal stability [184]. Subcutaneous injection of mutant AvPAL effectively lowered blood and brain phenylalanine in PKU mice over a 90 day trial period, coupled with reduced PKU manifestations and enhanced animal health [184]. Phenylalanine reduction was both dose- and load-dependent, with a higher dose and lower frequency of twice weekly dosing found to be more effective

than lower, daily dosing. This mutant (C503S and C565S mutations to reduce protein aggregation) and PEGylated AvPAL (mutant AvPAL) was then shown to have an optimal pH at 7.5-8.5, with both mutant AvPAL and RtPAL shown to retain activity after a 10 minute exposure to a broad pH range [185]. This highlights the possibility that if protected from proteases, these PAL enzymes could survive the low pH of the stomach and be active in the intestine, which in a fasting state is approximately pH 1.8 and rises to 5.4-6.2 immediately after a meal [186]. They also identified protease sites for trypsin and chymotrypsin that could be engineered in the future for oral administration, although this was not pursued, for both mutant AvPAL and RtPAL, with neither showing susceptibility to bloodstream proteases thrombin and factor X, beneficial for intravenous administration [185].

After this series of experiments just described, the mutant PEGylated AvPAL was chosen to enter human clinical trials [184]. BioMarin Pharmaceutical (a biotechnology company interested in enzyme replacement therapies) subsequently applied to the Food and Drug Administration (FDA) for approval to begin human trials with PAL in PKU. A phase I, multicentre clinical trial evaluated the safety, tolerability and efficacy of rAvPAL-PEG (recombinant *A. variabilis* PAL conjugated with PEG) in PKU patients [187]. Single subcutaneous injections of rAvPAL-PEG were administered in escalating doses from 0.001-0.1 mg/kg to 25 PKU adults that had blood phenylalanine >600 µmol/L, and followed up for 6 weeks. Treatment was effective in the patients receiving the highest dose, with a 58% reduction in phenylalanine observed for up to a week. It was concluded that the PAL was safe and well tolerated, despite 80% experiencing an adverse event, with injection-site reactions and dizziness reported most.

After separate parent phase II trials investigating rAvPAL-PEG (renamed pegvaliase) dosing [188,189], a longer term phase II extension study was carried out [190], evaluating long-term efficacy, safety and immunogenicity. Pegvaliase was either continued at the same or at a higher dose used in the parent study ranging between 2.5–375 mg/week or between 0.001–5 mg/kg/week, with doses and/or frequency adjusted for each patient to achieve a plasma phenylalanine concentration between 60–600 µmol/L. Pegvaliase was administered subcutaneously, rotating the site of injection, with a mean administration rate [range] of 2.5 [1.0-5.0] days/week in the parent study and 4.5 [1.0-6.9] days/week in the extension study. Overall mean treatment duration was approximately 3.4 years; 66% received pegvaliase for >2 years and 38% >4 years. Mean plasma phenylalanine was reduced by 60% at week 48, and 72% at week 120, with protein intake remaining relatively constant. Mean plasma phenylalanine decreased as mean pegvaliase dose increased, with both then remaining relatively stable from week 48–264. All participants reported at least one adverse event with

the most common being injection site reaction 72.5%, injection site erythema 67.5%, headache 67.5% and arthralgia 65.0%, with 12.5% and 76.3% of patients limited to mild and moderate adverse events, respectively, with serious adverse events experienced by 11.3%. One patient experienced anaphylaxis. All patients developed a sustained PAL antibody response, and a transient anti-PEG response. Hypersensitivity events were most frequent in the first 24 weeks then decreased to baseline levels near the end of the study. Differences in immune response is likely the reason why a variety of PAL doses in different patients were needed to achieve specific phenylalanine levels; patients with a lower antibody response had a greater phenylalanine reduction in early treatment.

Phase III clinical trials were then carried out called PRISM-1 and PRISM-2 [191,192]. PRISM-1 involved pegvaliase-naïve patients receiving either 20 or 40 mg/day pegvaliase via subcutaneous injection, using an induction (one weekly dose), titration (administered 2-7 days/week) and maintenance dosing regime, with daily dosing in all patients once the maintenance dose was reached. PRISM-2 involved continued pegvaliase treatment as an extension of previous trials, using doses of 5-60 mg/day, with daily subcutaneous administration. Out of 262 patients, mean blood phenylalanine was 1232.7 µmol/L at baseline, 564.5 µmol/L at 12 months and 311.4 µmol/L at 24 months, with improved neuropsychiatric outcomes associated with reduced phenylalanine. Adverse event findings similar to the previous trials were reported, with all participants reporting at least 1 adverse event, with overall adverse events decreasing in number over treatment duration. Serious adverse events still occurred, including anaphylaxis (2.7%) and hypersensitivity events (4.6%). The adverse events were considered manageable in most patients. In May 2018, pegvaliase was approved by the US FDA under the product name PALYNZIQ®. In May 2019, the EMA issued marketing authorisation for pegvaliase throughout the European Union for the treatment of PKU in adults and adolescents from 16 years of age.

1.2.6.4.4 TAL and tyrosinaemia

The use of PAL to degrade phenylalanine in PKU raises the question as to whether or not a similar strategy could be employed in nitisinone-induced tyrosinaemia in AKU patients, using TAL to degrade tyrosine. Despite the extensive research into PAL, TAL research is much further behind due to TAL enzymes being much rarer than PAL enzymes, with the first TAL discovered in 2001 [154] approximately 40 years after the first PAL [151]. If a TAL-based therapeutic is considered a plausible tyrosine-reducing strategy, the challenges and issues

documented throughout all stages of PAL development, which are likely to be applicable to TAL, should all be considered and evaluated carefully.

1.2.7 What remains to be identified in alkaptonuria for successful treatment?

Although the use of nitisinone in AKU patients has so far been very successful, nitisinone can only treat, not cure the disease. Tyrosinaemia, as discussed in section 1.2.6.3, is a consequence of nitisinone therapy that needs to be tackled in order to decrease or abolish the occurrence of keratopathy, and is on-going research. The next big step and ultimate treatment for single-gene diseases like AKU would be to treat the underlying genetic cause with gene/enzyme replacement therapy. Treatment of other inborn errors of metabolism related to the phenylalanine/tyrosine pathway by enzyme replacement has been attempted with some success [193]. In the past decade, liver-directed gene therapy has emerged as a promising alternative to transplantation in monogenic liver disorders such as AKU [194]. Gene therapy for AKU however has not yet been investigated. Before such work begins, there are some important questions however that must be addressed. It's currently unknown how much HGD (via enzyme or gene therapy) must be replaced in order to rescue the disease and whether HGD expression outside of the liver can affect the phenotype.

1.3 Animal models of disease

Model organisms such as fruit flies, worms, zebra fish and rodents have been used for many years to study elements of human disease. Many genes are conserved between species, in addition to many basic processes such as metabolism, cell division and growth. The house mouse (*Mus musculus*) is the most common laboratory model of human disease due to easy and cost-effective maintenance and breeding, similarities to humans in terms of phylogenetics, anatomy and physiology, and the ability to manipulate the genome. The ability to genetically modify the DNA of the mouse genome by manipulation technologies to create transgenic lines such as knock-in and knockout mouse models accelerated the use of mouse models in research, with thousands of strains now available.

1.3.1 Mouse model strategies

Mendelian diseases, such as AKU, are caused by a mutation in single gene, however the mode of inheritance can vary. Single-gene diseases for example can be autosomal recessive (i.e.

cystic fibrosis) requiring two mutated alleles or autosomal dominant (i.e. Huntington's disease) requiring one mutant allele. Genetic diseases can also be X-chromosome linked dominant (i.e. hypophosphatemia rickets) requiring one mutant gene on the X-chromosome and X-chromosome linked recessive (i.e. haemophilia) requiring one mutant X-chromosome in males and two mutant X-chromosomes in females. AKU is an autosomal recessive disease therefore both *Hgd* alleles need to be mutated to induce the AKU phenotype in mice. There are two main ways of creating a model of a genetic disease; directed and disease driven approaches, also known as reverse genetics, whereby a gene of interest is targeted, or non-directed and mutation based approaches, also known as forward genetics, whereby mice undergo random mutagenesis and subsequently screened for phenotypes [195,196].

1.3.1.1 Non-directed approaches (forward genetics)

1.3.1.1.1 Chemical mutagenesis

Ethylnitrosourea (ENU) mutagenesis is the most common mutagen used for large-scale phenotyping programs [197,198]. ENU acts as a point mutagen by transferring its ethyl group to oxygen or nitrogen radicals in DNA, resulting in mispairing and base-pair substitutions to occur at high rates in germ cells, particularly in spermatogonial stem cells. Within a single gene locus, the mutation frequency can reach up to 6×10^{-3} [199]. Point mutations can induce different types of mutated alleles, such as loss-of-function alleles, hypomorphic alleles that have reduced gene function, antimorphic alleles that antagonize the gene's normal function and gain-of-function alleles [198]. Dominant mutations can be screened in F1 generation screening, with recessive mutations identified among F3 offspring (heterozygous F2 females can be backcrossed to F1 males).

1.3.1.1.2 Insertional mutagenesis

Gene trap screens are another type of mutagenesis strategy, termed insertional mutagenesis, whereby phenotypes are identified after transfecting embryonic stem (ES) cells with a gene trap vector that can randomly integrate into the genome, causing mutations [195]. The mutant ES cells would then need to be re-introduced into an early-stage embryo, where they can contribute to the formation of the mouse. As with ENU mutagenesis, the offspring would require screening to identify a phenotype, which can be difficult and expensive, especially for recessive mutations that require F3 progeny. The inclusion of a promotorless reporter gene, typically β-galactosidase, into the gene trap can aid identification of the

mutant gene [200]. If inserted in an intron in the correct orientation and reading frame, a fusion transcript is formed between the endogenous interrupted gene and the reporter gene in the gene trap, mimicking its endogenous expression.

1.3.1.2 Directed approaches (reverse genetics)

Sequencing of the mouse (2002) and human (2001) genomes [201,202] led to an international effort to determine the function of protein-coding genes [203], with particular attention drawn towards inherited diseases (https://www.omim.org/statistics/geneMap) of which there are over 6,500 described, using mouse models to determine the genetic basis of these diseases. It was therefore more efficient and necessary to target specific genes in the genome of mice, rather than use a mutagenesis approach.

Once a disease gene has been identified, characterised and cloned, there are various methods that can be applied to create a genetic disease model, allowing the phenotypic consequences of a specific genetic mutation to be studied. In addition to genome modifying capabilities, the ability to harvest and grow mouse ES cells in culture that retain the ability to contribute to the formation of a mouse upon reintroduction into an early-stage embryo has established the mouse as the leading mammalian model system for studying the effect of genes *in vivo* [200]. Targeting a specific gene in ES cells with mutations has become the method of choice to create genetic models in mice, and is termed gene targeting.

Homologous recombination is a common technique used to precisely insert modified DNA into the mouse genome, usually designed to knockout a gene by replacing or deleting one or multiple coding exons [196]. At the very simplest, an artificial exogenous fragment of DNA in a gene targeting vector usually with a selectable marker such as an antibiotic resistance gene that allows selection of modified ES cells will have regions at either end that are homologous to endogenous gene of interest, allowing an exchange of the DNA between the two homologous regions, transferring the exogenous DNA into the host gene. This method can be used to delete a gene, remove exons, add in a gene and also introduce point mutations by modifying individual base pairs.

1.3.1.2.1 Transgenic mice

Transgenic mice can be generated via a simple random integration transgenic approach, whereby an exogenous gene is microinjected into the pronuclei of a 1 cell embryo which then

should incorporate into all future cells of the mouse [195,204]. The injected DNA construct inserts randomly into the genome, at one or more genetic loci, either as single or multiple copies, all of which can affect the level of gene expression. This approach is a targeted mutagenesis approach as a specific gene has been introduced and used to study simple overexpression. Although a gene of interest is injected, there is no control over the integration of the exogenous gene with this method, hence why targeting a specific gene in ES cells is a preferred method.

1.3.1.2.2 Gene targeting

Gene knockouts are the most common type of genetic model for studying disease. Using homologous recombination in ES cells to introduce a deletion of an important exon, or by a gene trap which disrupts a gene, creates a ubiquitous knockout where the gene is deleted/interrupted in every cell. The modified ES cells can then be introduced to an early-stage embryo and incorporated into the germ line [195,196]. This technique was then followed by the introduction of conditional alleles, whereby a gene could be deleted in a specific tissue and/or at particular time.

Currently, the most common technique to manipulate alleles to obtain conditional, tissue-specific and/or time-dependant deletion, is the use of the site specific recombination via the bacterial Cre/*LoxP* system [205,206], or the Flp/*FRT* system [207] from yeast [204]. Both *LoxP* and *FRT* sequences are not found within the mammalian genome. Exogenous *LoxP* (34 bp: ATAACTTCGTATAATGTATGCTATACGAAGTTAT [208]) or *FRT* (34 bp: GAAGTTCCTATTCTCTAGAAAGTATAGGAACTTC [209]) sequences can be introduced either side of a piece of DNA such as a coding exon in a gene of interest in the mouse genome, to generate a floxed allele or *FRT*-flanked allele, respectively, that does not affect transcription of the target gene. Cre recombinase or Flp recombinase enzymes can then recombine the *LoxP/FRT* sequences to excise the flanked target sequence or invert the sequence, see Figure 1.7. To achieve Cre recombination, which is the more common method, you need double transgenic mice that are genetically modified with a floxed target gene, generated by homologous recombination in ES cells, and must also express a Cre recombinase enzyme. Creating a floxed allele in an ES cell that transmits to the germ line results in every cell containing the floxed allele. If Cre is present under a ubiquitous promoter, the gene will be knocked out in all cells.

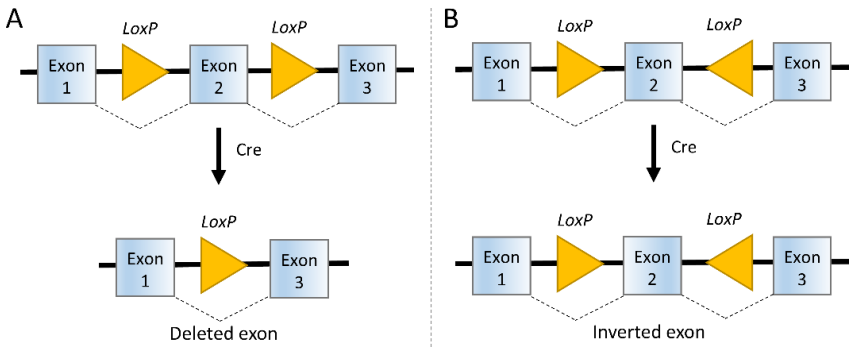

Figure 1.7. Cre/*LoxP* recombination.
(A) LoxP sites placed head-to-tail around a target sequence, in this case an exon, will cause the floxed sequence to be deleted by Cre recombinase. (B) *LoxP* sites placed head-to-head around a target sequence, in this case an exon, will cause the floxed sequence to be inverted by Cre recombinase. The mechanism of Flp/*FRT* recombination is the same as Cre/*LoxP* recombination.

Restricting the expression of the Cre recombinase enzyme using a tissue-specific or cell-specific promotor can restrict the deletion of the allele to a specific tissue or cell type. Different promotors can also be active at different developmental stages, allowing deletion of the floxed gene to occur after birth for example, which can be useful for genes that are embryonically lethal. Alternatively, Cre enzymes can be under the control of an inducible promoter, such as a drug responsive promotor, therefore deletion can also be induced at any developmental stage once the drug is given. An example of this is Cre ER where the Cre is fused to the oestrogen receptor (ER) and modified by a mutation to respond to tamoxifen and not oestrogen [210]. Once a double transgenic is given tamoxifen, the Cre is translocated to the nucleus where it can cleave floxed DNA, usually a critical coding exon to disrupt expression of the gene, creating a null allele via a deletion [204].

1.3.1.2.3 Knockout-first strategy

More recently, the International Knockout Mouse Consortium (IKMC), with the European Conditional Mouse Mutagenesis (EUCOMM) and the National Institutes of Health Knockout Mouse (KOMP) programs suggested another gene targeting strategy called knockout-first, which combines both gene trapping and conditional gene targeting [211]. The first allele generated is a *LacZ*-tagged knockout-first allele, which has an *FRT*-flanked gene trap vector inserted into an intron of a gene, see Figure 1.8A. The vector has a splice-acceptor sequence, then a *LacZ* reporter gene followed by a polyadenylation stop sequence, creating an in-frame fusion transcript of the gene of interest up to the position of the target vector that then terminates at the stop sequence, disrupting the gene. The *LacZ* gene is expressed as a fusion

transcript with the gene of interest but not as a fusion protein, due to an internal ribosome entry site (IRES) element between the splice acceptor site and the *LacZ* sequence, allowing independent translation. Downstream of the gene-trap cassette, the next exon is flanked by *LoxP* sites (floxed), but is usually not transcribed, although in some target genes low-level transcription may after the gene trap (hypomorphic mutation). This knockout-first allele is inserted into ES cells via homologous recombination, and will be present in every cell, therefore the allele is disrupted in every cell in which it is usually expressed.

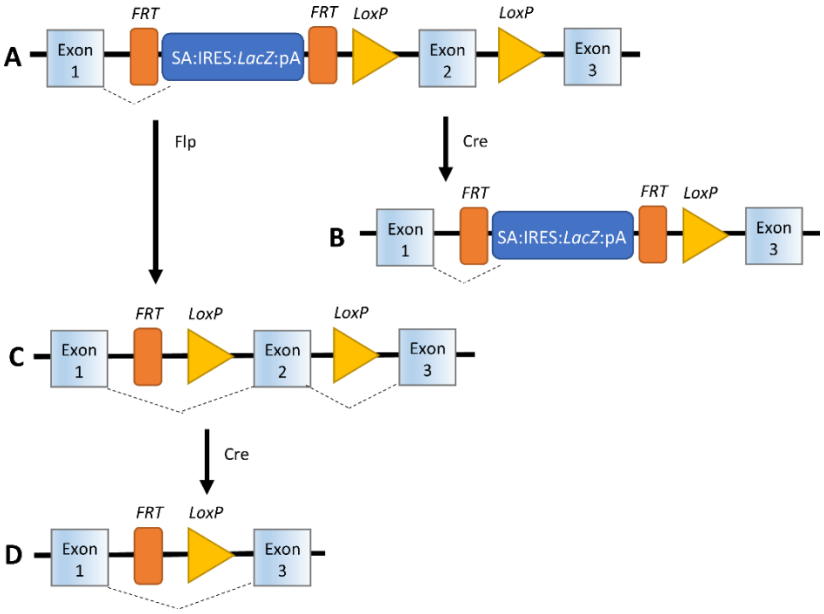

Figure 1.8. Knockout-first strategy.
A shows a knockout-first allele. A gene trap vector, flanked by *FRT* sites has been inserted into the intron of a gene. Within the gene trap vector is a splice-acceptor (SA), a *LacZ* reporter gene and a polyadenylation (pA) sequence that prematurely terminates transcription of the target gene. The *LacZ* gene is expressed as a fusion transcript with the start of the target gene, but not as a fusion protein due to the presence of an internal ribosome entry site (IRES) between the SA and *LacZ*. Adjacent to the gene trap, the next downstream exon is flanked by *LoxP* sequences. This allele would be interrupted by the gene trap. Cre recombinase can then convert this allele in A to become a null, *LacZ*-tagged allele as shown in B, by removal of the floxed target exon. Flp recombination of the allele in A results in removal of the gene trap vector, leaving behind a floxed target exon, with the gene being transcribed as normal (C). Exposure of the conditional allele (C) to Cre then creates a null allele (D) by Cre/*LoxP* recombination that removed the floxed target exon.

This knockout-first allele can then be modified by either Cre of Flp recombinase [211]. Cre recombination would remove the floxed exon, resulting in a null, *LacZ*-tagged allele (Figure 1.8B). Flp recombination on the other hand would result in a conditional allele (Figure 1.8C), where the gene trap has been removed, leaving a residual *FRT* site and the floxed downstream exon; this allele is transcribed as normal. The conditional allele can then be converted to a null allele (Figure 1.8D) by Cre recombination due to the presence of *LoxP*

sites that are usually flanking a critical exon. Any suitable Cre line can be used to obtain tissue-specific and/or time-specific deletion of the gene. This knockout-first strategy is versatile and has been to generate thousands of gene knockouts in ES cells through targeted mutagenesis programs such as the International Knockout Mouse Consortium [212], which was reported to have 17,473 targeted and trapped alleles for protein-coding genes in 2012.

1.3.1.2.4 RNA interference

The introduction of double-stranded RNA (dsRNA) that is homologous in sequence to a specific gene can results in its post-transcriptional silencing, first reported in 1998 in *C. elegans.* [213]. This type of gene silencing is termed RNA interference (RNAi). An enzyme called Dicer processes dsRNA into a smaller dsRNA fragments termed small interfering RNAs (siRNAs), which are incorporated into a nuclease complex called RISC (RNA-induced silencing complex) [204]. The RISC finds homologous target mRNAs using a strand of the siRNA as a guide strand, and then cleaves the target mRNA. It was first shown that siRNA could knockdown gene expression in mice in 2003 [214]. RNAi models are advantageous as the method is much more rapid and inexpensive in comparison to generating knockout mice as described in the above sections. On the other hand, the knockdown of genes via RNAi can be variable and transient, and can therefore be less reliable and reproducible than a knockout model. The RNAi can either be injected into mice or an RNAi expression cassette could be engineered into the genome of mice.

1.3.1.2.5 Other methods for genetic manipulation of DNA

In recent years, a series of programmable nuclease-based genome editing technologies have been developed, where site-specific nucleases are used to introduce specific DNA breaks in the genome [215]. The DNA break can then be repaired either by homology directed repair (HDR) mechanisms or via non-homologous end joining (NHEJ), resulting in genome editing. Programmable nucleases that use proteins to recognise the target DNA sequence, which require new proteins to be engineered each time, which is expensive and labour-intensive, include meganucleases, zinc-finger nucleases and transcription-activation-like effector nucleases. More recently, the clustered regularly interspaced short palindromic repeat (CRISPR) associated proteins 9 (CRISPR/Cas9) technology has been developed that uses RNAs for site recognition [216]. An engineered single guide RNA is used to find the target DNA and used to introduce a double strand break by the Cas9 endonuclease protein. CRISPR/Cas9

could be used to generate models of disease by introducing mutations into genes, and perhaps more importantly, it can be used as a tool for gene therapy to correct mutations in genetic diseases.

1.3.2 Mouse models of AKU

1.3.2.1 Importance of animal models in AKU

The primary metabolic consequences of AKU are relatively straightforward to study; metabolites such as HGA and tyrosine from urine [44,46] and blood [217] samples can be measured and monitored. More recently, technology and software has led to metabolomic analysis in AKU, enabling the wider consequences of this metabolic disease to be studied, which can be performed on blood/urine samples that are relatively easy to obtain [218]. Studying the ochronotic process in human joints however has been much more limited. Currently, only joints from patients undergoing joint replacement [57] or autopsy [55] are available to study as it is highly unethical and impractical to investigate younger, less diseased joints. Therefore, the only insight into human joint pathology in AKU is at the end stage of the disease.

The development of HGD deficient AKU mouse models has allowed examination of joints from the very onset of pigmentation. In addition, AKU mouse models can be used to study metabolites relevant to AKU, to further characterise disease pathophysiology and to investigate new and experimental treatments.

1.3.2.2 Early animal work in AKU

Many reports have documented spontaneous AKU in various animals such as the rabbit [219], chimpanzee [220], orangutan [221] and macaque [222], where urine was found to darken after standing, leading to the identification of AKU. However, no evidence of osteoarthropathy or pigmentation was found. In addition, these findings were all isolated case reports. Early animal work involved attempts to induce ochronosis by injection of HGA into rabbits, with intra-articular injection shown to produce joint ochronosis resembling that of human lesions [223]. Intravenous and intraperitoneal injection failed to produce ochronosis in this rabbit model. A dietary model was also reported, with rats fed a diet excess in tyrosine (8%) for a minimum of 9 months, which appeared to induce ochronosis [224].

These early reports of AKU occurred before the advent of genome modifying technology. The world's first transgenic mouse model was developed in 1976 and the first knockout mouse

in 1987 [225]. After the injection of HGA into rabbits to induce ochronosis in 1961, which did not attempt to create a model of AKU, it was not until the 1990s that a murine model for AKU was discovered.

1.3.2.3 BALB/c *Hgd*$^{-/-}$ mouse model of AKU

The first AKU mouse model was generated by ENU mutagenesis, whereby random mutations are induced into the genome [198]. The AKU phenotype was identified by Montagutelli et al. in 1994 at the Pasteur Institute (Paris, France) due to darkened cage bedding, caused by elevated HGA in the urine turning a dark brown/black colour [86]. Subsequent mice were confirmed to have AKU by urine spots on sodium hydroxide-soaked filter paper, which causes AKU urine to turn brown in 30–60 seconds (alkaline conditions speed up the colour change; urine eventually turns dark after standing for several days). An example of dark stained cage bedding from these AKU mice is shown in Figure 1.9. This *Hgd* mutation was then backcrossed onto the BALB/cByJ and C57BL/6J murine backgrounds. Urine analysis then confirmed that HGA was elevated to >0.55 mol/mol creatinine in homozygous mice and was non-detectable in wildtype and heterozygotes.

Figure 1.9. BALB/c *Hgd*$^{-/-}$ AKU mouse cage bedding.
Mice with deficient homogentisate 1,2-dioxygenase (HGD) activity (shown on the right) are unable to metabolise homogentisic acid (HGA), leading to its excretion into the urine, causing dark urine stained cage bedding after several days of exposure to the air. A wildtype mouse is shown on the left. Image used with the permission of Dr Jean Louis Guenet.

In 1997, the murine *Hgd* gene was cloned and the ENU-induced mutation was identified in 1998 to be a point mutation that resulted in a truncated HGD protein with 6% activity compared with wildtypes [226,227]. The mutation changed the splice donor site within intron 12, from G**T**AAGT → G**A**AAGT, leading to deletion of exon 12 and causing a frameshift mutation and premature stop codon at the start of exon 13 [228]. Despite the extreme level of pigmentation seen in human AKU cartilage, no connective tissue pigmentation in these

homozygous AKU mice was found, despite increased urinary HGA [45,86]. Ochronosis however was later detected using Schmorl's staining to intensify the colour of the pigment in a crossbred murine model of AKU, *Hgd*$^{-/-}$*Fah*$^{-/-}$, derived from the original ENU mutagenesis mouse from the Pasteur Institute, showing microscopic pigmentation synonymous to human ochronosis [229]. Pigmentation was shown to initiate in the pericellular matrix of chondrocytes found in calcified articular cartilage [229]. Although pigmentation was identified, the complex *Hgd*$^{-/-}$*Fah*$^{-/-}$ model was not deemed a suitable model for AKU due to the confounding HT-1 *Fah*$^{-/-}$ mutation that exhibits severe hepatic and renal pathology. Furthermore, the model requires nitisinone treatment from birth to survive by blocking the tyrosine pathway upstream of the fatal *Fah*$^{-/-}$ mutation, with subsequent removal in adulthood to cause spontaneous loss of heterozygosity from *Hgd*$^{+/-}$*Fah*$^{-/-}$ to *Hgd*$^{-/-}$*Fah*$^{-/-}$ in a subset of mice to generate the AKU genotype.

In 2014, a consistent murine model of AKU in the BALB/c background, *Hgd*$^{-/-}$, was described with no confounding HT-1 pathology [115]. This AKU model demonstrated relatively stable increased plasma HGA levels, the first reported in an AKU animal model, and extensive chondrocyte pigmentation via a modified Schmorl's stain. It was shown here that initial chondrocyte pigmentation is pericellular, progressing to the intracellular compartment. The ability to then score the number of pigmented chondrocytes in the tibio-femoral (knee) joint showed a linear increase in pigmentation with age. This AKU mouse model has provided the means to study early ochronosis in a predictable and systematic manner.

Establishment of this BALB/c *Hgd*$^{-/-}$ AKU model has led to work looking at various aspects of the disease, such as preventing HGA formation and therefore disease progression with nitisinone (discussed in section 1.3.2.4 below) [115,116], metabolomic evaluation of the wider effects of nitisinone [218,230,231], investigation of the ultrastructure of murine AKU calcified cartilage by electron microscopy [232], expression of enzymes related to tyrosine metabolism (Wilson et al., manuscript in preparation) and the effectiveness of tyrosine dietary restriction on nitisinone-induced tyrosinaemia [233] which is discussed in chapter 5.

1.3.2.4 Nitisinone-treatment in the BALB/c *Hgd*$^{-/-}$ AKU mouse model

As discussed in section 1.2.6, only palliative treatment such as analgesics and arthroplasty [28] were available for AKU, with low-protein diets, ascorbic acid and physiotherapy proven clinically ineffective [20,101,102]. Nitisinone, which blocks the HPPD enzyme that forms HGA, was shown to completely prevent chondrocyte pigmentation in the BALB/c *Hgd*$^{-/-}$ mouse model

[115]. This mouse study followed a human trial of nitisinone that saw a reduction in HGA, but was deemed inconclusive and ineffective due to no clinical joint improvement, assessed by hip rotation, which is now deemed an inappropriate primary outcome [40]. Further work in this mouse model showed that nitisinone can arrest, but not reverse, ochronosis progression, and also demonstrated a clear-dose response between nitisinone and plasma HGA [116].

The investigation of nitisinone in this BALB/c *Hgd*$^{-/-}$ model was highly influential, providing evidence of HGA reduction and disease prevention. This led to the off-label use of nitisinone at the NAC and within the DevelopAKure series of human clinical trials investigating the use of nitisinone in AKU [52,118], where its use has proven safe and effective (see section 1.2.6.2).

Although the use of nitisinone in these clinical trials has so far been very successful, nitisinone can only treat, not cure the disease. The next big step in single-gene diseases like AKU would be to treat the underlying genetic cause with gene/enzyme replacement therapy.

1.3.2.5 Why create a new AKU mouse model?

It is clear that the ENU mutagenesis *Hgd*$^{-/-}$ AKU mouse model has greatly contributed to our knowledge of AKU, in terms of both disease pathophysiology and treatment, and will continue to be utilised for AKU research. ENU mutagenesis however is not a targeted approach to create a model of genetic disease due to the high frequency of DNA mutations that ENU causes [197,198]. Other unknown and uncharacterised mutations could potentially exist in the mutagenesis AKU model that could affect the phenotype, as the ENU model has never been fully sequenced. Newer, more complex mouse models offering additional tools such as endogenous reporter genes and conditional potential are now available, whereby a specific gene is targeted. Conditional alleles in particular are extremely useful as they have the ability to be induced in a specific tissue and at a specific time point in the animal's life course.

1.4 Overall aims

1. The first aim of this work was to generate and phenotype a new targeted conditional mouse model of AKU, raised in the C57BL/6 background using a mutant knockout-first allele obtained from the KOMP repository (www.komp.org). The aim was to phenotype the mouse model biochemically by quantifying HGA and then histologically, investigating tissue ochronosis.

2. The second aim of this project was to use the *LacZ* reporter gene situated within the *Hgd* locus of the knockout-first mouse model to localise gene expression of *Hgd*. The Flp/FRT and Cre/*LoxP* site-specific recombination system within the new mouse model was then used to obtain an inducible and tissue-specific knockout, with the aim of investigating the effect of partial *Hgd* knockout on the AKU phenotype. With gene therapy becoming a likely tool in the future, this conditional mouse model was used to provide an insight into the level and location of *Hgd* expression that could rescue the AKU phenotype.

3. Treatment of AKU with the HGA-lowering drug nitisinone has emerged as the first and most promising disease-preventing treatment for AKU. Nitisinone therapy however is associated with tyrosinaemia that in a minority of patients causes keratopathy. The third major aim of this work was to investigate nitisinone-induced tyrosinaemia in AKU mice and potential strategies that may lower circulating tyrosine. Initially, dietary studies were carried out to investigate the effectiveness of reducing oral/intestinal uptake of tyrosine and/or phenylalanine. Subsequently, a bacterial enzyme with tyrosine degrading activity was investigated *in vitro*.

2 Methods

2.1 Mouse generation

Embryonic stem (ES) cells containing a modified *Hgd* allele, clones *Hgd* C10 and *Hgd* C11 (origin strain C57BL/6N-A^{tm1Brd} (non-*agouti* mutation; ES cell line JM8A3.N1), were purchased from the UC Davis KOMP repository (KOMP is now the Mutant Mouse Resource & Research Centres (MMRRC) at UC Davis; *Hgd* KOMP ES cell line https://www.mmrrc.org/catalog/cellLineSDS.php?mmrrc_id=56778). The ES cells were grown on G419-resistant primary embryonic fibroblasts, as described [234]. Following G418 antibiotic selection, healthy ES cells were injected into blastocysts of C57BL/6 (Harlan, UK) at the blastula stage, in the blastocoel cavity close to the inner cell mass. The modified blastocysts were then transferred into pseudopregnant recipient CD1 females (Charles River, UK), and chimeric offspring identified. Further breeding was used to confirm germline transmission of the modified allele. Only C10 chimeras achieved germline transmission, and were subsequently bred to homozygosity. The C10 line was then referred to as *Hgd tm1a*, either as homozygous (-/-) or heterozygous (-/+).

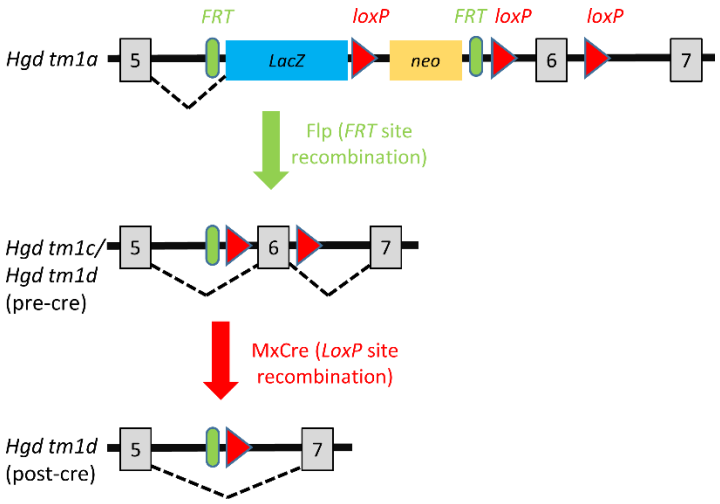

Figure 2.1. Modified *Hgd* alleles; *Hgd* tm1a, *Hgd* tm1c, *Hgd* tm1d.
The *Hgd* tm1a allele has an AKU phenotype due to disruption by the gene trap cassette situated between exons 5 and 6. Flp-mediated FRT site recombination removes the gene trap cassette, leaving *LoxP* sequences either side of exon 6 in the *Hgd tm1c* allele, which is transcribed as normal. The *Hgd tm1d floxed (fl/fl)* allele is obtained by breeding the *Hgd tm1c* floxed allele with *MxCre* mice *(Hgd tm1d (fl/fl) MxCre)* and is inducible. When MxCre expression is induced, the floxed sixth exon in *Hgd tm1d* is removed by Cre/LoxP site recombination, resulting in *Hgd* deletion (post-cre).

To obtain the conditional *Hgd tm1d* line, *Hgd tm1a* mice were crossed with Flpo mice to remove the FRT-flanked gene trap cassette, leaving a floxed target exon (*Hgd tm1c +/+*) [235], see Figure 2.1. Homozygote floxed *Hgd tm*1c mice were crossed with *MxCre* mice [236] (Mx-1 Cre); referred to as *Hgd tm1d* (fl/fl) *MxCre* (-/+ or WT). The removal of the floxed 6th exon in *Hgd tm1d* was induced with administration of polyinosinic: polycytidylic acid (pIpC)[236,237],

which increases interferon levels, driving the interferon-responsive Mx-1 promoter and therefore the Cre expression (see section 2.3.2 for more details).

2.1.1 Genotyping

Mice were ear notched after weaning at approximately three weeks of age in order to be identified and genotyped.

2.1.1.1 Ear Notch Digestion

100 µl of lysis buffer (50 mM tris-HCl (pH 8.0), 0.1 M NaCl, 1% SDS w/v, 20 mM EDTA in distilled H_20) and 10 µl of 10 mg/ml proteinase k (100 mg reconstituted in 10 ml 50% glycerol; Sigma Aldrich UK, P2308 or Bioline UK, BIO-37037)) were added to the ear notch in an Eppendorf, then incubated at 55°C overnight in a water bath. The following day, samples were removed from the water bath, cooled to room temperature and vortexed to ensure the tissue had been digested. DNA was then isolated from the digested ear notch using an isopropanol DNA extraction.

2.1.1.2 Isopropanol DNA extraction

DNA was isolated from digested ear notch tissue using an isopropanol DNA precipitation method.

1. Digested ear notch samples removed from 55°C water bath, cooled and vortexed.
2. Lysate was centrifuged at ≥12,000 g for 10 minutes to form a protein pellet.
3. Supernatant was transferred into a new Eppendorf, leaving the protein pellet behind.
4. An equal volume of 100% isopropanol at room temperature was added to the supernatant (usually about 80 µl).
5. The tubes were inverted several times to aid the DNA precipitation, then centrifuged at ≥12,000 g, for 10 minutes. DNA will form a pellet (may not be visible).
6. The supernatant was then removed and discarded.
7. 100 µl of 70% ethanol was then added to wash the DNA pellet, then discarded, followed by brief centrifugation for 30 seconds.
8. The remaining supernatant was then removed with a pipette, and the DNA pellets left to air dry for approximately 10 minutes.
9. The DNA pellet was then reconstituted in 1 X TE (tris-EDTA) buffer (25 µl).

After reconstituting the DNA, the concentration (ng/µl) was measured by spectrophotometry using Nanodrop™ 2000 (ThermoFisher Scientific). DNA was stored at -20°C if not being used straightaway. Extracted ear notch DNA was then used as the template for PCR reactions. See below for PCR reaction mixtures, cycling parameters and expected band sizes for the different mouse lines. See Table 2.1 for primer sequences.

Table 2.1 Genotyping primer sequences.

Primer Name	Sequence (5' to 3')	Mouse line	Source
Lox-F	GAGATGGCGCAACGCAATTAATG	*Hgd tm1a/c/d*	KOMP repository, supplied with modified ES cells
Hgd-R	CTTGGCTTTGGACTTGAACCCTAGC	*Hgd tm1a/c/d*	
Hgd-F	GCCTTTATCCCTACAAGTCTCCCCG	*Hgd tm1a/c/d*	
Hgd-ttR	TAGATGGATTTTGTGGGGAGAGGGC	*Hgd tm1a/c/d*	
MxCre F	CATGTGTCTTGGTGGGCTGAG	*Hgd tm1d MxCre*	Dr Takao Sakai [238]
MxCre R	CGCATAACCAGTGAAACAGCAT	*Hgd tm1d MxCre*	
Internal F	TGGACAGGACTGGACCTCTGCTTTCCTAGA	Used with *MxCre*	Prof George Bou-Gharios
Internal R	TAGAGCTTTGCCACATCACAGGTCATTCAG	Used with *MxCre*	
Hgd290 F	CATTTTCACCGTGCTGACTG	BALB/c *Hgd*$^{-/-}$	Dr Andrew Preston [115]
Hgd290 R	TTTAGTCGCTGCATCACCTG	BALB/c *Hgd*$^{-/-}$	

2.1.1.3 PCR Reaction Mixtures

GoTaq® G2 Flexi DNA polymerase (Promega, UK) was used to amplify DNA products for genotyping. Approximately 100 ng of template DNA was used in each reaction. Primers, purchased from Eurofins Genomics (Ebersberg, Germany) were reconstituted in 1 x TE buffer to a concentration of 100 pmol/µl, then diluted 1 in 10 in 1 x TE buffer to 10 pmol/µl; aliquots were stored at -20°C.

2.1.1.3.1 *Hgd tm1a* and *Hgd tm1c/d* (pre-cre)

To distinguish the genotype of the *Hgd* gene in *Hgd tm1a, Hgd tm1c* (post-flp) and *Hgd tm1d* (pre-cre), the same PCR reaction mixture and primers were used (Table 2.2), producing different bands for the different lines. The expected band sizes were as follows:

- *Hgd tm1a*
    - WT (2 unmodified alleles) has only 561bp band.
    - Homozygous *Hgd* flox (2 modified alleles) has only 257bp band.

- Heterozygous *Hgd* flox (1 modified allele, 1 unmodified allele) has 561bp and 257bp bands.

- *Hgd tm1c (fl/fl)* (post-flp) and *Hgd tm1d (fl/fl)* (pre-cre)
  - WT (2 unmodified alleles) has only 561bp band.
  - Homozygous *Hgd* flox (2 modified alleles) has 673bp and 257bp bands.
  - Heterozygous *Hgd* flox (1 modified allele, 1 unmodified allele) has 673bp, 561bp and 257bp bands.

Table 2.2 PCR reaction mixture and cycling parameters for *Hgd tm1a*, *Hgd tm1c* (post-flp)*/d* (pre-cre) genotyping.

PCR Reaction: *Hgd tm1a*, *Hgd tm1c/d* (pre-cre)				**Cycling parameters**		
		x1 (µl)		1	94°C	5 min
	5x Buffer	6		2	94°C	15 sec
	25 mM $MgCl_2$	2.1		3	65°C	30 sec
	10 mM dNTP	1		4	72°C	1 min
	DMSO	0.325		5	GOTO step 2, x10, -1°C per cycle	
	Go taq	0.3		6	93°C	1 min
10 pmol/µl	Lox-F primer	0.5		7	65°C	1 min
	Hgd-R primer	0.5		8	72°C	30 sec
	Hgd-F primer	0.5		9	GOTO step 2, x30	
	Hgd-ttR primer	0.5		10	72°C	5 min
Adjust to approximately 100 ng/µl DNA	H_20	17.2		11	4°C	∞
	DNA	1				
	Total	**30**				

2.1.1.3.2 MxCre

MxCre genotyping only produces a band when *MxCre* is present, it is unable to distinguish between homozygous or heterozygous; positive is denoted as +/-. To ensure that the PCR amplification was successful (i.e. to show that DNA was present in the reaction mixture at sufficient quality, to show that the PCR reaction worked) and to prevent false-negative results, the reaction mixture included primers for a control gene; specifically, exon 1 of the *Fabp2* (fatty acid-binding protein 2) gene. The PCR reaction mixture and cycling parameters are shown in Table 2.3. The expected bands are:

- WT has only a 194bp band corresponding to the internal control gene
- *MxCre* positive, denoted +/-, has both the internal control band at 194bp and a band at 520bp corresponding to *MxCre*. The Cre primers are specific to *MxCre*.

Table 2.3 PCR reaction mixture and cycling parameters for *MxCre* genotyping.

PCR Reaction: *MxCre*				**Cycling parameters**		
		x1 (µl)		1	95°C	3 min
	5x Buffer	5		2	94°C	30 sec
	25 mM $MgCl_2$	2		3	63°C	30 sec
	10 mM dNTP	0.5		4	72°C	30 sec
	Go taq	0.1		5	GOTO step 2, x9, -1°C per cycle	
	DMSO	1.25		6	95°C	30 sec
10 pmol/µl	MxCre F primer	0.5		7	53°C	30 sec
	MxCre R primer	0.5		8	72°C	30 sec
	Internal F primer	0.5		9	GOTO step 6, x35	
	Internal R primer	0.5		10	72°C	5 min
Adjust to approximately 100 ng DNA	H_20	13.15		11	4°C	∞
	DNA template	1				
	Total	**25**				

2.1.1.3.3 BALB/c *Hgd*$^{-/-}$

To genotype the BALB/c *Hgd*$^{-/-}$ colony, the region containing the AKU-causing mutation within the *Hgd* gene is amplified by PCR (see Table 2.4) to generate a 290bp sequence. In a wildtype, this sequence contains a $HypCH_4III$ restriction enzyme binding site; the mutated AKU sequence does not. A restriction enzyme digest (see

Table 2.5) followed by agarose gel electrophoresis (3% w/v gel) is used to determine the presence or absence of the AKU mutation. The expected bands are:

- WT would have two bands at 170bp and 120bp.
- Homozygous would have one non-digested band at 290bp.
- Heterozygous would have three bands at 290bp, 170bp and 120bp.

Table 2.4. PCR reaction mixture and cycling parameters for BALB/c *Hgd*$^{-/-}$ genotyping.

PCR Reaction: BALB/c *Hgd*$^{-/-}$				**Cycling parameters**		
		x1 (µl)		1	95°C	15 min
	Qiagen HotStarTaq Mastermix	12.5		2	94°C	30 sec
10 pmol/µl	Hgd290 F primer	0.5		3	52°C	30 sec
	Hgd290 R primer	0.5		4	72°C	1 min
Adjust to approximately 100 ng DNA	H_20	8.5		5	GOTO step 2, x30	
	DNA template	2		6	72°C	7 min
	Total	**25**		7	4°C	∞

Table 2.5. Restriction enzyme digest reaction mixture and incubation parameters for BALB/c *Hgd*$^{-/-}$ genotyping.

Reaction components	Volume (µl)	Cycling Parameters
NEB4 (New England BioLabs Buffer 4)	1.5	37°C for 2 hours
HypCH$_4$III	0.3	
H_20	11.7	
PCR product	1.5	
Total	**15**	

2.1.1.4 Gel electrophoresis

Agarose gels were used for gel electrophoresis to separate DNA bands from genotyping PCR reactions. Tris-acetic acid EDTA (ethylenediaminetetraacetic acid) (TAE) buffer was used to cast and run gels. 1x TAE buffer was obtained by diluting 50x TAE stock (242 g Tris base, 57.1 ml glacial acetic acid, 18.6 g EDTA disodium salt dehydrate in distilled H_2O to a total volume of 1 L). Gels of 1.5% w/v were typically used, unless stated otherwise, made using 1x TAE buffer and molecular grade agarose powder (Bioline UK, BIO-41025). To stain the gel, 2 µl of SYBR safe (10,000X concentrate; ThermoFisher Scientific, S33102, UK) per 50 ml gel is added (1 in 25,000 dilution). Gels were loaded with 20 µl of PCR product, and run in a Bio-Rad Sub-Cell® agarose gel electrophoresis system, in 1x TAE buffer, at 100 volts for 70 minutes. A Quick-Load® Purple 2log-DNA ladder (now called 1kb Plus DNA ladder (N3200S), New England BioLabs, US) was used to determine band sizes, unless indicated otherwise. A Bio-Rad ChemiDoc™ XRS+ Imaging System coupled with Bio-Rad Image Lab™ Software (Version 5.0), was used to image gels; UV light was used to excite the SYBR-safe nucleic acid stain.

2.2 Histology

2.2.1 Tissue processing

Tissues for paraffin wax embedding were processed following fixation in 10% formalin for a minimum of 24 hours. Hard tissues were decalcified in 10% EDTA pH 8.0 (changed a few to several times depending on the size of the tissue) until the tissue was flexible and soft enough to bend prior to processing to enable histological sectioning. For example, the knee joint of mice was decalcified over 1-2 weeks, with 3 changes of EDTA solution. Table 2.6 shows the tissue processing steps for soft tissues and hard tissues, using a Leica ASP300 tissue processor. After processing, tissues were embedded in paraffin wax blocks.

Table 2.6. Tissue processing stages for soft and hard tissues.

Step	Chemical	Soft tissue	Hard (decalcified) tissue
1	70% ethanol	30 mins	15 mins
2	90% ethanol	30 mins	1 hour
3	100% ethanol	10 mins	1 hour
4	100% ethanol	10 mins	1 hour
5	100% ethanol	10 mins	1 hour
6	100% ethanol	10 mins	1 hour
7	Xylene	30 mins	1 hour
8	Xylene	30 mins	1 hour
9	Paraffin wax	2 hours	2 hours
10	Paraffin wax	2 hours	2 hours
Total time		6 hours 40 minutes	11 hours 15 minutes

2.2.2 Sectioning of tissues

Leica RM 2235 or RM 2245 manual microtomes were used to section paraffin wax embedded tissues at a thickness of 5/6 µM. Sections were transferred to a 45°C water bath and mounted on glass Superfrost® Plus microscope slides (ThermoScientific, UK). Slides were then dried overnight in a 37°C oven. Frozen samples embedded in OCT (Leica Tissue Freezing Medium) were sectioned using a Leica CM 1900 cryostat, using glass Superfrost® Plus microscope slides (ThermoScientific, UK). Slides were then stored at -20°C until staining.

2.2.3 Staining of sections

Tissue sections were stained using the following protocols.

2.2.3.1 Haematoxylin and eosin

Haematoxylin and eosin (H&E) staining of paraffin sections was carried out according to Table 2.7.

Table 2.7. H&E staining of paraffin sections.

Step	Chemical	Duration
1	Xylene	3 minutes
2	Xylene	3 minutes
3	100% ethanol	2 minutes
4	90% ethanol	2 minutes
5	70% ethanol	2 minutes
6	Running tap water	1 minute
7	Harris Haematoxylin	5 minutes
8	Running tap water	1 minutes
9	Acid alcohol	15 seconds
10	Running tap water	5 minutes
11	Eosin Y (alcoholic)	3 minutes
12	Running tap water	15 seconds
13	70% ethanol	1 minute
14	90% ethanol	1 minute
15	100% ethanol	1 minute
16	Xylene	2 minutes
17	Xylene	2 minutes
18	Mount coverslip with DPX	-

2.2.3.2 Schmorl's staining

Schmorl's staining of paraffin sections to detect ochronotic pigment was carried out according to Table 2.8.

Schmorl's incubating solution

The incubating solution for Schmorl's staining (1% ferric chloride, 1% potassium chloride, in dH_2O) was prepared fresh prior to staining and was not used for more than 1 day.

Nuclear fast red

Nuclear fast red was filtered before staining, and stored in the fridge between use. To prepare the stain, 15 g of aluminium sulfate hexadecahydrate ($Al_2(SO_4)_3.16H_2O$) was dissolved in 300 ml dH_2O (approximately 5% solution), then 0.3 g nuclear fast red added (0.1%). The solution was heated and stirred until boiling, cooled to room temperature and then filtered. A few grains of thymol were added to prevent bacterial growth, then stored in the fridge.

Table 2.8. Schmorl's staining of paraffin sections.

Step	Chemical	Duration	Notes
1	Xylene	3 minutes	
2	Xylene	3 minutes	
3	100% ethanol	2 minutes	
4	90% ethanol	2 minutes	
5	70% ethanol	2 minutes	
6	Tap water	1 minute	Not running water
7	Schmorl's incubating solution	1 - 15 minutes	Usually 15 minutes
8	Running tap water	3 minutes	
9	1% acetic acid	5 minutes	Prevents overstaining
10	Nuclear fast red	2 – 4 minutes	Time dependant on intensity
11	Running tap water	5 minutes	Agitate
12	70% ethanol	2 minutes	
13	90% ethanol	2 minutes	
14	100% ethanol	2 minutes	
15	Xylene	3 minutes	
16	Xylene	3 minutes	
17	Mount coverslip with DPX	-	

2.2.3.2.1 Ochronosis scoring

To score the severity of ochronosis, the first coronal knee joint section, sectioned posterior to anterior, that encompassed the entire tibio-femoral joint (knee) containing all four joint quadrants (medial tibia, medial femur, lateral tibia, and lateral femur) was used as a representative section and stained with Schmorl's stain. The number of pigmented chondrons was recorded for each joint quadrant in the calcified articular cartilage and entheses of the femoral condyles where collateral ligaments attach, see Figure 2.2. This ochronosis scoring system was then adapted to the vertebral column; pigmented chondrons were counted in both the cranial and caudal endplates (then summed) either side of an IVD stained with Schmorl's stain, across 5 sections in the coronal plane. Scoring was carried out blind by two observers.

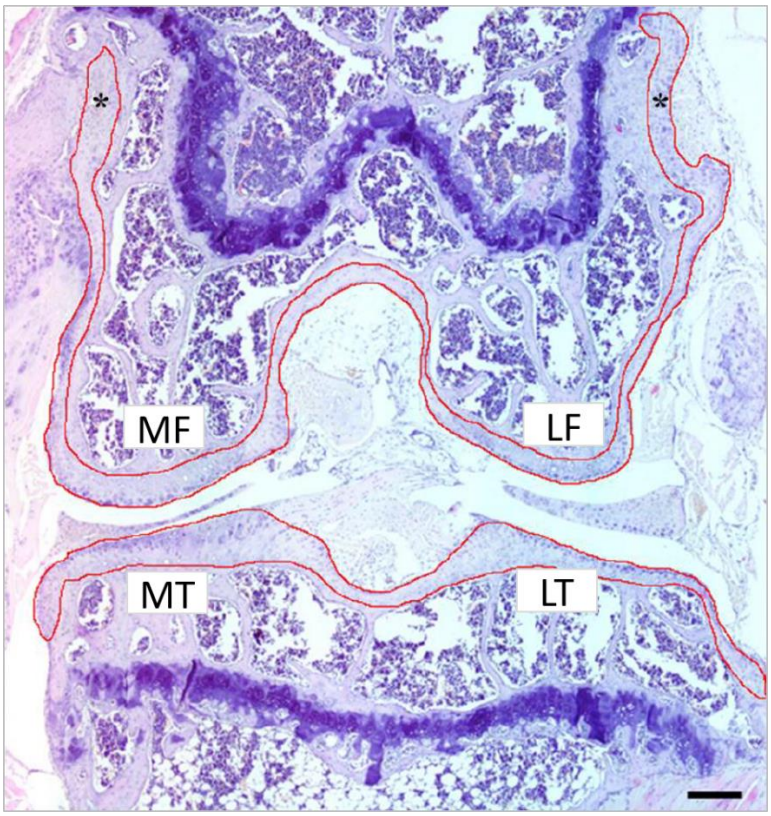

Figure 2.2. Areas of scoring ochronosis in the knee joint.
The red lines indicate the articular cartilage in the (tibio-femoral) knee joint where the number of pigmented chondrons were recorded in a representative section containing all four joint quadrants and the entheses of the femoral condyles (*). MT = medial tibia. LT = lateral tibia. MF = medial femur. LF = lateral femur. Haematoxylin & eosin stain. Scale bar = 50 µM. Image used with permission from Dr Craig Keenan [239].

2.2.3.3 Eosin

Eosin staining of paraffin sections was carried out according to Table 2.9. If the tissue had previously been *LacZ* stained, HistoClear was uses instead of xylene.

Table 2.9. Eosin staining of paraffin sections.

Step	Chemical	Duration	Notes
1	Xylene	2 minutes	HistoClear used if tissue was *LacZ* stained
2	Xylene	2 minutes	
3	100% ethanol	2 minutes	
4	90% ethanol	2 minutes	
5	70% ethanol	2 minutes	
6	Dip in running tap water	10 seconds	
7	Eosin Y (alcoholic)	2 minutes	
8	Dip in running tap water	10 seconds	
9	70% ethanol	30 seconds	
10	90% ethanol	30 seconds	
11	100% ethanol	30 seconds	
12	Xylene	30 seconds	HistoClear used if tissue was *LacZ* stained
13	Xylene	30 seconds	
14	Mount coverslip with DPX	-	

2.2.3.4 Nuclear fast red

Nuclear fast red staining of paraffin sections was carried out according to Table 2.10. If the tissue had previously been *LacZ* stained, HistoClear was uses instead of xylene.

Table 2.10. Nuclear fast red staining of paraffin sections.

Step	Chemical	Duration	Notes
1	Xylene	2 minutes	HistoClear used if tissue was *LacZ* stained
2	Xylene	2 minutes	
3	100% ethanol	2 minutes	
4	90% ethanol	2 minutes	
5	70% ethanol	2 minutes	
6	Dip in running tap water	10 seconds	
7	Nuclear Fast Red	2 – 4 minutes	Time dependant on intensity
8	Dip in running tap water	10 seconds	
9	70% ethanol	30 seconds	
10	90% ethanol	30 seconds	
11	100% ethanol	30 seconds	
12	Xylene	30 seconds	HistoClear used if tissue was *LacZ* stained
13	Xylene	30 seconds	
14	Mount coverslip with DPX	-	

2.2.3.5 Periodic acid Schiff/haematoxylin

Table 2.11 shows the protocol for paraffin section periodic acid Schiff/haematoxylin (PAS/H) staining. For frozen section PAS/H staining, slides were fixed in 10% formalin for approximately 20 minutes, rinsed with dH_2O then stained using the protocol in Table 2.11, commencing at step 7 (periodic acid). For PAS staining performed immediately after frozen section *LacZ* staining (section 2.2.5.6 below), slides were fixed in 10% formalin for approximately 20 minutes, rinsed with dH_2O then stained for PAS (Table 2.11), commencing at step 7 (periodic acid), without the haematoxylin counterstain (steps 12 and 13 omitted).

Table 2.11. PAS/H staining of paraffin sections.

Step	Chemical	Duration
1	Xylene	3 minutes
2	Xylene	3 minutes
3	100% ethanol	1 minute
4	90% ethanol	1 minute
5	70% ethanol	1 minute
6	Dip in tap water	5 seconds
7	0.5% periodic acid solution	10 minutes
8	Dip in running tap water	5 seconds
9	Rinse with distilled water	5 seconds
10	Schiff reagent	10 minutes
11	Wash in lukewarm tap water	5 minutes
12	Mayer's Haematoxylin	1 minute
13	Running tap water	5 minutes
14	70% ethanol	30 seconds
15	90% ethanol	30 seconds
16	100% ethanol	30 seconds
17	Xylene	30 seconds
18	Xylene	30 seconds
19	Mount coverslip with DPX	-

2.2.3.6 Safranin O fast green

Safranin O / fast green staining of paraffin sections was carried out according to Table 2.12.

Table 2.12. Safranin O / fast green staining of paraffin sections.

Step	Chemical	Duration
1	Xylene	10 minutes
2	Xylene	10 minutes
3	100% ethanol	2 minutes
4	90% ethanol	2 minutes
5	70% ethanol	2 minutes
6	Running tap water	1 minute
7	Harris Haematoxylin	30 seconds
8	Running tap water	5 minutes
9	0.2% fast green	10 minutes
10	1% acetic acid	20 seconds
11	1% acetic acid	20 seconds
12	Running tap water	10 seconds
13	0.5% safranin O	8 minutes
14	70% ethanol	2 minutes
15	90% ethanol	2 minutes
16	100% ethanol	2 minutes
17	Xylene	3 minutes
18	Xylene	3 minutes
19	Mount coverslip with DPX	-

2.2.4 Light microscopy

Histology slides were all examined using light microscopy. A Nikon Eclipse Ci microscope was used, with a Ds-Fi2 camera and NIS Elements Br software (version 4.13.04).

LacZ stained brain sections were imaged using light microscopy and stitched together using a using a Zeiss Axio Imager Z2 microscope and Zen Blue software.

2.2.5 *LacZ* staining

The *Hgd tm1a* mouse harbours a *LacZ* transgene between exons 5 and 6 of the modified *Hgd* gene that is transcribed before the gene is interrupted by the gene trap cassette. *LacZ* is a bacterial gene encoding the enzyme β-galactosidase, which will from a blue product when given the substrate X-gal (5-bromo-4-chloro-3-indolyl-β-D-galactopyranoside). By staining a tissue for the presence of *LacZ*, a blue colouration indicates the tissue is *LacZ* positive and therefore expresses *Hgd*.

2.2.5.1 Time-mated embryos

Mice were mated overnight and checked the next morning for signs of mating (a vaginal plug is usually observed). It is assumed that fertilization took place at night and that the embryos are half a day old by the morning (E0.5). The embryos were harvested a specific number of days after the plug was found, i.e. 11 days later would give E11.5 embryos.

The pregnant mother was culled by cervical dislocation in order to collect the time-mated embryos. The uterus was removed and immersed immediately in ice cold PBS until dissection. Embryos were removed from the uterus, and the yolk sac and placenta dissected away. Embryos were then used for *LacZ* staining, frozen sectioning or for mRNA collection. Embryos for frozen sectioning (for frozen *LacZ* staining) were fixed as for whole mount *LacZ* staining (see below), then placed into 30% sucrose until they sank. They were then embedded in OCT on dry ice and stored at -80°C until sectioning. Samples for mRNA (embryonic liver) were collected immediately after harvesting the embryos, and placed into either liquid nitrogen or RNA*later*, then stored at -80°C until mRNA isolation.

2.2.5.2 *LacZ* fix and stain solutions for embryos/whole tissues

X-gal fix solution: 50 ml

0.2% glutaraldehyde	400 µl of 25% solution
2% paraformaldehyde	12.5 ml of 8% solution
0.1 M Na Pi buffer at pH 7.4	5 ml of 1 M stock
5 mM EGTA (pH 8.0 with NaOH)	2.5 ml of 0.1 M stock
2 mM $MgCl_2$	100 µl of 1 M stock

Top up to 50 ml with dH_20

X-gal rinse solution: 1L

0.1 M Na Pi Buffer pH7.4	100 ml of 1 M stock
2 mM $MgCl_2$	2 ml of 1 M stock
0.1% sodium deoxycholate	1 g
0.2% NP40	2 ml

Top up to 1 L with dH_20

X-gal stain solution: 100 ml

5 mM potassium ferricyanide	165 mg (mw 329.2)
5 mM potassium ferrocyanide	211 mg (mw 422.4)
1 mg/ml X-gal	4 ml of 25 mg/ml stock (add fresh)

100 ml X-gal rinse solution

(Store wrapped in foil)

X-gal stock: 25 mg/ml

1 g X-gal (≥98.0%, VWR, 437132J, US)

40 ml N,N-dimethylformamide

2.2.5.3 *LacZ* staining of embryos

The procedure for *LacZ* staining time-mated embryos was as follows:

1. After separation from the placenta and yolk sac, embryos were fixed (X-gal fix) on ice at 4°C, using Table 2.13 as a guide for fixation time.

2. The fix solution was discarded and the embryos washed 3 times for 30 minutes in X-gal rinse, whilst rotating at room temperature.
3. X-gal substrate was then added to the prepared X-gal stain solution (X-gal always added fresh) to obtain a final concentration of 1 mg/ml X-gal. For example, 10 ml stain solution has 400 µl of 25 mg/ml X-gal.
    a. Embryos were immersed in X-gal stain solution, wrapped in foil (staining must be carried out in the dark) and stained overnight whilst rotating at room temperature.
4. After staining, 3 x 30-minute washes of the embryos were carried out in X-gal rinse solution, at room temperature whilst rotating.
5. Images were taken if required of the embryos (in a dish with PBS) using an Olympus SZX12 dissection microscope equipped with a QCapture camera and software (version 2.8.0, QImaging, Canada).
6. Embryos were then fixed overnight in 10% formalin.
7. Transferred to 70% ethanol.
8. If required, embryos were then processed for paraffin wax embedding using the soft tissue processing program (Table 2.6).

Table 2.13. Fixation times for time-mated embryos to be stained with *LacZ*.

Embryo Age	Fixation time	Notes
E7.5 – E8.5	10 minutes	
E8.5 – E9.0	20 minutes	
E9.5	30 minutes	
E10.0 – E11.5	45 minutes	
E12.5	1 hour	
E13.5	1.5 – 2 hours	
E14.5	2.5 hours	
E15.5	3 hours	Embryos aged E15.5 and over need to be opened by an incision through the abdomen and thorax to allow fix solutions to penetrate through skin that has begun to form
E16.5 – E17.5	4 hours	

2.2.5.4 *LacZ* staining of adult tissues

Adult tissues were *LacZ* stained by the same method used for embryos (section 2.2.5.3), with soft tissue fixation times adjusted relative to the size of embryos. Bones were cut to expose the stain solution to the medullary cavity of the bone. Bones were fixed for 4 hours prior to *LacZ* staining.

2.2.5.5 Frozen section *LacZ* fix and stain solutions

Frozen X-gal fix solution: 100 ml

0.2% glutaraldehyde 800 µl of 25% stock

100 ml PBS

Frozen X-gal stain solution: 100ml

0.1 M NaPi	10 ml of 1 M stock
2 mM $MgCl_2$	200 µl of 1 M stock
0.01% sodium deoxycholate	0.01 g
0.02% NP40	20 µl stock
5 mM potassium ferricyanide	165 mg (mw = 329.2)
5 mM potassium ferrocyanide	211 mg (mw = 422.4)
1 mg/ml X-gal	4 ml of 25 mg/ml stock (added fresh)

Top up to 100 ml with dH_2O

2.2.5.6 Frozen section *LacZ* staining

Embryos and adult tissues were harvested and fixed as for whole mount *LacZ* staining (2% PFA, 0.2% glutaraldehyde). Tissues were then placed in 30% sucrose until they sunk, embedded in OCT on dry ice and stored at -80°C until cryo-sectioning. Frozen sections were then stored at -20°C until staining. The frozen section *LacZ* staining protocol is as follows:

1. Fix slides on ice in 0.2% glutaraldehyde in PBS for 10 minutes if not fixed before cryo-embedding. Samples not fixed with this step if fixed prior to cryo-embedding.
2. 5 minutes wash in cold PBS (1).
3. 5 minutes wash in cold PBS (2).
4. 5 minutes wash in cold PBS (3).
5. Immerse slides in frozen X-gal stain in the dark at 37°C for a 2-3 hours, or at room temperature overnight.
    a. Embryos were stained overnight at room temperature.
    b. After optimization, adult liver and kidney were stained at 37°C for 2 hours.
6. After staining, rinse slides with PBS (use Pasteur pipette).
7. Fix slides in formalin (10%) for 20-30 minutes.
8. Rinse slides with PBS (use Pasteur pipette).
9. Rinse slides with distilled water (use Pasteur pipette).

a. If not counterstaining, coverslip with an aqueous mounting agent or dehydrate (70%, 90% and 100% ethanol), clear (HistoClear, not xylene) and mount with DPX.

10. Counterstain with eosin (aqueous) or nuclear fast red.
11. Dip in running tap water.
12. Coverslip with an aqueous mounting agent or dehydrate (70%, 90% and 100% ethanol), clear (HistoClear, not xylene) and mount with DPX.

2.3 Mouse studies

All mice were housed and maintained within the University of Liverpool Biomedical Services Unit (BSU) in specific pathogen-free conditions in accordance with UK Home Office Guidelines. Food and water were available *ad libitum*. Under the Animal (Scientific Procedures) Act 1986, Juliette Hughes held a personal licence (PIL 42023) allowing experiments and procedures to be carried out under two project licence holders; Professor George Bou-Gharios (PPL 70/9047) and Professor Jonathan Jarvis (PPL 40/3743, PA693D221).

2.3.1 Urine and Blood Collection

Urine samples of volumes <50 µl were acidified using 5% v/v 1 M H_2SO_4 and volumes >50 µl with 1% v/v 5 M H_2SO_4. Acidified urine was stored at -80°C until analysis via HPLC tandem mass spectrometry [46]. Venous tail bleed samples were collected by a small incision made into one of the lateral tail veins in lithium heparin microvettes (CB 300 LH, Sarstedt, UK) and kept on ice until processed. Whole blood was centrifuged at 1500 g for 10 minutes at 4°C and the plasma supernatant acidified using 10% v/v 5.8M perchloric acid and vortexed. The acidified plasma was then centrifuged at 1500 g for 10 minutes at 4°C, the supernatant removed (leaving behind a protein pellet) and stored at -80°C until analysis analysed via HPLC tandem mass spectrometry [47].

The amount of blood that can be withdrawn at any one time must be calculated to be within Home Office guidelines. A mouse has approximately 75 ml/kg blood (LASA Good Practice Guidelines), with a 25 g mouse having approximately 1.8 ml blood. Tail bleeding must include room for error as the bleeding site may not stop instantly (pressure is applied until bleeding stops). Therefore, 65 ml/kg was used here as an estimation of total blood volume for calculating bleed sizes, as also recommended by the LASA Good practice guidelines. A maximum of 10% of the total blood volume may be taken at any one time (≈160 µl per 25 g

mouse) and a maximum of 15% (≈240 µl per 25 g mouse) across a month across multiple bleeds.

2.3.2 *Hgd tm1d* liver-specific *Hgd* knockout

To remove the floxed 6th *Hgd* exon in *Hgd tm1d (fl/fl) MxCre* +/- mice, two intraperitoneal injections of polyinosinic: polycytidylic acid (pIpC, GE Healthcare: Poly(I).Poly(C), double strand, sterile, 27-4732-01) were given, initially at 10 µg/g body weight [237], see section 4.3. Injections of pIpC were mainly carried out by Dr Ke Liu. The initial pIpC stock solution was 5 mg/ml in sterile PBS, which was diluted 1 in 10 to 500 µg/ml in sterile PBS prior to injection. To obtain 10 µg/g body weight, injection volume was calculated for each mouse; a 25 g mouse would receive 500 µl of 500 µg/ml for example. A short-term and long-term study investigated the effect of two 10 µg/g body weight pIpC injections. A dose response study was then carried out, using diluted pIpC to obtain doses ranging from 3.33 µg/g to 0.01 µg/g body weight pIpC.

Hgd tm1a -/- mice were injected with pIpC (highest dose used in the experiment) as AKU controls and wildtype controls were either *Hgd tm1d (fl/fl) MxCre* WT mice injected with pIpC (highest dose used in the experiment) or *Hgd tm1d (fl/fl) MxCre* +ve mice injected with PBS. To assess the resulting phenotype, HGA was measured in plasma and urine samples collected pre-injection and at time points post-injection. Liver and kidney *Hgd* mRNA were analysed from all mice. In the long-term study, knee joints were collected for ochronosis scoring (see section 2.2.3.2.1).

2.3.3 Isotopic HGA injection

Hgd tm1a -/- (n=4) and *Hgd tm1a -/+* (n=4) mice were injected with $^{13}C_6$-HGA into the lateral tail vein, adjusted to body weight to achieve a final blood concentration of approximately 1 mmol/L. Injections were carried out by Dr Hazel Sutherland assisted by BSU technical staff. Venous tail bleeds were collected at various time points post-injection from 2-60 minutes. The whole procedure of injections and bleeds was carried out under isoflurane anaesthesia (0.8 L O_2, with up to 2% isoflurane to effect). Whole blood was centrifuged and the supernatant removed and immediately frozen.

Non-targeted metabolic flux analysis was performed to trace metabolism of $^{13}C_6$-HGA. Metabolic profiling was performed using a published mass spectrometric technique [218]. Briefly, plasma was diluted 1: 9 plasma: deionised water and HPLC performed on an Atlantis

dC18 column (3x100 mm, 3 µm, Waters, UK) coupled to a 6550-quadrupole time-of-flight (Q-TOF) mass spectrometer (Agilent, UK). An accurate-mass compound database with potential association to HGA was generated for data mining using Agilent Pathways to PCDL. Data were mined for these compound targets with an accurate mass window of ±5 ppm using 'batch isotopologue extraction' in Profinder (build 08:00, Agilent). Isotopologue extraction investigates association with the injected $^{13}C_6$-HGA by examining the relative abundances of the M+0 – M+6 isotopologues for compound targets.

2.3.4 Nitisinone treatment in mice

Mice received nitisinone in the drinking water at a concentration of 4 mg/L, which was freely available. For a 30 g mouse drinking approximately 6 ml/day, this equates to 0.8 mg/kg nitisinone.

2.3.5 Dietary restriction studies

To investigate the effect of tyrosine and phenylalanine dietary restriction on nitisinone-induced tyrosinaemia, BALB/c *Hgd*$^{-/-}$ AKU mice (groups of n=6; 3 male, 3 female) were treated with nitisinone for 1 week on a normal diet, then switched to either tyrosine/phenylalanine free or phenylalanine-only free diets with phenylalanine supplemented into the drinking water, whilst still on nitisinone. Controls remained on normal diet whilst still on nitisinone. Acidified plasma was collected pre-nitisinone, post-nitisinone and then during dietary restriction.

2.3.5.1 Diets

The normal control mouse diet (CRM(P), product code 801722, Special Diet Services (SDS), UK), contained 0.88% phenylalanine and 0.59% tyrosine. Restricted diets were synthetically made by SDS in pellet form. Synthetic raw materials were used to produce an amino acid defined diet which has an amino acid profile similar to the normal CRM(P) diet, with tyrosine and/or phenylalanine removed and balanced with maize starch.

2.3.5.2 Nitisinone and phenylalanine provision in the drinking water

Nitisinone was added to the drinking water at 4 mg/L. Phenylalanine was added to the drinking water at various doses (0-5 mg). Drinking water was freely available. Tyrosine supplementation in the drinking water was not investigated due to water insolubility.

2.4 Mass spectrometry

Analysis of tyrosine pathway metabolites (phenylalanine, tyrosine, HGA, HPPA and HPLA) in both urine and plasma samples was performed on an Agilent 6490 triple quadruple LC-MS/MS with Jet-Stream electrospray ionization (ESI-MS/MS) equipped with an Agilent 1290 infinity II Ultra High-Performance Liquid Chromatography pump and autosampler. Chromatographic separation of the sample was performed using an Atlantis C18 column (100 mm x 3.0 µm, 3 µm) (Waters, UK). Matrix-matched calibration standards were used to form a calibration curve used for quantification of metabolites.

2.4.1 Sample preparation

Samples, stored at -80°C until analysis, were defrosted and centrifuged at full speed for 5 minutes to ensure that any residual protein/debris/residue formed a pellet. 10 µl of the supernatant was pipetted into a 10 ml glass tube and diluted in 10 ml of the internal standard solution containing isotopically-labelled $^{13}C_6$-HGA, d_4-tyrosine, d_5-phenylalanine, with 0.1% formic acid in dH_2O. Samples <10 µl were diluted 1 in 1000 using smaller volumes, for example 5 µl in 5 ml. Tubes were capped and inverted to mix the sample. 1 ml of this solution was then pipetted into 2 ml mass spec vials (VI-03-12-01L, Chromatography Direct, UK) and capped or 500 µl pipetted into a 96 well plate (186002481, Waters, UK), which is heat sealed. The vials or plate were then loaded into the auto sampler. The samples, calibrators and quality control samples were prepared in an identical way and injected from the same type of container (i.e. vial or plate) within each analysis.

2.4.2 Plasma metabolite analysis

2 µl of the prepared plasma sample was injected into the HPLC system with a total run time of 7.0 minutes. Initial gradient conditions were 80:20 water: methanol with 0.1% formic acid (v/v) increasing linearly to 10:90 in 2.5 minutes. The mobile phase was maintained for a further 1.1 minutes, increased to 100% methanol for 1 minute and then returned to starting conditions (flow rate 0.4 ml/min). The column was reconditioned for 2 minutes prior to the next injection.

2.4.3 Urine metabolite analysis

2 µl of the prepared urine sample was injected into the HPLC system with a total run time of 7.0 minutes. The same chromatographic conditions were used as for plasma metabolite analysis (section 2.4.2) with a flow rate maintained at 0.6 ml/min.

2.4.4 Metabolite quantitation

For quantitative analysis, Mass Hunter software was used to process the data. For a more detailed description see Hughes et al., 2014 for the urine method [46] and Hughes et al., 2015 for plasma/serum method [47].

2.4.5 *In vitro* experiments

To measure tyrosine/phenylalanine in TAL/PAL *in vitro* experiments, the plasma metabolite method (section 2.4.2) was altered to measure only tyrosine and/or phenylalanine, using calibrators that were matrix-matched to the sample. The same sample preparation and HPLC mass spectrometry conditions were used.

2.5 RNA extraction and qPCR

2.5.1 Sample collection and RNA extraction

Fresh samples were either snap-frozen in liquid nitrogen or placed in RNA*later* RNA stabilization reagent (Qiagen) overnight in the fridge at 4°C, then the liquid removed and the sample stored at -80°C until needed. RNA was extracted using the Qiagen RNeasy Mini Kit and protocol. Samples were reconstituted in 30-50 µl RNase-free H_20. All samples were treated with DNase (RNase-Free DNase set, Qiagen).

Fresh RNA was immediately quantified using the Nanodrop™ 2000 (ThermoFisher Scientific). The concentration was recorded (µg/µl) as well as the 260/280 and 260/230 ratios to check purity/contamination. Synthesis of cDNA was carried out immediately from the fresh RNA, and if not used straight away, stored at -80°C.

2.5.2 cDNA synthesis

Reverse transcription of RNA to produce cDNA was carried out using the Applied Biosystems RNA-to-cDNA kit. 1 µg of RNA was loaded into the reaction mixture with water adjusted to make up the correct volume, see Table 2.14. For example, 1 µl of 1 µg/µl RNA would be used with 8 µl water. The final concentration of RNA in the reaction mixture is 50 ng/µl. The amplification conditions for cDNA synthesis are shown in Table 2.14. After synthesis, cDNA is diluted 1 in 10 (20 µl reaction in 180 µl) in nuclease-free H_20, then stored at -20°C.

Table 2.14. Reaction mixture for cDNA synthesis from RNA and the amplification conditions.

Reaction Components	**Volume (µl)**		**Amplification conditions**		
2x RT Buffer	10		1	37°C	60 mins
20x Enzyme Mix	1		2	95°C	5 mins
RNA	9 (total 1 µg RNA)		3	4°C	∞
Nuclease-free H_20					
	Total: 20 µl				

2.5.3 qPCR reaction

Quantitative PCR (qPCR) was performed with a Bio-Rad CFX Connect™ Real-Time System, using Bio-Rad 96 well Hard-Shell PCR plates, sealed with Bio-Rad optical tape. Bio-Rad iQ™ SYBR® Green Supermix was used for the reaction mixture; see Table 2.15 for the reaction mixture and amplification conditions. Samples were run in triplicate. A non-template control for each reaction mixture was run for each plate (reaction mixture, with water substituted in place of cDNA).

Table 2.15. Reaction mixture and amplification conditions used for qPCR.

Reaction Components	**Volume (µl)**		**Amplification conditions**			
SYBR green	7.5		1	95°C	3 mins	
Forward primer (5 µM)	1		2	95°C	30 secs	
Reverse primer (5 µM)	1		3	60°C	30 secs	plate read
Nuclease-free H_20	3.5		4	GOTO step 2, x39		
cDNA	2		5	95°C	10 secs	
	Total: 15µl		6	65°C to 95°C, increments of 0.5°C	5 secs for each increment	Melt curve. Plate read

2.5.4 qPCR primer design

The NCBI Primer-BLAST (Primer Basic Local Alignment Search Tool) online primer tool was used to design specific primers (https://www.ncbi.nlm.nih.gov/tools/primer-blast/), which utilises the Primer3 (http://bioinfo.ut.ee/primer3/) tool to design the primers for a specific gene and then uses BLAST to screen the primers against the whole genome of interest, in this case *Mus musculus*. Primer specifications were: 100-150bp product size, 18-22bp primer size, 58-62°C primer Tm (melting temperature) and 20-50% primer GC% content. DNA mfold (http://unafold.rna.albany.edu/?q=mfold/DNA-Folding-Form) was then used to look for secondary structures within the PCR product that the chosen primers will amplify, such as hairpin loops. The criteria for this search was: linear sequence type, 58-62°C folding temperature, and ionic conditions of 50 mM Na^+ and 3 mM Mg^{2+}. Beacon Designer (http://www.premierbiosoft.com/qOligo/Oligo.jsp?PID=1) was then used to check to see if the chosen primers dimerize with each other or create other structures. The search criteria were 500 nm nucleic acid, 50 mM mono ion and 3 mM free Mg^{2+}.

Once designed, primers were purchased from ThermoFisher Scientific as a lyophilized powder, see Table 2.16 for sequences. Primers were reconstituted to 100 µM in 1x TE buffer for storage at -20°C, then diluted 1 in 20 (nuclease-free H_20) to give a working concentration of 5 µM. The final concentration of the primers in the reaction mixture (1 in 15 dilution) was 333 nM.

Table 2.16. Primer sequences used for qPCR.

Name	Forward sequence	Reverse sequence	Notes
*Hgd*1	5'- TGTCCACGGAACACCAATAA-3'	5'- GCCAACTTCATCCCAGTTGT-3'.	spanning exons 3-4
*Hgd*2	5'-GACCCATCGGAGCAAATGGC-3'	5'-AGTGTAACCACCTGGCACTC-3'	spanning exons 9-10
18S	5'- GAAAATAGCCTTCGCCATCA -3'	5'-AGTTCTCCAGCCCTCTTGGT-3'	

2.5.5 Calculating primer efficiency

In order to test the primers for qPCR (*Hgd*1, *Hgd*2 and *18S*), the standard qPCR reaction, as shown in Table 2.15, was used with the primers with a range of cDNA concentrations. The primers were tested using a serial dilution of WT liver cDNA, with dilutions of 1/10, 1/50, 1/250, 1/1250, 1/6250, 1/31,250 (dilution factor of 5) and a non-template control (no cDNA), all in triplicate. The mean Ct (cycle threshold) value, the number of cycles required for the fluorescent signal to reach the threshold exceeding background levels, for each cDNA dilution

was plotted to produce a graph with a straight line for each primer. The R^2 value should be >0.980 (Bio-Rad Laboratories, Inc. Real-Time PCR Applications Guide, 2006). The R^2 for *Hgd*1, *Hgd*2 and *18S* was 0.9995, 0.9990 and 0.9993 respectively. The gradient of the slope was then used to calculate the efficiency of the primer using the following equation:

Efficiency = $100 \times n^{(-1/\text{gradient})} - 1$ (n = dilution factor, in this case 5)

The resulting efficiency must be in the range of 90-105% for the primers to be acceptable (Bio-Rad Laboratories, Inc. Real-Time PCR Applications Guide, 2006). The efficiencies calculated for *Hgd*1, *Hgd*2 and *18S* primers were 98.9%, 95.8% and 98.4% respectively.

2.5.6 Calculating relative gene expression

To calculate relative gene expression, the Ct values obtained from the qPCR were used. For each sample triplicate, mean Ct was calculated for the gene of interest and the housekeeping gene. Delta Ct (ΔCt) was then calculated (gene of interest Ct – housekeeping gene Ct). Relative expression was then calculated as $2^{(-\Delta Ct)}$.

2.6 PAL and TAL

2.6.1 *In vitro* PAL assay

Phenylalanine ammonia lyase (PAL) from *Rhodotorula glutinis* (yeast) was purchased from Sigma, UK (P1016) as a Grade I buffered aqueous glycerol solution. PAL was supplied in international enzymes units (U), with Sigma stating that 1U of PAL will deaminate 1.0 µmol/minute of L-phenylalanine to trans-cinnamic acid and NH_3 (ammonia) at pH 8.5 at 30°C. 1 mM stock solutions of L-tyrosine (Sigma, UK; T8566) (with tyrosine initially dissolved at 1 M in 5 M H_2SO_4) and L-phenylalanine (Sigma, UK; P5482) were prepared in 50 mM Tris-HCl (pH 8.5). These stock solutions were then used to prepare the working solutions (10-500 µmol/L) in an Eppendorf, combining the required amount of tyrosine or phenylalanine stock solution and PAL enzyme (either 0.01 or 0.1 U; added last when experiment is initiated), with a total volume of 1 ml made up with 50 mM Tris-HCl.

To begin the assays, PAL enzyme was added to each Eppendorf, gently vortexed and placed in a 30°C water bath. 50 µl aliquots of each experimental condition were taken at various time points, ranging from 0-24 hours. The aliquot was immediately acidified with 5 µl 5.8 M perchloric acid (10% v/v) to stop the enzymatic activity and to deproteinise the sample. The acidified samples were then centrifuged at full speed for 5 minutes, and the supernatant

removed and stored at -20°C until analysis. Tyrosine and phenylalanine were analysed by mass spectrometry, using matrix-matched tyrosine and phenylalanine calibrators made up in 50 mM Tris-HCl, see section 2.4.5.

2.6.2 TAL expression and purification

A pETDuet:Tal expression vector containing a synthetic, codon optimised *Rhodobacter capsulatus* TAL gene was obtained from The Protein Expression Facility, Manchester Institute of Biotechnology, University of Manchester, UK. Codon optimisation involves synonymous substitution mutations so that the same amino acid is encoded, with codons preferentially used by the host expression organism, in order to favour efficient soluble protein expression [240]. Chemically competent *Escherichia coli* JM109(DE3) bacteria (Promega, UK; P9801) was used for TAL protein expression.

Dr Peter Wilson carried out the transformation and expression of pETDuet:Tal in addition to the purification of the TAL protein, SDS-PAGE gel and protein quantitation procedures, all described below.

2.6.2.1 Transformation and expression of pETDuet:Tal

To transform the bacteria with the expression vector and to induce TAL protein expression, the following steps were carried out:

1. 0.5 µl pETDuet:Tal plasmid added to 100 µl competent JM109(DE3) cells then mixed by flicking the tube (not vortexed) and left on ice for 15 minutes.
2. The bacteria were then heat shocked at 42°C for 50 seconds and then placed on ice for 2 minutes.
3. 900 µl of LB broth was then added to the bacteria, which were then incubated for 1 hour at 37°C whilst shaking at 200 rpm.
4. 100 µl of the bacteria culture were then spread onto an LB agar plate containing 100 µg/ml ampicillin, air dried for 5 minutes and left overnight at 37°C, upside down.
    a. Bacterial colonies that have grown on the plate will have successfully been transformed with the pETDuet:Tal vector, as it has an ampicillin resistance gene.
5. A single colony was then selected to inoculate 30 ml selective LB broth containing 100 µg/ml ampicillin and grown over night at 37°C, shaking at 200 rpm.

6. 10 ml of this culture was then removed and added to 1 L of selective LB broth at 37°C, shaking at 200 rpm, until the cells reached an optical density (OD) of 0.6 at OD_{600}, measured using a spectrophotometer.
7. Protein expression was then induced with 0.2 mM IPTG (isopropyl β-D-1-thiogalactopyranoside), and grown for 20 hours at 25°C, at 200 rpm.
8. The culture was then spun at 4000 rpm, for 10 minutes, at 4°C, in 4 x 50 ml falcon tubes. This was repeated in the same tubes using all of the remaining culture.
    a. The cell pellets were then snap-frozen in liquid nitrogen and stored at -80°C.

2.6.2.2 Purification of TAL

To isolate and purify the TAL enzyme from the bacterial pellets, the following procedure was carried out.

1. 1 x 50 ml falcon tube containing the pellet of bacteria from the expression of TAL protein was thawed on ice.
2. The cell pellet was then re-suspended in 7.5 ml of lysis buffer (Buffer 1 (25 mM Tris-HCl pH 8.0, 300 mM NaCl, 10% glycerol) with 1:1000 proteinase inhibitor cocktail and 5 mM imidazole and 1% Triton X-100).
    a. An alternative lysozyme extraction method was also used. The cell pellet was re-suspended in 7.5 ml buffer 1 with 1:1000 proteinase inhibitor cocktail, 1% Triton X-100 and 2 mg lysozyme (imidazole left out as it inhibits lysozyme). The sample was gently mixed on a rocking platform for 30 minutes at 4°C. The sample was then clarified as stated in step 3, without the sonication, and then the rest of the purification procedure followed as below.
3. The sample was then sonicated 7 times for 30 seconds on ice at an amplitude of 6 microns, resting on ice in between to ensure the sample remained cold, and then clarified at 10,000 g for 30 minutes at 4°C.
    a. The supernatant, referred to as soluble fraction, was then taken for purification and kept on ice.
    b. The insoluble fraction (pellet) was frozen at -80°C.
4. 1 ml of the Ni-NTA (nickel-nitrilotriacetic acid) slurry (0.5 ml bead volume) (Ni-NTA agarose; 157049819, Qiagen, Germany) was prepared for purification of the supernatant, by briefly centrifuging in a 15 ml falcon tube, then the supernatant

removed. Lysis buffer (2 ml) was then added to the beads left in the tube, mixed and briefly centrifuged, then the supernatant removed.

5. The bacterial cell lysate supernatant, approximately 7.5 ml from step 3a, was then added to the Ni-NTA beads and mixed gently on a rotary shaker at 4°C for 1 hour.
6. This lysate-Ni-NTA mixture was then loaded into an empty PD10 column (17-0851-01, GE Healthcare), the cap removed and the flow through collected.
    a. At this stage, the TAL protein is bound to the Ni-NTA beads within the column via a His tag.
7. The column was then washed twice with 2.5 ml wash buffer (buffer 1 + 50 mM imidazole), and each wash fraction collected.
8. Bound TAL protein was then eluted with 2.5 ml elution buffer A (buffer 1 + 250 mM imidazole).
9. The eluted protein was then buffer exchanged using a PD10 desalting column (17-0851-01, GE Healthcare), to obtain a desalted fraction.
    a. The column was equilibrated with 25 ml elution buffer B (25 mM Tris-HCl pH 7.5, 150 mM NaCl, 10% glycerol) and the flow through discarded.
    b. Elute containing the TAL protein (2.5 ml) was added to the column, allowed to enter the packed bed completely, then the flow through discarded.
    c. The TAL protein was then eluted with 3.5 ml elution buffer B and the flow through collected.

2.6.2.2.1 SDS-PAGE gel protein visualisation

TAL protein purification was assessed by analysis of samples from each step of the process by SDS-PAGE (sodium dodecyl sulfate – polyacrylamide gel electrophoresis). 6.5 µl of each sample was added to 2.5 µl NuPAGE®LDS sample buffer (4X) and reduced with 1 µl NuPAGE® reducing agent (10X), heated at 70°C for 10 minutes before loading onto a NuPAGE® Bis-Tris 4-12% Mini Gel (IM-8042, Invitrogen, UK) and run for 55 minutes at 200 volts in NuPAGE™ MOPS SDS running buffer (NP00102, Invitrogen, UK) with 500 µl NuPAGE® antioxidant in the upper buffer chamber**.** 5 µl of a Full Range GE Healthcare Rainbow™ Molecular Weight Marker (11580684, FisherScientific) and 5 µl of a Novex™ Sharp Unstained Protein Standard (LC5801, ThermoFisher, UK) was used to identify the TAL protein. To visualise the protein bands, the gel was immersed in a 0.25% Coomassie Brilliant Blue R250 stain solution (0.25 g Coomassie Blue in 100 ml made up with 90 ml methanol: H_2O (1:1 v/v) and 10 ml glacial acetic acid) for 1 hour on a rocking platform at room temperature. The gel was then de-stained (de-

stain solution: 100 ml made up with 90 ml methanol: H_2O (1:1 v/v) and 10 ml glacial acetic acid) by immersion in de-stain solution for 1 hour, on a rocking platform at room temperature, repeated 2-3 times with fresh de-stain solution until the protein bands were visible. The gel was then photographed.

2.6.2.2.2 Protein quantitation

In order to quantify the amount of TAL protein purified, a Pierce™ BCA (bicinchoninic acid) protein assay kit (23225, Thermo Scientific, UK) and protocol was followed. The reaction involves the reduction of Cu^{2+} to Cu^{1+} by protein in an alkaline medium, followed by the chelation of 2 BCA molecules with 1 Cu^{1+} ion that produces a purple coloured reaction that exhibits strong linear absorbance at 562 nm with increasing protein concentration.

Briefly, the working reagent is prepared and mixed (50:1, Reagent A: B), and then mixed with albumin protein standards at known concentrations and unknown samples (TAL protein) (25 µl sample + 200 µl working reagent) and then incubated at 37°C for 30 minutes and then left to cool to room temperature. A spectrophotometer, set at 562 nm, was then used to measure the absorbance of the samples. A standard curve of absorbance was plotted against concentration (µg/µl), and used to determine the protein concentration of the unknown TAL samples.

2.6.2.3 *In vitro* TAL experiments

In vitro assays of the purified TAL enzyme were carried out using 2 mM TAL protein (unless otherwise stated) and 100 µmol/L L-tyrosine (Sigma, UK; T8566) (with tyrosine initially dissolved at 1 M in 5 M H2SO4 and then diluted using Tris-HCl) made up to 1 ml in 25 mM Tris-HCl (pH 8.5). The activity of TAL at different pH's was tested, using 25 mM Tris-HCl buffer at pH 1.5, 4.5 and 8.5. The assays were carried out at 37°C. 50 µl aliquots of each experimental condition were taken at various time points, ranging 0-24 hours. The aliquot was immediately acidified with 5 µl 5.8 M perchloric acid (10% v/v) to stop the enzymatic activity and to deproteinise the sample. The acidified samples were then centrifuged at full speed for 5 minutes, and the supernatant removed and stored at -20°C until analysis. Tyrosine was analysed by mass spectrometry, using matrix-matched tyrosine calibrators made up in 25 mM Tris-HCl pH 8.5, see section 2.4.5.

2.7 Statistical analysis

Statistical analysis was performed using Stats Direct 3 (UK) and GraphPad Prism 6 (USA). Significance is denoted as $p<0.05$ *, $p<0.01$ ** and $p<0.001$ ***. Error bars represent standard error of the mean (SEM). In order to see if there was a statistical difference between groups, various statistical tests were used:

- When comparing the means of two separate or unrelated samples/groups, a two-tailed unpaired t-test was used. This analysis was used to determine if significant differences were observed in Figure 3.13 (number of pigmented chondrons in the tail versus lumbar spine), in Figure 3.22 (OARSI scores for each joint quadrant between *Hgd tm1a -/-* and *-/+* mice) and in Figure 5.2 (tyrosine concentration in untreated mice versus nitisinone-treated mice).
- To compare the mean metabolite concentration in mice pre- and post-treatment, a two-tailed, paired t-test was used as the samples were from the same mice pre- and post- treatment. This analysis was used in Figure 3.25 (average metabolite level pre- and post- nitisinone in *Hgd tm1a -/-* mice) and Figure 5.1 (average metabolite level pre- and post- nitisinone in BALB/c $Hgd^{-/-}$ mice).
- When comparing the mean of 3 or more groups, one-way ANOVA was used to test for statically significant differences. Where ANOVA detected significant differences, a post-hoc multiple comparisons test was used to determine the significant pairwise differences between means.
    - Where group sizes were equal, one-way ANOVA was followed by a Tukey post hoc test. This analysis was used in the dietary restriction studies in Figure 5.3, Figure 5.4, and Figure 5.5, (differences in metabolite levels between the groups at each post-dietary restriction time point, in addition to comparing body weight changes between the groups), in Figure 5.6 (difference in metabolite level at three time points), and in Figure 5.7 (body weight changes between different dietary conditions).
    - Where group sizes were unequal, one-way ANOVA was followed a Tukey Kramer post hoc test. This analysis was used in Figure 3.6 (mean HGA concentration in different genotypes).

3 Results:

Generation and phenotyping of a targeted mouse model of alkaptonuria

3.1 Introduction

An existing HGD deficient AKU mouse model, BALB/c *Hgd*$^{-/-}$, created by ENU mutagenesis [86] has previously been shown to exhibit an AKU phenotype [115,116]. This mouse has been shown to have increased HGA in the plasma, and ochronosis of the knee joint presenting as pigmentation of individual chondrons within the calcified articular cartilage. This mouse has proven to be a useful model for studying both the pathological effects of AKU and the effectiveness of treatments. However, due to the high mutation efficiency of ENU mutagenesis, this ENU AKU model could potentially possess other unknown mutations in the genome [197], that could affect the phenotype. In addition to the mutagenic strategy used to generate the BALB/c *Hgd*$^{-/-}$ mouse, this model has no further tools such as a reporter gene or the presence of site-specific recombinase sequences to allow further manipulation of the model. More modern techniques now exist to generate targeted and specific mouse models that allow multiple alleles to be generated.

Here in this chapter, a new mouse model of AKU (*Hgd tm1a*) has been generated using a knockout-first strategy, whereby the *Hgd* gene is specifically disrupted by gene targeting, using a gene trap. This strategy ensures that no other potentially confounding mutations are present in the genome. Additionally, the gene trap cassette used to disrupt the gene contains a *LacZ* reporter gene which has been used for localising *Hgd* gene expression and contains site-specific recombinase sites that allow the generation of a conditional allele (both presented in the next chapter), both of which were unavailable in the ENU mutagenesis AKU model. The generation and phenotyping of this new *Hgd tm1a -/-* AKU model is presented in this chapter, reporting both the metabolic nature and joint pathology characteristics of AKU, including comparisons with the mutagenesis model.

3.2 Generation of conditionally targeted mouse model of alkaptonuria

3.2.1 Establishment of the conditionally targeted *Hgd* colonies

Two murine ES cell lines, clones *Hgd* C10 and C11, were obtained from the UC Davis KOMP repository, containing a modified *Hgd* allele. They were grown on G418-resistant primary embryonic fibroblast feeder cells, as described [234]. The *neo* gene within the gene trap cassette (see Figure 3.1A) allowed G418 antibiotic selection of healthy ES colonies, see Figure 3.2. The selected ES cells were then injected into blastocysts of C57BL/6 at the blastula stage, into the blastocoel cavity close to the inner cell mass (Figure 3.3). The modified blastocysts were then transferred into pseudopregnant recipient females. Chimeric offspring were then identified

by the presence of the non-*agouti* grey coat colour (C57BL/6N-A^{tm1Brd}), see Figure 3.4. Further breeding confirmed that only C10 chimeras achieved germline transmission of the modified allele. C10 mice were subsequently bred to homozygosity, using C57BL6/J and referred to as *Hgd tm1a* either as homozygous (-/-) or heterozygous (-/+).

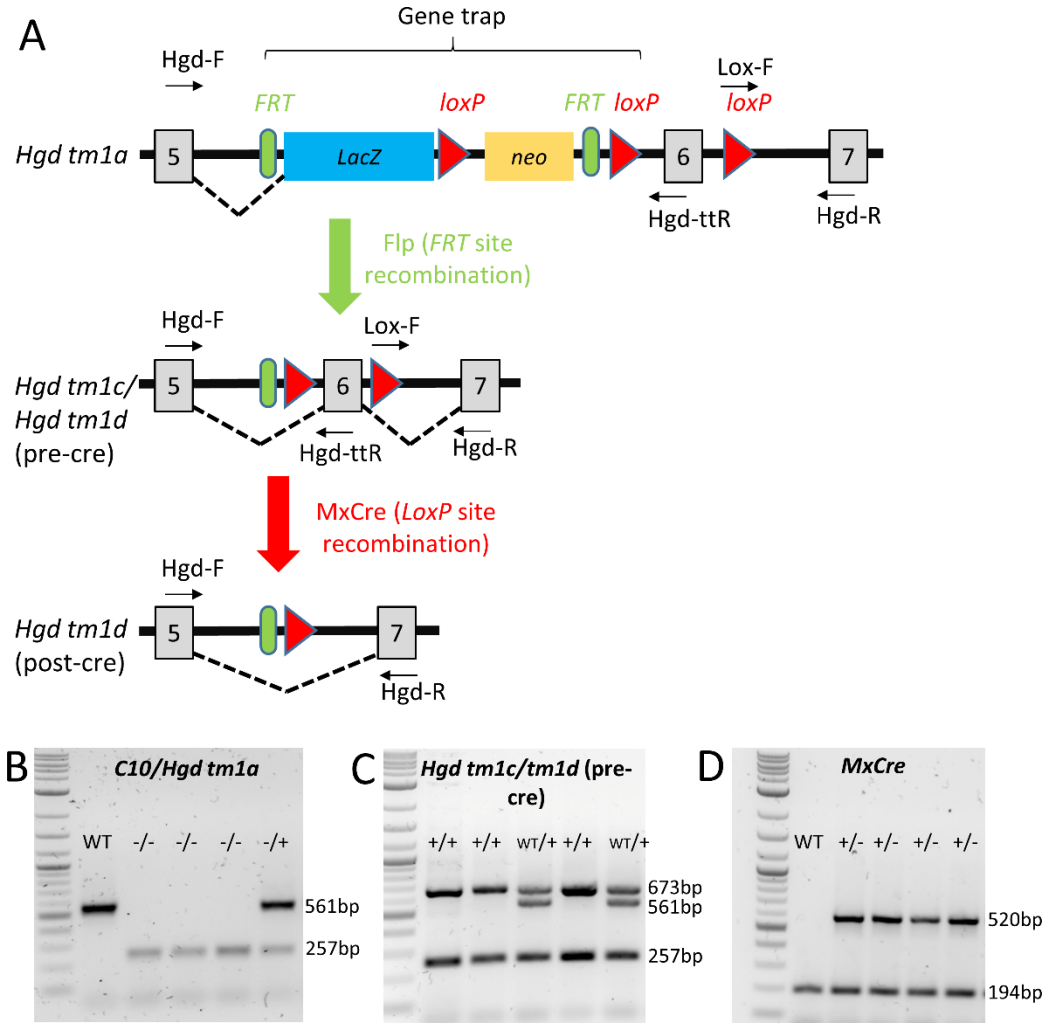

Figure 3.1. Schematic and genotyping of the modified *Hgd* allele.
A schematic of the modified *Hgd* allele is shown in A. *Hgd tm1a*: AKU phenotype. *Hgd tm1c/*Hgd tm1d (pre-cre): wildtype phenotype. *Hgd tm1d (post-cre)*: tissue specific and inducible deletion of *Hgd*. Using the primer pairs Hgd-F/Hgd-ttR and Lox-F/Hgd-R, B shows the genotyping of *tm1a*; C shows the genotyping of *tm1c*and *tm1d* (before cre recombination). D shows the genotyping of *MxCre* (top band) with the *Fabp2* control gene (bottom band). A 2-log DNA ladder was used in B-D.

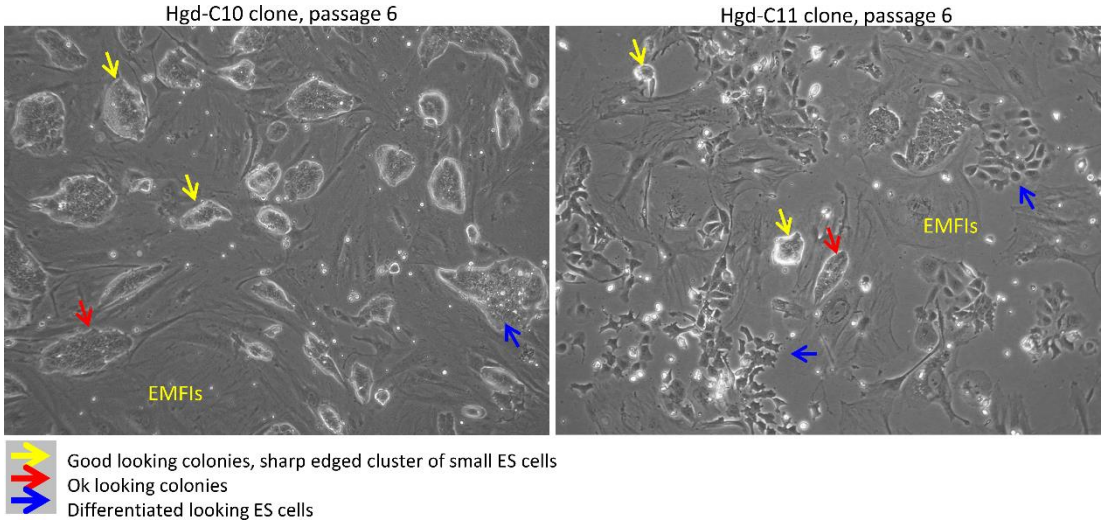

Figure 3.2. Culture of embryonic stem cell lines *Hgd*-C10 and *Hgd*-C11.
These stem cell lines contain a modified *Hgd* allele. The ES cells were grown on feeder cells; primary mouse embryonic fibroblasts (EMFIs). The modified *Hgd* allele contain a *neo* gene for G418 antibiotic resistance which was used for selection. ES cells from the good-looking colonies (yellow arrows) were used for subsequent blastocyst injection. ES cell culture carried out by Dr Antonius Plagge.

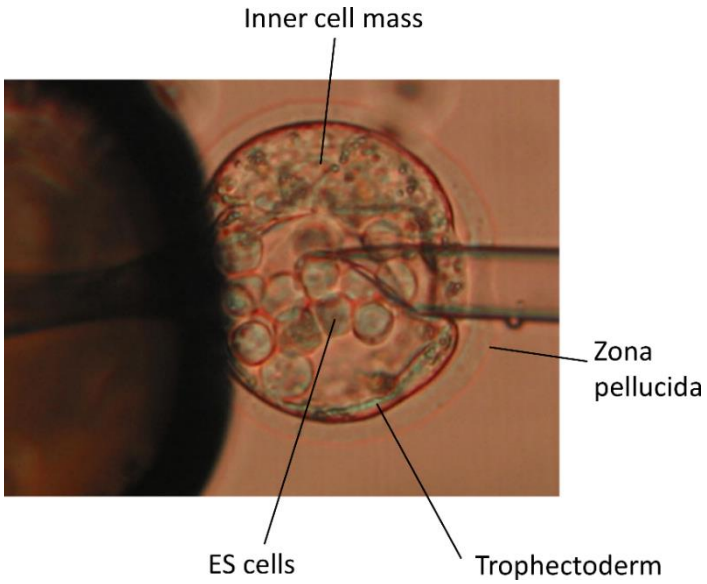

Figure 3.3. Injection of modified ES cells into a blastocyst at the blastula stage.
The ES cells were injected into the blastocoel cavity, close to the inner cell mass. Carried out by Dr Ke Liu.

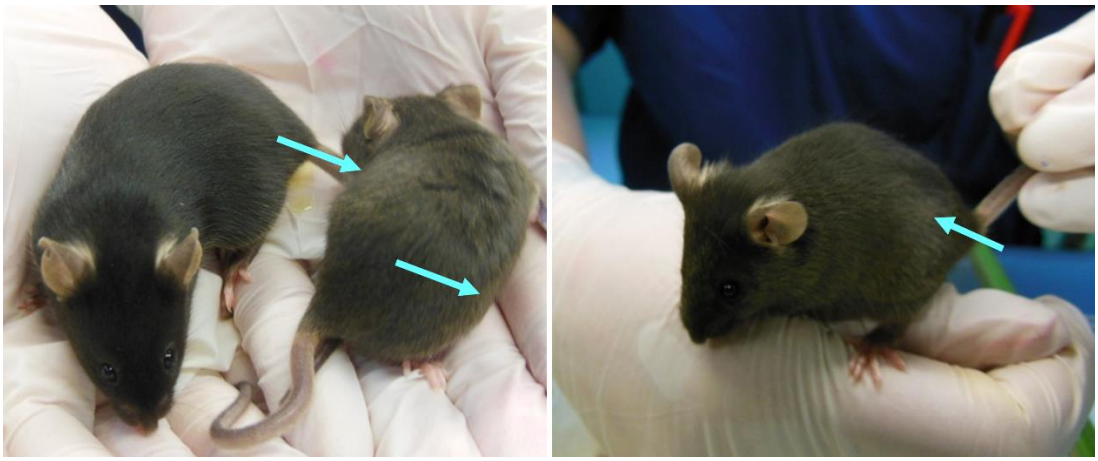

Figure 3.4. Selection of chimeric offspring carrying the non-*agouti* wildtype allele (A^{tm1Brd}).
Arrows indicate the non-*agouti* coat colour derived from the modified ES cells.

To obtain the conditionally targeted *Hgd tm1d* line, *Hgd tm1a* mice were crossed with Flpo mice to remove the FRT-flanked gene trap cassette, leaving a floxed target exon in the *Hgd tm1c (+/+)* allele, see Figure 3.1 [235]. Homozygote floxed *Hgd tm1c +/+* mice were crossed with *MxCre* mice [236] to obtain *Hgd tm1d* (fl/fl) *MxCre* (+/- or WT). The removal of the floxed sixth exon in *Hgd tm1d (fl/fl) MxCre +/-* was inducible with administration of polyinosinic: polycytidylic acid (pIpC) [236,237]. Removal of the floxed sixth exon causes a frameshift mutation, triggering nonsense medicated decay of the transcript.

These novel *Hgd* alleles can also be presented using the following nomenclature:

- *Hgd tm1a -/- or -/+* → $Hgd^{tm1a(KOMP)Wtsi}$ = $Hgd^{-/-}$ or $Hgd^{-/+}$.
- *Hgd tm1c +/+* → $Hgd^{tm1c(KOMP)Wtsi}$ = $Hgd^{flox/flox}$.
- Pre-Cre *Hgd (fl/fl) tm1d MxCre +/-* → $Hgd^{flox/flox}Mxcre^{+/-}$
- *Hgd tm1d MxCre +/-* post-cre → $Hgd^{tm1d(KOMP)Wtsi}$ = $Hgd^{\Delta Mx\text{-}1/\Delta Mx\text{-}1}$

Here in this thesis, the alleles are termed *Hgd tm1a -/- or -/+, Hgd tm1c +/+* and *Hgd tm1d (fl/fl) MxCre +/-* or *WT*.

3.2.2 Genotyping

DNA extracted from ear notch tissue was used to genotype mice; see section 2.1.1 for a detailed description. Briefly, tissue was digested using proteinase k and lysis buffer at 55°C overnight, followed by an isopropanol DNA extraction to isolate genomic DNA. PCR amplification of specific sequences using the isolated DNA as a template was then carried out using specific primers, followed by gel electrophoresis to separate and visualise DNA bands. The resulting DNA bands were used to determine the genotype of mice.

3.2.2.1 *Hgd tm1a, tm1c* and *tm1d* colonies

ES cells from clone C10 resulted in chimeras which achieved germline transmission. This knockout-first allele (*Hgd tm1a*) contained a promotorless IRES:*LacZ* gene trap cassette, flanked by an En2 splice acceptor and polyadenylation (poly(A)) sequence, and a promoter-driven *neo* cassette, flanked by a human beta-actin promoter (*hBactP*) and poly(A) sequence, inserted into the fifth *Hgd* intron with the sixth exon flanked by *LoxP* sequences, see Figure 3.1 (adapted from Collins and Rossant, 2007 [241]; Skarnes et al., 2011 [211]). The poly(A) sequence in the *LacZ* trapping element causes early termination of *Hgd* gene transcription; *Hgd* is transcribed up to exon 5 as a fusion transcript with *LacZ,* but are translated independently due to the IRES element. Homozygous *Hgd tm1a* mice showed an AKU phenotype due to *Hgd* gene disruption. In C10/*Hgd tm1a* mice, Lox-F/Hgd-R primers amplified the *LoxP* sequence (257bp) showing the allele was floxed (Figure 3.1B). Hgd-F/Hgd-ttR primers produced a 561bp band in the wildtype allele only; the gene trap cassette sequence in the modified allele was too large to be amplified. Homozygous *Hgd tm1a* therefore had only the 257bp floxed band, heterozygous had both the floxed 257bp and wildtype 561bp bands and wildtype had only the 561bp band (Figure 3.1B).

Hgd tm1c +/+ had restored *Hgd* gene expression due to removal of the gene trap and was shown to have a wildtype phenotype. To achieve inducible and conditional *Hgd* deletion, the floxed *Hgd tm1c +/+* line was bred with an interferon-inducible *Mx-1* (Interferon-Induced GTP-binding protein Mx1) cre recombinase mouse line, *MxCre* [236], generating the *Hgd tm1d MxCre* line. In the *Hgd tm1c* (restored *Hgd* allele, floxed) and pre-cre *Hgd tm1d* (floxed) alleles (*tm1c* and *tm1d* are both *Hgd* floxed alleles, with the *Hgd tm1d* mouse line name demonstrating that it has been bred with an *MxCre* line), Lox-F/Hgd-R primers showed the allele was floxed (257bp) and Hgd-F/Hgd-ttR primers showed that Flp recombination had occurred (673bp), see Figure 3.1C. Wildtype *Hgd tm1c/d* (WT/WT; not shown as no mice with this genotype were generated) would only have the 561bp band (Hgd-F/Hgd-ttR). Homozygously floxed *Hgd tm1c/d (+/+)* had both the 257bp floxed bands with the 673bp post-flp band and heterozygously floxed *Hgd tm1c/d (WT/+)* had all three bands (257bp floxed, 673bp post-flp and 561bp wildtype). Primers specific to *MxCre* (one primer in the *Mx-1* promoter, one primer in the cre sequence) produced a band at 520bp when *MxCre* was present (Figure 3.1D), denoted as +/-. The genotyping for *MxCre* does not distinguish the copy number as either heterozygous or homozygous. To prevent false-negative *MxCre* genotyping, control primers were included in the PCR reaction mix that amplify exon 1 of the *Fabp2* gene, a sequence that should always be present, showing that DNA was present in the

reaction mixture and that the PCR amplification was successful, preventing false-negative genotyping. The control primers produce a band at 194bp, see Figure 3.1D.

3.2.2.2 BALB/c *Hgd*$^{-/-}$ colony

In addition to the new targeted *Hgd tm1a* AKU colony, the existing BALB/c *Hgd*$^{-/-}$ AKU mice [115] were used for experiments, established at the University of Liverpool using the original ENU AKU mouse from the Pasteur Institute [86]. The BALB/c *Hgd*$^{-/-}$ colony is bred homozygous x homozygous, meaning that genotyping was not necessary as all resulting offspring would be homozygous. Periodically however, the colony must be genotyped to ensure that the mice are still the correct genotype. To identify the mutation present in these AKU mice, the region within *Hgd* containing the AKU mutation is amplified by PCR, producing a 290bp band. Within this region in the wildtype, there is a HypCH_4III restriction enzyme binding site. This binding site is not present in the AKU mutant sequence. Digestion with HypCH_4III is therefore used to detect the AKU mutation. With reference to Figure 3.5, wildtype mice show bands at 170bp and 120bp, due to the action of the restriction enzyme. Homozygous BALB/c *Hgd*$^{-/-}$ show a single intact band at 290bp due to the inability of the restriction enzyme to cut the DNA. Heterozygous mice would therefore exhibit bands at 290bp, 170bp and 120bp (not shown as no DNA was available from heterozygous mice).

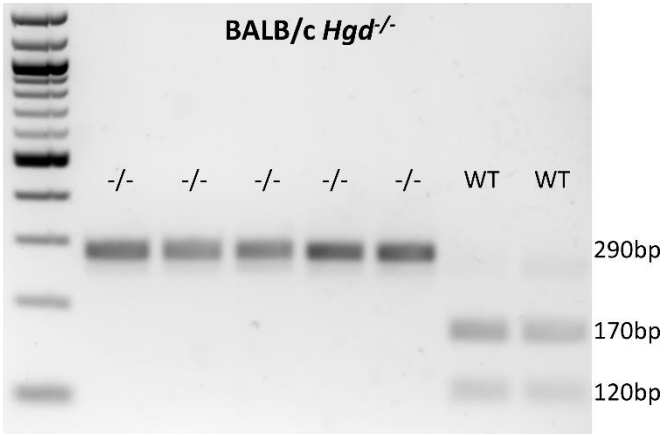

Figure 3.5. Genotyping of BALB/c *Hgd*$^{-/-}$.
Following amplification of the region within *Hgd* containing the AKU mutation, a restriction enzyme digest is used to determine the presence or absence of the AKU mutation. The absence of the restriction enzyme binding site results in a single intact band in homozygous BALB/c *Hgd*$^{-/-}$ mice. Wildtype (WT) mice show 2 bands as a result of the restriction enzyme cleaving the DNA. A 100bp ladder was used.

3.3 Phenotyping

3.3.1 Homogentisic acid

One of the first signs of AKU in humans is urine that turns dark brown/black after several hours due to exposure to the air, due to the presence of HGA. Figure 3.6A demonstrates dark urine stained cage bedding from *Hgd tm1a -/-* mice. This was the first observed sign that this new targeted model had AKU. Heterozygous cages did not have any dark urine stained cage bedding.

Following this, HGA was measured in urine and plasma of mice (Figure 3.6B-C). Urinary HGA (mean ±SEM) was increased approximately 10,000 - 100,000-fold (99,575 ±30,851 µmol/L) and plasma HGA elevated about 50-fold (100.5 ±34.9 µmol/L) in the *Hgd tm1a -/-* mice compared to *Hgd tm1a -/+* (plasma: 2.0 ±0.5 µmol/L; urine: 15 ±25.3 µmol/L), *Hgd tm1c* +/+ (plasma: 2.0 ±1.0 µmol/L; urine: 2.4 ±2.9 µmol/L) and C57BL/6 wildtype (plasma: 1.7 ±0.6 µmol/L; urine: 0.8 ±0.2 µmol/L) mice. These differences were all statistically significant ($p<0.001$; one-way ANOVA, Tukey-Kramer post-hoc). For comparison, urine and plasma HGA levels (mean ±SEM) for BALB/c *Hgd*$^{-/-}$ mice (n=48) are shown in Figure 3.7, and were 151,520 ±3,508 µmol/L and 108.8 ±9.2 µmol/L, respectively.

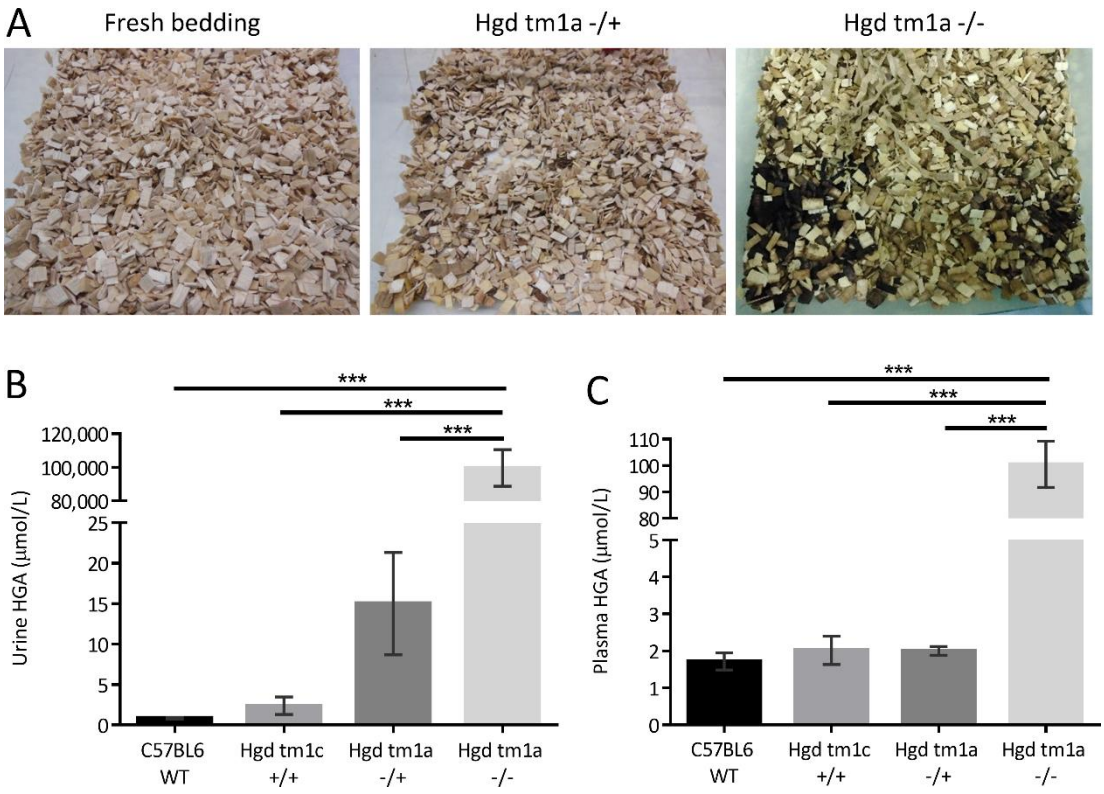

Figure 3.6. HGA levels in *Hgd tm1a -/-* AKU mice compared to non-AKU controls.
A shows dark urine stained cage bedding of *Hgd tm1a -/-* mice compared to *Hgd tm1a +/-* and fresh bedding. B and C show urine and plasma HGA levels respectively. Urinary HGA is increased approximately 10,000 - 100,000-fold in *Hgd tm1a -/-* mice (n=8; mean age [range] = 18.7 [9.0-31.1] weeks; 7 M, 1 F) compared with C57BL/6 wildtype (n=4; all 26.0 weeks, all F), *Hgd tm1c +/+* (n=7; mean age [range] = 23.1 [18.3-25.4] weeks; 2 M, 5 F) and *Hgd tm1a -/+* (n=16; mean age [range] = 24.6 [7.3-43.6] weeks; 12 M, 6 F) controls. Plasma HGA is increased approximately 50-fold in *Hgd tm1a -/-* mice (n=16; mean age [range] = 16.1 [7.1-31.1] weeks; 13 M, 3 F) compared to C57BL/6 wildtype (n=7; mean age [range] = 24.9 [22.3-26.0] weeks; 5 F, 2 M), *Hgd tm1c +/+* (n=7; mean age [range] = 24.1 [18.3-26.7] weeks, 2 M, 5 F) and *Hgd tm1a -/+* (n=18; mean age [range] = 23.9 [7.3-43.6] weeks, 12 M, 6 F) controls. HGA = homogentisic acid. M = male. F = female. Significance: $p<0.05$ *, $p<0.01$ ** and $p<0.001$ ***. Error bars represent SEM.

AKU is present at birth therefore plasma HGA was measured in day 1 *Hgd tm1a -/-* pups (2 pools of n=3; gestation: 19.5 days), see Figure 3.8. Plasma HGA (mean ±SEM) was elevated 3-fold in day 1 pups (308.8 ±18.9 µmol/L) compared with adult *Hgd tm1a -/-* mice (100.5 ±8.7 µmol/L).

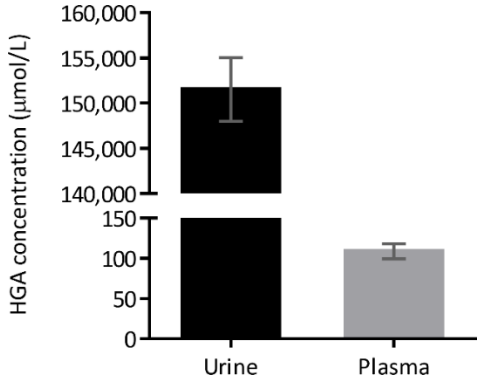

Figure 3.7. HGA levels in BALB/c *Hgd*$^{-/-}$ mice.
Urine and plasma HGA levels from 48 adult BALB/c *Hgd*$^{-/-}$ AKU mice. Mean age [range] = 31.9 [5.8-60.1] weeks. 24 males, 24 females. HGA = homogentisic acid. Error bars represent SEM.

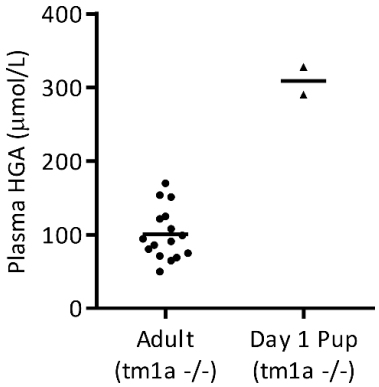

Figure 3.8. HGA levels in day 1 *Hgd tm1a -/-* pups.
Plasma samples from the pups were combined due to volume constraints into 2 pools of n=3. HGA levels were compared to adult *Hgd tm1a -/-* mice from Figure 3.6. HGA = homogentisic acid.

3.3.2 Ochronosis

In the BALB/c *Hgd*$^{-/-}$ mouse model, ochronosis has previously been reported in the tibio-femoral (knee) joint, using a modified Schmorl's stain to stain pigment a dark-blue colour [81,229]. Ochronosis was therefore initially assessed in the knee joints of the *Hgd tm1a -/-* mice for comparison, followed by investigation of other joints and tissues.

An example of Schmorl's staining from the tibia of a 52-week-old *Hgd tm1a -/-* AKU mouse is shown in Figure 3.9A. Several pigmented chondrons can be seen in the calcified articular cartilage, stained a dark-blue colour, indicated by arrows. An unstained section was also observed (Figure 3.9B), in which native, unstained ochronotic pigment can be seen, appearing yellow-brown (or ochre) in colour. This confirms that the Schmorl's stain is

identifying ochronotic pigment, which allows for easier identification of pigmented cells. The use of a nuclear fast red as a counterstain with Schmorl's stain allows other, non-pigmented cells to be identified.

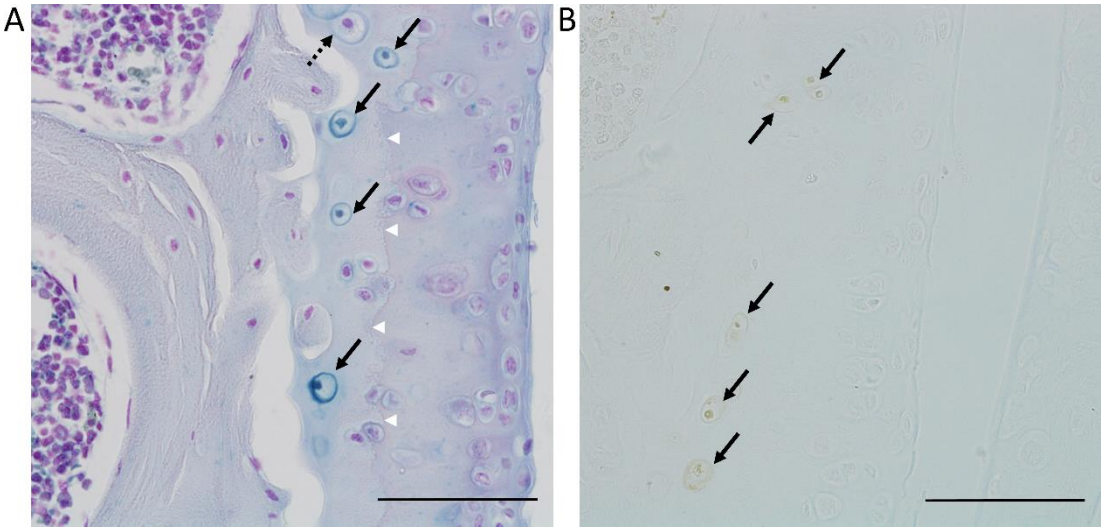

Figure 3.9. Identification of ochronotic pigment.
A shows Schmorl's staining of the tibio-femoral joint of a 52-week-old *Hgd tm1a -/-* mouse; arrows indicate pigmented chondrons found within the calcified articular cartilage of the tibia. The dashed arrow shows a chondron with pericellular pigmentation only. White arrow heads show the tidemark separating the calcified articular cartilage from the hyaline cartilage. B shows native ochronotic pigment without Schmorl's staining. Scale bar = 50 µM.

3.3.2.1 Knee joint ochronosis

In order to determine when ochronosis first appears, knee joints from *Hgd tm1a -/-* mice aged 7–15 weeks were examined for pigmentation. Ochronosis was only found in the calcified articular cartilage (Figure 3.10A), first appearing at 9 weeks of age (Figure 3.10B). The pigment was initially pericellular (9-11 weeks) and very infrequent. At 26 and 40 weeks of age in *Hgd tm1a -/-* (Figure 3.10C and E respectively), the number and intensity of pigmented chondrons was increased and showed advancement of pigmentation to the intracellular compartment, including the nucleus. At 40 weeks of age, pigmentation was still confined to the calcified articular cartilage. Heterozygous controls (*Hgd tm1a -/+*) showed no pigmentation at 26 and 40 weeks of age (Figure 3.10D and F respectively).

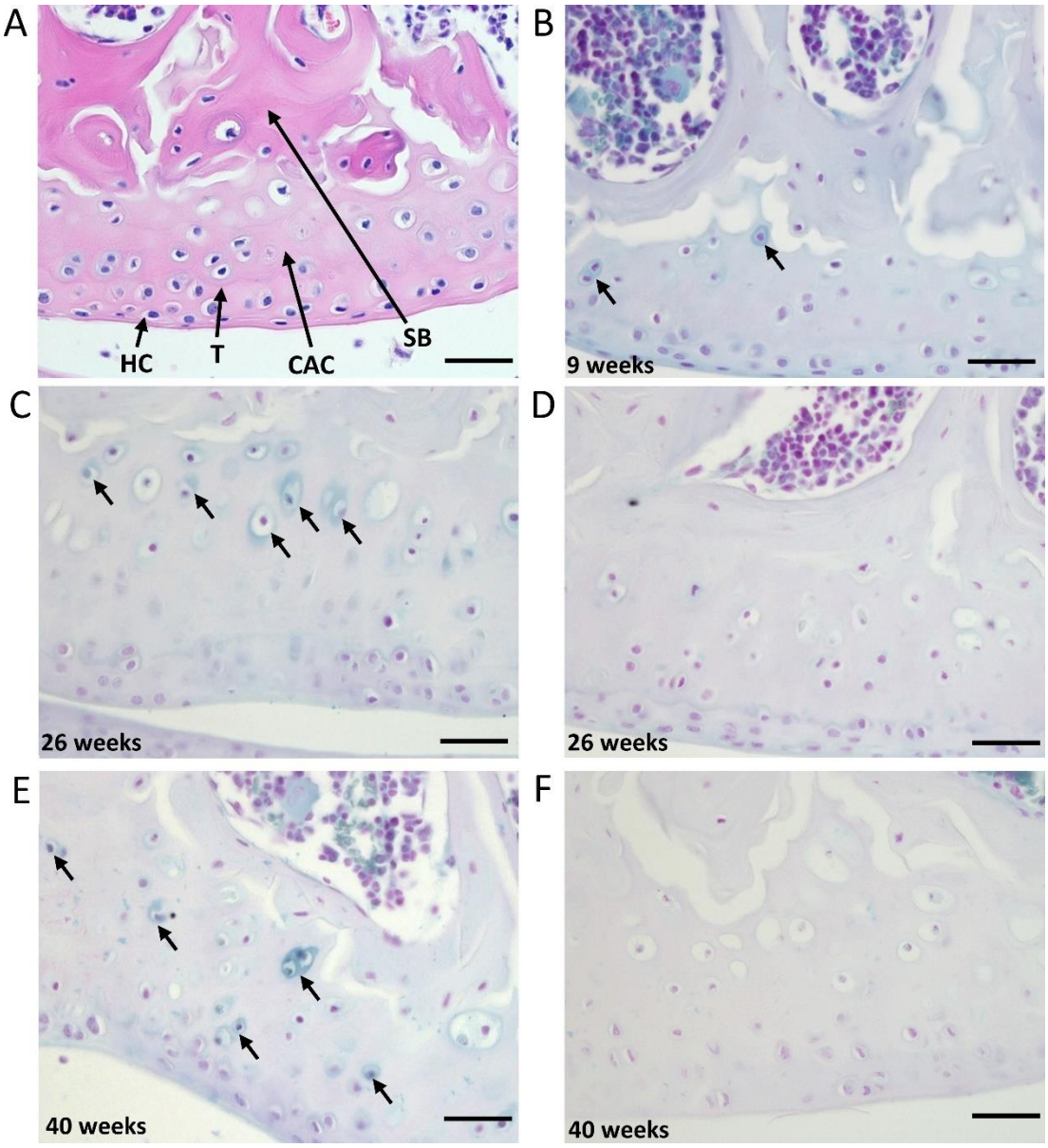

Figure 3.10. Initiation and progression of ochronosis in *Hgd tm1a -/-* mice.
H&E staining in A shows the division of the articular cartilage into different zones: hyaline cartilage (HC) and calcified articular cartilage (CAC) separated by the tidemark (T). Deep to CAC is subchondral bone (SB). B–F show femoral condyles from *Hgd tm1a* mice that have been Schmorl's stained (stains ochronotic pigment a blue colour). B shows pericellular pigmentation of chondrocytes situated in the CAC in a 9-week-old *Hgd tm1a -/-* femoral condyle. C and E show the femoral condyle of *Hgd tm1a -/-* mice at 26 and 40 weeks of age respectively. The pigmentation has advanced to the inner compartment of the cell, with more numerous affected chondrocytes showing varying pigment intensities. The pigmentation is still confined to the CAC layer. *Hgd tm1a -/+* mice at 26 and 40 weeks of age (D and F respectively) show no pigmentation. H&E, haematoxylin and eosin. All sections: 6 µM. Scale bar = 25 µM.

The lifetime progression of the number of pigmented chondrons within the knee joint of the BALB/c *Hgd*$^{-/-}$ colony has previously been reported by both Preston et al. [115] and Keenan et al. [116], with a linear pattern of increase observed with increasing age. To show the progression of ochronotic pigment with age in the *Hgd tm1a -/-* colony, knee joints from *Hgd tm1a -/-* mice aged 7-52 weeks were scored; the total number of pigmented chondrons in a

representative knee joint section encompassing all 4 joint quadrants was obtained (see section 2.2.3.2.1 of methods). With reference to Figure 3.11, the previously reported BALB/c *Hgd*$^{-/-}$ pigmentation progression is compared with that of the newer *Hgd tm1a -/-* model. The progression of the pigmentation observed is comparable in both models, with both showing a remarkably similar linear increase in the number of pigmented chondrons with increasing age.

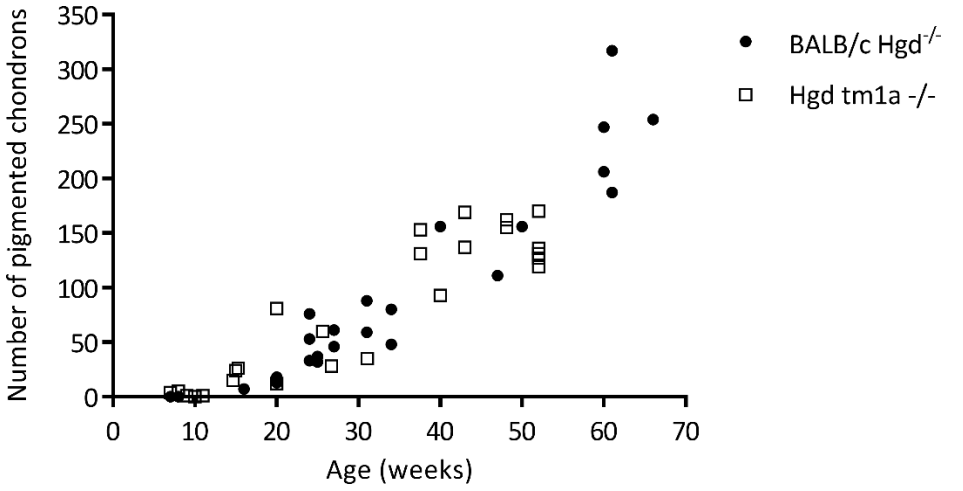

Figure 3.11. Quantification of pigmented chondrons with age in BALB/c *Hgd*$^{-/-}$ and *Hgd tm1a -/-* mice.
The number of pigmented chondrons were quantified in a representative knee joint section from mice of various ages from both the BALB/c *Hgd*$^{-/-}$ (n=28; 16 female aged 7-66 weeks, 12 male aged 8-47 weeks) and *Hgd tm1a -/-* (n=25; 8 female aged 8-48 weeks, 17 male aged 7-52 weeks) mouse models. Progression of pigmentation is similar in both models, with the number of pigmented chondrons increasing with age. BALB/c *Hgd*$^{-/-}$ data from Dr Craig Keenan's thesis and used with his permission [239], some of which was also reported in Preston et al. 2014 [115].

3.3.2.2 Investigation of ochronosis in other tissues

Previously, ochronotic pigmentation in AKU mice has only been reported in the calcified articular cartilage of the knee joint. Histological analysis of the elbow, hip and shoulder joints identified the presence of ochronotic pigmentation within these joints (Figure 3.12A-C), as pigmented chondrons within the calcified articular cartilage. No pigmentation was observed in the non-calcified hyaline cartilage, bone, periosteum, nor within ligaments or tendons associated with these joints. Within the vertebral column, pigmentation was only associated

with chondrons located in the calcified endplates of the vertebral bodies, adjacent to the growth plate, located either side of the IVD, and not within the disc itself Figure 3.13D).

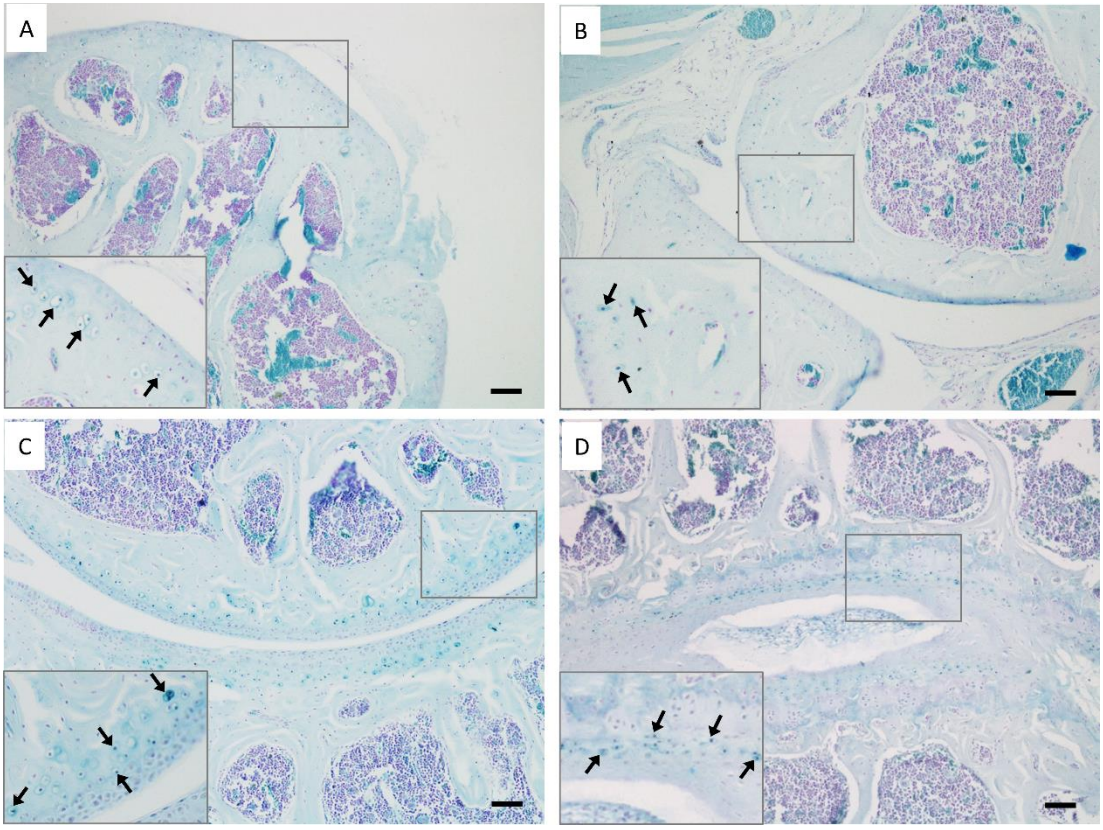

Figure 3.12. Schmorl's staining showing ochronotic pigmentation in various joints.
Pigmented chondrons can be observed within the calcified articular cartilage located on the femoral head of the hip joint (A), the articulation of the humerus and radius of the elbow joint (B), and the humeral head and glenoid fossa of the shoulder joint (C). Within the vertebral column (D), pigmented chondrons are observed in the calcified endplates of the vertebral bodies, either side of the intervertebral disc, but not within the disc itself. A-D from 52-week-old *Hgd tm1a -/-*. Scale bar = 50 µM.

The severity of pigmentation appeared to be affected by mechanical loading and force. With reference to Figure 3.13, significantly more pigmented chondrons (mean ±SEM) were observed within the endplates of the vertebral bodies adjacent to the 2nd lumbar (L2) IVD (48.4 ±4.5) compared to an IVD from the base of the tail (2.2 ±0.6) ($p = 0.002$). Clustering of pigmented chondrons was observed in areas of greater tensile stress such as the insertion of tendons and ligaments in joints; the Achilles tendon on the calcaneus in the ankle (Figure 3.14A), the cruciate ligaments on the intercondylar area of the tibial plateau in the knee joint (Figure 3.14B), and calcified fibrocartilage found at the entheses attached to the femoral condyle where collateral ligaments insert (Figure 3.14C). Pigmentation was also observed

within the calcified fibrocartilage of the meniscus of the knee joint associated with chondrons (Figure 3.14D) that is subjected to compressive loading. No pigmentation was observed in 52-week-old *Hgd tm1a -/+* control joint tissue, that includes the shoulder, hip, elbow, knee and vertebral column (not shown).

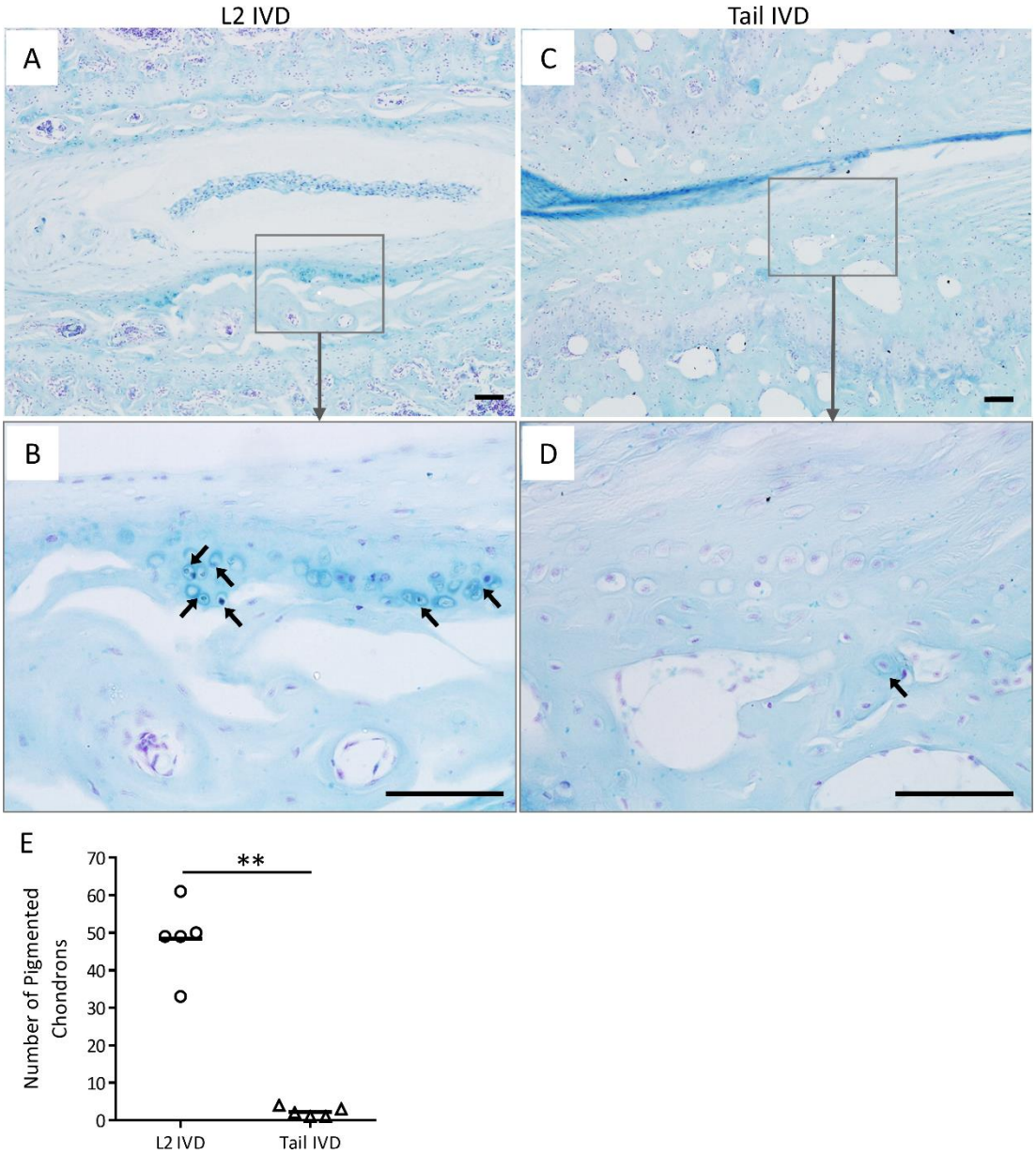

Figure 3.13. Comparison of pigmentation within the endplates of tail and lumbar IVDs.
A+B shows numerous pigmented chondrons within the vertebral endplates of the 2nd lumbar(L2) IVD from the lumbar spine. C+D shows the presence of few pigmented chondrons present in the vertebral endplates of an IVD from the base of the tail. E shows the difference in the number of pigmented chondrons within the endplates of the L2 and tail IVD; 5 sections were scored, taken every 3rd slide. IVD = intervertebral disc. Two-tailed, unpaired t-test; p = 0.002. Significance: p<0.05 *, p<0.01 **, p<0.001 ***. Tissue from 52-week-old *Hgd tm1a -/-*, sectioned sagittal plane. Scale bar = 50 µM.

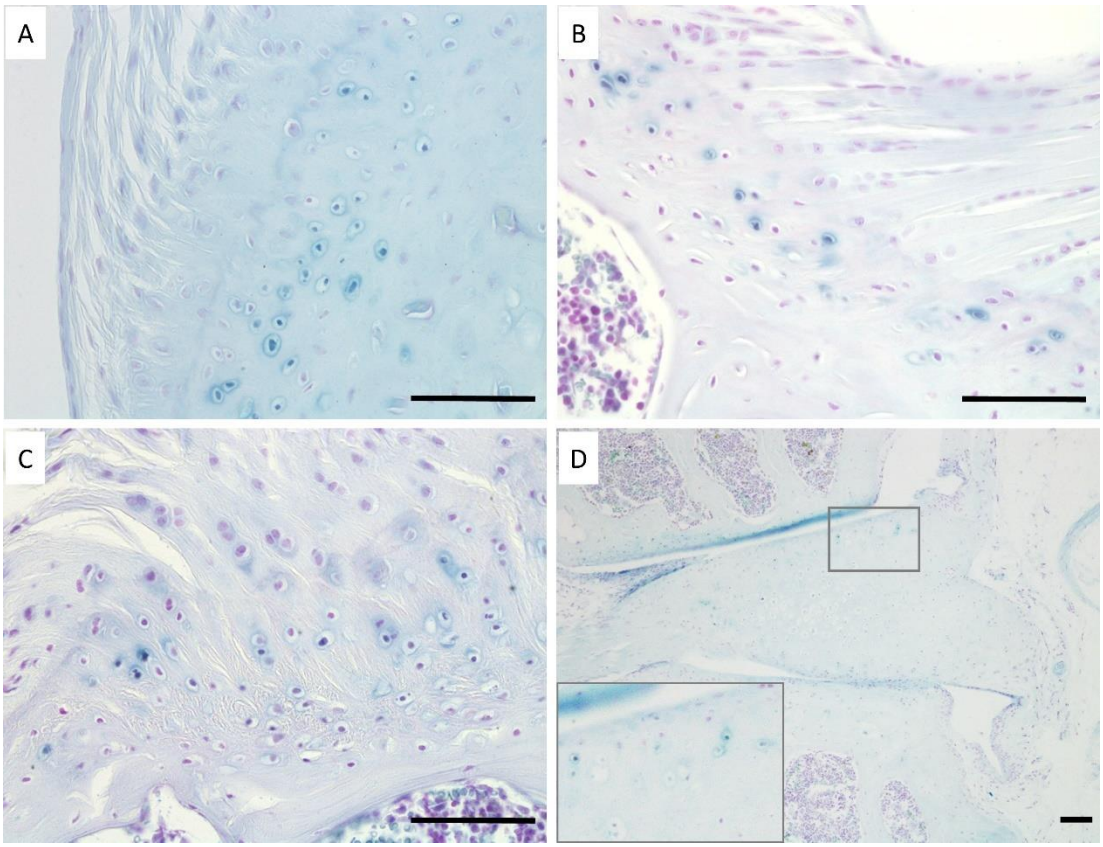

Figure 3.14. The relationship between ochronotic pigment and mechanical loading and force.
Large numbers of pigmented chondrons can be seen adjacent to the insertion of the Achilles tendon on the calcaneus of the ankle (A) and adjacent to the insertion of a cruciate ligament on the intercondylar area of the tibial plateau (B). Pigmented chondrons are observed in the calcified fibrocartilage of entheses attached to the femoral condyles (C) and the calcified fibrocartilage within the meniscus of the knee joint (D). A from 65.7-week-old BALB/c *Hgd*$^{-/-}$. B from 40-week-old *Hgd tm1a -/-*. C from 38-week-old *Hgd tm1a -/-*. D from 52-week-old *Hgd tm1a -/-*. Scale bar = 50 µM. Image A used with permission from Dr Craig Keenan [239].

In addition to musculoskeletal tissues, sections from the larynx, ear, eye and heart of a 52-week-old *Hgd tm1a -/-* mouse were stained with Schmorl's stain to look for ochronotic pigmentation and compared to a 52-week-old *Hgd tm1a -/+* (non-AKU) control. Ochronotic pigmentation was not observed in the hyaline laryngeal cartilage (Figure 3.15), nor the hyaline cartilages of the trachea, and was comparable with the non-AKU control. Ochronotic pigmentation was not observed in the eye, where only the dark-black pigmentation of the pigmented retinal epithelium was observed (Figure 3.16), nor the ear (Figure 3.17), and was comparable to the non-AKU control. In the heart, no ochronotic pigmentation was observed in the roots and walls of the vessels nor in the muscular wall/septum of the heart chambers. Interestingly, a dark, punctate black pigment was observed within the heart valves of the AKU *Hgd tm1a -/-* heart, however due to the presence of this pigmentation also in the non-AKU valves it is not thought to be ochronotic pigment (Figure 3.18). This pigment also did not stain a dark-blue colour with Schmorl's staining. This black, punctate pigment was also

observed macroscopically within the hearts of *Hgd tm1a -/-, Hgd tm1a -/+* and C57BL/6 WT mice during whole *LacZ* staining, see Figure 3.19. Sections from the liver (Figure 3.20) and kidney (Figure 3.21) of 52-week-old AKU (*Hgd tm1a -/-*) and non-AKU (*Hgd tm1a -/+*) were also stained with Schmorl's stain, with no differences observed.

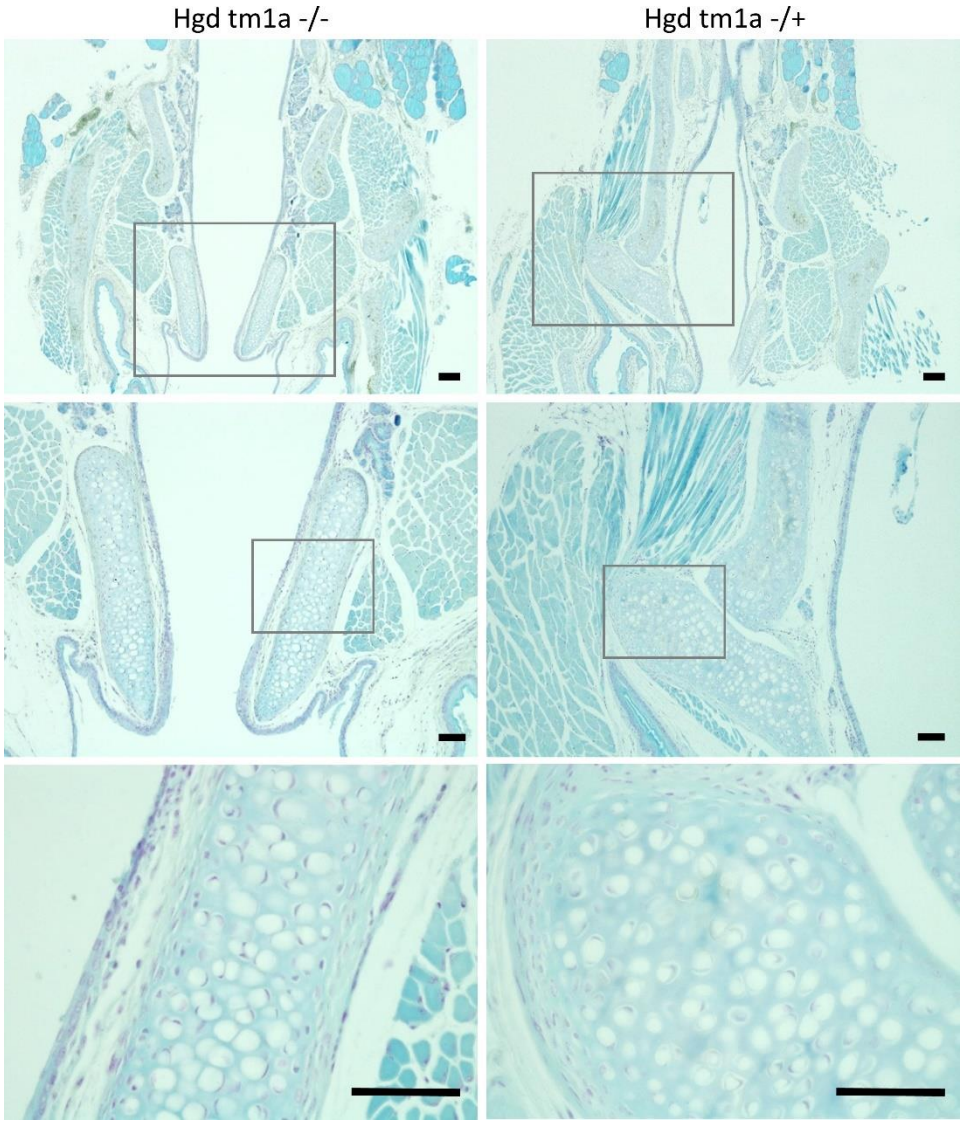

Figure 3.15. Schmorl's staining of laryngeal cartilage from AKU and non-AKU mice.
Sections from *Hgd tm1a -/-* (AKU) showed no ochronotic pigmentation in the laryngeal cartilage and was comparable *with Hgd tm1a -/+* (non-AKU). Boxes show area of magnification. Tissue from 52-week-old mice. Scale bar in top row = 100 µM. Scale bar in middle and bottom row = 50 µM.

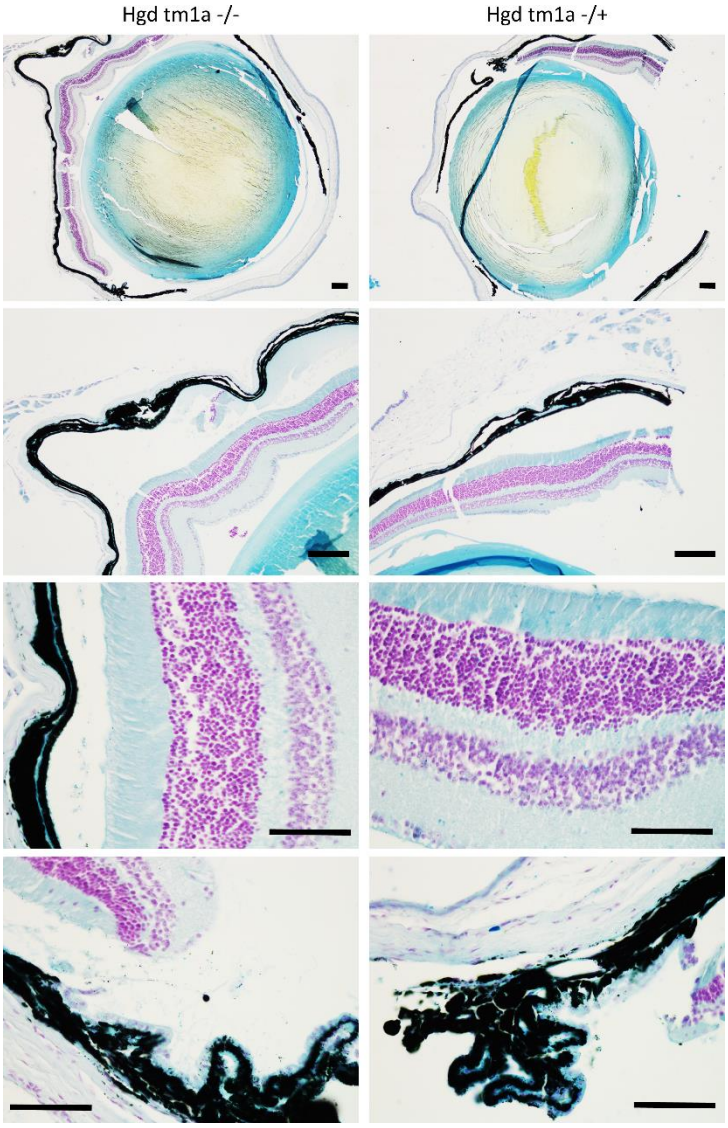

Figure 3.16. Schmorl's staining of eyes from AKU and non-AKU mice.
Sections from *Hgd tm1a -/-* (AKU) showed no ochronotic pigmentation (only the pigmented retinal epithelium shows pigmentation) and were comparable with *Hgd tm1a -/+* (non-AKU) eyes. The pigmented retinal epithelium showed a dark black pigment as expected in both *Hgd tm1a -/-* and *Hgd tm1a -/+*. Eyes from 52-week-old mice. Scale bar in top two rows = 100 µM. Scale bar in bottom two rows = 50 µM.

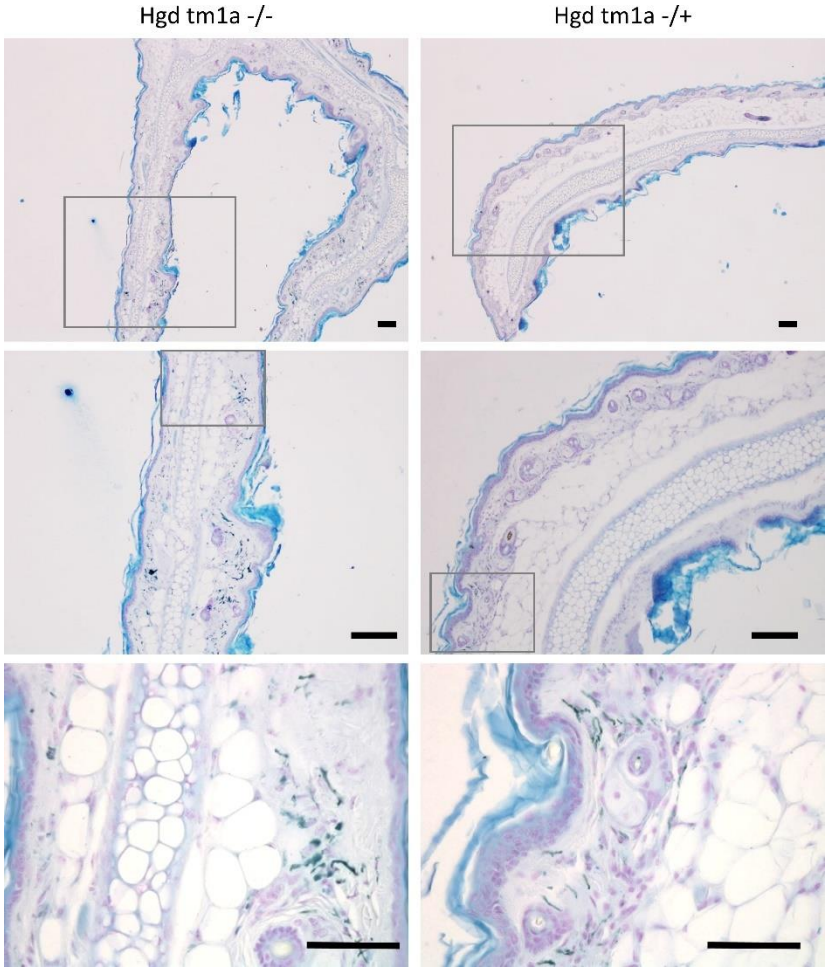

Figure 3.17. Schmorl's staining of ear tissue from AKU and non-AKU mice.
Sections from *Hgd tm1a -/-* (AKU) showed no ochronotic pigmentation and were comparable with *Hgd tm1a -/+* (non-AKU) ear tissue. Ear tissue from 52-week-old mice. Scale bar in top two rows = 100 µM. Scale bar in bottom row = 50 µM.

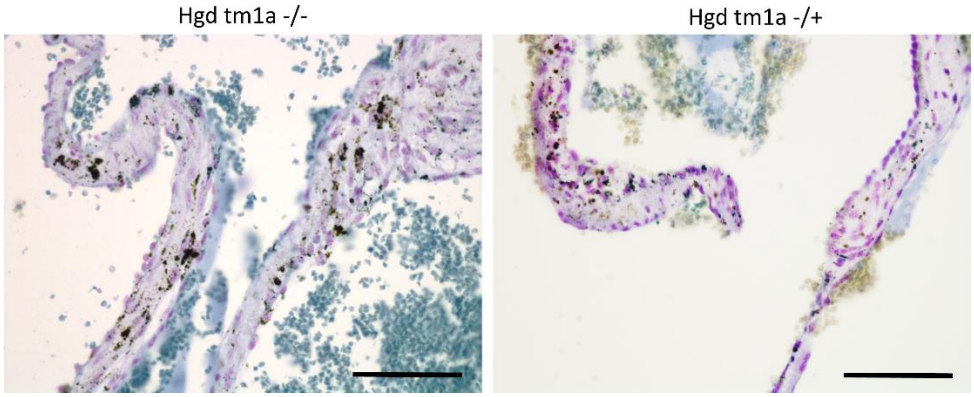

Figure 3.18. Schmorl's staining of the heart valves from AKU and non-AKU mice.
The presence of a black pigment was observed in histological sections of the heart valves of both AKU *(Hgd tm1a -/-*) and non-AKU (*Hgd tm1a -/+*) mice, aged 52 weeks. Scale bar = 50 µM.

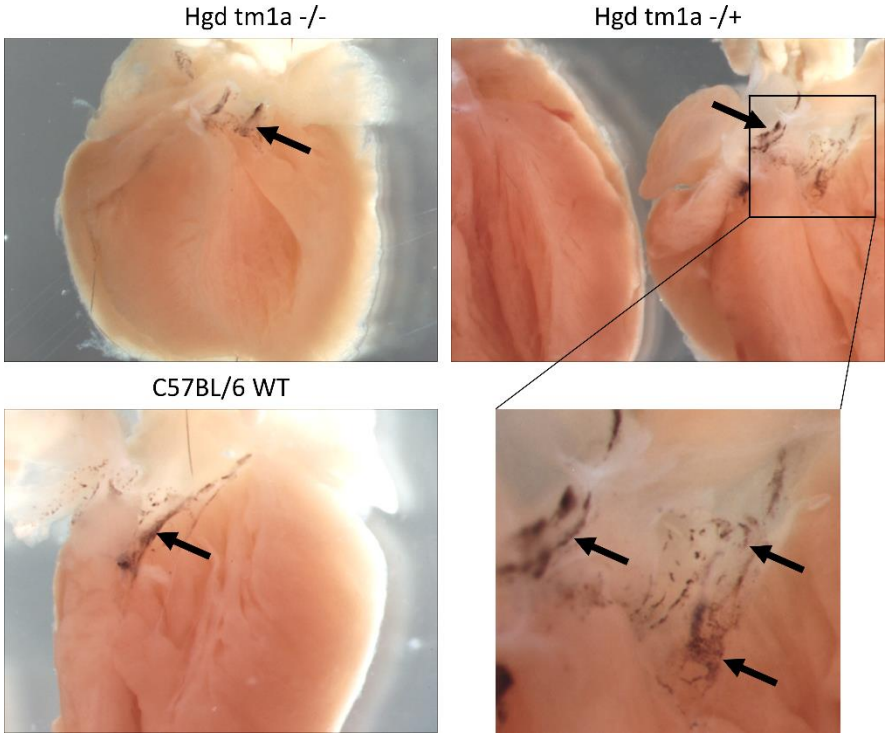

Figure 3.19. Presence of a black pigment within the heart valves of AKU and non-AKU mice.
The presence of a black, punctate pigment was observed in the heart valves of both AKU (*Hgd tm1a -/-*, 31 weeks old) and non-AKU (*Hgd tm1a -/+*, 23 weeks old; C57BL/6 WT, 22 weeks old) mice, indicated by arrows.

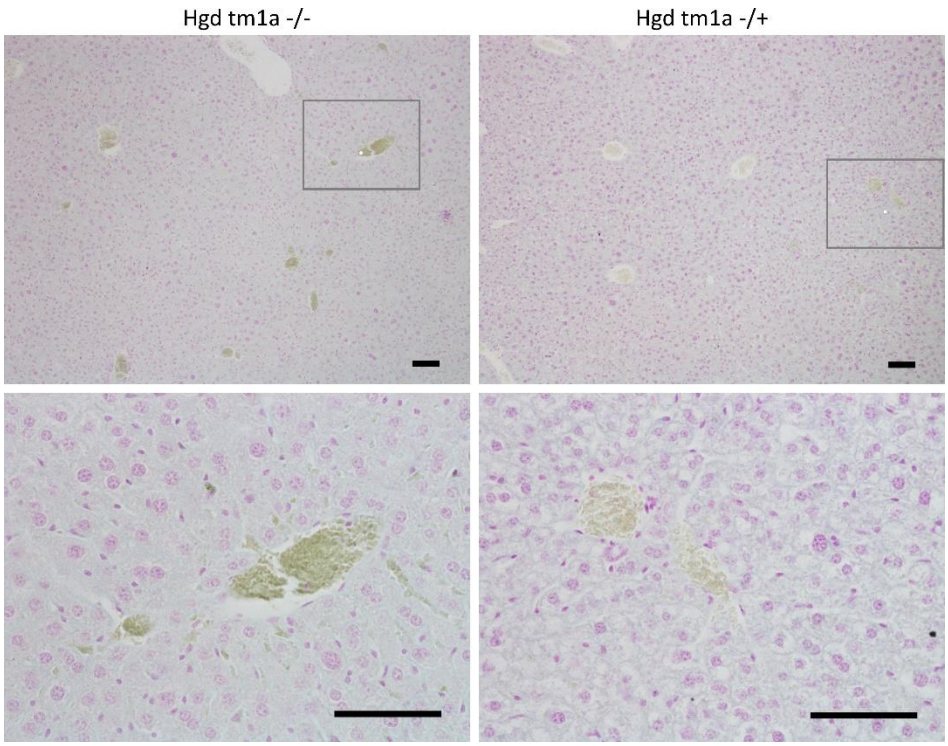

Figure 3.20. Schmorl's staining of liver from AKU and non-AKU mice.
Sections from AKU *Hgd tm1a -/-* showed no ochronotic pigmentation and were comparable with non-AKU *Hgd tm1a -/+* control liver sections. Tissue from 52-week-old mice. Scale bar = 50 µM.

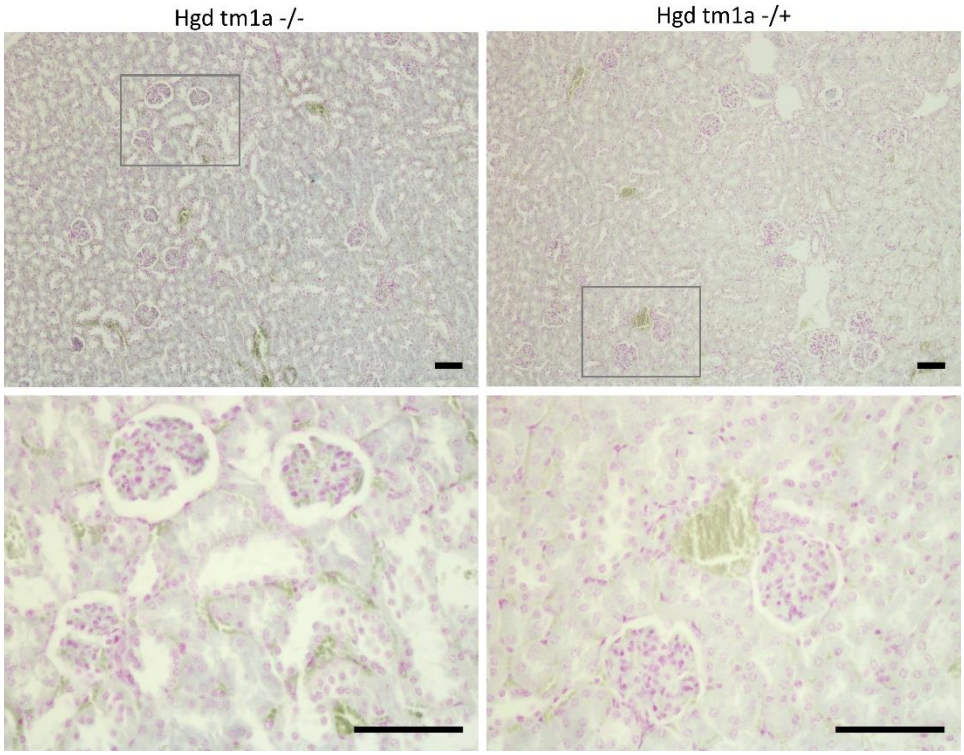

Figure 3.21. Schmorl's staining of kidney from AKU and non-AKU mice.
Sections from AKU *Hgd tm1a -/-* showed no ochronotic pigmentation and were comparable with non-AKU *Hgd tm1a -/+* control kidney sections. Tissue from 52-week-old mice. Scale bar = 50 µM.

3.3.2.3 Osteoarthritis

To investigate whether the AKU phenotype causes osteoarthritis in the *Hgd tm1a -/-* mouse model, knee joints from *Hgd tm1a -/+* (n=5) and *Hgd tm1a -/-* (n=5) male mice aged 52 weeks were taken. Every fourth, coronal paraffin section was stained with safranin O/fast green. Safranin-O stains cartilage red, with the intensity reflecting the proteoglycan content, and fast green stains the bone green. This staining allows the cartilage to be scored histologically for osteoarthritis, using the OARSI histopathology initiative scoring system [242]. Briefly, each joint quadrant throughout the knee joint is scored individually, given a score between 0 and 6. Normal cartilage would score 0. Proteoglycan loss only, with no structural changes would score 0.5. Minor damage, with superficial vertical clefts and some loss of the surface lamina would score 2. Scores of 3-6 would represent vertical clefts/erosion to the calcified cartilage, ranging from <25% of the articular surface (score 3) to >75% of the articular surface (score 6).

OARSI scores are presented as both the mean OARSI score and maximum OARSI score for each joint quadrant (medial tibia; medial femur, lateral tibia and lateral femur). With reference to Figure 3.22, no significant differences (two-tailed, unpaired t-test) were

observed between *Hgd tm1a -/+* and *Hgd tm1a -/-* mice, across all 4 joint quadrants, for both the mean and maximum OARSI scores. Figure 3.23 shows safranin O/fast green staining of the knee joint cartilage from 52-week-old *Hgd tm1a -/-* and *Hgd tm1a -/+* mice, which look comparable. No subchondral bone sclerosis was observed in *Hgd tm1a -/-* or *-/+*. The presence of osteophytes was also documented; an osteophyte was observed in one *Hgd tm1a -/-* mouse (on the medial tibia), and an osteophyte observed in three *Hgd tm1a -/+* mice (2 on the medial tibia 1 on the medial femur), see Figure 3.24.

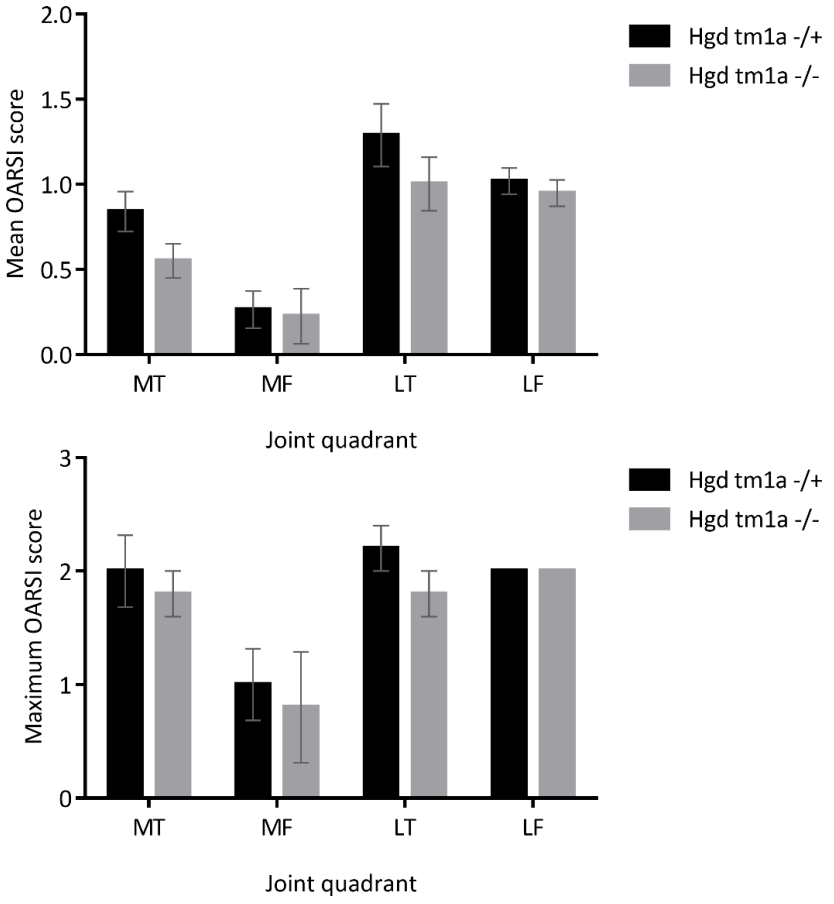

Figure 3.22. Osteoarthritis scoring of the knee joint in *Hgd tm1a -/+* and *Hgd tm1a -/-* mice.
Coronal knee joint paraffin sections from 52-week-old, male *Hgd tm1a -/+* (n=5) and *Hgd tm1a -/-* (n=5) were stained with safranin-O/fast green and the cartilage scored using the OARSI scoring system. No significant differences were found between *Hgd tm1a -/+* and *Hgd tm1a -/-* mice for the mean and maximum OARSI score across all joint quadrants (two-tailed unpaired t-test). MT = medial tibia. MF = medial femur. LT = lateral tibia. LF = lateral femur. Knee joints sectioned by Dr Craig Keenan.

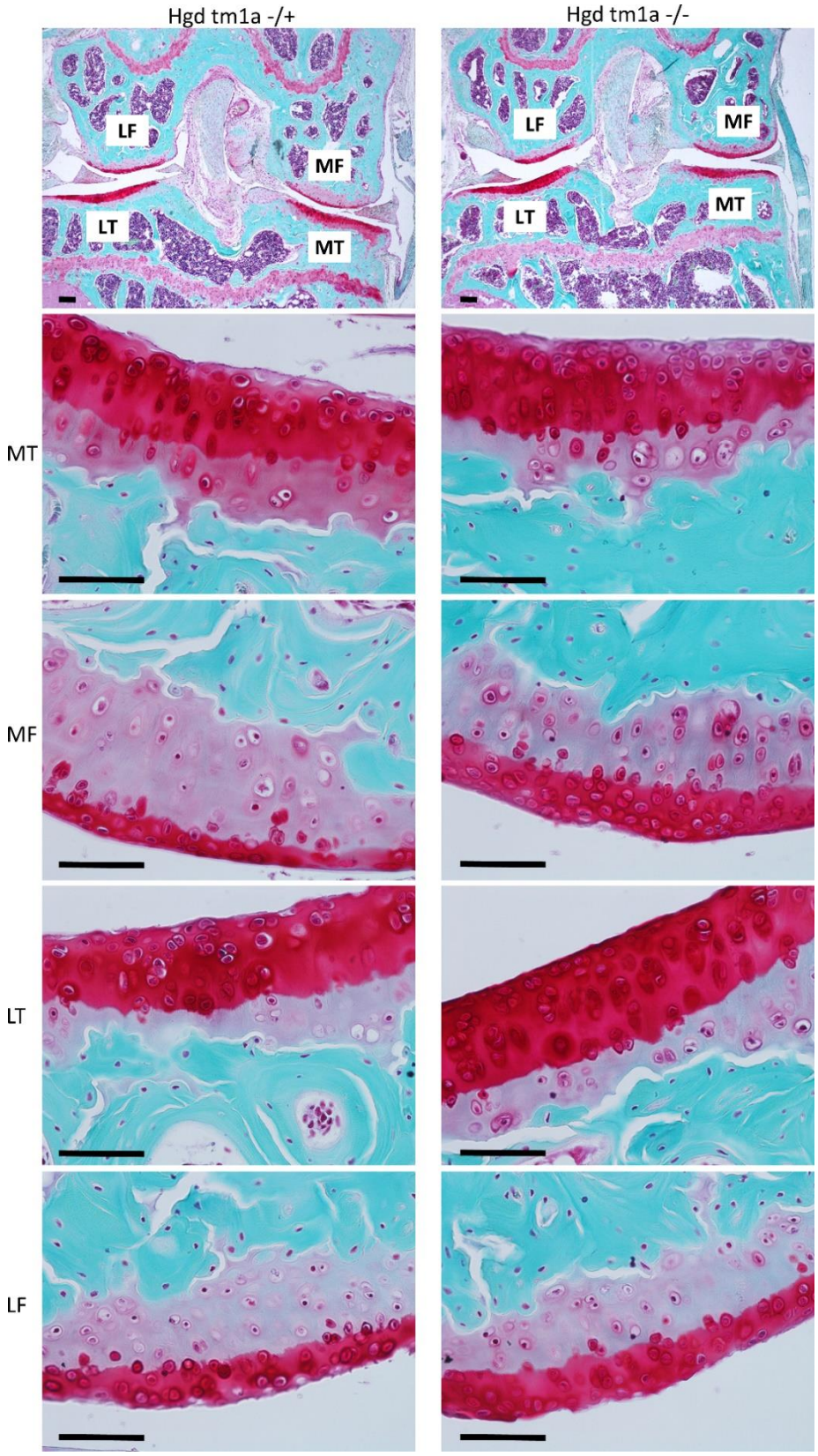

Figure 3.23. Safranin-O/fast green staining of 52-week-old *Hgd tm1a -/+* and *Hgd tm1a -/-* knee joint cartilage. Coronal paraffin section of the knee joints from 52-week-old, male *Hgd tm1a -/+* (n=5) and *Hgd tm1a -/-* (n=5) were stained with safranin-O/fast green and the cartilage scored using the OARSI scoring system. No differences were observed between *Hgd tm1a -/-* and *Hgd tm1a -/+* knees. Top row shows a whole knee joint. MT = medial tibia. MF = medial femur. LT = lateral tibia. LF = lateral femur. Scale bar in top row = 100µM. Scale bar in bottom four rows = 50 µM.

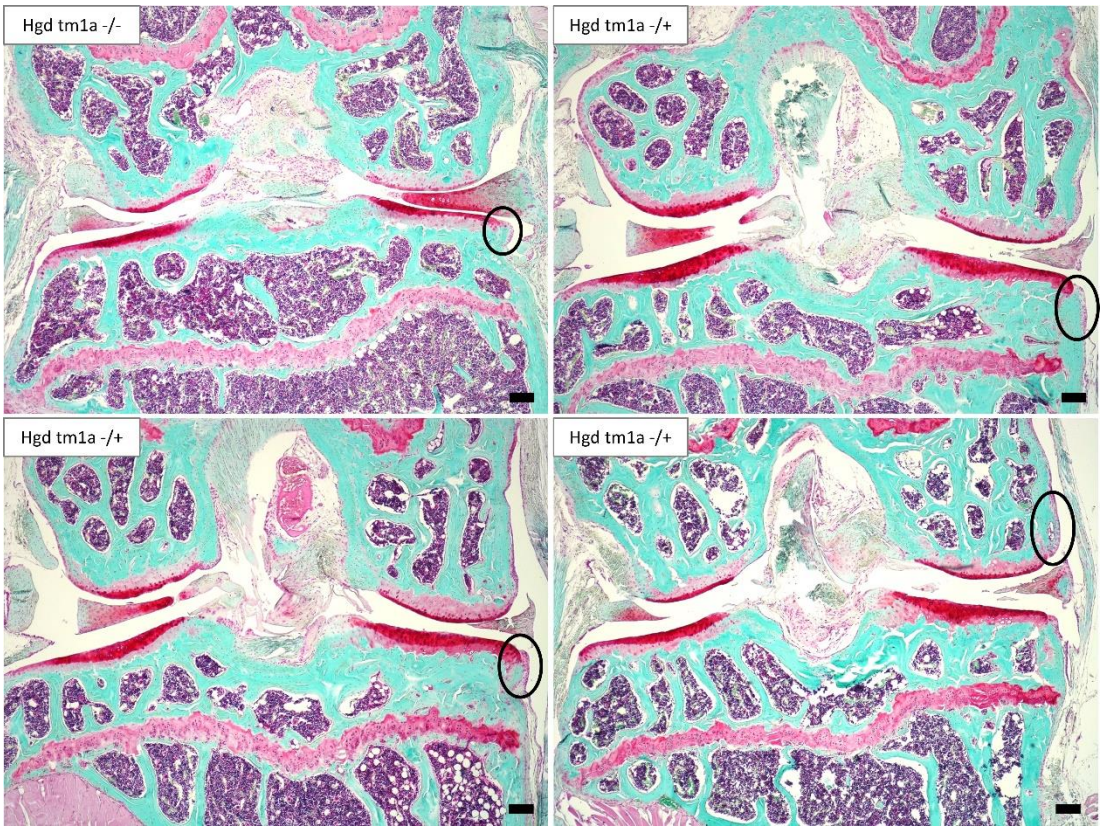

Figure 3.24. Presence of osteophytes in 1-year AKU and non-AKU mice.
Safranin O/fast green staining of knees from 5 *Hgd tm1a -/-* (AKU) and 5 *Hgd tm1a -/+* (non-AKU) male mice revealed the presence of osteophytes (indicated by circles). An osteophyte was observed on 1 AKU mouse knee on the medial tibia. Osteophytes were observed on 3 non-AKU mouse knees; 2 on the medial tibia and 1 on the medial femur (bottom right). Each section: femur top, tibia bottom, lateral towards left, medial towards right. Scale bar = 100 µM.

3.4 Response to nitisinone therapy

Nitisinone has been tested in both the existing BALB/c *Hgd*$^{-/-}$ mouse model and in human patients, where it has been shown to lower circulating HGA and increase tyrosine. *Hgd tm1a -/-* mice (n=6) were therefore treated with 4 mg/L nitisinone (the dose previously used in AKU mice), with tail bleed samples taken pre- and post-treatment to assess the response of HGA, tyrosine and other associated metabolites.

With reference to Figure 3.25, HGA (mean ±SEM) was decreased 10-fold from 81.7 ±10.5 µmol/L to 8.2 ±0.6 µmol/L whilst all other metabolites increased; all changes were significant (two-tailed paired t-test). Tyrosine increased 14-fold from 65.3 ±10.3 µmol/L to 940.3 ±55.7 µmol/L. Phenylalanine increased 1.2-fold from 78.1 ±2.1 µmol/L to 95.8 ±5.2 µmol/L. HPPA increased 9-fold from 18.0 ±0.4 µmol/L to 169.3 ±29.0 µmol/L. 4-hydroxyphenyllactic acid (HPLA) increased 16-fold from 1.8 ±0.2 µmol/L to 29.1 ±3.0 µmol/L.

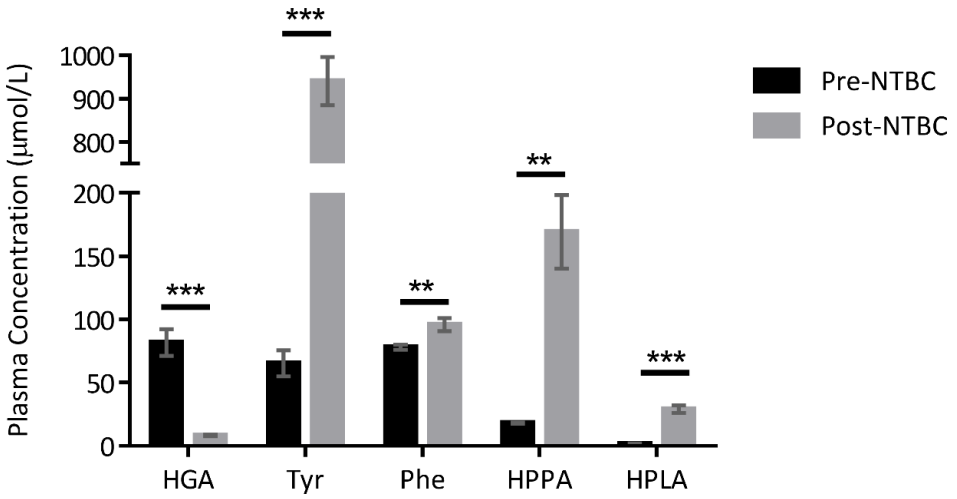

Figure 3.25. Nitisinone treatment of *Hgd tm1a -/-* mice.
Hgd tm1a -/- mice (n=6; 3 male, 3 female; mean age [range]: 12.2 [11.1-17.3] weeks) were treated with 4 mg/L nitisinone (NTBC) for 1 week, with tail bleed samples taken pre- and post-treatment. HGA = homogentisic acid. Tyr = tyrosine. Phe = phenylalanine. HPPA = 4-hydroxyphenylpyruvic acid. HPLA = 4-hydroxyphenyllactic acid. Error bars represent SEM. Paired t-test (two-tailed) significance: $p<0.05$ *, $p<0.01$ **, $p<0.001$***.

3.5 Discussion

The pathophysiology of AKU has been investigated in *ex vivo* tissue samples [57,78,99], *in vitro* models [81,100] and also within an ENU mutagenesis mouse model of AKU, BALB/c *Hgd*$^{-/-}$ [115]. To investigate the metabolic consequences of AKU and novel therapeutic approaches further, a new conditionally targeted mouse model of AKU in the C57BL/6 background has been generated using a mutant knockout-first *Hgd* allele obtained from the UC Davis Knockout Mouse Project (KOMP) Repository.

Targeted gene disruption in *Hgd tm1a* removes any potentially confounding mutations that could be present in the existing BALB/c *Hgd*$^{-/-}$ ENU AKU mouse model [115], as ENU mutagenesis causes a high frequency of genomic mutations [198]. The *LacZ* reporter gene within the *Hgd* gene locus has enabled precise localisation of *Hgd* expression, which is shown in chapter 4. Manipulation of this *Hgd tm1a* knockout-first allele by FRT/flp and Cre/*LoxP* site-specific recombination enabled liver-specific *Hgd* deletion in double transgenic *Hgd tm1d MxCre +/-* mice, highlighting important considerations for future therapy in AKU, which is also shown in chapter 4. Here within this chapter, the new conditional *Hgd tm1a* mouse model of AKU has been phenotyped, showing that the model exhibits the main characteristics of AKU.

3.5.1 Phenotyping the new *Hgd tm1a* mouse model

The new targeted mouse model of AKU (*Hgd tm1a -/-*) was shown to exhibit an AKU phenotype comparable to the BALB/c *Hgd*$^{-/-}$ mouse, of increased HGA in the urine and plasma, and joint pigmentation [243].

Plasma HGA levels in *Hgd tm1a -/-*, which were on average about 100 µmol/L, were comparable to the values previously reported in the ENU BALB/c *Hgd*$^{-/-}$ model [115,116], which ranged from approximately 100-200 µmol/L, measured via a different HPLC system. Serum HGA values in human AKU patients are lower than that of AKU mice; fo example the mean [range] serum HGA reported in 40 patients was 29.2 [5.8-45.5] µmol/L [52] and in 3 patients was 49.3 [30-75] µmol/L [47]. The methods used here to quantitate HGA, both in plasma and urine, are state-of-the-art, clinically validated assays, developed for use on human samples at the NAC and for the SONIA-1 and SONIA-2 clinical trials [46,47]. Shown for the first time are HGA values for heterozygous mice (*Hgd tm1a -/+*) that do not have AKU, with HGA levels comparable to C57BL/6 or *Hgd tm1c +/+* wildtype control mice. Also reported for the first time are urine HGA values in AKU mice, which are on average 100,000 µmol/L in *Hgd tm1a -/-* mice, which had not previously been reported for the BALB/c *Hgd*$^{-/-}$ model within recent publications in 2014 [115] nor 2015 [116], where only plasma HGA was reported. Urine HGA had been reported for the original ENU BALB/c *Hgd*$^{-/-}$ model in 1994, determined by organic solvent extraction and GC/MS, and determined to be >0.55 mol/mol creatinine [86], which is not a comparable measure to the urine HGA levels obtained here. Therefore, for a direct comparison, urine and plasma HGA was measured in BALB/c *Hgd*$^{-/-}$ mice, taken from the pre-treatment values of a separate experiment to this thesis, measured via the same HPLC system used to analyse samples from *Hgd tm1a -/-*. The plasma HGA in BALB/c *Hgd*$^{-/-}$ was comparable, at approximately 100 µmol/L, and urine HGA was approximately 150,000 µmol/L, which is higher than the approximate 100,000 µmol/L level reported in *Hgd tm1a -/-,* but still within the same order of magnitude. This urinary HGA difference could be due to differences in urine concentration, as the urine HGA values (and plasma) are not normalised to creatinine, which can minimise variation due to the differences in sample concentration. In human AKU patients, HGA is measured in urine that is collected over a 24-hour period. For a direct comparison, mice would have to be single-housed in metabolic cages, which was not deemed necessary in this case as it is very stressful [244]. The HGA quantitation method used here has very recently been developed to incorporate creatinine quantitation for both plasma and urine (Andrew T Hughes, unpublished) and would be more ideal to use in the future, especially for urine samples where the concentration can vary drastically.

Both the BALB/c *Hgd*$^{-/-}$ and *Hgd tm1a -/-* AKU models reflect the metabolic nature of AKU, demonstrating increased HGA, and both show signs of ochronosis, as pigmentation of chondrocytes located within calcified articular cartilage (see section 3.5.1.1 below for a more in-depth discussion on pigmentation). The appearance and progression of ochronosis is very similar between the two models. The new targeted *Hgd tm1a -/-* AKU model presenting with an almost identical metabolic and joint phenotype to the mutagenesis BALB/c *Hgd*$^{-/-}$ model provides confidence that no confounding mutations affecting the AKU phenotype, with regards to HGA and joint pigmentation at least, are present in the BALB/c *Hgd*$^{-/-}$ model; other mutations affecting aspects of the disease not yet investigated could exist. In addition, this comparison highlights that either model is suitable for further AKU research and can be used interchangeably.

3.5.1.1 Ochronosis

With the introduction of Schmorl's staining in AKU [81], ochronosis was first detected in a mouse model of AKU (BALB/c *Hgd*$^{-/-}$ *Fah*$^{-/-}$) in the calcified articular cartilage of the knee joint, as pigmented chondrocytes with dense intracellular granular pigmentation and a uniform pigmentation of the territorial matrix [229]. No pigmentation was identified in the bone or hyaline cartilage, nor in the inter-territorial matrix. Pigmented kidney nodules were observed in this *Hgd*$^{-/-}$ *Fah*$^{-/-}$ AKU model but were deemed to be associated with the severe renal pathology caused by the confounding HT-1 (*Fah*) mutation. Subsequently, ochronosis was studied in a specific mouse model of AKU, BALB/c *Hgd*$^{-/-}$[115]. The earliest sign of pigmentation was identified in the pericellular matrix of chondrocytes which then progressed to the intracellular compartment, appearing synonymous with the initial stages of ochronosis described in human calcified cartilage [57]. Pigmented chondrons were only observed on the calcified articular cartilage with no end stage blanket pigmentation of any cartilage layers observed, even at 71 weeks of age, with the authors suggesting that lifespan and loading differences due to quadrupedal gait and size between mice and humans may account for this [115].

Pigmentation of knee joint chondrons in BALB/c *Hgd*$^{-/-}$ mice were quantified, with pigmentation shown to begin at 15 weeks of age (mice aged 6, 8 and 15 weeks were investigated), then progress linearly with age. In *Hgd tm1a -/-* mice aged 7-15 weeks, pericellular pigmentation was first identified at 9 weeks within the calcified articular cartilage (Figure 3.10); progression was then similar to BALB/c *Hgd*$^{-/-}$ AKU mice. The ability to score the

progression of ochronosis in AKU mice is a very useful method for assessing future therapeutic interventions, as utilised by Keenan et al. in 2015, where nitisinone was shown to prevent ochronosis from birth and halt ochronosis progression when given mid-life [116]. The counting of pigmented chondrons however is not a perfect quantitation/assessment of joint pigmentation; the observer has to decide whether or not a chondron is pigmented, which can sometimes be unclear. The scoring here, and in the previous BALB/c *Hgd*$^{-/-}$ publications, was also carried out using one section to represent the whole joint, which is the first coronal section to encompass all joint quadrants (medial and lateral parts of both the femur and tibia) when sectioning posterior to anterior through the knee. Although the knees are embedded for sectioning in the same orientation, the position is also not always perfect and may lead to areas of the joint being positioned slightly different to other joints for example. This pigment scoring system could be slightly improved, by using a method similar to the osteoarthritis scoring system, in which the joint is scored in multiple sections taken at fixed intervals across a joint (i.e. every 4th slide encompassing all joint quadrants), which would eliminate variation due to positioning of the joint and the location of the section.

3.5.1.1.1 Anatomical distribution of ochronotic pigment

Pigmentation within the BALB/c *Hgd*$^{-/-}$ and *Hgd tm1a -/-* models had previously only been reported in the knee joint, within the calcified articular cartilage. Here, other large weight bearing hyaline joints were investigated with similar findings; ochronosis was only found as pigmentation of chondrons within the calcified articular cartilage of the femoral head, shoulder joint and elbow joint. Investigation of the vertebral column revealed pigmented chondrons within the calcified cartilaginous endplates of the vertebral bodies, however no pigmentation was found within the fibrocartilaginous annulus fibrosis of the IVD itself, which is a reported site of pigmentation in humans [55,58]. Pigmentation was observed within the fibrocartilaginous menisci within the knee of mice, which is calcified, and also a site of pigmentation in humans.

It would appear in mice, that non-calcified tissue, including non-calcified cartilage, is not susceptible to pigmentation. The superficial layer of hyaline articular cartilage, hyaline laryngeal cartilages, elastic cartilage within the pinna of the ear and the fibrocartilaginous IVDs, which are all composed of non-calcified cartilage, did not show pigmentation even though humans with AKU show pigmentation in these tissues. Pigmentation was also absent in the eyes, tendon, ligament and heart valves. The calcified articular cartilage is clearly the

initial site of pigment deposition in mice and if the lifespan of mice was longer, or if the disease process could somehow be accelerated, they may also eventually exhibit pigmentation of non-calcified tissue such as hyaline cartilage.

3.5.1.1.2 Loading and force influences ochronotic pigment

From the observations here in mice, it would appear that mechanical loading increases pigmentation, as a significantly greater number of pigmented chondrons were observed in the lumbar vertebral endplates compared to those found in the base of the tail. The degree of loading and compression in the mouse lumbar spine is much greater than that of the tail. Furthermore, clustering of pigmented chondrons at the insertion of both ligaments and tendon, such as the Achilles tendon on the calcaneous and the cruciate ligament on the tibia, into calcified articular cartilage appears to reflect the increased tensile stress exerted in these areas.

The effect of physical stress/loading on pigmentation has also been seen in human AKU patients. It has been reported that macroscopic pigmentation on the surface of human calcified articular cartilage appears to be centralised rather than peripheral, and found to be localised in areas of greater loading such as the medial tibial plateau compared to the lateral tibial plateau of the knee joint [57]. Additionally, an autopsy of an AKU patient revealed that whilst the aortic valve of the heart was heavily pigmented along with the mitral valve, the tricuspid valve was unaffected and minimal pigmentation was observed in the pulmonary valve [55]. The authors suggested that the difference in blood pressure and haemodynamic factors between the pulmonary and systemic circulation may influence ochronotic pigmentation. Further to this, prominent pigmentation has been observed in the carotid sinus, which is known to have more turbulent blood flow than the rest of the common carotid artery, which showed little pigmentation [245]. Lichtenstein and Kaplan also documented that pigment was barely found in veins which are under less pressure than the arterial system [58]. Pigmentation within the sclera of the eye is also postulated to be due to UV light damage and stress arising from ocular muscle contractions [83]. This pattern of pigmentation in both mice and humans supports the exposed collagen hypothesis that increased mechanical loading may lead to damage of collagen fibrils within the ECM resulting in loss of protective molecules, increasing the susceptibility of the collagen fibrils to pigment deposition [79]. This would suggest that the ECM associated with chondrons located in calcified cartilage is the

first matrix to exhibit damage through normal physiological loading and ageing, becoming susceptible to HGA-derived pigmentation.

The relationship of mechanical loading with ochronotic pigment could be investigated further using the AKU mouse model. In humans, AKU is a rare form of osteoarthritis, exhibiting a severe and early-onset osteoarthropathy caused by ochronotic pigment deposition. Osteoarthritis is commonly studied using mouse models, investigating pathophysiology, therapeutic interventions/prevention measures or the involvement of specific genes using genetically-modified mice for example. Histological analysis is the main method of evaluating osteoarthritis in the mouse, often utilising scoring systems to compare the severity of cartilage destruction such as the OARSI scoring system [242]. This system was used here to compare the knee joints of untreated *Hgd tm1a -/-* mice with the non-AKU *Hgd tm1a -/+*. Although human AKU patients experience a very severe osteoarthropathy, no differences in OARSI scores were observed at 52-weeks of age in the AKU mice. Although the OARSI scores were not significantly different, the *Hgd tm1a -/+* mice had slightly increased OARSI scores in all the knee joint compartments except for the lateral femur which was comparable. Also, more osteophytes were also observed in *Hgd tm1a -/+* mice than *Hgd tm1a -/-,* which are a common feature of osteoarthritis. This may suggest that the initial, localised chondrocyte pigmentation could actually be protective in *Hgd tm1a -/-* mice, although only a small number of mice were investigated for osteoarthritis here. We know from human AKU patients however that this is not the case for more advanced ochronosis where extreme joint degeneration occurs and pigmentation is clearly not protective, but is detrimental to the joint. If the mice were aged for longer, perhaps a difference in OARSI scores would be observed. Induction of experimental osteoarthritis in the knee joint of the AKU mice however could provide an alternative, quicker way of investigating osteoarthritis; the severity of cartilage damage could be assessed and compared to the non-AKU controls.

Various different murine osteoarthritis models are used in the literature. In addition to using spontaneous mouse models of osteoarthritis such as the STR/ort mouse [246], other post-traumatic models are available where an osteoarthritic phenotype is induced such as intra-articular collagenase injection [247], surgical models such as anterior cruciate ligament transection (ACLT) [248] or destabilisation of the medial meniscus (DMM) [249], and non-invasive joint loading/injury [250,251].

Glasson et al. compared ACLT and DMM, concluding that DMM had good reproducibility, was less invasive and resulted in slower disease progression than ACLT, in which erosion of tibial

subchondral bone could be observed [249]. DMM however still produces moderate-to-severe osteoarthritis by 4-8 weeks post-surgery [249]. Non-invasive joint injury involves using externally applied mechanical loading to the knee that does not break the skin or disrupt the joint capsule to initiate osteoarthritic joint degeneration by injuring the cartilage [251]. Cyclic tibial compression of articular cartilage is a commonly used loading method, whereby cyclic axial compressive loads, considered to be sub-injury forces, are applied to the lower leg through the knee and ankle joints, with the ability to adjust the compressive load, the number of cycles and the frequency that loading is carried out [251]. Cyclic tibial compression is also a very consistent and repeatable method, with the loading controlled by a machine, and is versatile as the loading force, time that the knee is loaded for, how often the knee is loaded and the length of time post-loading can all be altered.

Techniques that induce osteoarthritis in mice could be applied to the AKU *Hgd tm1a -/-* mouse model, to see how changes in loading caused by either surgically-induced joint instability (i.e. DMM) or increased ex-vivo mechanical loading affect both pigmentation of chondrons with the knee joint, and the severity of the induced osteoarthritis. For pigmentation scoring to be possible however, the calcified articular cartilage must remain intact to enable quantification of chondrons within this region. Additionally, as discussed above, pigmentation may be a time-dependant process as the first pigmented chondrons were observed at 9 weeks in *Hgd tm1a -/-* mice, meaning that a period longer than 8 weeks for pigmentation changes to be observed post-injury or post-loading may be required. DMM would therefore most likely be unsuitable, as knees are typically analysed 8-12 weeks post-surgery, where erosion of the calcified articular cartilage may occur, destroying the region where pigmented chondrons need to be counted [252]. The adjustability of the cyclic tibial compressive loading model, coupled with the milder joint degeneration observed due to the sub-injury forces used, representing chronic overuse rather than acute injury, would probably make it the most suitable experimental osteoarthritis model to apply to AKU mice to investigate the effect of mechanical loading on pigmentation and severity of joint degeneration.

3.5.1.1.3 Extracellular matrix and collagen

In human tissue, it has been shown that ochronotic pigment has an affinity for fibrillar collagen surrounded by glycosaminoglycan-rich ground substance, particularly in hyaline cartilage [67]. Analysis of the ligamentous capsule of an AKU hip joint revealed intracellular

pigmentation of fibroblasts and extracellular granular pigmentation associated with collagen fibres that varied in position, distribution and intensity, with individual collagen fibres showing a periodic banding pattern of pigment [78]. It was this work that preceded the exposed collagen hypothesis, with Taylor et al. suggesting that the ECM is normally resistant to pigmentation, becoming susceptible after biochemical or mechanical damage [57]. They also demonstrated that pigmented cartilage is much stiffer than non-pigmented cartilage and suggested that focal pigmentation of individual chondrocytes and their associated collagen is likely to make the ECM prone to damage through normal loading, leading to further damage in an inevitable downward spiral. This then led to the exposed collagen hypothesis as the small granule pigmentation observed on collagen fibres was similar to the pattern of proteoglycan binding, leading to the theory that proteoglycan and glycosaminoglycan loss exposes collagen fibrils, allowing initial HGA/pigment binding that acts as a nucleation point for pigment aggregation [79].

In addition to tissue calcification and loading, it is likely that other factors influence pigmentation as many non-calcified tissues in humans are pigmented, such as the sclera of the eye, the walls of blood vessels and the hyaline articular cartilage of various joints. Differences in the composition of the ECM between tissues could be a factor in ochronotic pigment deposition. With collagen being the most abundant protein in the ECM, the collagen distribution (amount and type) in different tissues may explain why some tissues are more susceptible to ochronosis, in addition to differential expression of other ECM proteins. Furthermore, tissues with different compositions of ECM will likely transmit force/load differently, which may cause damage to occur at different rates. The initiation of pigmentation in the calcified cartilage before any other tissue matrix suggests it is the first matrix to become damaged and subsequently susceptible to attack, as demonstrated by the presence of pigmentation in AKU. Cellular activity may also have a role in pigmentation, as the pigment first identified in mice is associated with the chondrocytes of the calcified articular cartilage and their immediate pericellular matrix. It has been shown *in vitro* that culture media incubated with HGA took weeks to darken in the absence of cells, compared to a few days in the presence of cells (osteosarcoma cell lines), highlighting that cellular activity accelerates pigment deposition [81]. Interestingly, of the osteosarcoma cell lines incubated with HGA, SaOS-2 cells were the most pigmented, but synthesised the least amount of collagen (the opposite was true for TE85 cells), suggesting that the amount of collagen is not a key factor associated with pigmentation [81]. The authors suggested that the ECM formed *in vitro* is not assembled correctly into a highly organised and complex matrix,

with no periodicity observed in fibres, and may explain the rapid pigment deposition by a lack of protective factors. This work suggests that the type of collagen and associated proteins may have a role in pigment deposition, or protection from pigmentation, as certain matrices maybe be more easily damaged than others, whilst others such as mineralised bone are protective in AKU. The absence of pigmentation within tendons and ligaments of mice may be due to the structural organisation of collagen fibrils into fibril bundles, fascicles and then fibre bundles, which may initially protect the collagen from HGA binding. If this assumption was correct, ligaments and tendons may eventually pigment in mice. It is unknown in human AKU patients whether the initiation of pigmentation in calcified articular cartilage occurs at the same time as ligament and tendon pigmentation. Although mentioned above that cellular activity may be a factor accelerating ochronosis, tissues such as cartilage, tendon and ligament have comparatively less cells, in addition to substantially less blood flow or none in the case of cartilage, than tissues such as liver that does not show any pigmentation despite being extremely cellular, very well perfused and the main site of HGA production. The liver is mainly composed of equal amounts of type I and type III collagen, in addition to non-fibrillary basement membrane collagens [253]. The main collagen found within articular cartilage is type II [254], with ligaments and tendons mainly composed of type I collagen [255,256]. The organic matrix of bone is also mainly formed of type I collagen, alongside type V collagen, and is resistant to pigmentation; perhaps mineralized collagen is protected from HGA binding.

3.5.1.1.4 Mice represent the early stages of human ochronosis

No pigmentation was identified in the eyes, ears, laryngeal cartilage, IVDs or the heart valves of the AKU mice, which are all sites of pigmentation in humans. The black punctate pigment seen within the heart valves of both the AKU (*Hgd tm1a -/-*) and non-AKU (*Hgd tm1a -/+*) mice has been reported in normal C57BL/6 mice, thought to be produced by melanocytes derived from a neural crest cell lineage [257]. The AKU mice here appear to represent only the early stages of human ochronosis, with pigmentation only observed in calcified cartilage. The initial site of ochronosis in human tissues may also be chondrons within calcified articular cartilage of the joints, with other tissues subsequently becoming pigmented. The deposition of ochronotic pigment is likely to be a time-dependant process that is related to the composition of the extracellular matrix and is accelerated by loading/physical stress.

3.5.2 Limitations of AKU mouse models

Both the mutagenesis and targeted AKU mouse models exhibit the main characteristics of AKU. The degree of pigmentation however appears to reflect early-stage joint disease even when aged up to 52-80 weeks [115] which is comparable with 40-60 years in humans [258], with no pigmentation observed in the superficial hyaline cartilage, despite humans exhibiting a severe blanket pigmentation present in all layers of articular cartilage [57]. Furthermore, AKU patients develop an early-onset and severe osteoarthritis which is not seen in the AKU mouse models at 1 year of age, with no difference in OARSI scores between homozygous and heterozygous *Hgd tm1a* mice, supported by Preston et al. reporting that the rate of development of osteoarthritis in the BALB/c *Hgd*$^{-/-}$ model was not greater than the spontaneous osteoarthritis rate reported for the background strain [115]. The absence of osteoarthritis in AKU mice is likely due to the ochronotic phenotype being mild and early-stage.

In addition to the absence of macroscopic and microscopic hyaline cartilage pigmentation, there has been no pigmentation observed in other connective tissues such as tendons, ligaments, and the cardiovascular system in mice, that are pigmented in humans. Endogenous vitamin C production in mice [259] has previously been suggested as a protective mechanism against the formation of ochronotic pigmentation due to its anti-oxidant activity. In the 1990s, the absence of pigmentation in the first ENU BALB/c *Hgd*$^{-/-}$ mice aged up to 14 months was attributed to vitamin C production. Differences in urinary excretion of HGA in mice and humans may also have explained the lack of joint pigmentation. However, with subsequent detection of ochronotic pigment and plasma HGA levels that were 3-4-fold greater than human levels [115,116,243], differences in ochronosis severity cannot be attributed to increased urinary excretion nor vitamin C production. Furthermore, treatment with vitamin C in human patients has not proven to be clinically effective [28]. Lack of severe pigmentation in mice could be attributable to their smaller size and quadrupedal gait, and therefore reduced mechanical loading of the joints compared to humans, although it should be noted that the shoulders, which are a non-weight bearing joint in humans, are affected in human patients. If ochronotic pigment deposition is a time-dependant process, the short mouse lifespan may prevent the accumulation of ochronotic pigment to the severe level observed in humans. As discussed in section 1.2.5.3, several different *HGD* mutations exist in human AKU patients, which can have different impacts on the residual activity of the enzyme [93,95,260]. The BALB/c *Hgd*$^{-/-}$ model, was shown to have <6% HGD activity compared to WT, due a truncated protein [86]. Residual activity in the *Hgd tm1a -/-* model has not been reported or

investigated, however no mRNA is detected after the gene trap which causes early termination of transcription (chapter 4 includes liver and kidney *Hgd* mRNA data from *Hgd tm1a -/-* in the *Hgd* deletion studies, Figure 4.31B+C Figure 4.32B+C Figure 4.33B+C, using primers after the gene trap cassette spanning exons 9-10). A recent study reporting the first human genotype-phenotype data however suggests that different residual HGD activity due to the nature of the different mutations is likely not responsible for the observed differences in ochronosis between mice and humans. No differences in serum or 24-hour urine HGA, eye pigmentation and hip bone density were found between patients with 1% or 31-34% residual HGD activity [93].

3.5.3 Future of AKU mouse models

Both the mutagenesis BALB/c *Hgd*$^{-/-}$ and targeted *Hgd tm1a -/-* model show a very similar phenotype of increased plasma and urine HGA and joint pigmentation, therefore either model is suitable for future AKU research. Although these AKU mouse models may not exhibit a severe joint pathology like the human condition, they provide insight into early joint disease that currently cannot be investigated in human patients. Biochemically however, these models represent the AKU phenotype very well, showing the same metabolic features of increased HGA and response to nitisinone. AKU mouse models provide controlled conditions in which to test potential therapies where the effectiveness can be investigated to a much greater extent than is possible in humans, in addition to the opportunity to conduct research into the slow, progressive pathophysiology of AKU, which is not achievable in human patients where disease manifestation takes decades to present. The requirement for these AKU mouse models will exist whilst new therapies and potential treatments are being established, such as enzyme replacement and gene therapy, the latter being the ultimate cure for AKU and other Mendelian diseases.

Studying a rare disease such as AKU can also provide valuable lessons for other more common diseases such as osteoarthritis, as AKU exhibits a severe and early osteoarthropathy. Additionally, attempts to treat the metabolic defect in AKU, via enzyme replacement or gene therapy, will undoubtedly uncover fundamental information applicable to other genetic disorders of the liver.

4 Results:

Localisation of *Hgd* expression and conditional *Hgd* knockout

4.1 Introduction

It is well known that HGD is expressed in the liver and the kidney, where other enzymes in the tyrosine metabolism pathway are also present. There have however been reports that *HGD* is also expressed in the small intestine, colon and prostate [90], the brain [99] and also within osteoarticular cells [100]. Here in this chapter, the tissues in which *H*gd is expressed in the mouse was investigated using the new *Hgd tm1a* model that expresses a *LacZ* reporter gene as a fusion transcript with the first 5 exons of *Hgd.* The initiation of *Hgd* expression in embryonic development was also investigated.

Having determined the location of *Hgd* expression, the *Hgd tm1a* model was then manipulated to create the conditional knockout model *Hgd tm1d*. The aim was to investigate the effect of *Hgd* removal on the AKU phenotype in order to determine the minimum level of *Hgd* mRNA required. In determining which Cre to use the following points were considered; which cells in the liver expressed *Hgd* and can the Cre be used at different levels in order to achieve a dose response curve of the deletion. The main liver Cre available worldwide was the albumin Cre. However, when we looked at the expression of HGD in liver, the albumin expressing cells were not the same as the HGD cells, (data extracted from Aizarani et al. (2019) [261]). *MxCre* has been shown to delete floxed genes in the liver [236] in addition to being inducible and able to produce a dose response.

Mx-1 Cre (*MxCre*) was therefore used here for liver-specific deletion of *Hgd* as firstly it is an inducible model, using pIpC to increase interferon levels in order to promote MxCre expression, which allowed phenotyping before and after deletion to be carried out. Secondly, the use of this interferon-inducible MxCre allowed for a dose response study to be performed by using a range of pIpC doses, resulting in different levels of residual *Hgd* expression. Although Mx-1 is active in other tissues outside of the liver, *Hgd* is only expressed in the liver and kidney, therefore *Mx-1* activity which is low in the kidney will only remove *Hgd* from the liver. In addition to the investigating the amount of liver *Hgd* mRNA needed to rescue AKU, other important considerations for future therapy are addressed in this chapter.

4.2 *Hgd* expression

LacZ, a bacterial gene not found within the mammalian genome, encodes the enzyme β-galactosidase (β-gal). The presence of this enzyme in tissues can be determined *ex vivo* by staining tissues for *LacZ*, where the colourless substrate x-gal (5-bromo-4-chloro-3-indolyl-β-D-galactopyranoside) is converted into galactose and 5-bromo-4-chloro-3-hydroxyindole;

the latter dimerizes and oxidises to 5,5'-dibromo-4,4'-dichloro-indigo, an intense blue product that can be visualised. The *Hgd tm1a* mouse has a *LacZ* reporter gene situated within the gene trap cassette, see Figure 4.1. Positive blue *LacZ* staining therefore represents *Hgd* expression.

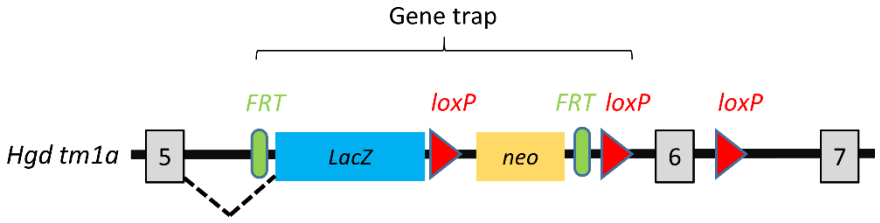

Figure 4.1. Position of *LacZ* within the *Hgd tm1a* allele.
In the *Hgd tm1a* allele, the *LacZ* gene is situated within the gene trap cassette between exons 5 and 6. This *LacZ* gene, which follows a splice acceptor sequence and internal ribosome entry site (IRES), is expressed as a fusion transcript with the first 5 exons of the *Hgd* gene, after which the gene is then interrupted by a poly(A) sequence in the gene trap. The first 5 *Hgd* exons and the *LacZ* gene are translated independently due to the IRES element. Positive *LacZ* expression therefore indicates the expression of the *Hgd* gene.

4.2.1 Whole-tissue *LacZ* staining

Macroscopic *LacZ* staining was carried out across a variety of adult tissues from *Hgd tm1a -/-* mice to identify the tissues expressing *Hgd*. Briefly, tissues were dissected, lightly fixed in 2% paraformaldehyde, 0.2% glutaraldehyde on ice (fixation for too long will diminish/abolish activity of the β-gal enzyme), rinsed in X-gal rinse solution, then stained in X-gal stain solution containing 1 mg/ml X-gal in the dark, at room temperature whilst rotating. Tissues were then rinsed in X-gal rinse, then photos taken with the tissue submerged in PBS, followed by fixation in 10% formalin for a minimum of 24 hours, and then transferred to 70% ethanol.

Tissues from *Hgd tm1a -/-* and -/+ mice containing the *LacZ* reporter gene were stained for *LacZ* alongside tissues from control mice that do not have a *LacZ* gene. These *LacZ* negative controls included *Hgd tm1c +/+*, *Hgd tm1d (fl/fl) MxCre WT or +/-* and C57BL/6 WT; the controls varied due to availability at the time of staining. Positive *LacZ* staining was observed macroscopically in the liver and kidney (Figure 4.2, Figure 4.3) of *Hgd tm1a* mice. Positive staining was observed across the liver parenchyma. In the kidney, only the cortex stained positive; the medulla and renal pelvis did not stain. At 1 and 2 hours, the intensity of *LacZ* staining in the heterozygous liver was less intense than the staining in the homozygous liver. After overnight staining, the difference in staining intensity was no longer obvious. In *Hgd tm1a -/-* mice, kidney expression was observed at 2 hours but not at 1 hour as was observed in the liver. In *LacZ* negative controls, the liver and kidney both stained negative after overnight staining.

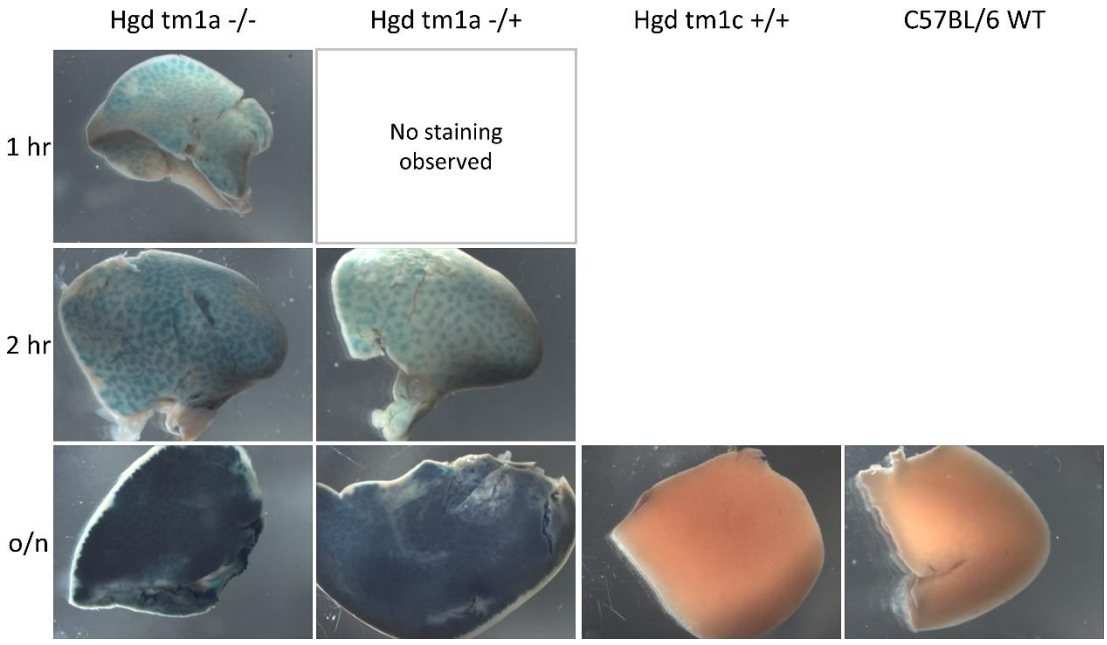

Figure 4.2. *LacZ* staining of adult liver.
Liver from *Hgd tm1a -/-* (31.1 weeks) and *Hgd tm1a -/+* (23.1 weeks) stained *LacZ* positive indicated by the blue colour. Liver from *LacZ* negative *Hgd tm1c +/+* (26.7 weeks) and C57BL/6 WT (22.3 weeks) controls did not stain. o/n = overnight.

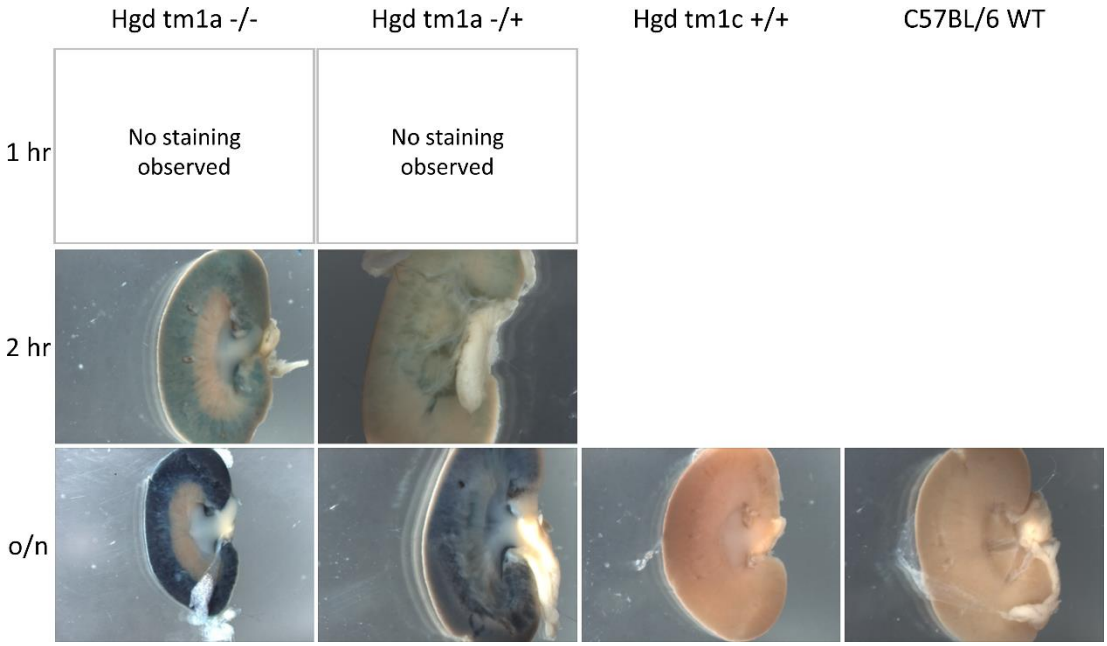

Figure 4.3. *LacZ* staining of adult kidney.
The kidney cortex, and not the medulla, from *Hgd tm1a -/-* (31.1 weeks) and *Hgd tm1a -/+* (23.1 weeks) stained *LacZ* positive indicated by the blue colour. Kidney from *LacZ* negative *Hgd tm1c +/+* (26.7 weeks) and C57BL/6 WT (22.3 weeks) controls did not stain. o/n = overnight.

To determine the histological localisation of positive *LacZ* staining in the liver and kidney, overnight *LacZ*-stained tissue was paraffin sectioned. Upon sectioning however, it became apparent that the *LacZ* staining was only at the periphery of the tissue, and in the area immediately surrounding blood vessels, see Figure 4.4. Upon sectioning, the tissues were also very crumbly; it was very difficult to obtain a section that didn't shatter. This suggested that the tissue was not fixed or processed sufficiently. *LacZ* staining was performed overnight; this is standard procedure for *LacZ* staining. The *Hgd* gene here is highly expressed, taking only an hour for blue staining to appear in the *Hgd tm1a -/-* mice. During staining, the X-gal must penetrate the tissue. Here, the blue product (5,5'-dibromo-4,4'-dichloro-indigo), which is insoluble, appears to have formed a physical barrier that prevented further penetration of the stain deeper into the tissue. This insoluble layer may also have prevented proper fixation and processing of the tissue for paraffin embedding; poor cell morphology of the liver was observed, see Figure 4.4B. The same issues were observed with the kidney. Frozen section *LacZ* staining (section 4.2.2) was therefore undertaken in order to determine the histological location of positive *LacZ* staining in the liver and kidney.

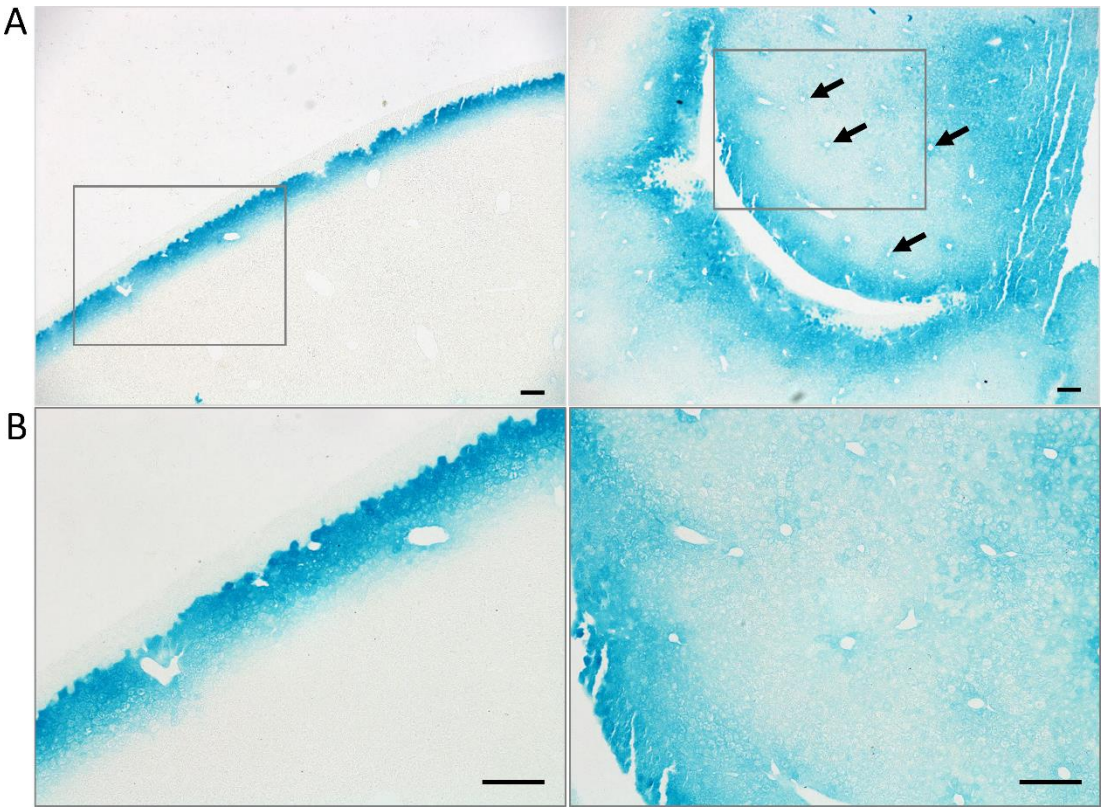

Figure 4.4. Paraffin wax sectioning of *LacZ* stained liver from *Hgd tm1a -/-*.
A shows intense blue *LacZ* staining that can only be seen at the periphery of the liver (top left) and the area immediately surrounding blood vessels (arrows in top right). Penetration of the *LacZ* stain appears to be limited. Higher magnification images are shown in B. Scale bar = 100 µM.

The adrenal gland, situated at the superior pole of the kidney, was also *LacZ* stained; no *LacZ* staining was observed macroscopically after overnight staining, with the adrenal gland from *Hgd tm1a -/-* looking comparable to that of *Hgd tm1d (fl/fl) MxCre +/-,* which does not possess a *LacZ* gene, see Figure 4.5A. Histological sectioning confirms that no blue *LacZ* staining was observed at the histological level, see Figure 4.5B.

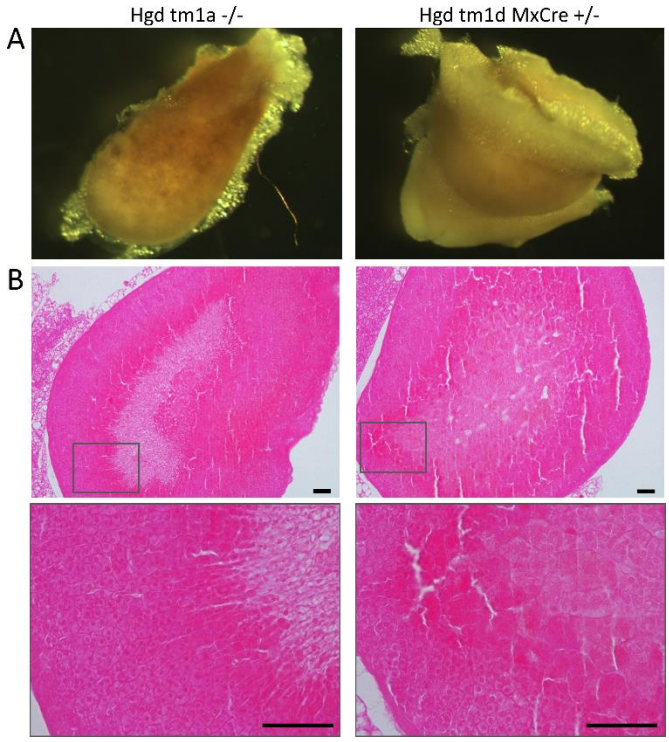

Figure 4.5. Overnight *LacZ* staining of the adult adrenal gland.
A shows overnight *LacZ* staining of the adrenal gland from *Hgd tm1a -/-* (16.3 weeks), which did not show any positive blue staining, and was comparable to the *LacZ* negative *Hgd tm1d (fl/fl) MxCre +/-* (5.4 weeks) control. B shows histological sections of overnight *LacZ* adrenal glands, counterstained with eosin. No *LacZ* staining was observed histologically in *Hgd tm1a -/-* (13.1 weeks) nor the *LacZ* negative control. Scale bar = 50 µM.

With reference to Figure 4.6, the heart, lung and spleen were *LacZ* negative. Staining was observed in the intestinal lumen (indicated by arrows) of *Hgd tm1a -/-* and *Hgd tm1a -/+* mice, however this was due to false-positive bacterial staining, also seen in the *LacZ* negative C57BL/6 WT intestine. The intestine was further investigated via histology; histological sections of *LacZ* stained small intestine (Figure 4.7), caecum (Figure 4.8) and large intestine (Figure 4.9) all show that the blue *LacZ* staining is within the intestinal lumen, and not within the cells making up the intestinal wall, in both the *Hgd tm1a -/-* and *LacZ* negative *Hgd tm1d (fl/fl) MxCre WT* control tissue.

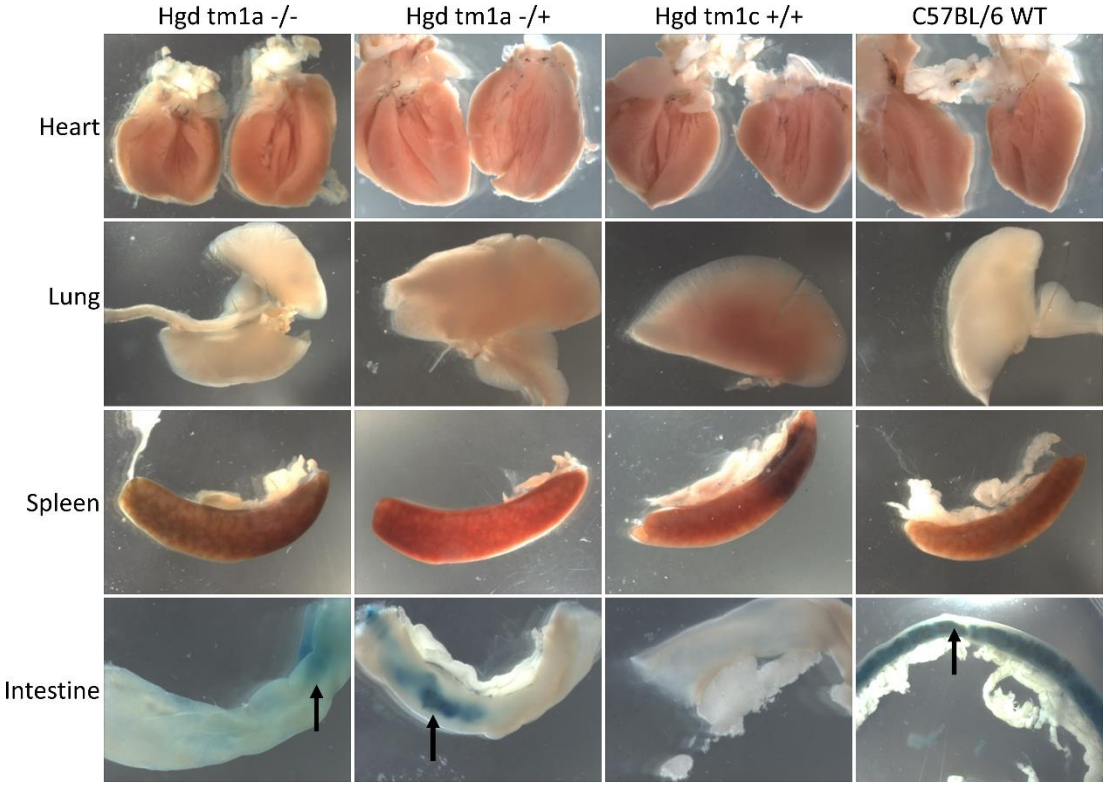

Figure 4.6. Overnight *LacZ* staining of adult heart, lung, spleen and intestine.
The heart, lung and spleen were *LacZ* negative in *Hgd tm1a*. *LacZ* staining was seen in the lumen of the intestine in *Hgd tm1a* and also in the WT *LacZ* negative control, due to false-positive bacterial *LacZ* staining. *Hgd tm1a -/-* = 31.1 weeks. *Hgd tm1a -/+* = 23.1 weeks. *Hgd tm1c +/+* weeks = 26.7 weeks. C57BL/6 WT = 22.3 weeks.

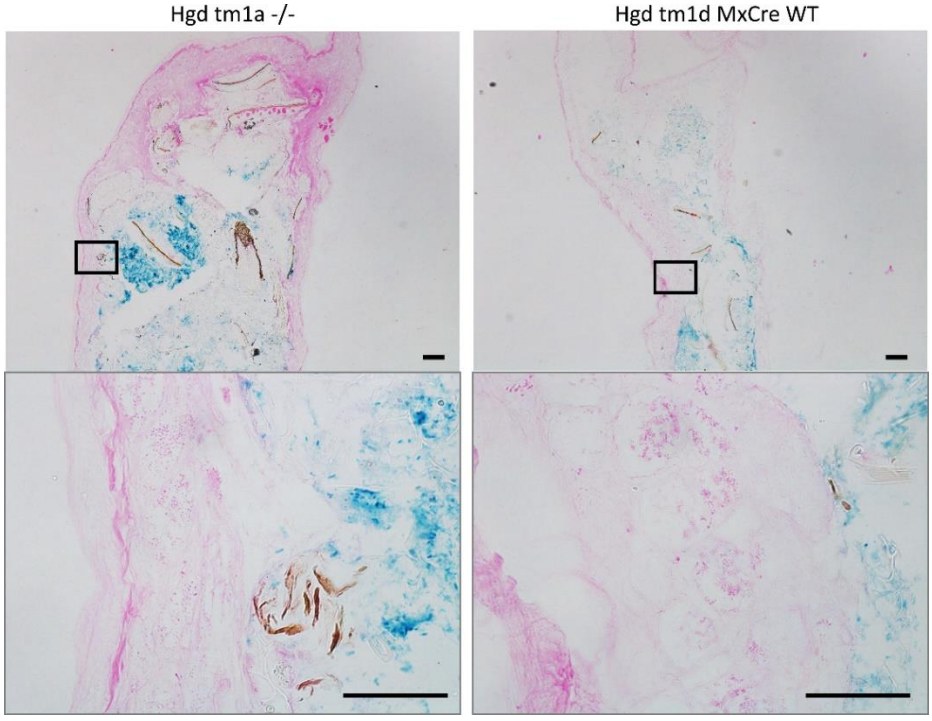

Figure 4.7. Histological sectioning of *LacZ* stained small intestine.
After *LacZ* staining overnight and fixation, the tissue was paraffin sectioned and counterstained with eosin. False-positive *LacZ* staining was observed within the lumen of the small intestine, in both in *Hgd tm1a -/-* (aged 42.7 weeks) and the *LacZ* negative *Hgd tm1d (fl/fl) MxCre WT* (aged 34.4 weeks). No *LacZ* staining was observed within the cells of the intestinal wall. Scale bar in top row = 100 µM. Scale bar in bottom row = 50 µM.

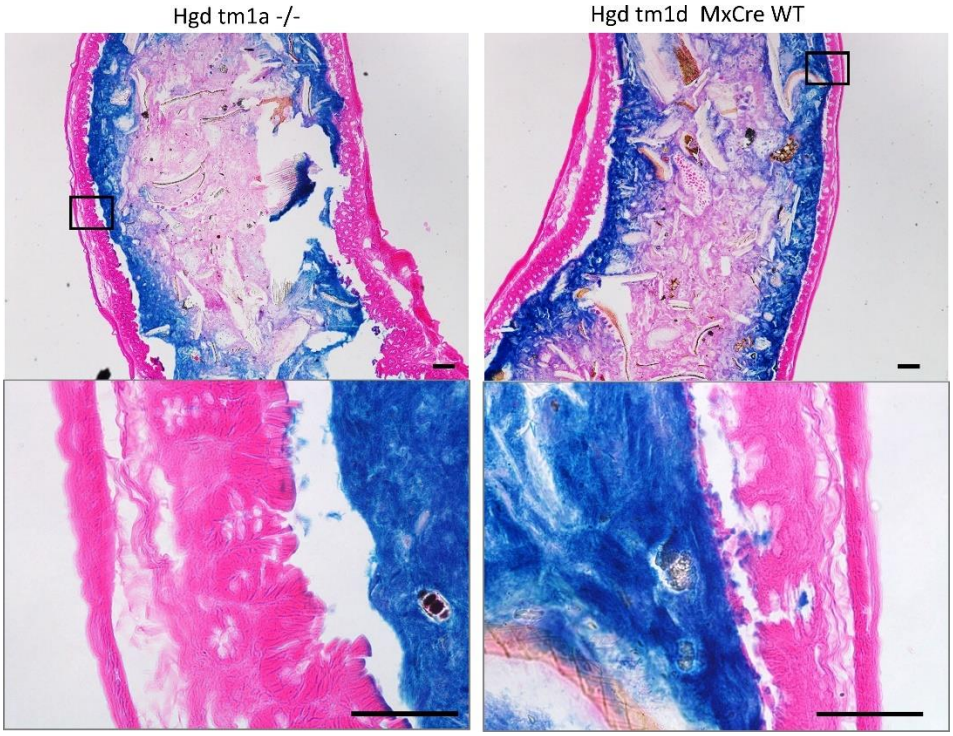

Figure 4.8. Histological sectioning of *LacZ* stained caecum.
After *LacZ* staining overnight and fixation, the tissue was paraffin sectioned and counterstained with eosin. False-positive *LacZ* staining was observed within the lumen of the caecum, in both in *Hgd tm1a -/-* (aged 42.7 weeks) and *LacZ* negative *Hgd tm1d (fl/fl) MxCre WT* (aged 34.4 weeks). No *LacZ* staining was observed within the cells of the caecum intestinal wall. Scale bar in top row = 100 µM. Scale bar in bottom row = 50 µM.

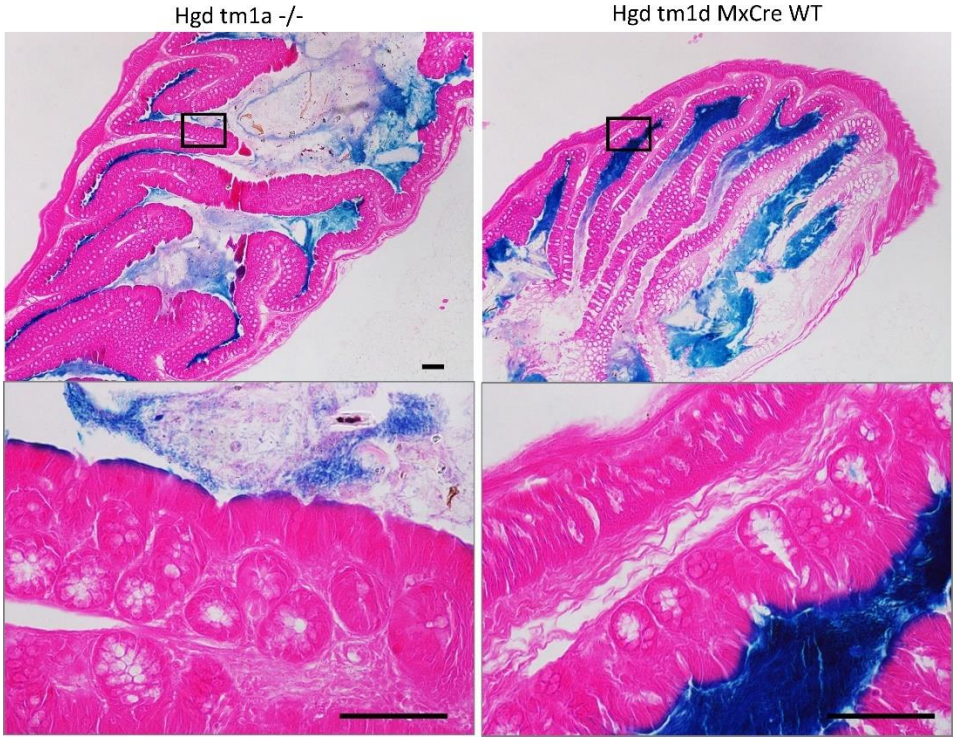

Figure 4.9. Histological sectioning of *LacZ* stained large intestine.
After *LacZ* staining overnight and fixation, the tissue was paraffin sectioned and counterstained with eosin. False-positive *LacZ* staining was observed within the lumen of the large intestine, in both in *Hgd tm1a -/-* (aged 42.7 weeks) and *LacZ* negative *Hgd tm1d (fl/fl) MxCre WT* (aged 34.4 weeks). No *LacZ* staining was observed within the cells of the intestinal wall. Scale bar in top row = 100 µM. Scale bar in bottom row = 50 µM.

With reference to Figure 4.10, the muscle, skin, eye and brain also showed no macroscopic *LacZ* staining; *Hgd tm1a* tissues were comparable with the *LacZ* negative controls. Due to the eye being naturally dark and pigmented, histological sectioning was performed to ensure that there was no positive *LacZ* staining masked by the dark colour of the eye. Histologically, the eye from *Hgd tm1a -/-* and C57BL/6 WT mice are both comparable; no *LacZ* staining observed Figure 4.11.

Brain that had been *LacZ* stained was also histologically sectioned to ensure that it was *LacZ* negative. Areas of particular interest was the cerebral cortex, cerebellum, midbrain, basal forebrain and hippocampus and striatum (caudate putamen), see Figure 4.12A. Figure 4.12B shows H&E staining of C57BL/6 WT and *Hgd tm1a -/+* sagittal brain sections encompassing all of the specific areas of interest. The H&E stain was used to help identify regions of the eosin stained sections from the C57BL/6 wildtype control and *Hgd tm1a -/+* sections. At this low magnification, no blue *LacZ* staining was observed. Figure 4.13 then shows specific areas of the brain in higher magnification, in which no blue *LacZ* staining was identified.

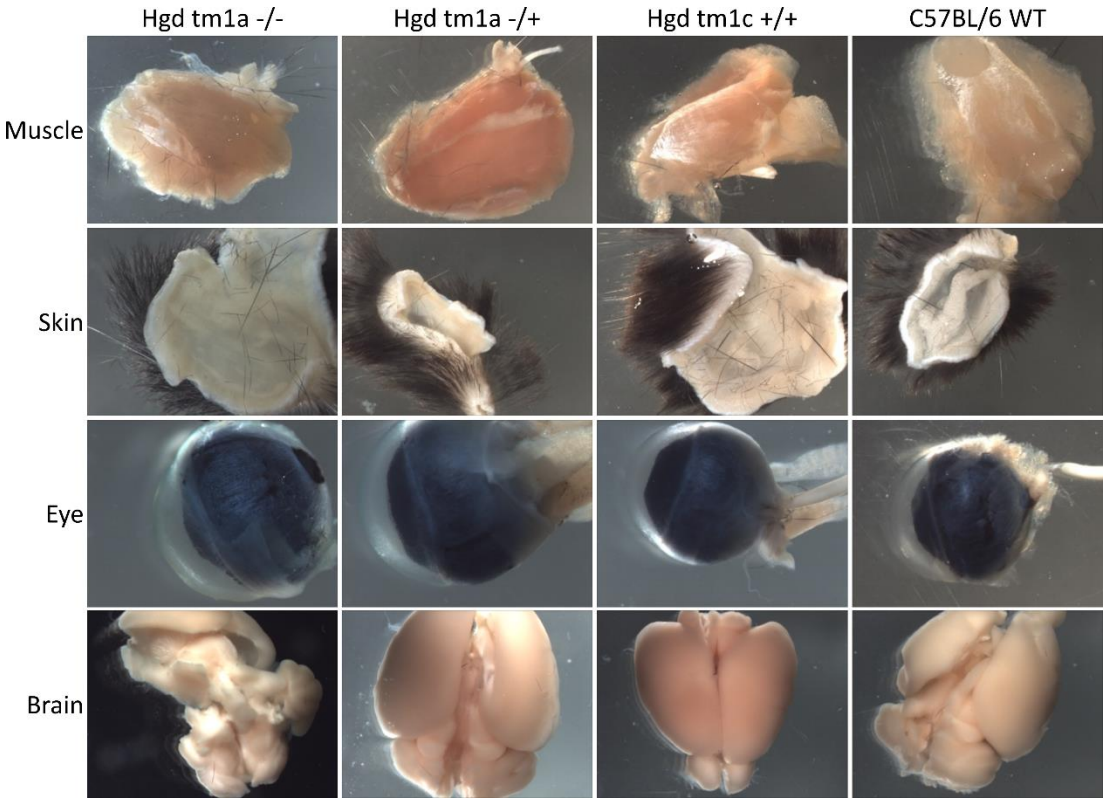

Figure 4.10. Overnight *LacZ* staining of muscle, skin, eye and brain.
No *LacZ* staining was observed in any of these tissues from *Hgd tm1a* mice or *LacZ* negative controls. *Hgd tm1a -/-* = 31.1 weeks. *Hgd tm1a -/+* = 23.1 weeks. *Hgd tm1c +/+* weeks = 26.7 weeks. C57BL/6 WT = 22.3 weeks.

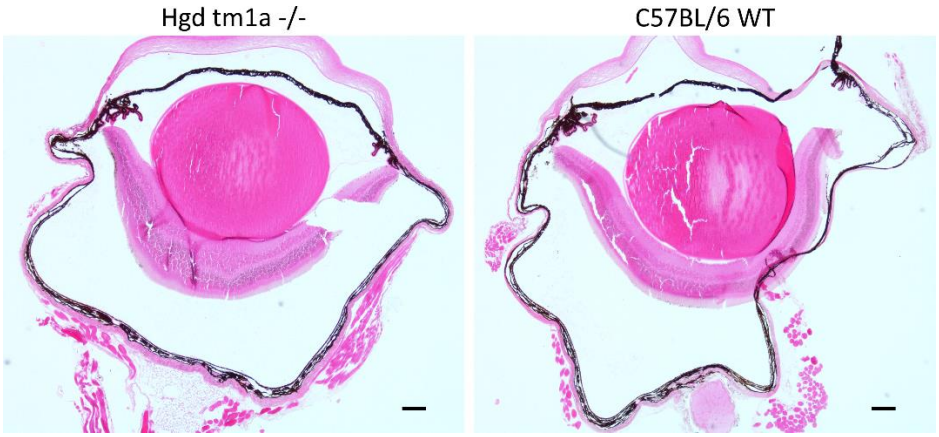

Figure 4.11. Histological sectioning of *LacZ* stained eyes.
After *LacZ* staining overnight and fixation, eyes were paraffin sectioned and counterstained with eosin. No positive *LacZ* staining was observed in *Hgd tm1a -/-* (31.1 weeks) nor the *LacZ* negative C57BL/6 WT (22.3 weeks) eyes. Scale bar = 100 µM

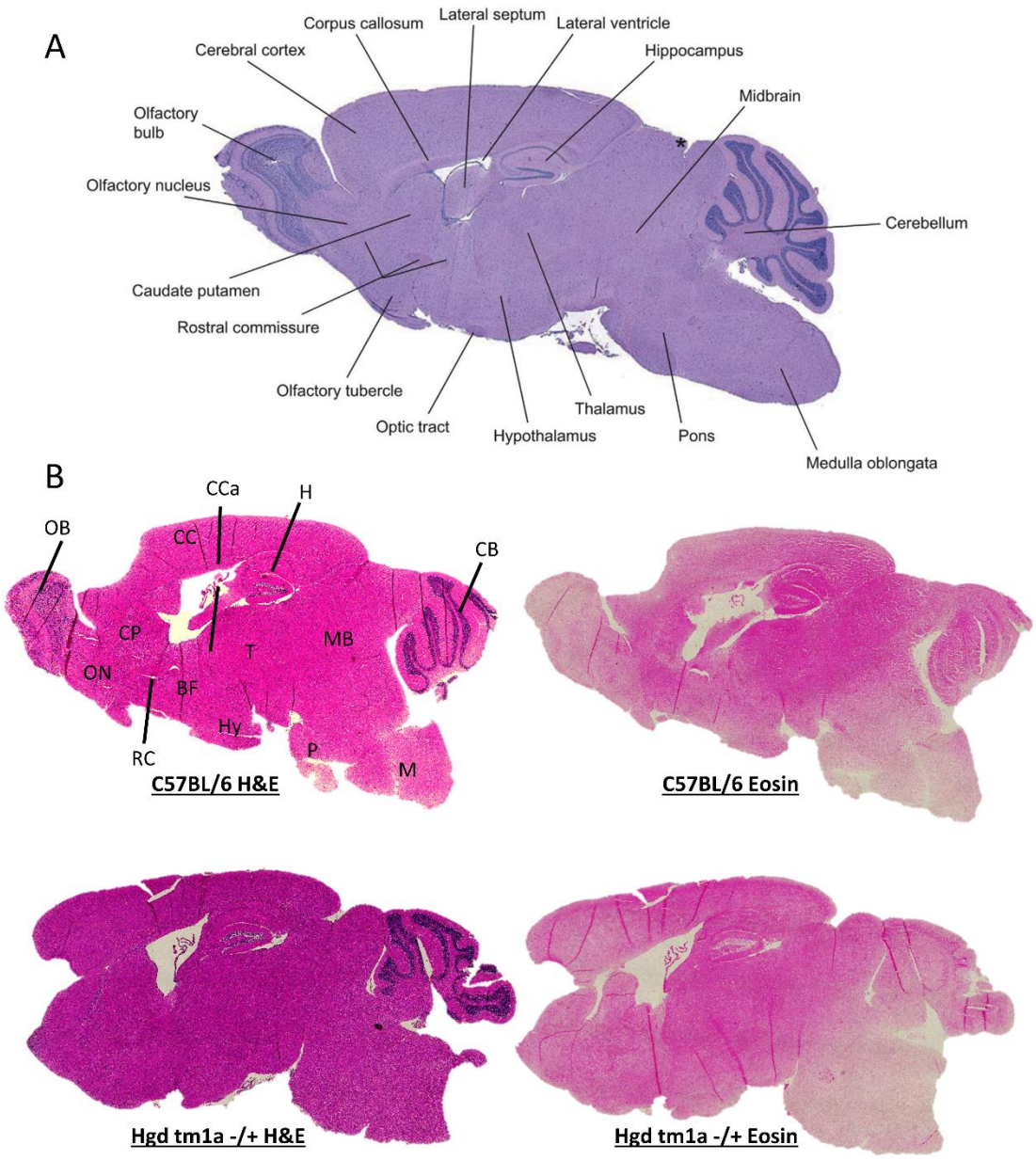

Figure 4.12. Histological anatomy of *LacZ* stained brain sections.
A shows the anatomy of the mouse brain. After *LacZ* staining overnight and fixation, brains were paraffin sectioned in the sagittal plane and counterstained with eosin (B; right). Additional sections were also stained with H&E to aid localisation of structures within the brains (B; left). Individual images were stitched together in order to visualise the whole brain section, to allow anatomical areas of the brain to be identified more easily. At low resolution, no positive *LacZ* staining (blue) was observed in *Hgd tm1a -/+* (23.1 weeks) or the *LacZ* negative C57BL/6 WT (22.3 weeks) brain sections. BF, basal forebrain; CB, cerebellum; CCa, corpus callosum; CP, caudate putamen; H, hippocampus; Hy, hypothalamus; M, medulla; MB, midbrain; OB, olfactory bulb; ON, olfactory nucleus; P, pons; RC, rostral commissure; T, thalamus. H&E, Haematoxylin and eosin. Source of image used in A: Snyder et al. (2018) [262]. Dr Joni Roachdown imaged and stitched the images together in B.

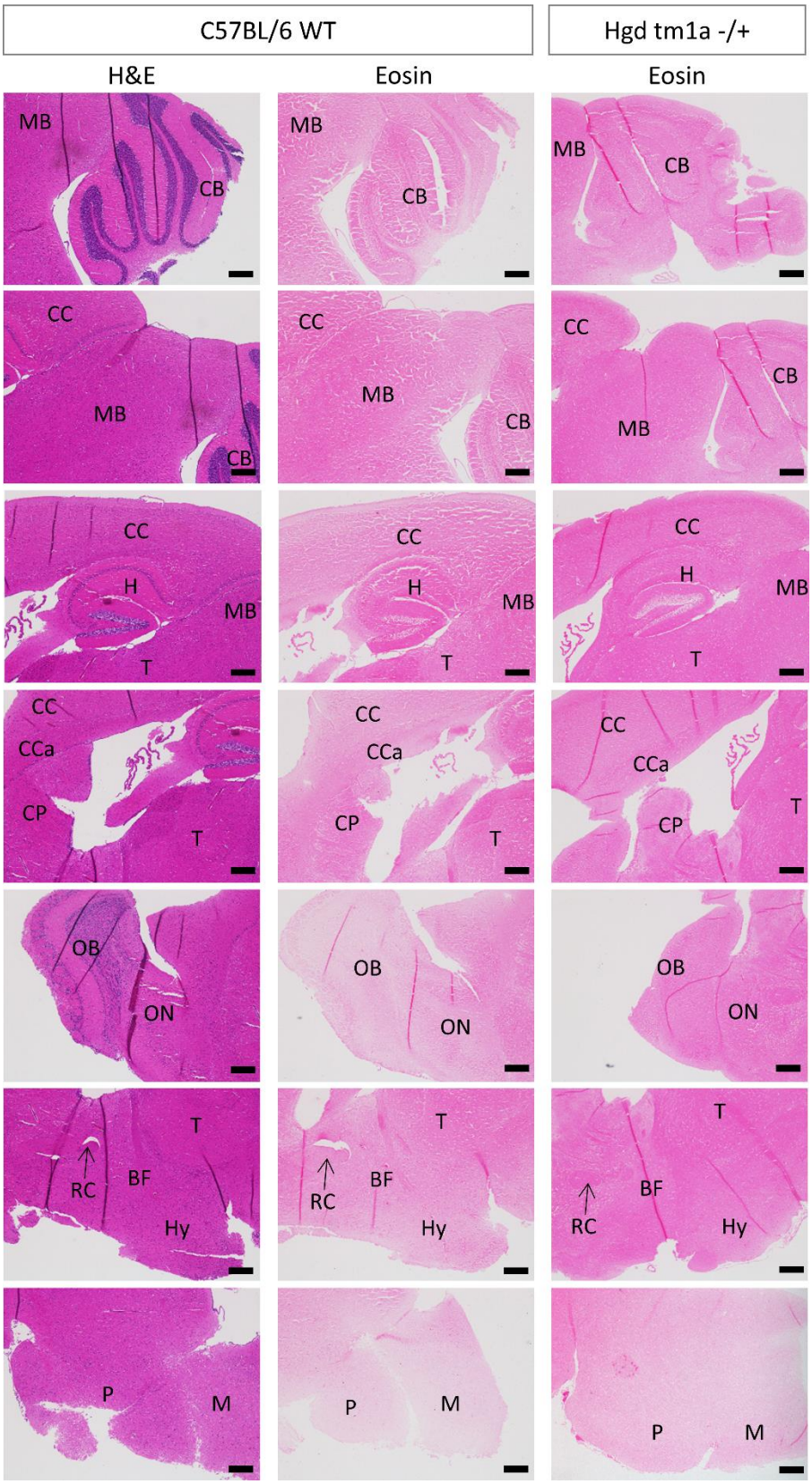

Figure 4.13. Histological sectioning of *LacZ* stained brains.
After *LacZ* staining overnight and fixation, brains were paraffin sectioned and counterstained with eosin, in addition to H&E staining to aid identification of brain regions. No positive *LacZ* staining (blue) was observed in *Hgd tm1a -/+* or C57BL/6 WT brain sections. BF, basal forebrain; CB, cerebellum; CCa, corpus callosum; CP, caudate putamen; H, hippocampus; Hy, hypothalamus; M, medulla; MB, midbrain; OB, olfactory bulb; ON, olfactory nucleus; P, pons; RC, rostral commissure; T, thalamus. Scale bar = 200 µM.

With reference to Figure 4.14, cartilage was *LacZ* negative; the hip did not show any staining. Overall, bones of the knee (femur and tibia), hip (femur) and ribs were *LacZ* negative. There was however positive blue staining present at the growth plates observed in both *Hgd tm1a* and wildtype *LacZ* negative controls, see the arrows in Figure 4.14. The presence of staining in the wildtype *LacZ* negative control mice suggests this is false-positive staining. Paraffin sectioning of the ribs in Figure 4.15 shows that the blue staining is localised to multinucleate osteoclasts present at the resorption zone of the growth plate. False-positive osteoclast staining has been previously reported [263]. Further staining was then carried out in other skeletal areas. The vertebral column was *LacZ* stained and shown to be negative, with no macroscopic staining observed in the vertebrae, intervertebral disc and spinal cord, see Figure 4.16. Also investigated were the bones of the lower jaw and craniofacial skeleton, which are derived from the neural crest of the ectodermal germ layer, whereas the bones of the rest of the body are derived from the mesodermal germ layer. Overnight *LacZ* staining of these bones showed no positive *LacZ* staining, see Figure 4.16.

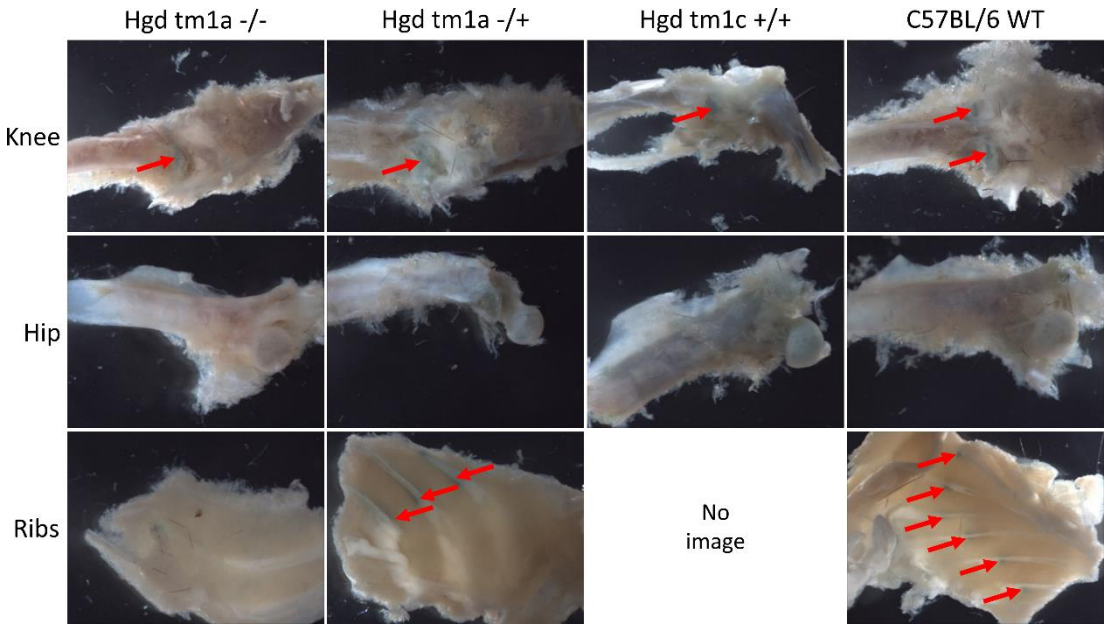

Figure 4.14. Overnight *LacZ* staining of bone and cartilage from the knee, hip and ribs.
In some of tissues where the growth plate is observable, positive blue staining was observed in the growth plates (indicated by arrows), including from the *LacZ* negative *Hgd tm1c +/+* and C57BL/6 WT controls that do not possess a *LacZ* reporter gene. No other staining was observed. *Hgd tm1a -/-* = 31.1 weeks. *Hgd tm1a -/+* = 23.1 weeks. *Hgd tm1c +/+* weeks = 26.7 weeks. C57BL/6 WT = 22.3 weeks.

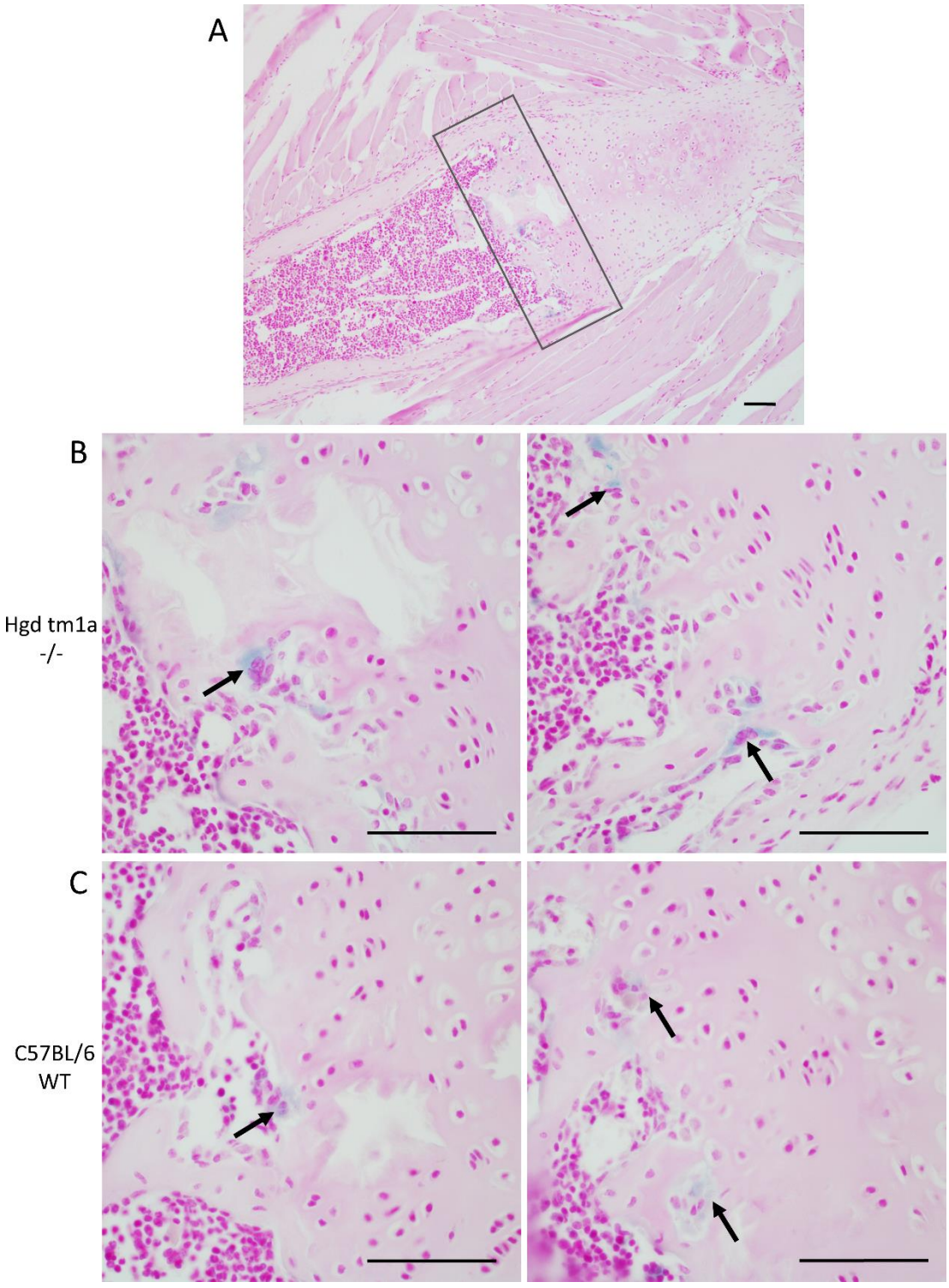

Figure 4.15. False-positive *LacZ* staining of osteoclasts within the rib growth plate.
Rib tissue was stained for *LacZ* overnight, fixed, embedded in paraffin wax, sectioned and counterstained with nuclear fast red. A shows the region of the rib in which false-positive *LacZ* staining (blue) of osteoclasts was found in *Hgd tm1a -/-* mice (B) and C57BL/6 WT mice (C), indicated by arrows. *Hgd tm1a -/-* = 31.1 weeks. C57BL/6 WT = 22.3 weeks. Scale bar = 50 µM.

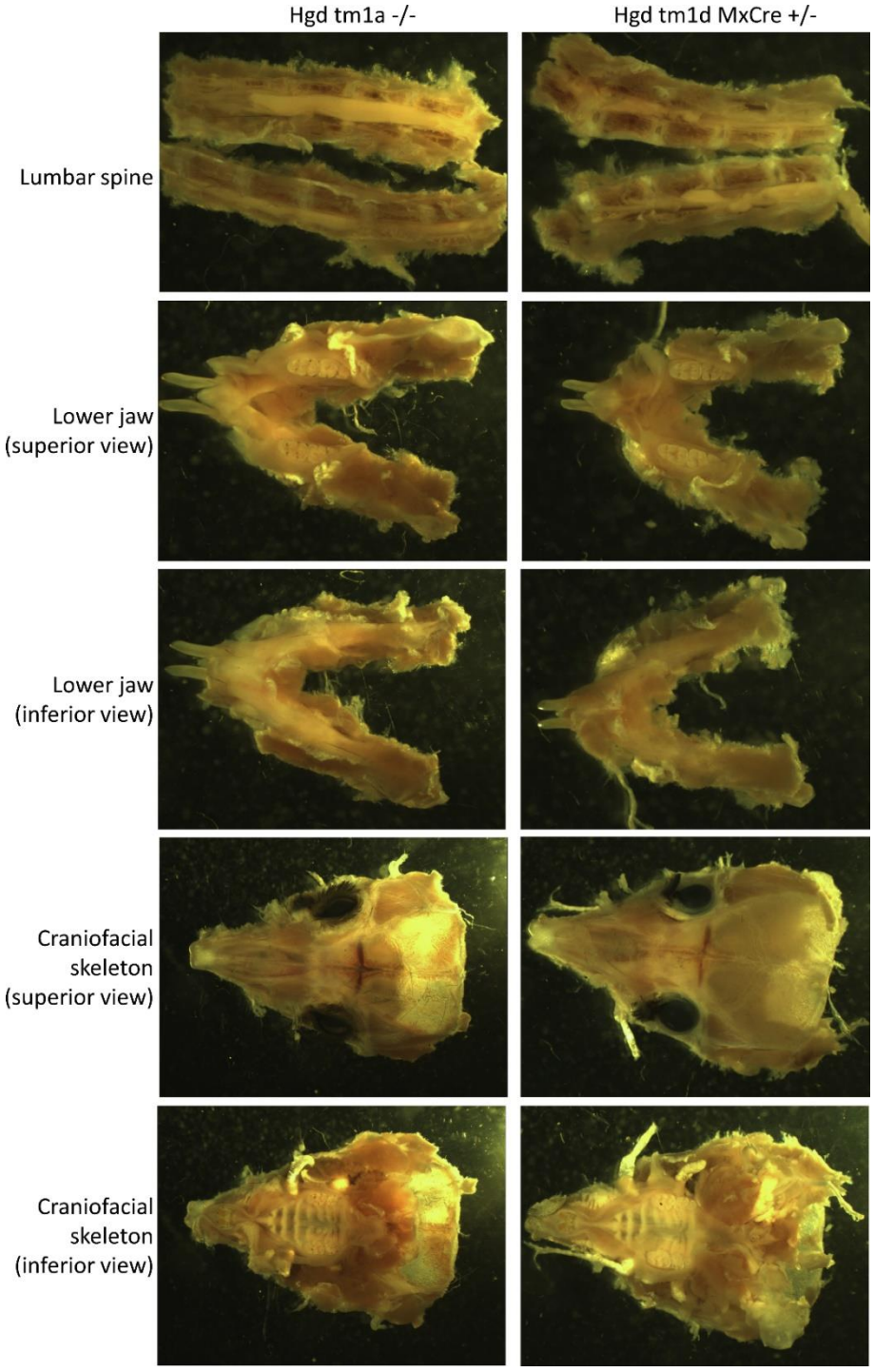

Figure 4.16. Overnight LacZ staining of bone and cartilage from the lumbar spine, lower jaw and craniofacial skeleton.
No *LacZ* staining was observed in *Hgd tm1a -/-* (spine 13.1 weeks, jaw and craniofacial skeleton 16.3 weeks), with the staining comparable to the *LacZ* negative *Hgd tm1d (fl/fl) MxCre +/-* (all tissue 5.4 weeks) control.

As it was previously reported that *HGD* is expressed in the human prostate, the prostate from male mice was *LacZ* stained, along with the bladder, seminal vesicles, urethra and vas deferens, see Figure 4.17A. Positive *LacZ* staining was seen in the vas deferens, in addition to slightly less intense positive *LacZ* staining in the prostate, in both *Hgd tm1a -/-* and the *LacZ*

negative *Hgd tm1d (fl/fl) MxCre WT* mice, see Figure 4.17B. In order to show that the staining is false-positive, the prostate and vas deferens were paraffin sectioned, see Figure 4.18, to demonstrate that the pattern of staining in the *Hgd tm1a -/-* mice was identical to the staining observed in *Hgd tm1d (fl/fl) MxCre WT* mice, where a *LacZ* gene is not present, and is therefore not representative of *Hgd* expression. Within the vas deferens, the staining was localised to the luminal border of the tubule wall (Figure 4.18A), with no blue staining present within the luminal contents which consists of mature sperm. Within the prostate, small diffuse spots of blue staining were observed (Figure 4.18B).

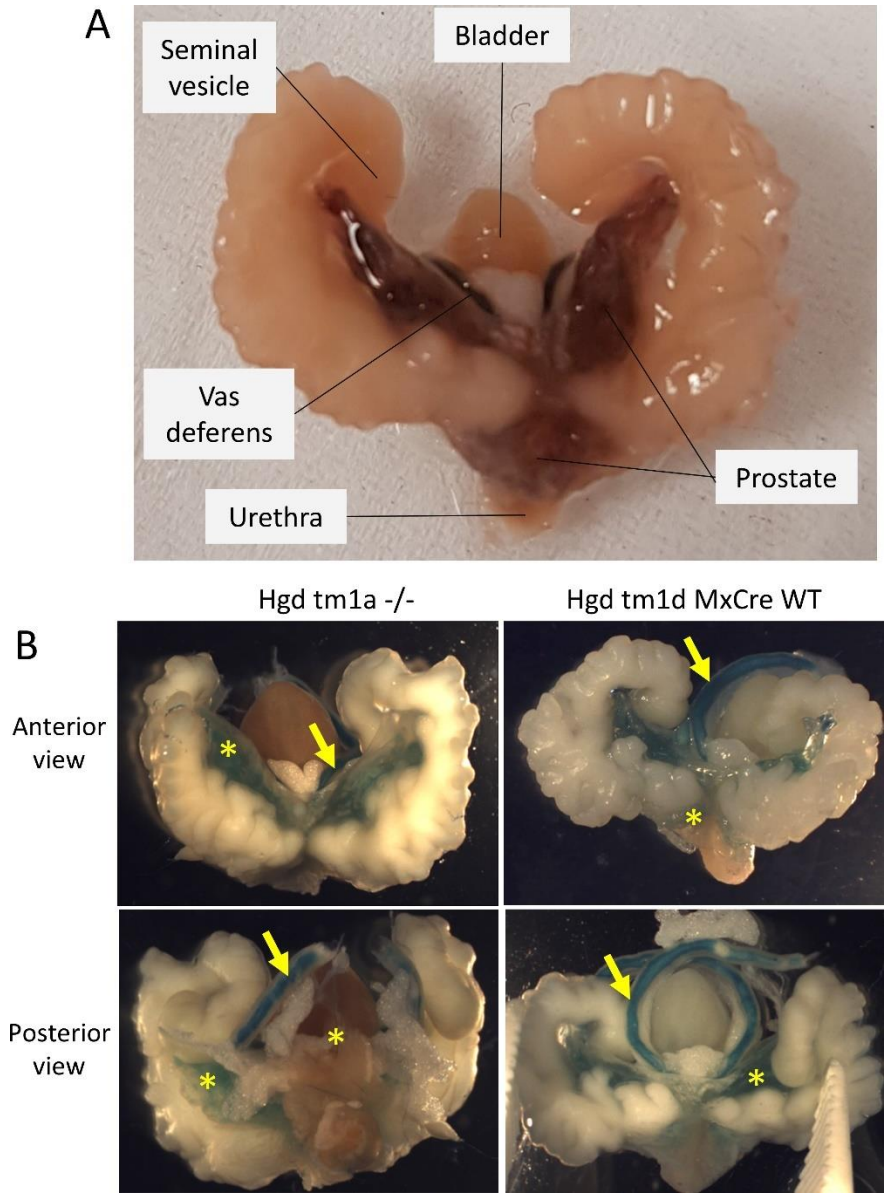

Figure 4.17. Overnight *LacZ* staining of the prostate.
A shows the anatomical location of the prostate, which surrounds the urethra, below the urinary bladder. In B, *LacZ* staining was not observed in the seminal vesicles, urethra or bladder. Positive *LacZ* staining was observed in the vas deferens (arrows) and prostate (asterix) of *Hgd tm1a -/-* (29.3 weeks), however this was also present in wildtype *LacZ* negative (*Hgd tm1d (fl/fl) MxCre WT*; 13.0 weeks) tissue.

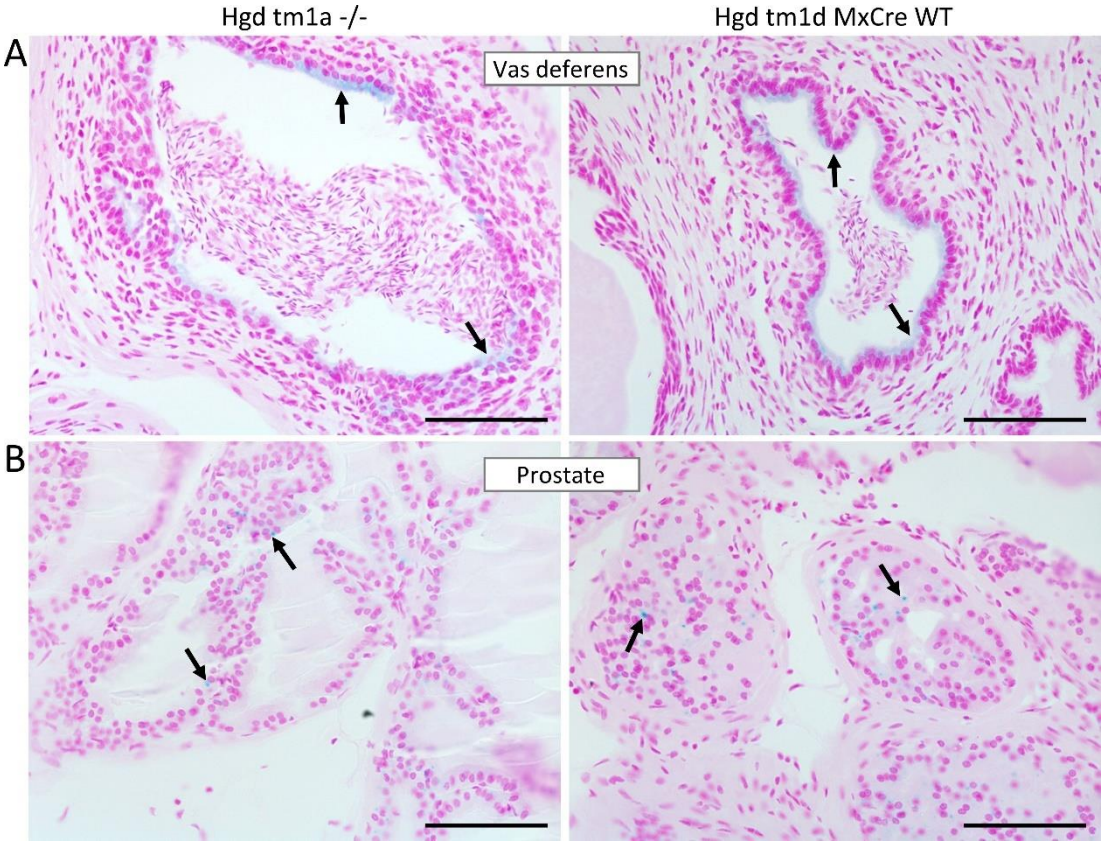

Figure 4.18. Histological sectioning of *LacZ* stained vas deferens and prostate.
After *LacZ* staining overnight and fixation, the prostate and vas deferens were paraffin sectioned and counterstained with nuclear fast red. A shows the vas deferens and B shows the prostate from *Hgd tm1a -/-* (29.3 weeks) and *Hgd tm1d (fl/fl) MxCre WT* (13.0 weeks) mice. Blue staining in both the vas deferens and prostate, indicated by arrows, was present in both *Hgd tm1a -/-* mice and in the *LacZ* negative control *Hgd tm1d (fl/fl) MxCre WT* mice, indicating false-positive *LacZ* staining. The pattern and intensity of staining in the *Hgd tm1a -/-* tissue is the same as the *Hgd tm1d (fl/fl) MxCre WT* tissue. Scale bar = 50 µM.

The gonads were also *LacZ* stained. With reference to Figure 4.19, macroscopic *LacZ* staining revealed that the ovary, fallopian tubes and uterus in female mice did not stain *LacZ* positive in *Hgd tm1a -/-* mice. Histological sectioning confirmed that no blue *LacZ* staining was observed (Figure 4.20), and was comparable with the *LacZ* negative control. Overnight *LacZ* staining of the testis, epididymis and part of the vas deferens revealed positive blue staining in *Hgd tm1a -/-*, see Figure 4.21. Due to positive blue staining also being observed in the *LacZ* negative control mouse (*Hgd tm1d (fl/fl) MxCre WT*) within the epididymis and vas deferens, only the testis positive staining was thought to be true *LacZ* staining representing *Hgd* expression.

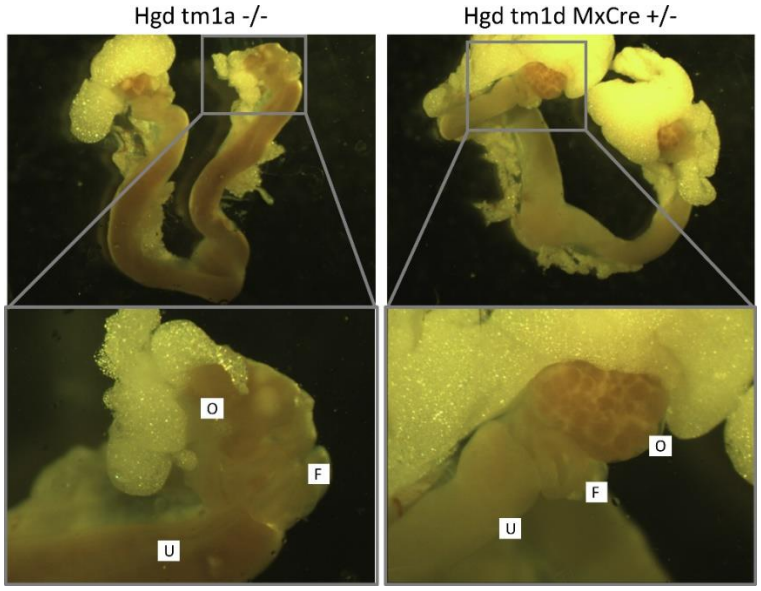

Figure 4.19. Overnight *LacZ* staining of adult ovaries, fallopian tubes and uterus.
After overnight *LacZ* staining, no positive staining was observed in the ovaries, fallopian tubes and the uterus from female *Hgd tm1a -/-* (13.1 weeks). The *Hgd tm1a -/-* staining was comparable to the *LacZ* negative *Hgd tm1d (fl/fl) MxCre +/-* (5.4 weeks) control. O = ovary, F = fallopian tube, U = uterus.

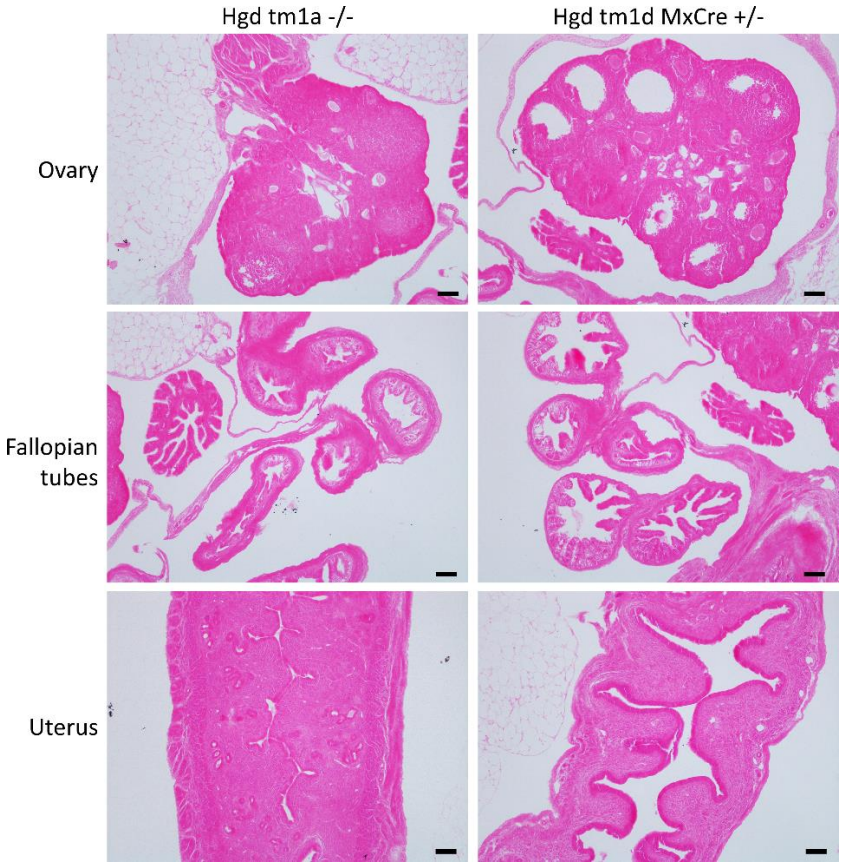

Figure 4.20. Histological sectioning of *LacZ* stained ovary, fallopian tubes and uterus.
After *LacZ* staining overnight and fixation, the ovary, fallopian tubes and uterus were paraffin sectioned and counterstained with eosin. No positive *LacZ* staining was observed in any of these tissues from *Hgd tm1a -/-* (13.1 weeks), which were comparable to the *LacZ* negative *Hgd tm1d (fl/fl) MxCre +/-* (5.4 weeks) control. Scale bar = 50 µM.

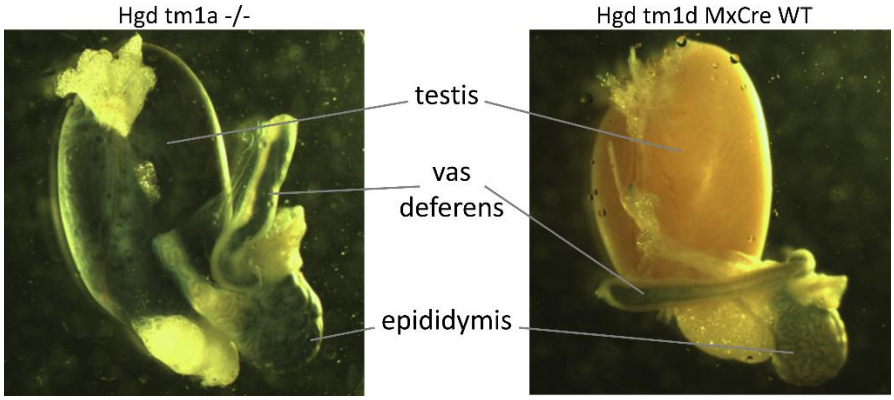

Figure 4.21. Overnight *LacZ* staining of adult testis and epididymis.
Positive blue *LacZ* staining was observed in the testis, epididymis and part of the vas deferens from male *Hgd tm1a -/-* (16.3 weeks). The *LacZ* negative control (*Hgd tm1d (fl/fl) MxCre WT*; 23.1 weeks) shows positive blue staining in the epididymis and vas deferens, but not in the testis.

Histological sectioning of the testis and epididymis is shown in Figure 4.22; the vas deferens was investigated above in Figure 4.18 with the prostate. Within the testis, positive blue staining was observed within the luminal aspect of the seminiferous tubules of *Hgd tm1a -/-* , and not within the *LacZ* negative control, which indicated that *Hgd* is expressed in the testis, see Figure 4.22A-C. The middle tubules of the testis were not stained blue, most likely due to the stain solution not penetrating the centre of the tissue fully. The staining was not observed within the extra-tubular Leydig cells or peri-tubular myoid cells. The positive blue staining appears to be in the cytoplasm of the developing sperm, which progress through a series of developmental stages, beginning at the basal aspect of the seminiferous tubule then passing through the somatic Sertoli cells that form the walls of the tubules (these are very hard to identify even with histology), finishing at the luminal aspect of the seminiferous tubule wall, with the spermatozoa tails projecting into the lumen, see Figure 4.23. The blue staining shown in *Hgd tm1a -/-* matches the pattern of staining observed within the testis of a different knockout mouse model called *Paskin -/-* in the literature, where the authors report positive blue staining within the cytoplasm of developing spermatids and spermatozoa, see Figure 4.22D [264]. The positive blue staining in Figure 4.23B appears to be within the cytoplasm of secondary spermatocytes, round spermatids and the elongated spermatozoa towards the luminal side of the seminiferous tubules. The small punctate dots near the basal surface may be cytoplasmic residual bodies released from the round spermatids as they alter their morphology to become elongated spermatozoa.

Within the epididymis (see Figure 4.24), positive blue *LacZ* staining was observed within the innermost aspect of the tubule wall (see arrows) in both *Hgd tm1a -/-* and the *LacZ* negative

Hgd tm1d (fl/fl) MxCre WT control, indicating that the staining is false-positive and does not represent *Hgd* expression. Although not identified macroscopically in Figure 4.21, there was positive blue *LacZ* staining with in the lumen of the tubules of the epididymis in *Hgd tm1a -/-*. This staining is could either be within the cytoplasm of the spermatozoa contained within the epididymis and/or the cytoplasm droplets from the developing spermatids released from the seminiferous tubules. The epididymis from the *Paskin* -/- mice shown in Figure 4.22D also showed patchy blue staining in the epididymis [264].

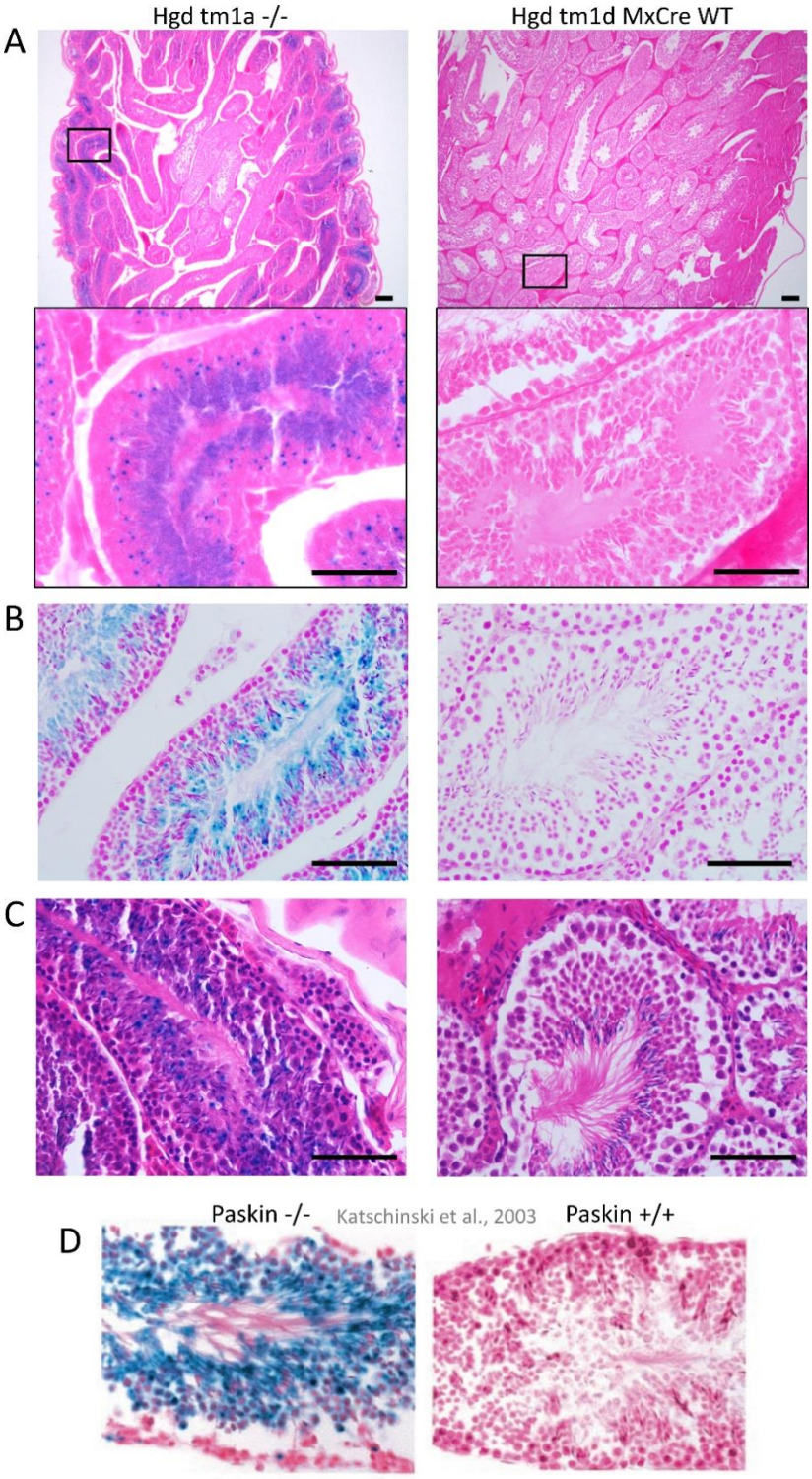

Figure 4.22. Histological sectioning of *LacZ* stained testis.
After *LacZ* staining overnight and fixation, the testis was paraffin sectioned and counterstained with eosin (A), nuclear fast red (B) or stained with haematoxylin & eosin (C). Positive blue *LacZ* staining can be observed within the tubules of the testis from *Hgd tm1a -/-*. The testis of the *LacZ* negative control (*Hgd tm1d (fl/fl) MxCre WT*) shows no *LacZ* staining. The blue *LacZ* staining appears to be within the developing germ cells undergoing spermatogenesis. D shows positive blue *LacZ* staining in cryosectioned testis from *Paskin -/-* (has *LacZ* reporter gene) and *Paskin +/+* (*LacZ* negative) mice, counterstained with neutral red, reported by Katschinski et al. in 2003 [264]. The blue *LacZ* staining is localised to the developing germ cells within the seminiferous tubules around the luminal surface, specifically within the cytoplasm of spermatids and within the tail region of maturing spermatozoa. The pattern of blue staining in D is comparable to B. *Hgd tm1a -/-* 16.3 weeks. *Hgd tm1d (fl/fl) MxCre WT* 23.1 weeks. Scale bar in top row of A = 100 µM. Scale bar in bottom row of A and in B and C = 50 µM.

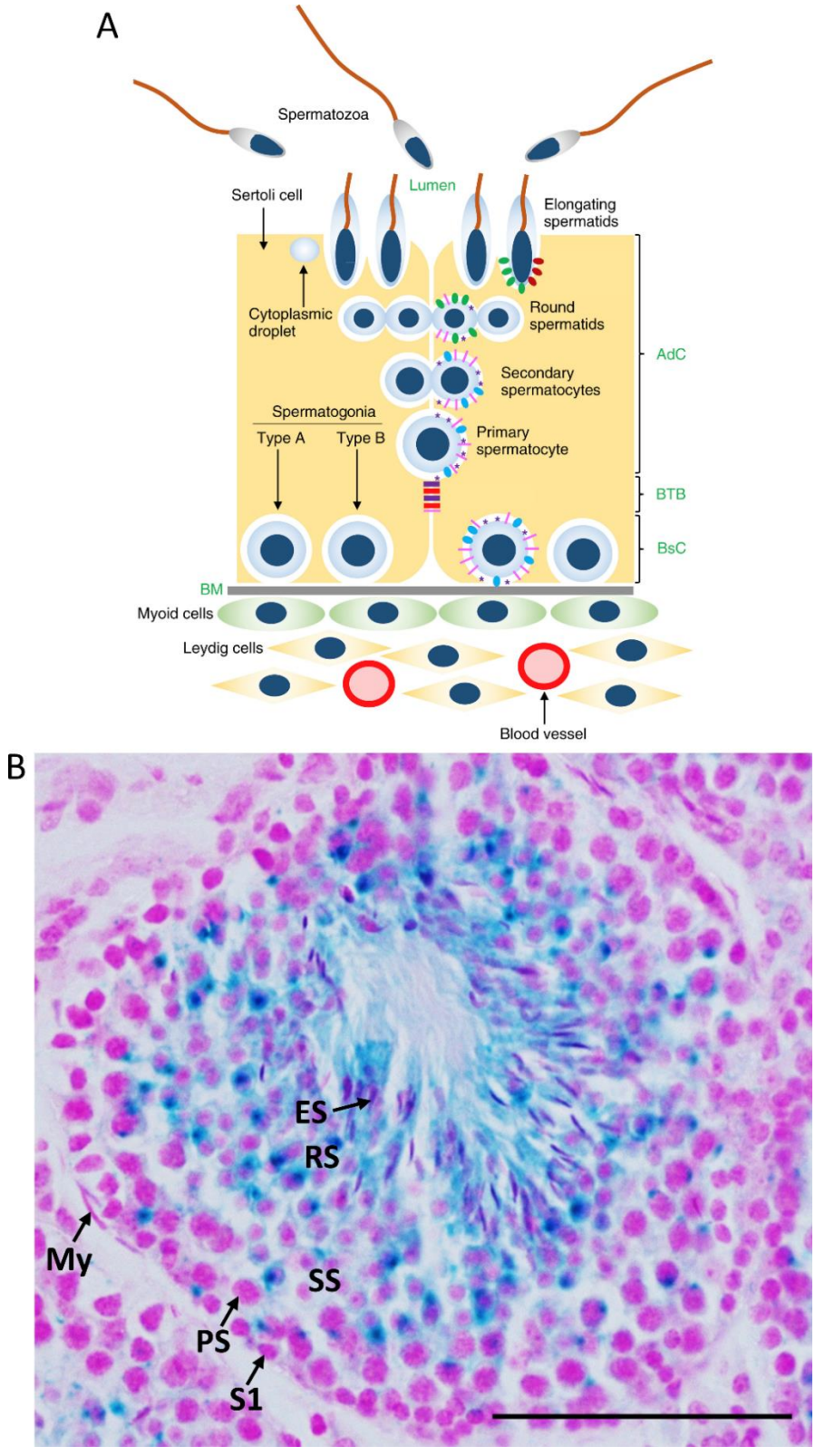

Figure 4.23. Histological identification of the cell types within the testis.
A shows a schematic representation of the cell types, both somatic and germ cells, within the testis. B shows nuclear fast red counterstaining of *LacZ* stained testis from *Hgd tm1a -/-.* The developing germ cells that migrate through the seminiferous tubule germinal epithelium have been identified. Abbreviations: BM, basement membrane; AdC, adluminal compartment; BTB, blood testis barrier; BcS, basal compartment; Le, Leydig cells; My, myoid cells; S1, spermatogonia; PS, primary spermatocytes; SS, secondary spermatocytes; RS, round spermatids; ES, elongated spermatozoa. Scale bar = 50 µm. Part A adapted from Nishimura & L'Hernault, 2017 [265].

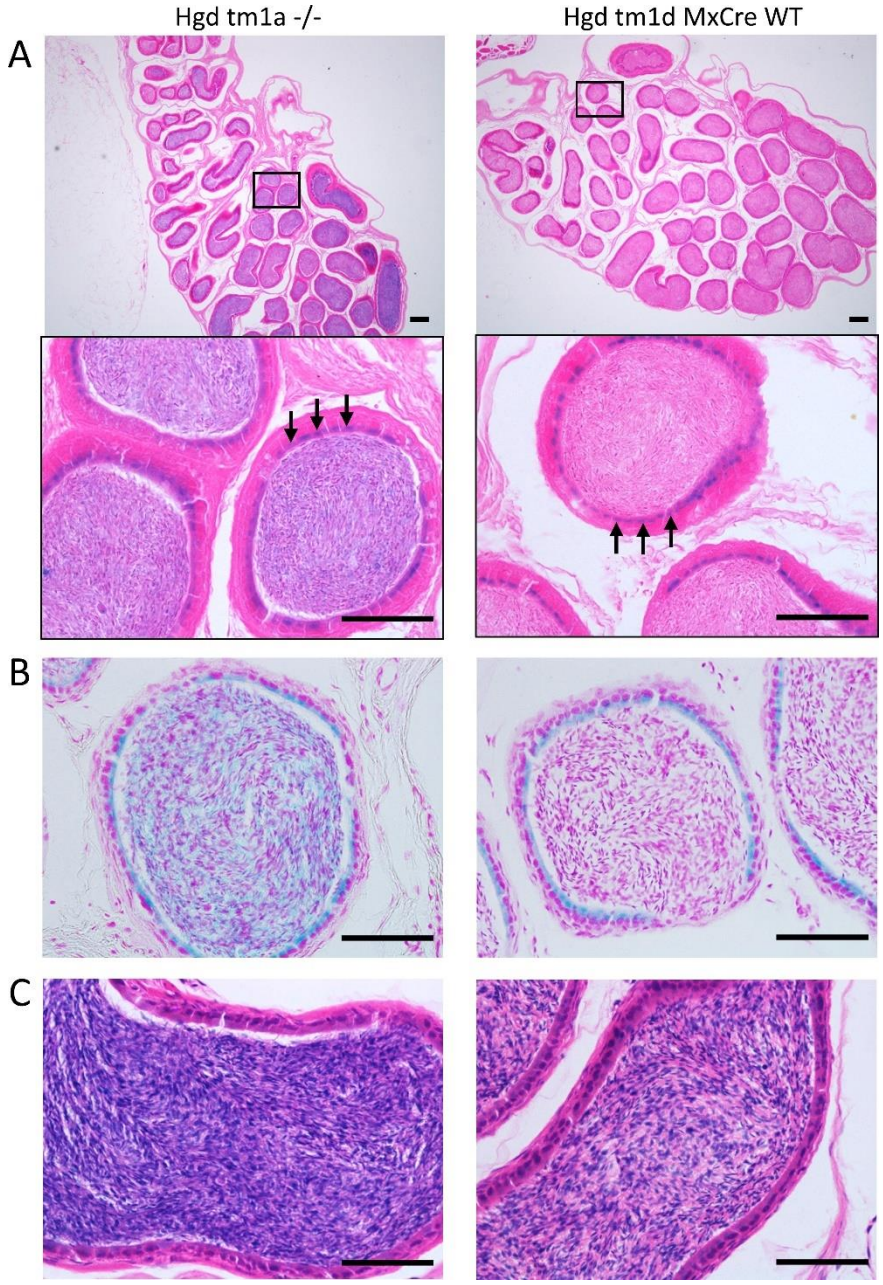

Figure 4.24. Histological sectioning of *LacZ* stained epididymis.
After *LacZ* staining overnight and fixation, the epididymis was paraffin sectioned and counterstained with eosin (A), nuclear fast red (B) or stained with haematoxylin & eosin (C). Positive blue *LacZ* staining can be observed at the luminal edge of the tubule walls within the epididymis (indicated by arrows) in both *Hgd tm1a -/-* and the *LacZ* negative *Hgd tm1d (fl/fl) MxCre WT* control. Positive blue *LacZ* staining is also observed within the lumen of the epididymis tubules in *Hgd tm1a -/-*, which is not observed in the control. *Hgd tm1a -/-* 16.3 weeks. *Hgd tm1d (fl/fl) MxCre WT* 23.1 weeks. Scale bar in top row of A = 100 µM. Scale bar in bottom row of A, and in B and C = 50 µM.

4.2.2 Frozen section *LacZ* staining

OCT-embedded frozen liver and kidney from *Hgd tm1a -/-* were sectioned with a cryostat to obtain frozen tissue sections. As with *LacZ* staining of whole tissue, fixing the section before staining is required if the tissue was not fixed prior to cryo-embedding. X-gal was used at the

same concentration as whole tissue staining, at 1 mg/ml. Protocols in the literature were greatly varied, therefore the frozen section *LacZ* staining procedure required optimization, with regards to fixation time, staining temperature and staining duration. Initially, a 3-minute 0.2% glutaraldehyde (GA) fix was used, followed by staining overnight at 37°C, with the section fully immersed in the frozen X-gal stain solution. With reference to Figure 4.25, the sections were overstained, with a poor cell morphology, likely due to prolonged exposure to 37°C. The same staining procedure was then undertaken at room temperature; the staining intensity was better and not overstained, however the morphology of the cells was still poor. This may have been due to the 3-minute GA fix not being long enough, and also due to the tissue being immersed in stain solution for too long. Thinner sections would also improve tissue morphology. Eosin, a cytoplasmic stain, was also tested as a counterstain, and was not useful in the liver, as the *LacZ* staining was present in the cytoplasm. Subsequently, a 10-minute GA fix with staining at 37°C for 2 hours to minimise the time in the stain solution but with a quicker reaction was performed, on 6 µM sections. The staining intensity and tissue morphology were improved, with nuclear fast red acting as a more suitable counterstain.

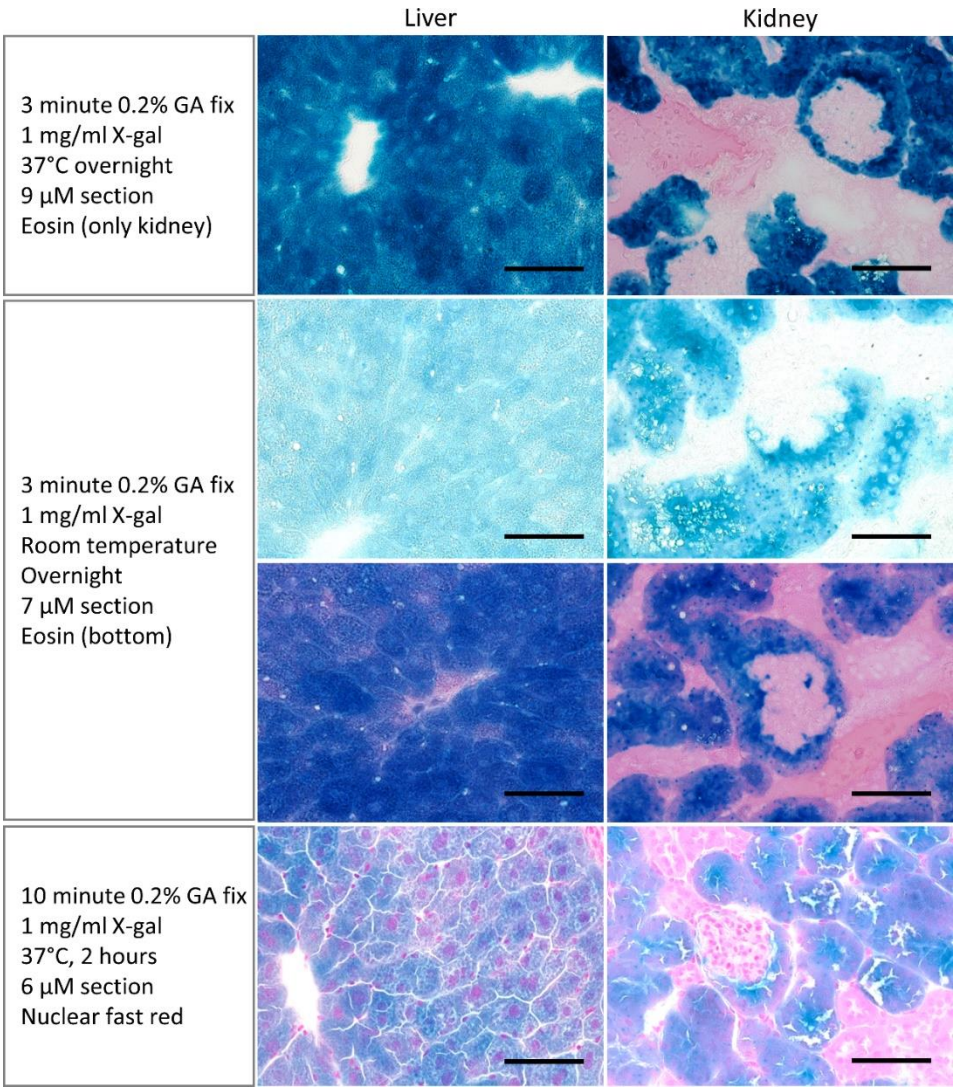

Figure 4.25. Optimisation of frozen section *LacZ* staining of liver and kidney from *Hgd tm1a -/-*.
Liver and kidney tissue from 26.7-week-old *Hgd tm1a -/-*. GA, glutaraldehyde. Scale bar = 50 µM.

Positive *LacZ* staining, and therefore *Hgd* expression, was observed throughout the parenchyma of the liver, in the cytoplasm of hepatocytes and not in the nucleus (Figure 4.26A). In the kidney cortex, staining was also observed in the cytoplasm of certain tubule cells with no staining seen in the glomeruli (Figure 4.26B). In order to determine whether the tubule cells that stained positive were proximal convoluted tubule (PCT) or distal convoluted tubule (DCT) cells, a periodic acid Schiff (PAS)/haematoxylin stain was performed. Figure 4.26C shows PAS/haematoxylin staining of a paraffin section of kidney cortex and how it distinguishes PCTs by the presence of a PAS-positive dark pink/purple brush border that is not present on DCTs. The PAS/haematoxylin stain was then performed on frozen sectioned kidney cortex to ensure the stain was suitable for frozen sections and gave the same result (Figure 4.26D). Frozen section *LacZ* staining of the kidney cortex was then performed,

followed immediately by PAS staining with no haematoxylin which is too similar in colour to the *LacZ* staining, see Figure 4.26E. The blue *LacZ* staining was localised with the PAS-positive tubules, identifying the *Hgd* expressing cells in the kidney cortex to be PCT cells of the kidney cortex.

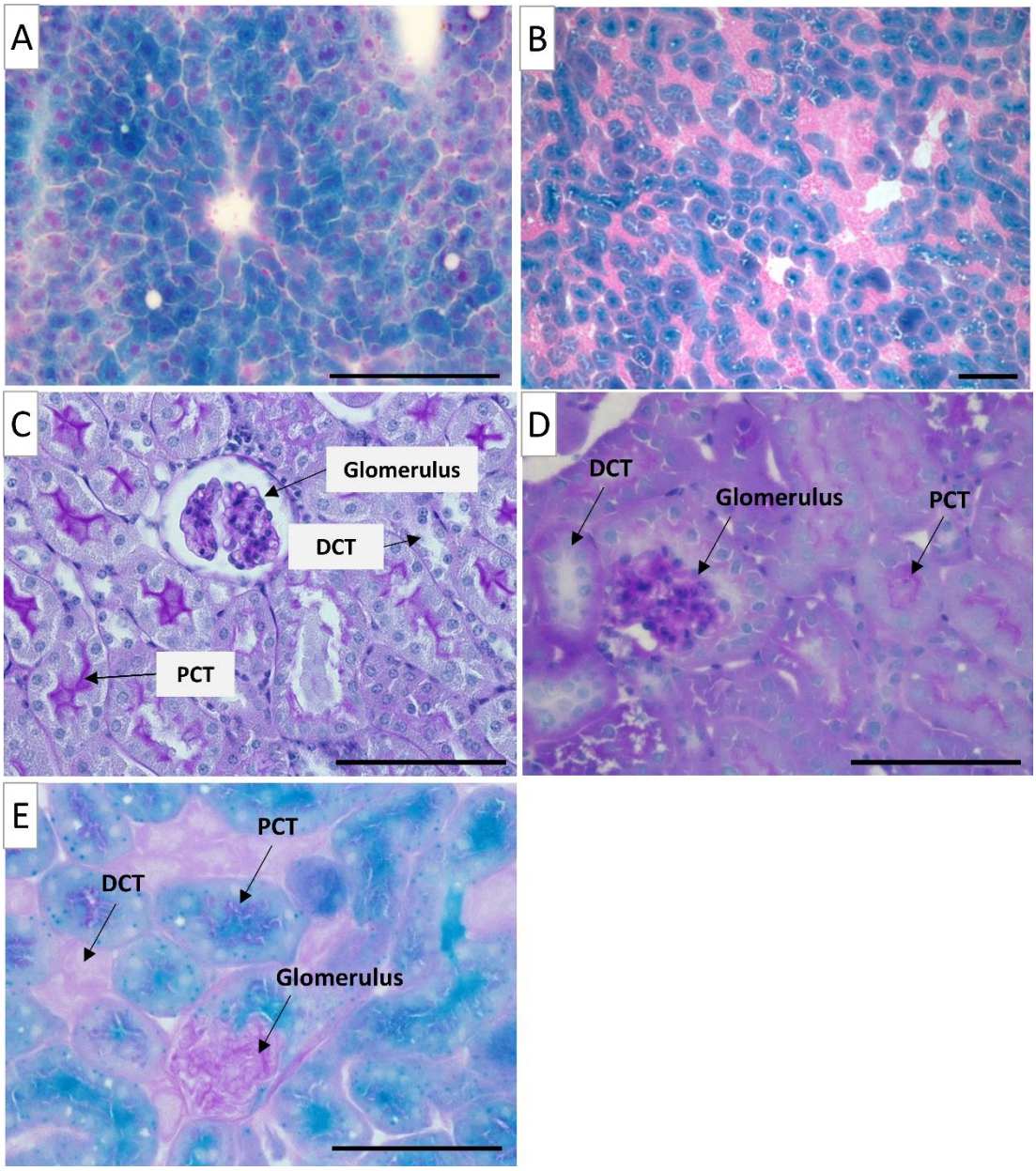

Figure 4.26. Histological location of *Hgd* in the liver and kidney cortex.
Liver (A) and kidney cortex (B) from *Hgd tm1a -/-* (26.7 weeks) show positive *LacZ* staining after 2 hours (counterstain = NFR). In the liver, positive staining is throughout the parenchyma, in the cytoplasm of hepatocytes. In the kidney cortex, staining is not in the glomerulus, and is only in some of the tubule cells. PAS/H staining of paraffin sectioned (C) and frozen sectioned (D) kidney cortex distinguishes PCTs from DCTs by the presence of a PAS-positive dark pink/purple brush border. Combined *LacZ* and PAS staining (with no haematoxylin) of the kidney cortex (E) localises the *LacZ* positive blue cells with the PAS-positive PCT cells. All sections: 6 µM. NFR, nuclear fast red. PAS, periodic acid Schiff. H, haematoxylin. PCT, proximal convoluted tubule. DCT, distal convoluted tubule. Scale bar = 100 µM.

4.2.3 *Hgd* mRNA distribution

In addition to using the *LacZ* reporter gene to localise *Hgd* expression, qPCR analysis of *Hgd* mRNA was also performed. A range of tissues from *Hgd tm1d (fl/fl) MxCre WT* mice (male; n=4) were harvested, immediately frozen in liquid nitrogen or immersed in RNA*later* solution. RNA was then isolated, reverse transcribed to produce cDNA and qPCR performed using *Hgd*-specific primers. *Hgd* mRNA expression was found within the liver and kidney, with no expression detected within the skin, cartilage, bone, brain, spleen, eye, intestine, lung, heart or muscle (Figure 4.27).

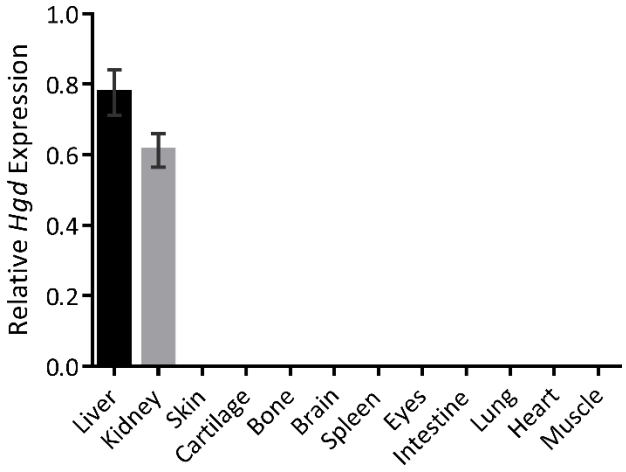

Figure 4.27. Analysis of *Hgd* mRNA expression by qPCR.
Relative *Hgd* expression, normalised to *18S*, is shown in a variety of adult *Hgd tm1d (fl/fl) MxCre WT* (male, n=4; mean age [range] = 16.5 [16-18] weeks) tissues. *Hgd* expression was found in the liver and kidney. *Hgd*1 primers (spanning exons 3-4). Error bars represent SEM. Dr Peter Wilson performed the RNA extraction, cDNA synthesis and qPCR.

Due to *LacZ* staining indicating that *Hgd* is expressed in the developing germ cells of the testis and epididymis, mRNA was collected from the testis, epididymis and liver of adult *Hgd tm1a* -/- mice (male, n=3, aged 13.9 weeks). Primers were used that span exons 3-4 before the gene trap cassette. With reference to Figure 4.28, the *Hgd* expression detected via qPCR in the testis was 7,612-fold lower than the liver, and in the epididymis was 2,036-fold lower. Although the mean value for the epididymis was higher than the testis, it was only one value of the three that was higher, with the other values being comparable. With the highest epididymis value removed, the expression of *Hgd* mRNA is 16,700-fold lower than the liver in the epididymis, which would reflect the lower staining intensity observed in the lumen of the epididymis compared to the tubules in the testis. This analysis by qPCR confirms the

presence of *Hgd* mRNA, albeit a very low level of expression comparted to the liver, within the testis and epididymis.

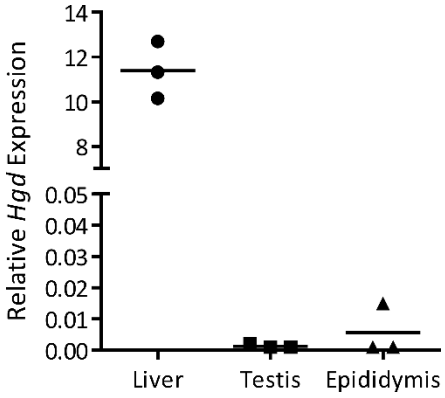

Figure 4.28. Analysis of *Hgd* mRNA expression by qPCR in the testis and epididymis.
Relative *Hgd* expression, normalised to *18S*, is shown in the testis and epididymis of *Hgd tm1a* -/- mice (male, n=3, aged 13.9 weeks) and compared with the liver from the same mice. *Hgd*1 primers (spanning exons 3-4).

4.2.4 Embryo *Hgd* expression

To investigate when *Hgd* expression begins during development, time-mated *Hgd tm1a -/-* embryos were collected and used for *LacZ* staining, both as whole embryos and for frozen section staining, in addition to *Hgd* mRNA analysis from the liver (the kidney was too small to isolate).

Macroscopically, *LacZ* staining of whole embryos showed positive staining at E14.5 onwards in the liver (Figure 4.29A). Frozen section *LacZ* staining at the histological level however revealed positive, punctate *LacZ* staining at E12.5 onwards in the liver (Figure 4.29B). In the kidney, positive *LacZ* staining was observed at E15.5 in some of the developing kidney tubules (Figure 4.29C). All other embryonic tissues examined in frozen sections, including the brain, eye, bones and other internal organs were *LacZ* negative.

Liver *Hgd* mRNA expression in *Hgd tm1a -/-* was analysed by qPCR (*Hgd*1 primers spanning exons 3–4 before gene trap cassette) at E12.5 (n=3), E13.5 (n=3), E14.5 (n=4) and E15.5 (n=3), day 1 pups (n=6) and compared with adult mice (n=4, male, mean age 18.9 weeks), see Figure 4.29D. Compared to the adult, liver *Hgd* mRNA expression was 0.3% at E12.5, 0.8% at both E13.5 and E14.5, and 2.3% at E15.5. This considerable difference in *Hgd* mRNA was reflected in the *LacZ* staining intensity seen between the adult liver (Figure 4.26A) compared to the

embryo liver (Figure 4.29B). Day 1 pup liver *Hgd* expression was 12.6% of the adult expression level (8-fold lower).

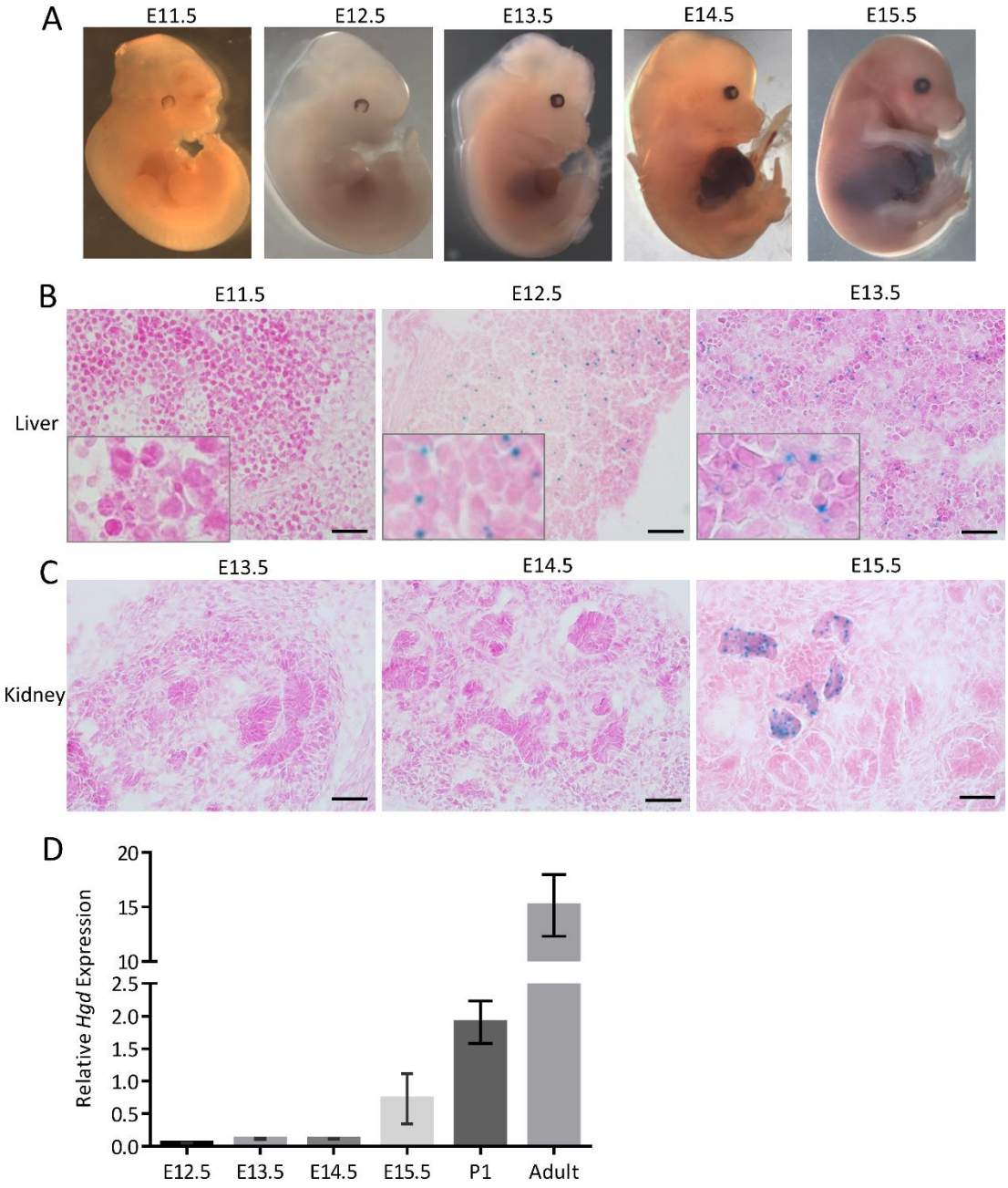

Figure 4.29. *Hgd* expression in *Hgd tm1a -/-* embryos.
A shows macroscopic *LacZ* staining of time-mated embryos, with positive blue *LacZ* staining seen at E14.5 onwards in the liver. B shows microscopic *LacZ* staining of liver from E11.5 to E13.5. At E11.5, the liver showed no visible *LacZ* staining; positive *LacZ* staining was seen at E12.5 onwards. C shows microscopic *LacZ* staining of the kidney, with positive *LacZ* staining seen at E15.5. D shows *Hgd* mRNA expression in E12.5 (n=3), E13.5 (n=3), E14.5 (n=4) and E15.5 (n=3) embryos, day 1 pups (P1) (n=6) and adult *Hgd tm1a -/-* mice (n=4; all male; mean age [range] = 18.9 [16.6-19.7] weeks), analysed via qPCR (*Hgd*1 primers spanning exons 3-4). Sections: 7 µM. Error bars represent SEM. Scale bar = 25 µM. Dr Hazel Sutherland cryosectioned the embryos.

4.3 Inducible and liver-specific *Hgd* knockout

The HGD enzyme is expressed in the liver and kidney where it metabolises HGA as part of the tyrosine metabolism pathway. In order to investigate liver-specific *Hgd* gene deletion in mice, the double transgenic *Hgd tm1d (fl/fl) MxCre* line was generated. *Hgd tm1c +/+* mice with a floxed *Hgd* gene were bred with another transgenic mouse line expressing *MxCre* recombinase. *MxCre* is a cre recombinase under the control of the *Mx-1* promotor. This *Mx-1* promotor should be silent in healthy mice, therefore pre-cre, *Hgd tm1d (fl/fl) MxCre +/-* mice have a wildtype phenotype as they are expressing *Hgd.* Only when the *Mx-1* promotor is induced will cre recombination remove the floxed target exon within *Hgd*. *Mx-1* (interferon-induced GTP-binding protein Mx-1) encodes the interferon-induced GTP-binding protein Mx-1 protein which has antiviral activity. *Mx-1* activity can be induced by interferon alpha/beta, viral infection or synthetic double-stranded RNA, causing it to accumulate in the cytoplasm where it acts to inhibit viral replication. In mice, *Mx-1* is responsible for the antiviral state against influenza. The C57BL/6J genome contains a mutation in *Mx-1* that results in a non-functional gene product (https://www.ncbi.nlm.nih.gov/gene/17857). Here pIpC (polyinosinic: polycytidylic acid), a synthetic double-stranded RNA, is used to induce the *Mx-1* promotor, see Figure 4.30. Intra-peritoneal injection of pIpC increases levels of interferon alpha/beta, which induces the *Mx-1* promotor and therefore the Cre expression (referred to as *MxCre*), see Figure 4.30A. The expression of MxCre then leads to site-specific Cre/*LoxP* recombination within the floxed *Hgd* gene (Figure 4.30B), removing the floxed 6th exon, as depicted in the post-cre *Hgd tm1d* allele. The *Mx-1* promotor is very active in the liver but not in the kidney, therefore pIpC injection into *Hgd tm1d (fl/fl) MxCre +/-* mice should result in an inducible and liver-specific knockout of *Hgd*.

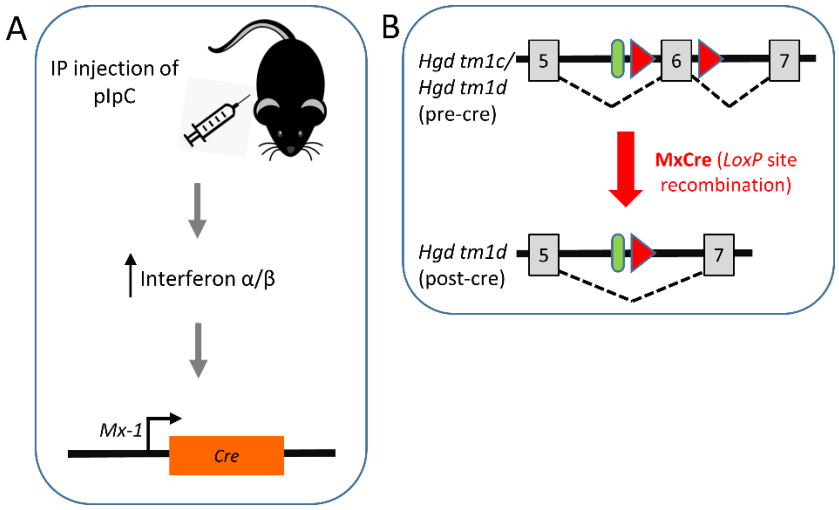

Figure 4.30. Induction of *MxCre* by pIpC.
Injection of pIpC, a synthetic double-stranded RNA, into mice can replicate a viral infection (A). Levels of interferon α/β subsequently are increased, inducing the interferon-responsive *Mx-1* promotor that is controlling Cre expression. With pIpC injection, cells that are interferon responsive with the *Mx-1* promotor will express Cre (referred to as *MxCre*). Where *MxCre* has been induced, site-specific cre recombination via *LoxP* sites will occur, removing the floxed 6th exon within the *Hgd tm1d* allele (B). IP, intraperitoneal.

To investigate the effect of liver-specific *Hgd* gene deletion, double transgenic *Hgd tm1d (fl/fl) MxCre +/-* mice (n=5; *MxCre +ve*) and *Hgd tm1d (fl/fl) MxCre WT* (n=3; wildtype control) and *Hgd tm1a -/-* (n=4; AKU control) controls were injected with pIpC. Blood and urine samples were collected according to the scheme in Figure 4.31A. Fifteen days after the first pIpC injection (post-cre activation), *MxCre +ve* mice showed a 77.6% decrease in liver *Hgd* mRNA compared with wildtype controls (Figure 4.31B). Kidney *Hgd* expression in *MxCre +ve* mice did not change and was comparable to wildtype controls (Figure 4.31C). AKU mice had no *Hgd* mRNA expression as expected (primers span exons 9–10 after gene trap cassette).

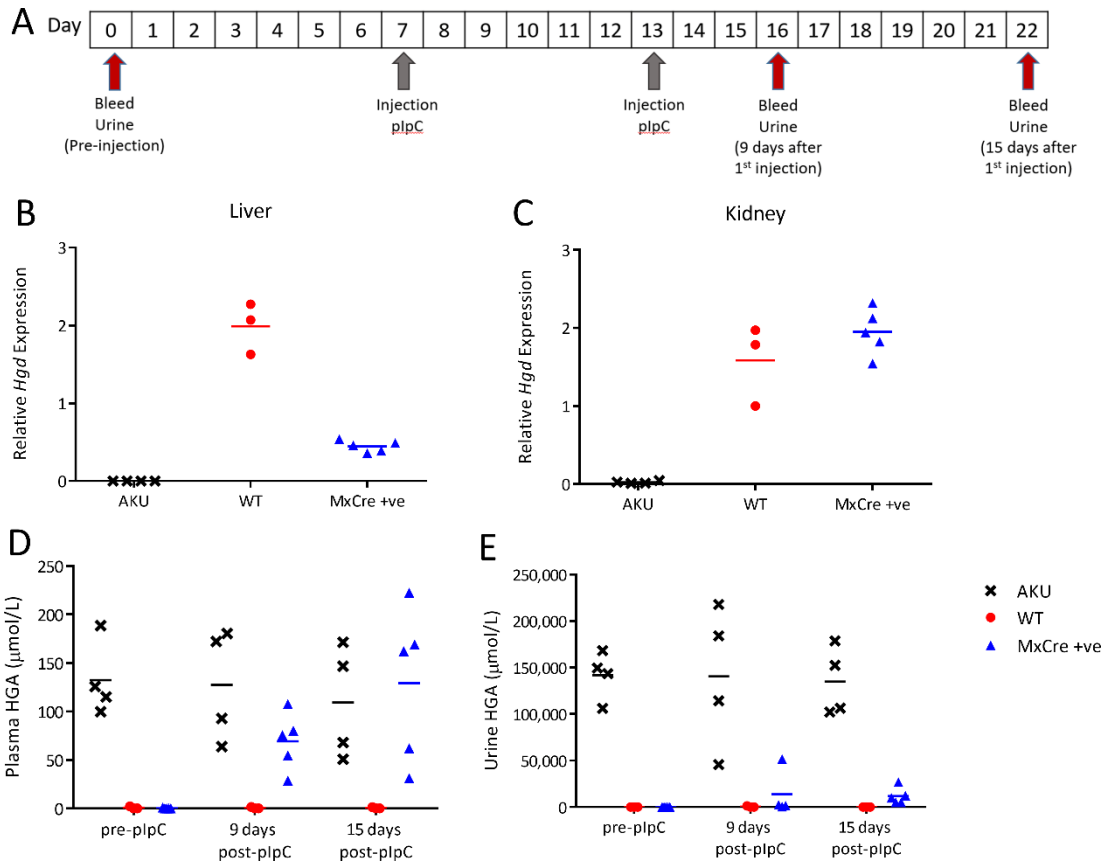

Figure 4.31. Liver-specific *Hgd* knockout, induced by pIpC injection, in *Hgd tm1d (fl/fl) MxCre +/-* mice.
A shows the timescale of blood and urine sampling and pIpC injections. B and C show *Hgd* mRNA (*Hgd*2 primers; relative to *18S*) in *Hgd tm1a -/-* (AKU controls, n=4, 2 M, 2 F, mean age [range] = 19.4 [19.0-19.7] weeks), *Hgd tm1d (fl/fl) MxCre WT* (WT controls, n=3, 1 M, 2 F, mean age [range] = 15.1 [13.4-16.6] weeks) and *Hgd tm1d (fl/fl) MxCre +/-* mice (*MxCre +ve*, n=5, 5 M, mean age [range] = 15.1 [9.1-18.7] weeks) in the liver and kidney respectively, 15 days after pIpC injection. *MxCre +ve* mice show reduced liver, but not kidney, *Hgd* expression compared to WT controls. D and E show plasma and urine HGA, respectively, at pre-injection and at 9 and 15 days after pIpC injection. Pre-injection, HGA in the plasma is not detected in *MxCre +ve* or WT mice. *Hgd tm1a -/-* mice show high HGA. Post-pIpC, plasma HGA in *MxCre +ve* mice is increased. Pre-injection, urinary HGA is low in *MxCre +ve* and WT mice compared to *Hgd tm1a -/-*. Post-pIpC, urinary HGA shows a relatively small increase in *MxCre +ve* mice. M = male. F = female.

Following the knockout of approximately 78% liver *Hgd* mRNA in *MxCre +ve* mice, mean plasma HGA (±SEM) increased from 0.2 ±0.2 µmol/L to 129.3 ±35.6 µmol/L at 15 days post-pIpC (Figure 4.31D). *MxCre +ve* urinary HGA (Figure 4.31E) was increased from 9.4 ±7.1 µmol/L to 11,807 ±974 µmol/L at 15 days post-pIpC but remained low in comparison to AKU controls (134,948 ±18,479 µmol/L). Both plasma and urinary HGA remained high in AKU controls and low in wildtype controls as expected.

4.4 Long-term liver-specific *Hgd* knockout

MxCre +ve mice (*Hgd tm1d (fl/fl) MxCre +/-*; n=15) and AKU *Hgd tm1a -/-* controls (n=5) were injected with pIpC. *MxCre +ve* mice were injected with PBS (*Hgd tm1d (fl/fl) MxCre +/-*; n=5) as wildtype controls. Injections and sampling of blood and urine was carried out according to

the scheme in Figure 4.32A. *MxCre +ve* mice injected with pIpC were culled at 9 (n=5), 15 (n=5) and 20 (n=5) weeks post-injection, with wildtype and AKU controls culled at 20 weeks only. Liver and kidney mRNA were taken for analysis and knee joints were taken to assess ochronosis.

As with the previous study, liver *Hgd* mRNA was reduced in pIpC-injected *MxCre +ve* mice (post-cre activation), which was sustained to 20 weeks post-injection, see Figure 4.32B. Compared to wildtype controls, *Hgd* expression was 11.7%, 17.7% and 18.4% at 9, 15 and 20 weeks respectively. Kidney *Hgd* expression in the *MxCre +ve* mice remained comparable to wildtype controls (Figure 4.32C). The reduction of liver *Hgd* mRNA in the *MxCre +ve* mice subsequently caused plasma HGA to increase (Figure 4.32D) to a level comparable with AKU controls. Urinary HGA (Figure 4.32E) was increased in the *MxCre +ve* mice but not to that of AKU controls. Knee joint sections stained with Schmorls' stain were scored to obtain the number of pigmented chondrons found in a representative knee joint section (Figure 4.32F). Few or no pigmented chondrons were found in the *MxCre +ve* knee joints at 9 weeks post-pIpC, increasing in number at 15 and 20 weeks. Wildtype controls showed no pigmentation. AKU controls showed pigmentation as expected.

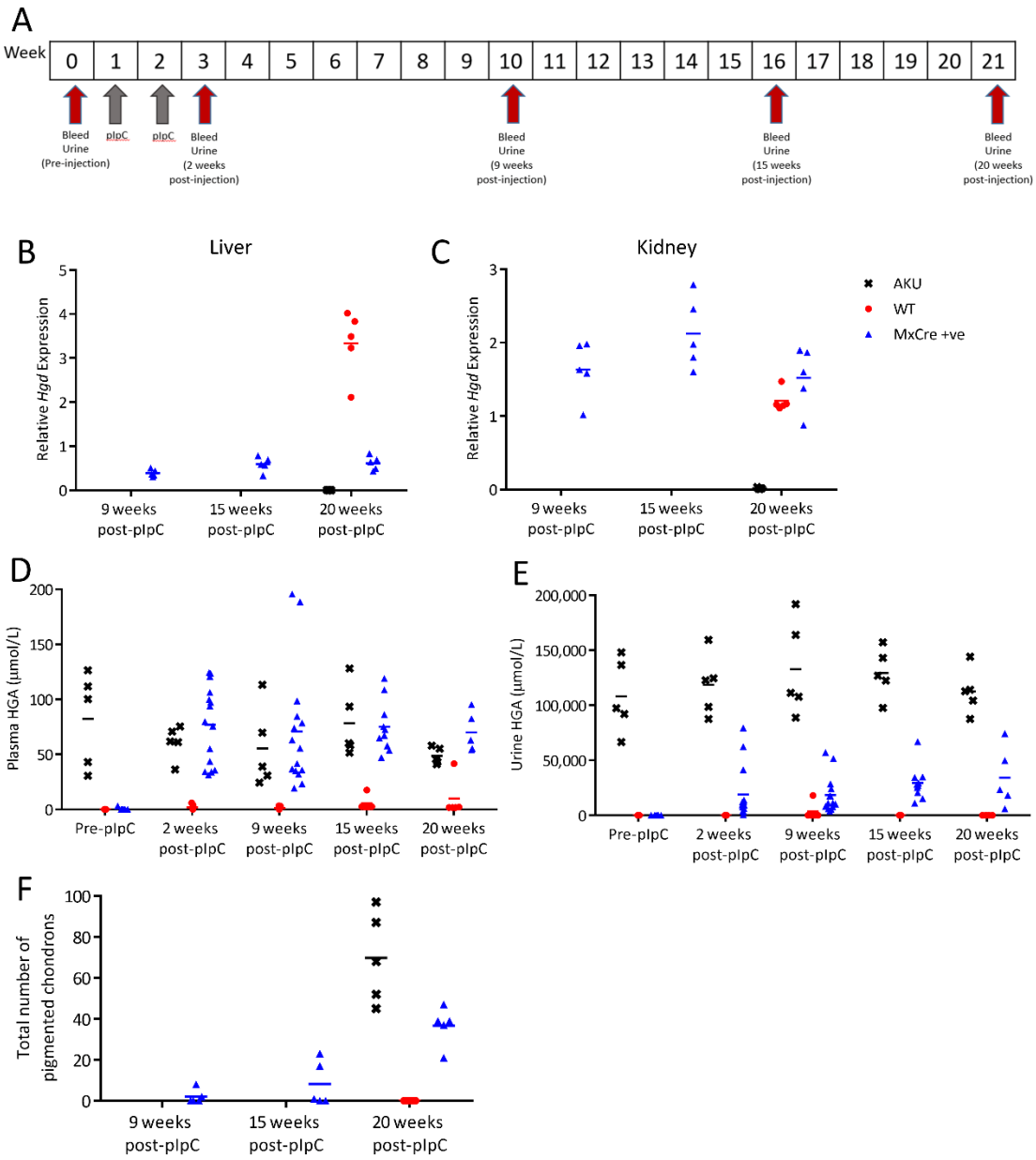

Figure 4.32. Long-term study of *Hgd tm1d (fl/fl) MxCre +/-* mice injected with pIpC.

A shows the timescale of blood and urine sampling and pIpC injections. *Hgd tm1a -/-* were injected with pIpC (AKU controls, n=5, 4 M, 1 F, mean age [range] = 16.6 [7.1-23.6] weeks). *Hgd tm1d (fl/fl) MxCre +/-* were injected with PBS (WT controls, n=5, all M, mean age [range] = 19.9 [13.6-31.7] weeks). *Hgd tm1d (fl/fl) MxCre +/-* mice were injected with pIpC (*MxCre +ve*, n=15, all M, mean age [range] = 18.9 [12.1-29.4] weeks). B and C show relative *Hgd* mRNA (*Hgd*2 primers; relative to *18S*) in the liver and kidney respectively, of *MxCre +ve* mice at 9-, 15- and 20-weeks (n=5) after the first injection, and in AKU and WT controls at 20 weeks. Liver *Hgd* mRNA was reduced compared to WT controls in *MxCre +ve* mice at 9 weeks and was sustained at this level until 20 weeks. Kidney expression was not reduced by pIpC injection in *MxCre +ve* mice. D and E show plasma and urine HGA levels respectively, pre-injection, and at 2-, 9-, 15- and 20-weeks post-injection. Pre-injection, plasma HGA is not detected in *MxCre +ve* or WT mice and AKU mice showed increased HGA. Post-pIpC, plasma HGA in *MxCre +ve* mice was increased at 2 weeks and remained at this level at 20 weeks. Pre-injection, urinary HGA is low in *MxCre +ve* and WT mice compared with AKU controls. Post-pIpC, urinary HGA showed a relatively small increase in *MxCre +ve* mice compared with AKU controls. The total number of pigmented chondrons in a representative section of the knee joint, stained with Schmorl's stain, is shown in F, at 9-, 15- and 20-weeks post-injection. M = males. F = females.

4.5 Liver-specific *Hgd* knockout: dose response

In order to investigate the effect of varying *Hgd* mRNA expression levels on the AKU phenotype, a short-term dose response study was carried out. Figure 4.33A demonstrates the study design. *MxCre +ve* mice (*Hgd tm1d (fl/fl) MxCre +/-*) were given two injections of pIpC at the following doses; 3.33 μg/g (n=3), 1 μg/g (n=3), 0.33 μg/g (n=3), 0.1 μg/g (n=5), 0.03 μg/g (n=3) and 0.01 μg/g (n=3) body weight. AKU (*Hgd tm1a -/-*; n=4) and wildtype (*Hgd tm1d (fl/fl) MxCre WT*; n=7) controls were given the highest dose of 3.33 μg/g pIpC. With the exception of the 0.01 μg/g group, liver *Hgd* mRNA in *MxCre +ve* mice was reduced at 15 days post-injection (Figure 4.33B) in all groups, with a dose response observed at the lower pIpC doses. The mean liver *Hgd* mRNA expression in *MxCre +ve* mice 15 days post-pIpC compared to wildtype controls was 17.0%, 20.5%, 20.5%, 53.4%, 54.5% and 107.2% (decreasing pIpC doses). Kidney expression was unchanged (Figure 4.33C).

Mean (±SEM) plasma HGA in *MxCre +ve* mice at 15 days post-pIpC were 75.0 ±20.9, 57.9 ±20.9, 27.2 ±9.6, 22.7 ±13.4, 26.1 ±24.1 and 1.3 ±0.4 μmol/L with decreasing pIpC doses (Figure 4.33D), in a dose responsive manner. Mean (±SEM) urine HGA demonstrated a dose response at 15 days post-pIpC, at 45,074 ±14,977, 14,169 ±13,783, 6,137 ±6,064, 5,717 ±5,667, 31,043 ±31,041 and 2.0 ±0.2 μmol/L with decreasing pIpC doses (Figure 4.33E). These were increased compared with wildtype (1.9 ±0.2 μmol/L), but lower than AKU (113,067 ±10,609 μmol/L) controls. Figure 4.33F-G shows the relationship between liver *Hgd* mRNA (expressed as percentage of the mean wildtype level) and HGA in both the plasma and urine. A non-linear, exponential curve has been fitted to the *MxCre +ve* mice in Figure 4.33F, to show the relationship between *Hgd* expression and plasma HGA ($R^2 = 0.592$).

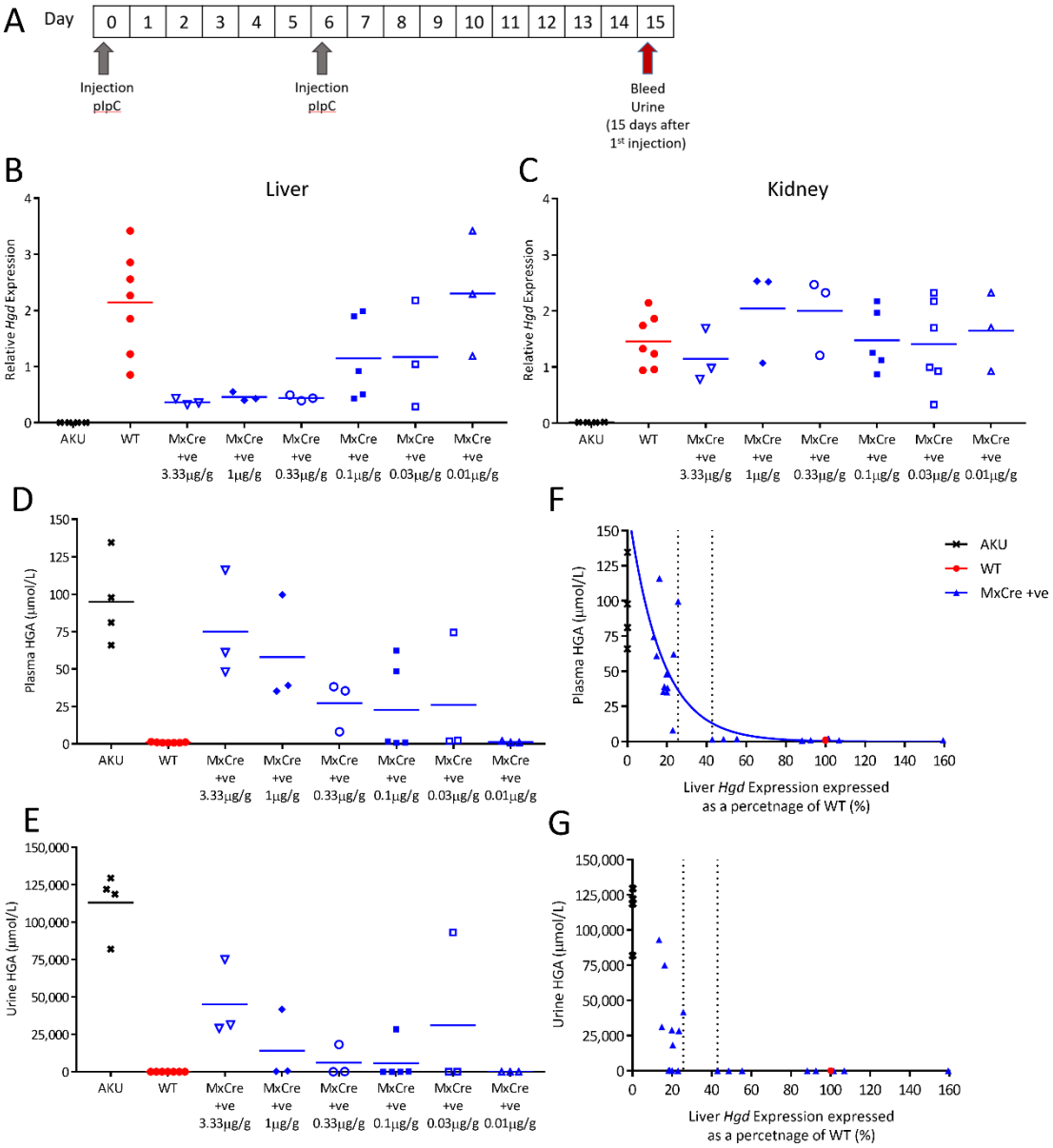

Figure 4.33. Liver-specific *Hgd* knockout, induced by decreasing doses of pIpC, in *Hgd tm1d (fl/fl) MxCre +/-* mice.

A shows the timescale of blood and urine sampling and injections of pIpC. B and C show relative *Hgd* expression (*Hgd*2 primers; relative to *18S*) in *Hgd tm1a -/-* (AKU controls, n=4, 4 M, mean age [range] = 52.8 [51.0-56.9] weeks), *Hgd tm1d (fl/fl) MxCre WT* (WT controls, n=7, 2 M, 5 F, mean age [range] = 22.9 [20.3-26.4] weeks) and *Hgd tm1d (fl/fl) MxCre +/-* mice (*MxCre +*ve; 3.33 µg/g, n=3; 0.1 µg/g, n=3; 0.33 µg/g, n=3; 0.1 µg/g, n=5; 0.03 µg/g, n=3; 0.01 µg/g, n=3) in the liver and kidney respectively, 15 days post-pIpC. Varying the dose of pIpC resulted in a range of liver *Hgd* expression in the *MxCre +ve* mice, with lower doses resulting in higher *Hgd* expression. Kidney *Hgd* expression was unchanged by pIpC. D and E show plasma and urine HGA, respectively, 15 days post-pIpC. A dose response in HGA was observed in both the plasma and the urine of *MxCre +ve* mice, with higher pIpC doses resulting in more elevated HGA. HGA was elevated in *Hgd tm1a -/-* and was low in WT controls. F and G show the relationship between liver *Hgd* mRNA (expressed as a percentage of the mean WT level) with plasma and urinary HGA respectively, at 15 days post-pIpC. *MxCre +ve* mice sex and mean age [range]; 3.33 µg/g = 1 M, 2 F, 9.3 [8.4-9.9] weeks; 1 µg/g = 2 M, 1 F, 8.9 [8.4-9.9] weeks; 0.33 µg/g = 2 M, 1 F, 8.9 [8.4-9.7] weeks; 0.1 µg/g = 3 M, 2 F, 14.2 [8.4-27.0] weeks; 0.03 µg/g = 2 M, 1 F, 17.1 [12.4-26.4]; 0.01 µg/g = 2 M, 1 F, 17.1 [12.4-26.4]. M = males. F = females.

4.6 Metabolism of circulating HGA

To determine if circulating HGA can be taken up by HGD-expressing cells to be metabolised intracellularly, both *Hgd tm1a -/-* (n=4) and *Hgd tm1a -/+* (n=4) mice were injected with $^{13}C_6$-HGA into the tail vein. Plasma samples were then collected at various time points, from 2–60 minutes post-injection. HGA in its native form (m+0) was detected in plasma of *Hgd tm1a -/-* mice at all time points, and was absent in *Hgd tm1a -/+* mice (Figure 4.34). $^{13}C_6$-HGA was detected in both *Hgd tm1a -/-* and *Hgd tm1a -/+* mice after injection (Figure 4.35). M+6 isotopologues of fumarylacetoacetic acid ($^{13}C_6$-FAA)/maleylacetoacetic acid ($^{13}C_6$-MAA), $^{13}C_6$-labelled downstream metabolites of HGA, were detected in *Hgd tm1a -/+* mice after $^{13}C_6$-HGA injection, and were not detected in *Hgd tm1a -/-* mice. Native FAA/MAA was not detected in either *Hgd tm1a -/-* or -/+ mice (Figure 4.34).

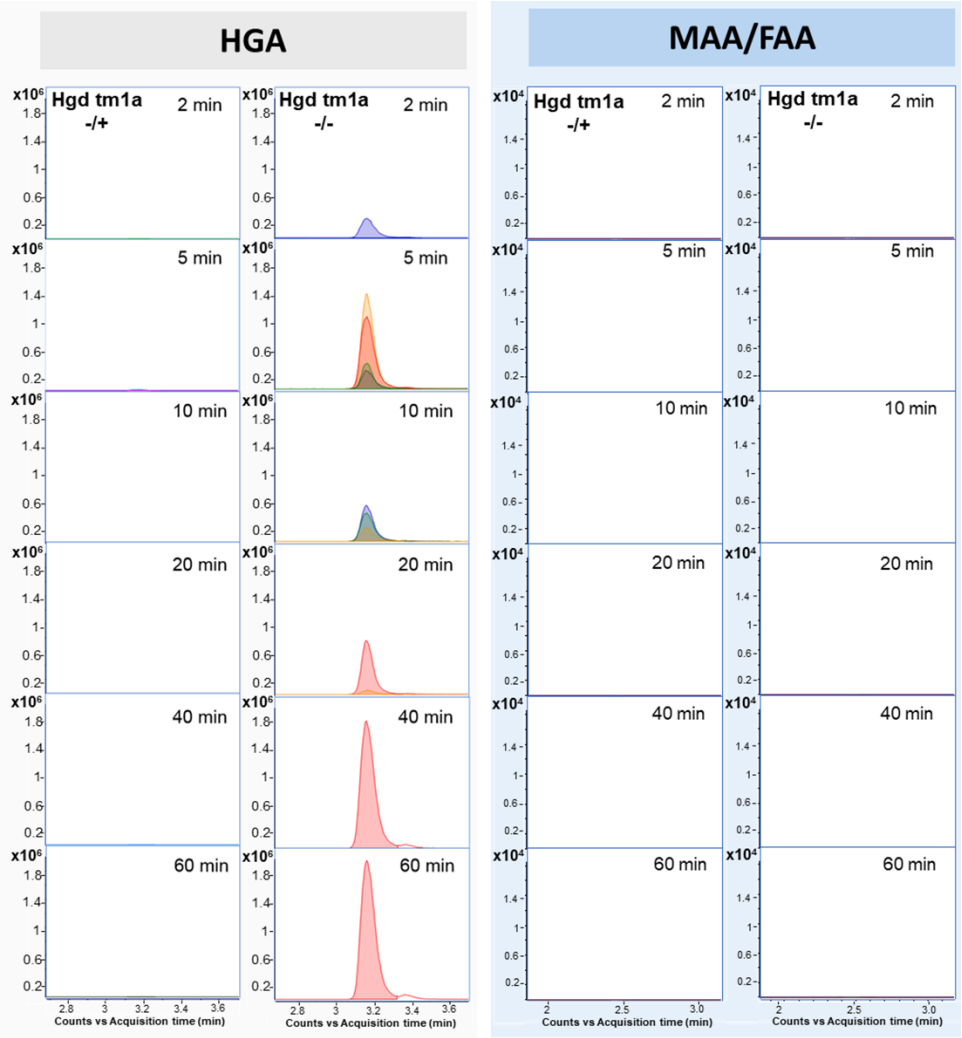

Figure 4.34. LC-QTOF-MS plasma flux analysis data for native compounds acquired following injection of *Hgd tm1a -/-* and *Hgd tm1a -/+* mice with $^{13}C_6$-HGA.

Plots show extracted ion chromatograms (theoretical accurate mass ±5 ppm) for HGA and fumarylacetoacetic acid (FAA)/maleylacetoacetic acid (MAA). Traces are for individual plasma samples taken 2-60 minutes post-injection and colour-coded to represent individual mice. HGA was detected in *Hgd tm1a -/-* only. FAA/MAA was not detected in either *Hgd tm1a -/+* or *Hgd tm1a -/-*. *Hgd tm1a -/+* mice; n=4; all females; mean age [range] = 58.9 [58.7-59.0]. *Hgd tm1a -/-* mice; n=4; 3 males, 1 female; mean age [range] = 56.8 [55.0-58.6]. Sample analysis performed by Dr Brendan Norman.

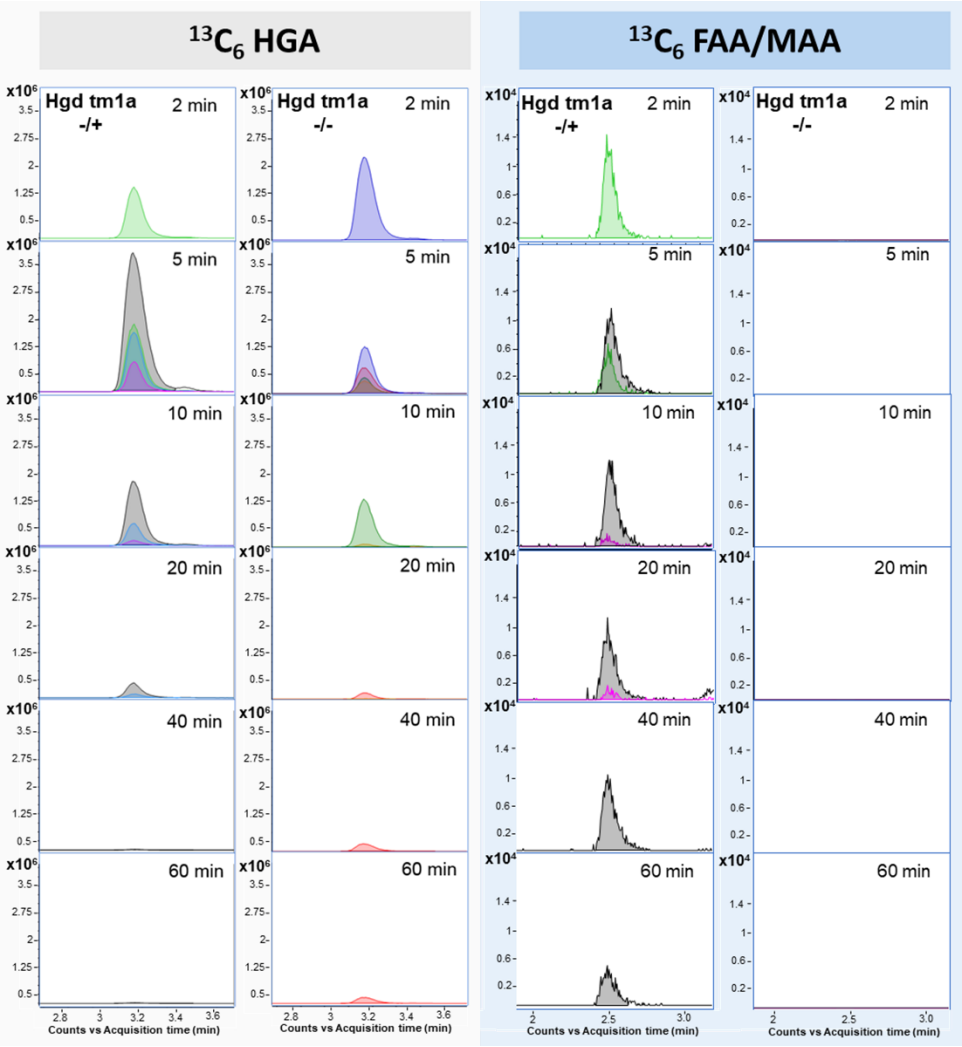

Figure 4.35. LC-QTOF-MS plasma flux analysis data for isotopically-labelled compounds acquired following injection of *Hgd tm1a -/-* and *Hgd tm1a -/+* mice with $^{13}C_6$-HGA.
Plots show extracted ion chromatograms (theoretical accurate mass ±5 ppm) for $^{13}C_6$-HGA and $^{13}C_6$-fumarylacetoacetic acid (FAA)/$^{13}C_6$-maleylacetoacetic acid (MAA). Traces are for individual plasma samples taken 2-60 minutes post-injection and colour-coded to represent individual mice. $^{13}C_6$-HGA was detected in *Hgd tm1a -/-* and *Hgd tm1a -/+* indicating presence of the tracer. $^{13}C_6$-MAA/FAA was observed at 2-60 minutes post-injection in *Hgd tm1a -/+*, and was not observed in *Hgd tm1a -/-* at any time point. *Hgd tm1a -/+* mice; n=4; all females; mean age [range] = 58.9 [58.7-59.0]. *Hgd tm1a -/-* mice; n=4; 3 males, 1 female; mean age [range] = 56.8 [55.0-58.6]. Sample analysis performed by Dr Brendan Norman.

4.7 Discussion

The BALB/c *Hgd*$^{-/-}$ AKU model is deficient in HGD, however it has no ability to be manipulated further nor does it possess a reporter gene. The targeted *Hgd tm1a* model on the other hand has a *LacZ* reporter gene within the gene trap cassette situated in the *Hgd* locus, which has enabled precise localisation of *Hgd* expression to hepatocytes and proximal convoluted cells of the kidney cortex, in addition to determining when embryonic expression of *Hgd* initiates. Low level expression of *Hgd* was also discovered in the testis and epididymis, specifically within the developing sperm cells contained within these organs. Furthermore, this

knockout-first *Hgd tm1a* allele contains FRT and *LoxP* sequences which enabled a double transgenic conditional *Hgd* knockout mouse to be generated using Flp/Cre site-specific recombination [211,241]. The use of *Mx-1* Cre recombinase (*MxCre*) allowed inducible and liver-specific knockout of *Hgd* mRNA by removal of the *LoxP* flanked (floxed) sixth *Hgd* exon in the *Hgd tm1d (fl/fl) MxCre +/-* conditional mouse model which has highlighted important considerations for gene/enzyme replacement therapy.

4.7.1 *Hgd* expression

The endogenous *LacZ* reporter gene has enabled both temporal and spatial histological localisation of *Hgd* showing that *Hgd* was expressed throughout the liver parenchyma and kidney PCT cells. This expression was then verified by qPCR analysis of *Hgd* mRNA. A few reports however have suggested HGD expression in various other tissues. In 1996, in addition to the liver and kidney, it was reported that *HGD* was expressed in human small intestine, colon and prostate tissue via northern blot hybridisation using a human cDNA clone as a probe for *HGD* (the spleen, thymus, testis, ovary, peripheral blood lymphocytes, heart, brain, placenta, skeletal muscle, lung and pancreas were reported negative) [90]. Although positive *LacZ* staining of the intestine, colon and prostate was observed in the *Hgd tm1a* mice, the same pattern of staining was also observed in *LacZ* negative control tissue, indicating false-positive staining and therefore no *Hgd* expression.

Histological sectioning of the intestine, caecum and large intestine (also known as colon) demonstrated that the *LacZ* staining was present in the intestinal lumen where bacteria are present (*LacZ* is a bacterial gene), and not within the cells making up the intestinal wall, in both the *Hgd tm1a* and *LacZ* negative control tissue. False-positive *LacZ* staining has been reported in C57BL/6 wildtype mice within the gastrointestinal tract [266]. In addition, no *Hgd* mRNA was found in the intestine via qPCR. In the prostate, macroscopic *LacZ* staining was observed alongside positive staining within the vas deferens, both of which were also observed in the *LacZ* negative control tissues. Histological sectioning of the *LacZ* stained prostate and vas deferens showed an identical pattern of staining in *Hgd tm1a* and the *LacZ* negative control, indicating false-positive staining and no *Hgd* expression. It has been reported in the literature that non-specific *LacZ* staining is a particular problem in the male reproductive tract, with positive staining observed in wildtype C57BL/6 in the testis, epididymis, vas deferens and prostate [266]. This reported non-specific *LacZ* data in wildtype mice of the same background strain as the mice used here supports the false-positive findings

presented here, that *Hgd* is not expressed in the gastrointestinal tract or male prostate or vas deferens.

Another tissue later investigated was the male testis and epididymis. Macroscopically, positive *LacZ* staining was observed in the testis of *Hgd tm1a -/-*, and not within the *LacZ* negative control. Histological sectioning revealed the staining within the testis to be of the developing male germ cells within the seminiferous tubules, and not within the somatic Sertoli cells that form the tubule wall, nor within the extra-tubular Leydig cells or peri-tubular myoid cells. The staining appeared to be localised within the cytoplasm of the developing sperm cells, which undergo a series of stages called spermatogenesis as they move from the basal surface of the Sertoli cell where they begin as round spermatogonia, ending up elongated, motile spermatozoa at the luminal edge of the Sertoli cell [265,267]. Identifying the cell types staining blue in the *Hgd tm1a -/-* testis using histology was a challenge but was aided by a report of a gene called *Paskin* that was identified in the mouse testis using *LacZ*, that had the same pattern of staining as the *Hgd tm1a -/-* testis, see Figure 4.22D [264]. The expression of *Paskin* was found to be localised to spermatids and spermatozoa within the seminiferous tubules. This provided confidence that the cells identified in *Hgd tm1a* were indeed developing male germ cells.

Spermatogonia in the seminiferous tubules of the testis undergo mitosis to produce primary spermatocytes, which then undergo meiosis I to become secondary spermatocytes, which then undergo meiosis II to become spermatids, all of which are round cells, progressing from the basal surface towards the luminal surface [265,268]. The round, non-motile spermatids then undergo a process called spermiogenesis, where the spermatid becomes an elongated, motile spermatozoa that has a rectangular head and a tail, with the latter projecting into the lumen of the seminiferous tubule [268]. During spermiogenesis, the elongating spermatids shed most of their cytoplasm as they leave the seminiferous tubule in a process called spermiation, discarding the cytoplasm as residual bodies, leaving behind a small intracellular cytoplasmic residue known as the cytoplasmic droplet [265,269,270]. Most of the residual bodies are phagocytosed by the Sertoli cells. The residual bodies may explain the presence of small punctate blue *LacZ* staining near the basal edge of the seminiferous tubules, which have migrated towards the basal side of the Sertoli cells before being phagocytosed. Within the epididymis, the spermatozoa then mature into sperm that have the ability to fertilize an egg.

Positive blue *LacZ* staining was present within the contents of the epididymal tubules in *Hgd tm1a -/-* that was not present in the *LacZ* negative control, suggesting that the expression of

Hgd was within the spermatozoa and/or within the cytoplasm droplet that was shed during spermiogenesis; the histology is not able to clearly show which of the aforementioned structures is staining blue within the epididymal lumen. Within the *Paskin -/-* mice mentioned above, diffuse blue *lacZ* staining was also observed within the epididymal lumen, which the authors attributed to be due to cytoplasmic droplets [264].

Cytoplasmic droplets are believed to play a role in osmoregulation in sperm [271]. A report in 2013 however also demonstrated that the cytoplasmic droplet is a transient organelle with an additional role in energy metabolism essential for epididymal sperm maturation; proteomic analysis of cytoplasmic droplets purified from murine epididymal spermatozoa revealed that 68% of the identified proteins were enzymes involved in energy metabolism, particularly glycolytic enzymes [271]. There is evidence to suggest that mitochondrial activity is low in the sperm of mice in the epididymal head and body, coupled with lower ATP levels, compared to the caudal end which has increased mitochondrial activity and more ATP production [271]. Pyruvate levels are also higher in at the epididymal head and body compared to the tail end [271]. Pyruvate is an intermediate substrate of both glycolysis and the TCA cycle; it can be converted to lactate for anaerobic glycolysis or into acetyl-coenzyme A to enter the TCA cycle for ATP production.

No tyrosine pathway enzymes were identified in the proteomic analysis of cytoplasmic droplets described in the previous paragraph [271]. The proteomic analysis however did not analyse all proteins present in the purified cytoplasmic droplets, but instead analysed 5 selected bands from an SDS-PAGE gel that represented proteins unique or highly enriched in purified cytoplasmic droplets compared to the rest of the spermatozoa. It is therefore possible that HGD and other tyrosine pathway enzymes was missed due to being expressed in both the cytoplasmic droplet and the remaining cytoplasm of the spermatozoon, and was therefore not present in one of the investigated groups of proteins in the report. The *LacZ* staining presented here, along with mRNA evidence, suggests that *Hgd* is present in the cytoplasm of spermatids and spermatozoa in the testis, and in the remaining cytoplasmic droplet and/or cytoplasm of the sperm itself within the epididymis. Downstream metabolites of HGA include fumaric acid and acetoacetic acid which can both enter the TCA cycle, in addition to acetoacetic acid being an intermediate metabolite for ketogenesis and fumaric acid for gluconeogenesis. It could therefore be hypothesized that *Hgd* expression in sperm within the testis and epididymis also has a role in energy metabolism in the absence of mitochondrial activity, providing alternative metabolic pathways to glycolysis. Once the mitochondrial production of ATP has increased at the caudal epididymis, perhaps the

expression of *Hgd* and other energy metabolism enzymes are then downregulated, as no blue *LacZ* staining was observed within the vas deferens that was in close proximity to the prostate gland, where mature sperm could be observed in the lumen via histology.

Further investigation of *Hgd* expression within the testis and epididymis was carried out via qPCR analysis of *Hgd* mRNA. The expression of *Hgd* in the testis of adult mice aged 13.9 weeks (sexually mature) was approximately 7600-fold lower than that of the liver, and 2000-fold lower in the epididymis compared with the liver. This enormous difference in *Hgd* expression suggests that the expression in the testis and epididymis is very unlikely to contribute towards metabolism of the HGA pool within the circulation, which would be metabolised by the liver and kidney in non-AKU individuals. Due to being expressed at a low level, the absence of *Hgd* within the developing and maturing sperm within the testis and epididymis is unlikely to affect male fertility if the role of HGD here is to contribute towards energy metabolism, as other major glycolytic pathways would be capable of generating enough energy. It is likely that the role of HGD in sperm is fairly insignificant with regards to the AKU phenotype.

Recently, there has been a report suggesting that HGD is expressed in brain tissue from both mice and humans using western blotting [99]. Specifically, HGD was reported in the midbrain, cerebellum, basal forebrain and hippocampus of male CD-1 mouse brain, and within the cortex, hippocampus, basal forebrain, cerebellum and striatum of human brain samples obtained from a tissue archive. The mouse brain from *Hgd tm1a* mice was therefore *LacZ* stained, with no positive staining observed in any region of the brain via histology, with particular attention paid towards the regions stated in the aforementioned report, some of which were very large regions such as the cerebellum. In addition to negative *LacZ* staining, no *Hgd* mRNA was found in the brains of mice here. Perhaps the anti-body used in the western blotting paper investigating brain tissue was not specific; there was no reported use of HGD-positive or -negative control tissue. The brain was also negative in the northern blot hybridisation study from 1996, although the interpretation of that data set should perhaps be approached with caution, as the *LacZ* and mRNA findings presented here for the intestine and prostate did not support the findings of the northern blot study [90].

Other work from the same group reporting HGD expression within the brain also reported that HGD is expressed in human osteoarticular cells [100]. Using western blotting with an anti-HGD antibody from the same source as used for the brain expression data, the authors report that HGD is expressed in chondrocytes, synoviocytes and osteoblasts, and demonstrate *HGD*

expression via qPCR in human primary cultured chondrocytes. *LacZ* staining in *Hgd tm1a -/-* however did not show that *Hgd* is expressed in these tissues. False-positive osteoclast staining was observed in the *Hgd tm1a* and *LacZ* negative controls along the resorption zone of the growth plate and were identified via histological sectioning, which showed no other *LacZ* positive cells, indicating that no *Hgd* is expressed there. False-positive staining of epiphyseal growth plates is reported in the literature and has been attributed to endogenous galactosidase activity within osteoclasts along the resorption zone of the epiphyseal growth plates where they phagocytose apoptosing chondrocytes [263]. In addition, qPCR analysis did not detect any *Hgd* mRNA in bone (taken from the femur) nor cartilage (hip joint femoral head), further supporting the lack of *LacZ* staining and the absence of *Hgd* in these tissues.

The major sites of *Hgd* expression have been identified here, with the expression localised to the cytoplasm of hepatocytes in the liver and of PCT cells in the kidney cortex. *H*gd expression was also identified in the cytoplasm of developing and maturing sperm cells within the testis and epididymis, but at a level that is unlikely to contribute to the metabolism of HGA in the rest of the body, but is possibly required for energy production in the sperm, which are isolated from the rest of the body by the blood-testis barrier. The liver and kidney are the major sites of expression of other tyrosine pathway enzymes, such as PAH, TAT, HPPD and FAH, see Table 4.1 for a summary of tissue expression for these enzymes from the literature. The liver is a metabolically active organ and directly receives the blood from the digestive tract which will be rich in amino acids such as tyrosine and phenylalanine. The kidney proximal convoluted tubule is also the main site of amino acid reabsorption from the filtrate back into the blood. The presence of *Hgd* within the liver and kidney is therefore not surprising considering the role of HGD, which is an intermediate enzyme in tyrosine and phenylalanine metabolism.

Table 4.1. Expression of tyrosine pathway enzymes in the literature.

Enzyme	Tissue	Species	Method	References
PAH	Liver[1], kidney[1] (PCTs[2,3]), pancreas[1], brain[1a]	Human	[1]northern blot, [2]RNA ISH, [3]immunoperoxidase staining	Lichter-Konecki et al, 1999 [272]
	Liver[1,2]	Mouse	[1]western blot, [2]mRNA	Shedlovsky et al, 1993 [176]
	Liver[1,2]	Rat	[1]enzyme assay, [2]flux assay	Stanley et al, 1985 [273]
TAT	Liver[1]	Human	[1]enzyme assay	Kida et al, 1982 [274], Goldsmith et al, 1979 [275]
	Liver[1,2,3]	Mouse	[1]northern blot, [2]mRNA (primary hepatocytes), [3]enzyme assay	Ruppert et al, 1992 [276], Endo et al. 1991 [277], Grompe et al, 1993 [278]
	Liver[1b,e,2]	Rat	[1]enzyme assay, [2]flux assays	Lock et al, 1996 [120], Stanley et al, 1985 [273], Hargrove & Mackin, 1984 [279]
HPPD	Liver[1,2], kidney[1c]	Human	[1]enzyme assay, [2]cDNA sequence analysis	Kida et al, 1982 [274], Endo et al, 1992 [280], Fellman et al, 1972 [281]
	Liver[1,2]	Mouse	[1]enzyme assay, [2]immunoblot	Endo et al. 1991 [277]
	Liver[1,2,3]	Pig	[1]cDNA sequence analysis, [2]enzyme assay, [3]immunoprecipitation	Endo et al, 1992 [280], Roche et al, 1982 [282]
	Liver[1], kidney[1]	Monkey[d]	[1]enzyme assay	Fellman et al, 1972 [281]
	Liver[1e], kidney[1c]	Rat[d]	[1]enzyme assay	Fellman et al, 1972 [281], Lock et al, 1996 [120]
FAH	Liver[1,2,3,4,5], kidney[1] (PCTs)[3]	Mouse	[1]northern blot, [2]mRNA (primary hepatocytes), [3]ISH, [4]enzyme assay, [5]southern blot	Ruppert et al, 1992 [276], Endo et al. 1991 [277], Grompe et al, 1993 [278]
	Liver[1,2], kidney[2]	Rabbit	[1]western blot, [2]IHC	Li et al, 2017 [283]
	Liver[1,2], kidney[1,2]	Rat	[1]northern blot, [2]western blot	Labelle et al, 1991 [284]

Abbreviations: PAH, phenylalanine hydroxylase. TAT, tyrosine aminotransferase. HPPD, 4-hydroxyphenylpyruvic acid dioxygenase. FAH, fumarylacetoacetate hydrolase. PCT, proximal convoluted tubules. ISH, *in situ* hybridisation. IHC, immunohistochemistry.

Footnotes

[a] PAH brain activity never demonstrated; no activity using ^{14}C-Phe-hydroxylation assay and no protein detected by western blotting in crude brain tissue (McDonald et al. 2002)[285].

[b] kidney, heart and brain negative (Hargrove & Mackin, 1984)[279]

[c] shown to be cytosolic in rat kidney (Fellman et al, 1972)[281]

[d] negative in heart, muscle and brain (Fellman et al, 1972)[281]

[e] also report HGD activity in liver (Lock et al, 1996)[120]

After determining that *Hgd* is expressed mainly in the liver and kidney, time-mated embryos were investigated to determine when expression begins in these tissues although the developing testis was not investigated here. Macroscopic *LacZ* staining was limited in its detection of *Hgd* as the embryonic kidneys were too small and the staining in the liver was microscopic. Frozen section *LacZ* staining of time-mated embryos was therefore used to demonstrate that hepatic *Hgd* expression begins at E12.5 as a diffuse staining. This expression was then further verified by qPCR analysis of liver *Hgd* mRNA from E12.5-E15.5. During embryonic development, hepatic cords that contain hepatoblasts, have formed by E10.0 in the developing liver alongside haematopoietic cells. The liver then expands due to hepatoblast proliferation and haematopoietic activity from E10.5-E11.5 [286]. Haematopoietic

activity then rapidly increases, peaking at E13.5 and does not start to decline until E15.5 [286]. Haematopoietic cells encompass almost 75% of total liver volume at E13.0 [287], with hepatoblasts at E13.5 having limited contact with each other [286], explaining the diffuse and punctate *LacZ* staining and low *Hgd* mRNA level in the embryonic liver compared to the adult expression. Murine hepatoblasts begin to differentiate into hepatocytes at E14.5 [286]. Haemaotpoietic activity continues into the first post-natal week, which may explain why day 1 pups have about an eighth of adult *Hgd* expression [286]. Adult *LacZ* staining suggests that the *LacZ* positive cells observed at E15.5 in the kidney are developing PCT cells of the kidney nephron.

Hgd expression has been shown here to begin in embryonic development at a very low expression level compared to adult mice. It was also shown that the *Hgd* expression level in day 1 *Hgd tm1a -/-* pups was approximately 8-fold lower than that of adults, in conjunction with a 3-fold greater HGA level in the plasma. In addition to highlighting the importance of HGD and its role in HGA metabolism, this high HGA/low *Hgd* expression at birth suggests that therapeutic strategies such a nitisinone [52] or gene/enzyme replacement therapy should begin at birth or as soon as possible in order to prevent any detrimental or pathological effects of the HGA within the body. Knee joint pigmentation was observed here as early as 9 weeks of age in *Hgd tm1a -/-* mice (section 3.3.2.1). Due to similar concentrations of HGA being observed in both humans and mice, and due to the greater size of humans and therefore greater loading, it's plausible that human children too could begin to show the earliest stages of ochronotic pigmentation at a similar time point to mice. The onset of pigmentation in human children has not yet been investigated.

4.7.2 Liver-specific *Hgd* deletion

Management of inborn errors of metabolism such as AKU has traditionally consisted of dietary and supportive therapy. However, other treatment options have become available, including enzyme inhibition [53,110], enzyme replacement [193], cell and organ transplantation [194], gene therapy [194] and CRISPR technology [288]. Before curative strategies such as enzyme replacement and gene therapy are implemented in disease such as AKU, it's important that the target cells have been identified and that the level of enzyme activity and/or gene expression required to rescue the phenotype has been determined. Having demonstrated that the liver and kidney are the main *Hgd*-expressing tissues, liver-specific *Hgd* deletion was investigated using *MxCre* recombinase for liver-specific *Hgd* deletion within double

transgenic *Hgd tm1d (fl/fl) MxCre +/-* mice [236,289]. The deletion of *Hgd* from the liver here gives an insight into the contribution of non-hepatic *Hgd* mRNA (i.e. renal) towards overall HGA metabolism, and whether or not the liver and/or kidney should be a target for gene/enzyme therapy for AKU.

Both the short-term and long-term *Hgd tm1d MxCre* studies used two doses of 10 μg/g body weight pIpC that resulted in resulted in an approximate 80% reduction in liver *Hgd* mRNA post-cre, whilst kidney *Hgd* mRNA was maintained at the wildtype level, at 15 days post-pIpC and at 20 weeks post-pIpC administration respectively. This reduction of liver *Hgd* mRNA caused a subsequent increase in plasma HGA in both studies to a level comparable with AKU controls, suggesting that hepatic HGD activity, and not kidney HGD which is intact, is crucial for HGA metabolism and clearance from the plasma. The intact kidney *Hgd* mRNA in the pIpC injected *Hgd tm1d (fl/fl) MxCre +/-* mice did not have an impact on plasma HGA, but instead caused reduced urinary HGA compared to AKU controls.

In the short-term *Hgd tm1d MxCre* study, urinary HGA was increased with the removal of 80% of liver *Hgd* mRNA in the *MxCre +ve* mice compared to the wildtype controls, but the level was substantially lower than the urinary HGA of the AKU controls. This elevation in urinary HGA was slightly more evident in the long-term study, but again, the urinary HGA in the *MxCre +/-* mice was not elevated to the level of the AKU control. This was a surprising finding; with HGA being increased to an 'AKU' level in the plasma, it would have been expected that the HGA in the urine would also be increased to the 'AKU' level. This effect of reduced urinary HGA in the presence of elevated plasma HGA suggests the PCT cells are reabsorbing HGA from the filtrate, which is most likely already transmitting its maximum load of HGA from the circulation to be excreted, that is then metabolised by the intact HGD within the PCT cells. In addition, HGA-derived from the reabsorption and breakdown of tyrosine/phenylalanine from the filtrate within the PCT cells will also likely be metabolised by the intact HGD.

The mechanism of HGA transport within the kidney, including reabsorption and tubular secretion, is currently unknown, but has recently been elucidated to by Ranganath et al. [290]. The authors determined that the amount of HGA within the urine of AKU patients is far more than the theoretical amount that can be accounted for by filtration and maximal renal blood flow alone, emphasizing that the tubular secretion of HGA, that is likely produced by the breakdown of tyrosine and phenylalanine in the PCT cells, contributes significantly to the renal production and secretion of HGA into the filtrate; the HGA derived from

tyrosine/phenylalanine in non-AKU individuals would be metabolised by HGD and is therefore not detectable in the urine. This would suggest that the difference in the *Hgd tm1d MxCre +/-* HGA levels in the urine post-cre recombination compared to AKU control mice could be the amount of HGA that can be metabolised by kidney HGD. Perhaps crossing the floxed *Hgd tm1d* mouse line with a kidney-specific Cre recombinase system, such as the *Pax8*-CreER^{T2} transgenic line that is directed to all renal tubular compartments or a *Slc22a6*-CreER^{T2} knock-in line that is specific to the epithelium of the proximal convoluted tubules, both of which are tamoxifen-inducible, would enable a more in-depth study of *Hgd*/HGA in relation to the kidney [291]. Fundamentally, the importance of this finding is that intact kidney *Hgd* does not rescue the disease and therefore liver *Hgd* is critical for the correction of AKU.

A report of an AKU patient who received a kidney transplant in 2002 reportedly had normalised plasma HGA and decreased urinary HGA , both approximately half pre-transplant levels, inferring that kidney transplantation would benefit AKU patients [104]. Liver-specific *Hgd* deletion shown here in mice however suggests that kidney *Hgd* mRNA is unlikely to rescue the AKU phenotype as blood HGA levels were elevated. The improvement reported with kidney transplantation was likely due to improved renal elimination as the patient had renal failure (a case where renal transplantation would be beneficial) and subsequently very high HGA pre-transplant, rather than donor *HGD* expression.

The elevation of plasma HGA in the absence of 80% liver *Hgd* mRNA, and the presence of renal *Hgd* mRNA, indicates that future gene/enzyme replacement therapy should target the liver in order to combat increased plasma HGA that causes ochronosis in AKU. The intact kidney HGD was unable to metabolise the HGA load within the circulation. The importance of the liver is supported by a case report of an AKU patient receiving a liver transplant, after which they found no HGA in the urine and reported a halt in progressive arthropathy [103]. The data here in mice suggests that approximately 20% liver *Hgd* mRNA, delivered by gene therapy for example, will not rescue AKU; the increased HGA subsequently caused ochronosis in the knee joints of the mice in the long-term study. Full liver *Hgd* mRNA knockout was not achieved with two 10 µg/g doses in the short-term and long-term *Hgd tm1d MxCre* studies. Further reducing liver *Hgd* mRNA however would not provide further insight into the level of liver *Hgd* mRNA required to rescue the phenotype, as the HGA level at an 80% reduction in liver *Hgd* mRNA was comparable to AKU controls. A pIpC dose response study, using lower pIpC doses, in the *Hgd tm1d (fl/fl) MxCre +/-* mice was therefore carried out in order to try and determine the amount of liver *Hgd* mRNA required to rescue the phenotype.

The dose response study intended to estimate how much liver *Hgd* mRNA would lower circulating HGA. A dose response was observed in both the plasma and urine HGA levels. However, for liver *Hgd* mRNA, there was only a dose response between the lower four pIpC doses (0.33-0.01 µg/g), with no dose response observed at the higher doses (3.33-0.33 µg/g). One possible explanation for *Hgd* mRNA not corresponding to plasma HGA in the higher dose groups could be that the mRNA:protein ratio is not linear. The dose response data obtained however indicates that the minimum level of liver *Hgd* mRNA required to eliminate circulating HGA must fall between the dashed lines of Figure 4.33F, between 26% and 43% of liver *Hgd* mRNA.

4.7.3 HGD activity and HGA metabolism: considerations for gene therapy

Restoring HGD activity in all cells, via gene therapy or enzyme replacement, is currently unachievable by any current method, but the data here suggests that it is not necessary. In heterozygous mice and humans, one functioning copy of the *HGD* gene is sufficient to deal with HGA metabolism. Assuming heterozygous mice possess 50% of the *Hgd* mRNA compared to wildtypes (adult *LacZ* staining suggests this assumption is correct), then 50% *Hgd* mRNA in every hepatocyte can rescue AKU. Deletion of liver *Hgd* by 80%, leaving 20% residual *Hgd* mRNA expression, did not rescue the phenotype. However, it could not be determined how many cells were expressing the gene, either as one or two alleles, nor the distribution of expression which could be variable from cell to cell. The proportion of corrected cells and the level of therapeutic gene expression per cell required to rescue AKU is therefore still not clear. A recent study providing the first human genotype-phenotype correlation data for the three most frequent *HGD* mutation variants (this included 33 patients homozygous for these variants) identified in the SONIA-2 trial supports the data here that between 26% and 43% is the minimum level of *Hgd* mRNA required to rescue AKU [93]. This genotype-phenotype study demonstrated no difference in baseline visit serum or 24-hour urine HGA, or clinical symptoms such as eye pigmentation, hip bone density or degree of scoliosis between patients predicted to have either 1% (16 patients) or 31%-34% (17 patients) residual HGD catalytic activity that was determined *in vitro* against wildtype recombinant human HGD enzyme [93]. Other studies have also reported no correlation between the presence or absence of any type of *HGD* mutation with HGA excretion or disease severity, although residual enzyme activity was not reported [20,260].

Another consideration is whether or not hepatocytes can take up HGA from the circulation/extracellular fluid/other hepatocytes and then metabolise it. A scenario could exist whereby hepatocytes with insufficient HGD activity post-therapy are unable to metabolise HGA, with neighbouring HGD-restored cells unable to take up this non-metabolised HGA, leading to its accumulation in the circulation. The ability of hepatocytes to take up HGA is an important consideration for gene/enzyme therapies, and may be a key factor in the success of these strategies. The uptake of HGA into *Hgd* expressing-cells was therefore investigated using both AKU (*Hgd tm1a -/-*) and non-AKU (*Hgd tm1a -/+*) mice. Intravenous injection of isotopically labelled HGA ($^{13}C_6$-HGA) provides evidence that circulating HGA can re-enter *Hgd*-expressing cells to be metabolised by intracellular HGD, as isotopically labelled FAA/MAA was detected in the blood of the non-AKU *Hgd tm1a -/+* mice. Thus, it should not be necessary to repair 100% of liver cells because HGA produced by HGD-deficient hepatocytes could be taken up and metabolised by genetically repaired cells, see Figure 4.36.

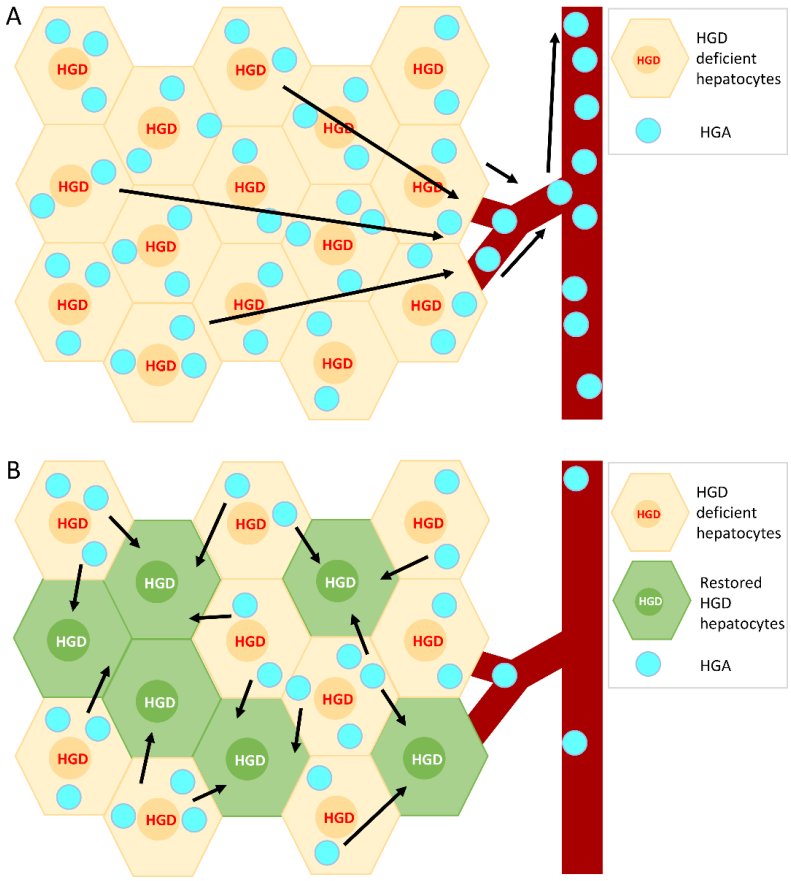

Figure 4.36. HGA uptake by hepatocytes and gene therapy.
A represents the hepatocytes within AKU liver. The hepatocytes are deficient in HGD and cannot breakdown HGA, which accumulates and enter the circulation. B represents a liver that has restored HGD activity in some of the hepatocytes, which can metabolise HGA. Some of the hepatocytes however are still deficient in HGD and are producing HGA, which can be taken up into the restored hepatocytes to be metabolised, as can HGA from the circulation. HGA = homogentisic acid. HGD = homogentisate 1,2-dioxygenase.

5 Results:

Nitisinone-induced tyrosinaemia

5.1 Introduction

The treatment of AKU with the 4-HPPD inhibiting drug nitisinone has proven to be effective at reducing circulating HGA in both humans [52,53] and mice, and has been shown to completely prevent ochronotic pigmentation in AKU mice [115,116]. A consequence of nitisinone treatment however is elevated tyrosine, or tyrosinaemia, which can cause eye and skin keratopathy. A strategy/treatment option that could reduce circulating tyrosine would improve nitisinone treatment in AKU patients by removing this potentially damaging tyrosinaemia side effect. Here, the effectiveness of dietary restriction of tyrosine and phenylalanine at reducing tyrosinaemia was investigated in nitisinone-treated AKU mice. Additional observational data in human AKU patients is also discussed.

Also reported in this chapter are a series of preliminary *in vitro* experiments investigating a potential tyrosine-reducing strategy. The expression, purification and *in vitro* activity of a tyrosine-degrading, bacterial enzyme called tyrosine ammonia lyase (TAL) is shown. The potential application of TAL to nitisinone-induced tyrosinaemia is discussed.

5.2 Dietary restriction studies

5.2.1 Dietary restriction study design

To investigate the effect of tyrosine and phenylalanine dietary restriction on nitisinone-induced tyrosinaemia and on other tyrosine pathway metabolites, AKU BALB/c *Hgd*$^{-/-}$ mice (groups of n=6; 3 male, 3 female) were treated with nitisinone for 1 week on a normal diet, then switched to either tyrosine/phenylalanine free or phenylalanine-only free diets with phenylalanine supplemented into the drinking water to investigate dose response (tyrosine is not water soluble), whilst still on nitisinone. Controls remained on normal diet whilst still on nitisinone. Blood samples were taken pre-nitisinone, after 1 week of nitisinone and then during dietary restriction (see schemes in Figure 5.3A, Figure 5.4A, Figure 5.5A) to assess tyrosine and other related metabolites in the pathway.

5.2.1.1 Calculating dietary restriction

The level of dietary restriction in the following studies was estimated using the approximate food and water intake for the background strain of the mice used, which were all BALB/c *Hgd*$^{-/-}$ in this chapter. Daily food and water intake is approximately 5 g and 6 ml respectively, per 30 g bodyweight for the BALB/cByJ strain [292]. These values are used to estimate the level of dietary restriction of tyrosine and phenylalanine, with a 30 g mouse on the normal CRM(P)

diet consuming approximately 44 mg/day phenylalanine and 29.5 mg/day tyrosine. Table 5.1 shows the estimated consumption of tyrosine and phenylalanine across the dietary restriction studies.

Table 5.1. Estimated tyrosine and phenylalanine consumption.

Study (Figure)	**Diet**	**Phe supplementation in drinking water (mg/ml)**	**Estimated level of tyr / phe consumed (%)**
Tyr/phe free diet study (Figure 5.3).	Tyr/phe free	5	0% tyr / 68% phe
		2.5	0% tyr / 34% phe
		1.25	0% tyr / 17% phe
Lower tyr/phe free diet study (Figure 5.4).		0.625	0% tyr / 8.5% phe
		0.3125	0% tyr / 4.25% phe
		None	0% tyr / 0% phe
Phe free diet study (Figure 5.5).	Phe free diet	2.5	100% tyr / 34% phe
		0.625	100% tyr / 8.5% phe
		None	100% tyr / 0% phe
Abbreviations: tyr = tyrosine; phe = phenylalanine			

5.2.2 The effect of nitisinone on tyrosine pathway metabolites

To show the effect that nitisinone has on tyrosine pathway metabolites, BALB/c *Hgd*$^{-/-}$ (n=24) were treated with 4 mg/L nitisinone in the drinking water, available *ad libitum*. Blood samples were taken pre-nitisinone, and after 7 days of treatment. With reference to Figure 5.1, HGA (mean ±SEM) was decreased 8-fold from 255.1 ±43.2 µmol/L to 32.9 ±3.2 µmol/L whilst all other metabolites increased; all changes were significant ($p<0.001$; two-tailed paired t-test). Tyrosine increased 11-fold from 72.9 ±3.6 µmol/L to 813.3 ±37.6 µmol/L. Phenylalanine increased 1.5-fold from 67.3 ±2.4 µmol/L to 100.8 ±4.9 µmol/L. HPPA increased 14.5-fold from 10.5 ±0.4 µmol/L to 151.8 ±12.9 µmol/L. 4-Hydroxyphenyllactic acid (HPLA) increased 19-fold from 2.0 ±0.2 µmol/L to 38.6 ±3.0 µmol/L.

Although mice are not reported to experience keratopathy of the eye in response to nitisinone-induced tyrosinaemia, the eyes of AKU mice were taken from another nitisinone study (not in this thesis), in order to determine the concentration of tyrosine within the eye. The eyes were dissected from both control BALB/c *Hgd*$^{-/-}$ mice (normal drinking water; n=4) and nitisinone-treated BALB/c *Hgd*$^{-/-}$ mice (4 mg/L in drinking water; n=4), homogenised in 70% methanol, centrifuged and the supernatant collected. The mass spectrometry method used to measure tyrosine in plasma [47] was used to quantitate tyrosine within the eye supernatants. The obtained concentrations however may not be truly representative of the actual concentration, as matrix-matched calibrators were not used (calibrators with a serum

matrix were used to quantitate tyrosine in the samples that were homogenised in a methanol/water matrix); but importantly, the control and nitisinone-treated groups will be comparable, as they were measured by the same method. The concentrations obtained from mass spectrometer were then multiplied by 33.3 as the eyes were diluted in 70% methanol at 30 mg/ml for homogenisation, which diluted the tyrosine within the eye by 33.3-fold. With reference to Figure 5.2, tyrosine within the eyes (mean ±SEM) of nitisinone-treated AKU mice was 4.4-fold greater than the controls, at 1,175.0 ±66.9 µmol/L and 270.8 ±35.3 µmol/L respectively. This difference was extremely significant ($p<0.0001$). Plasma tyrosine (mean ±SEM) was also measured in these mice and was 10.6-fold greater in the nitisinone-treated mice at 609.3 ±52.8 µmol/L, compared to the controls at 57.1 ±4.3 µmol/L ($p<0.0001$). In the nitisinone-treated mice, tyrosine within the eyes was 1.9-fold greater than the plasma. In the untreated mice, tyrosine within the eyes was 4.7-fold greater than the plasma.

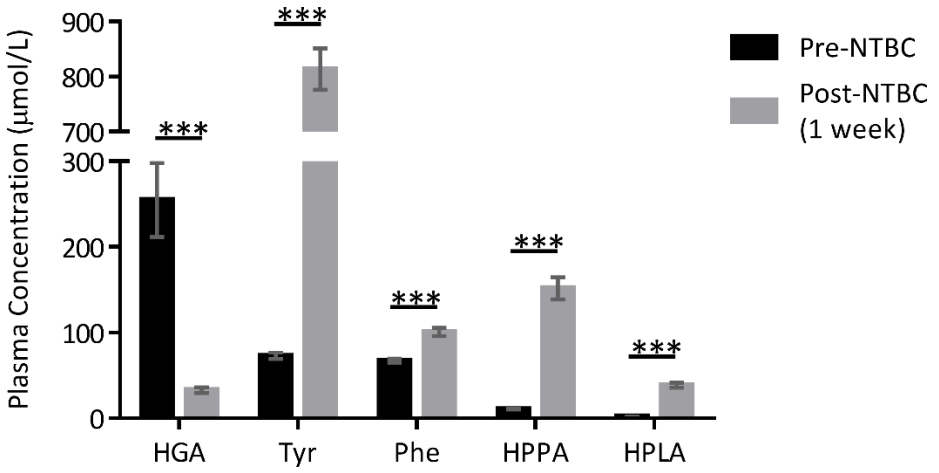

Figure 5.1. Changes in tyrosine pathway metabolites after 1 week of nitisinone treatment.
BALB/c *Hgd*$^{-/-}$ AKU mice were (n=24; 12 males, 12 females; mean age [range] = 42 [9-55] weeks) treated for 1 week with nitisinone (NTBC), with tail bleed samples taken pre- and post-treatment. HGA was significantly reduced, whilst the other metabolites were significantly increased. HGA = homogentisic acid. Tyr = tyrosine. Phe = phenylalanine. HPPA = 4-hydroxyphenylpyruvic acid. HPLA = 4-hydroxyphenyllactic acid. Error bars represent SEM. Paired t-test (two-tailed) significance: $p<0.05$ *, $p<0.01$ **, $p<0.001$***.

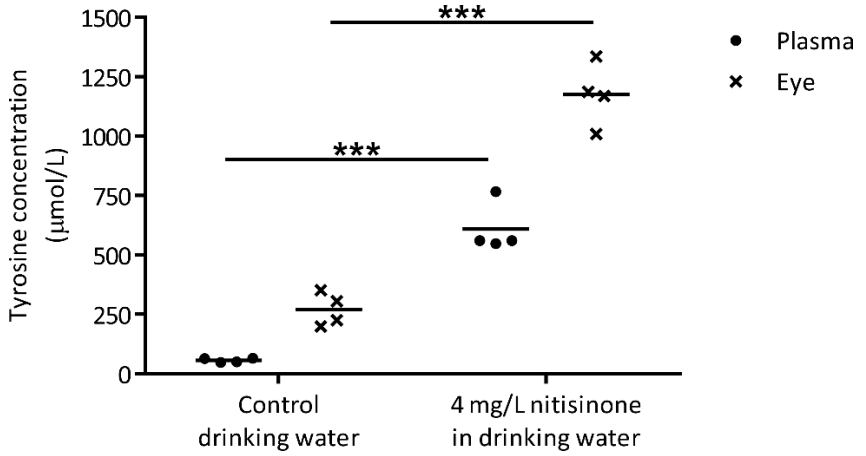

Figure 5.2. Tyrosine concentration within the plasma and eye after 1 week of nitisinone treatment.
After 1 week of treatment, plasma was taken and the eyes dissected from control (normal drinking water; n=4; male; mean age [range] = 30.1 weeks [29.0-31.1]) and nitisinone-treated (4 mg/L nitisinone; n=4; male; mean age [range] = 29.8 [25.7-31.1] weeks) BALB/c *Hgd*$^{-/-}$ mice. The eyes were homogenised and the supernatant collected. Tyrosine was quantitated in both the plasma and eye supernatant. Tyrosine was significantly greater in both the eyes and plasma of nitisinone-treated mice. Unpaired t-test (two-tailed) significance: $p<0.05$ *, $p<0.01$ **, $p<0.001$ ***.

5.2.3 Tyrosine/phenylalanine dietary restriction

To investigate the effect of tyrosine and phenylalanine dietary restriction on nitisinone-induced tyrosinaemia and on other tyrosine pathway metabolites, BALB/c *Hgd*$^{-/-}$ mice were given nitisinone (4 mg/L) in drinking water, and then whilst still on nitisinone fed a tyrosine and phenylalanine free diet. To look at dose response, phenylalanine was supplemented into the drinking water at three different doses (5 mg/ml, 2.5 mg/ml and 1.25 mg/ml) in the restricted groups. A control group remained on the normal diet with nitisinone treatment. Blood samples were taken according to the scheme in Figure 5.3A.

With reference to Figure 5.3B, tyrosine (mean ±SEM), which was increased from 72.9 ±3.6 µmol/L to 813.3 ±41.5 µmol/L (all groups, n=24) after 1 week of nitisinone treatment, is reduced in the restricted groups after 3 days of dietary restriction in a dose responsive manner (389.3 ±42.3 µmol/L, 274.8 ±6.3 µmol/L, 144.3 ±13.0 µmol/L). After 14 days of restriction, this reduction was still maintained in all groups. All comparisons to the control group at both 3 and 14 days were significant ($p<0.001$; one-way ANOVA, Tukey post-hoc). After 3 days of dietary restriction, significant reductions in the other metabolites investigated (phenylalanine, HGA, HPPA and HPLA) were present, however the dose response was not as clear in these metabolites (Figure 5.3B). After 14 days of dietary restriction, only HGA and HPLA showed significant reductions compared to the control group (but trends were similar at 3 and 14 days).

Individual body weight was monitored over the duration of dietary restriction. At 14 days of restriction, the restricted groups showed no significant change in body weight (Figure 5.3C) compared to the control group (one-way ANOVA; p=0.841).

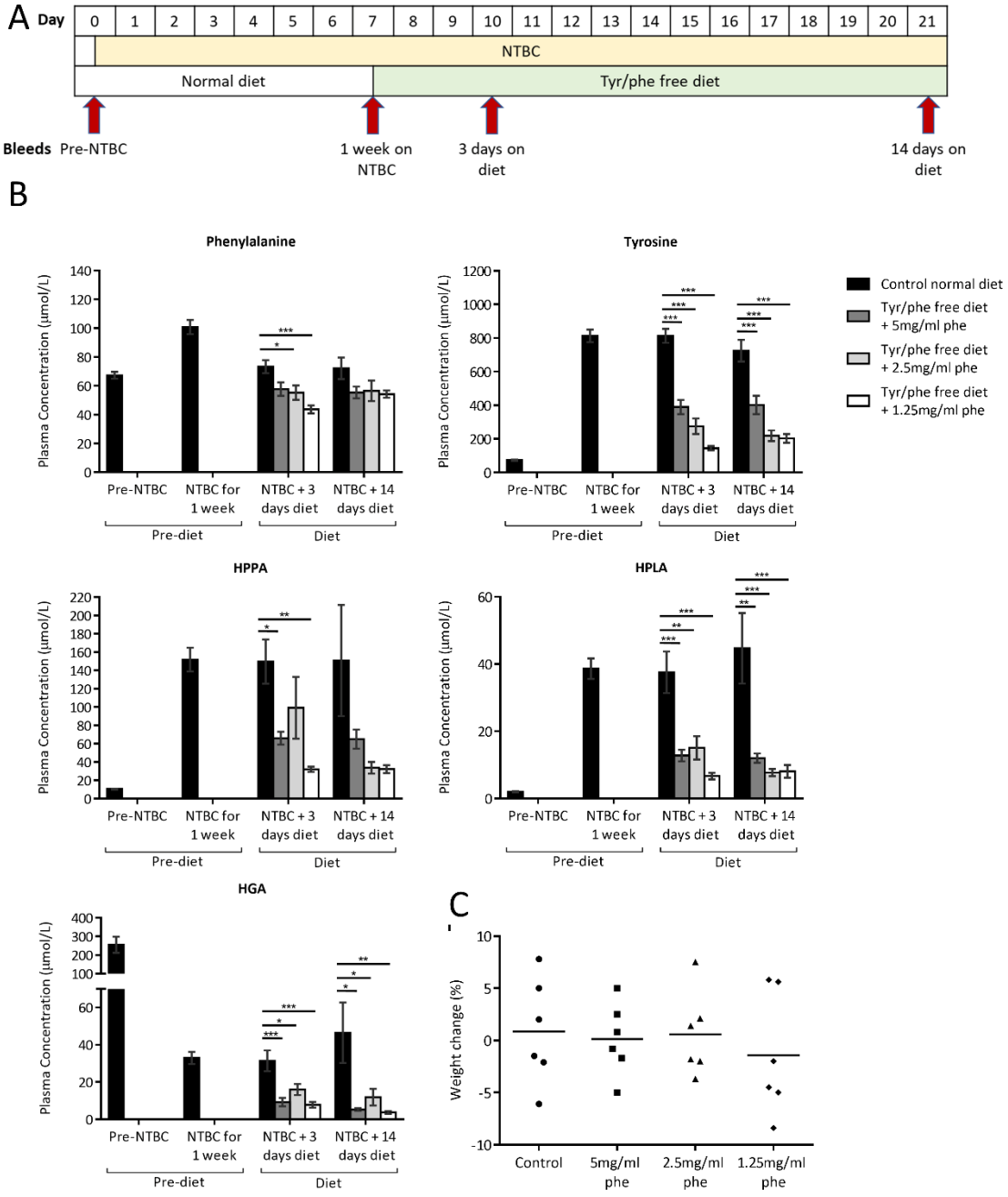

Figure 5.3. Dietary restriction of tyrosine and phenylalanine in NTBC-treated BALB/c *Hgd*$^{-/-}$ AKU mice.
A shows when blood samples were taken and when diet conditions were altered. B shows the plasma metabolite levels before NTBC treatment (all mice; n=24; 12 males, 12 females; mean age [range] = 42 [9-55] weeks), after 1 week of NTBC treatment (all mice; n=24), then after 3 (n=6) and 14 days (n=6) of diet restriction of tyrosine and phenylalanine. C shows the change in bodyweight of individual mice in each group from day 7 (start of dietary restriction) and day 21 (after 14 days of dietary restriction). Mean age [range] of each group; control = 39.6 [9-48] weeks; 5 mg/ml = 39.6 [25.4-49.4] weeks; 2.5 mg/ml = 43.4 [11.6-50.0] weeks; 1.25 mg/ml = 45.5 [14.4-55.0]. NTBC = nitisinone. HGA = homogentisic acid. HPPA = 4-hydroxyphenylpyruvic acid. HPLA = 4-hydroxyphenyllactic acid. Error bars represent SEM. One-way ANOVA (Tukey post-hoc) significance: p<0.05 *, p<0.01 **, p<0.001 ***.

5.2.4 Lower tyrosine/phenylalanine dietary restriction

To investigate the effect of further dietary restriction on nitisinone-induced tyrosinaemia, a second study was conducted using the tyrosine/phenylalanine free diet, supplementing less phenylalanine than was used in Figure 5.3. One of the restricted groups in this study was given no phenylalanine supplementation to investigate a diet completely free in both tyrosine and phenylalanine. Although no weight loss was seen in the previous study with higher phenylalanine supplementation, this study was shorter in anticipation of weight loss (project license weight loss limits must be adhered to and considered when planning/carrying out a study).

With reference to Figure 5.4B, tyrosine (mean ±SEM) which is increased from 59.0 ±2.0 µmol/L to 548.8 ±43.2 µmol/L (all groups, n=24) after 1 week of nitisinone treatment, is reduced in the restricted groups after 3 days of dietary restriction to 112.3 ±14.3 µmol/L, 170.6 ±12.0 µmol/L, 180.9 ±30.0 µmol/L in the 0.625 mg/ml, 0.3125 mg/ml and 0 mg/ml groups. After 4 days of restriction, this reduction was still maintained in all groups with no further decrease. All comparisons to the control group at both 3 and 4 days were significant ($p<0.001$; one-way ANOVA, Tukey post hoc). No dose response was seen at 3 or 4 days of restriction.

After both 3 and 4 days of dietary restriction, significant reductions in the other metabolites investigated (phenylalanine, HGA, HPPA and HPLA) were seen with dietary restriction, with the 4-day levels being comparable to the 3-day levels. As observed with tyrosine in this study, no dose response affect was observed.

Body weight was monitored over the duration of the dietary restriction. Figure 5.4C shows the weight change of individual mice at 4 days of dietary restriction. No significant differences were observed; the restricted groups showed weight changes comparable with the control group (one-way ANOVA; $p=0.798$).

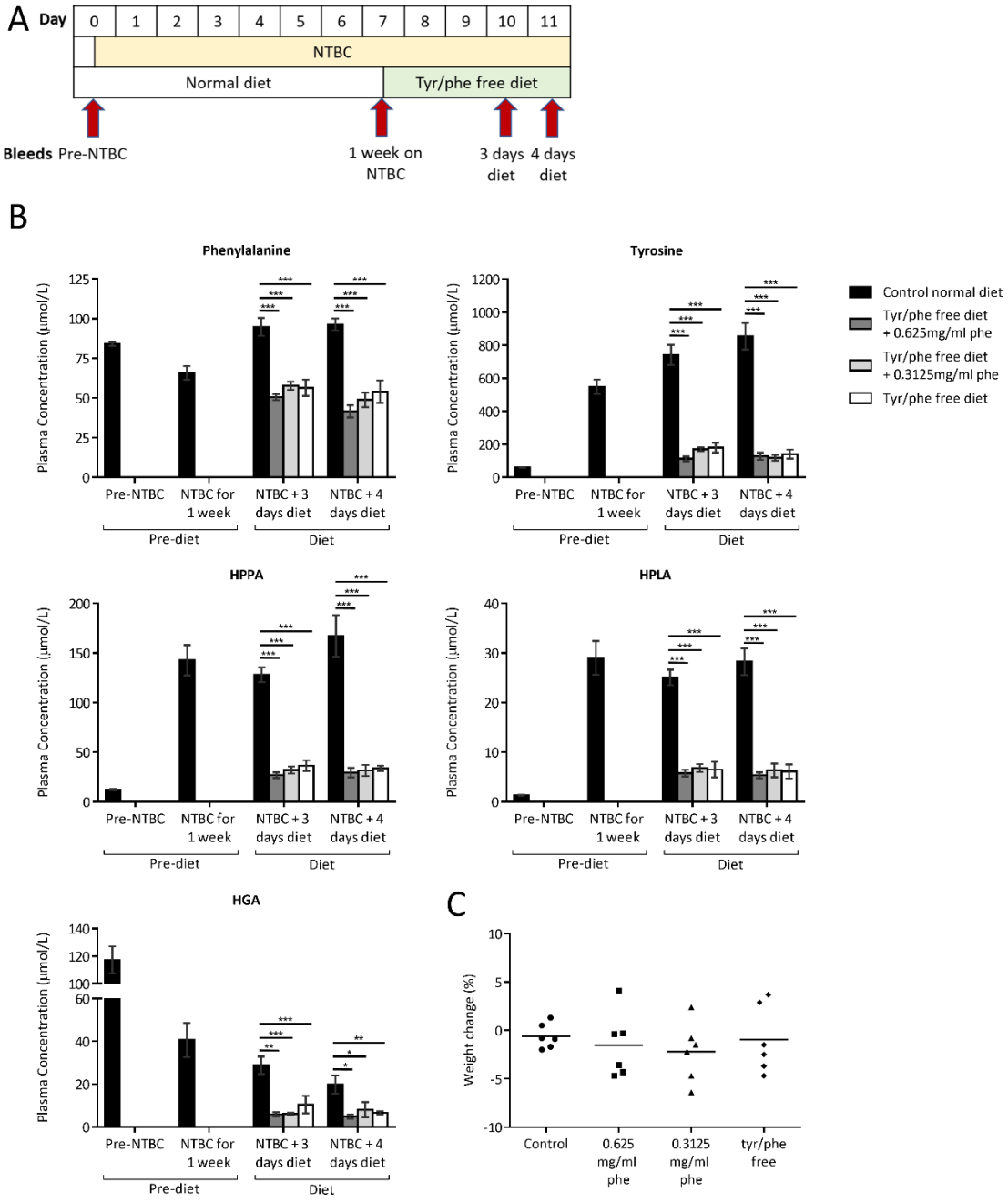

Figure 5.4. Lower dietary restriction of tyrosine and phenylalanine in NTBC-treated BALB/c *Hgd*$^{-/-}$ AKU mice.
A shows when blood samples were taken and when diet conditions were altered. B shows the plasma metabolite levels before NTBC treatment (all mice; n=24; 12 males, 12 females; mean age [range] = 23.2 [8.1-27.9] weeks), after 1 week of NTBC treatment (all mice; n=24), then after 3 (n=6) and 4 days (n=6) of diet restriction of tyrosine and phenylalanine. C shows the change in bodyweight of individual mice in each group from day 7 (start of dietary restriction) and day 11 (after 4 days of dietary restriction). Mean age [range] of each group; control 26.3 [24.9-27.9] weeks; 0.625 mg/ml = 20.7 [8.1-27.4] weeks; 0.3125 mg/ml = 21.8 [8.1-24.9] weeks; tyr/phe free = 24.1 [23.6-24.9] weeks. NTBC = nitisinone. HGA = homogentisic acid. HPPA = 4-hydroxyphenylpyruvic acid. HPLA = 4-hydroxyphenyllactic acid. Error bars represent SEM. One-way ANOVA (Tukey post-hoc) significance: p<0.05 *, p<0.01 **, p<0.001 ***.

5.2.5 Phenylalanine-only dietary restriction

To investigate the effect of phenylalanine-only dietary restriction on nitisinone-induced tyrosinaemia, BALB/c *Hgd*$^{-/-}$ mice were given nitisinone in the drinking water, then fed a phenylalanine free diet with normal tyrosine, whilst still on nitisinone, with phenylalanine supplemented in the drinking water (2.5 mg/ml, 0.625 mg/ml and 0 mg/ml) to look at dose response. Blood samples were taken according to the scheme in Figure 5.5A.

With reference to Figure 5.5B, plasma tyrosine was 63.5 ±2.7 µmol/L pre-nitisinone and increased to 748.9 ±26.8 µmol/L post-nitisinone (n=24, all groups). After 3 days of phenylalanine restriction, tyrosine levels were 757.3 ±54.9 µmol/L, 533.2 ±28.8 µmol/L and 656.2 ±69.6 µmol/L, with only the latter two groups, (0.625 mg/ml and phenylalanine free), being significantly different to control ($p<0.001$ and $p=0.014$, respectively). A clear dose response effect was not seen in plasma tyrosine with dietary restriction of phenylalanine after 3 days. After 7 days of dietary restriction, none of the restricted groups had a significantly lower tyrosine level compared with the control group.

Significant reductions in plasma phenylalanine were seen at both 3 days (all groups $p<0.001$ compared to control) and after 7 days (0.625 mg/ml and phenylalanine free, both $p<0.001$ compared with control; 2.5 mg/ml not significantly different, $p=0.065$) of phenylalanine dietary restriction. HPLA demonstrated significant differences after 3 days in the 0.625 mg/ml and phenylalanine free groups however these significant differences were not maintained after 7 days. HGA showed significant differences after 7 days of dietary restriction in all the restricted groups however these differences were not seen after 3 days. HPPA was not significantly reduced in the restricted groups compared with control, at neither 3 nor 7 days of dietary restriction.

Figure 5.5C shows the changes in body weight after 7 days of restriction. One-way ANOVA demonstrated a significant difference in weight change between the groups ($p=0.014$). Post-hoc Tukey tests demonstrate that the differences were between the 2.5 mg/ml group compared with the 0.625 mg/ml ($p=0.023$) and phenylalanine free ($p=0.021$) groups. None of the restricted groups however showed a weight change that was significantly different to the control group.

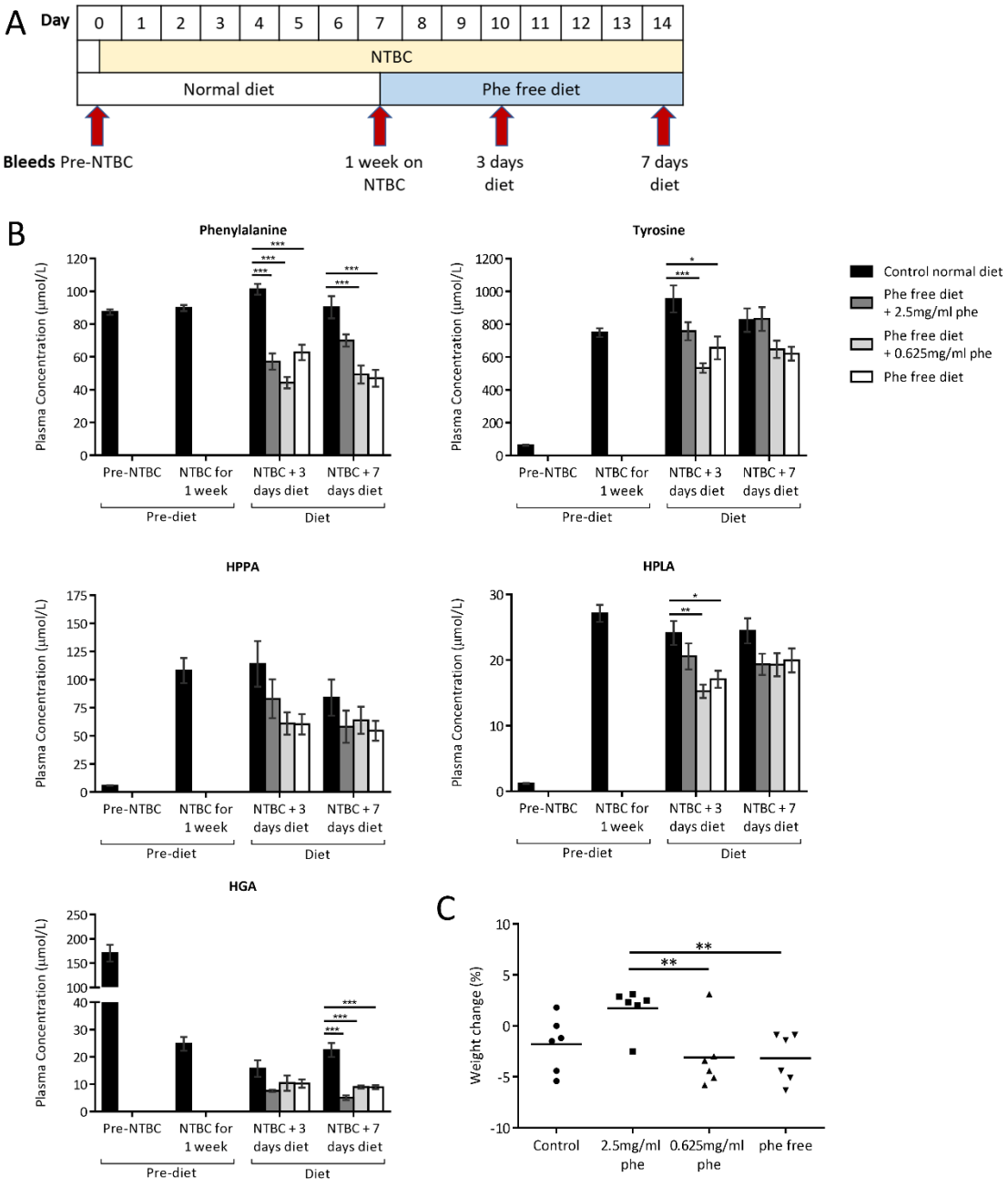

Figure 5.5. Dietary restriction of phenylalanine in NTBC-treated BALB/c *Hgd*$^{-/-}$ AKU mice.
A shows when blood samples were taken and when diet conditions were altered. B shows the plasma metabolite levels before NTBC treatment (all mice; n=24; 12 males, 2 females; mean age [range] = 27.7 [16.4-53.9] weeks), after 1 week of NTBC treatment (all mice; n=24), then after 3 (n=6) and 14 (n=6) days of diet restriction of phenylalanine. C shows the change in bodyweight of individual mice in each group from day 7 (start of dietary restriction) and day 14 (after 7 days of dietary restriction). Mean age [range] of each group; control = 32.9 [19.3-53.9] weeks; 2.5 g/ml = 19.5 [16.4-20.3] weeks; 0.625 mg/ml = 27.1 [20.3-31.6] weeks; phe free = 26.1 [20.3-34.7] weeks. NTBC = nitisinone. HGA = homogentisic acid. HPPA = 4-hydroxyphenylpyruvic acid. HPLA = 4-hydroxyphenyllactic acid. Error bars represent SEM. One-way ANOVA (Tukey post-hoc) significance: p<0.05 *, p<0.01 **, p<0.001 ***.

5.2.6 Tyrosine and phenylalanine restriction in the absence of nitisinone treatment

Phenylalanine, and tyrosine in the absence of sufficient phenylalanine, are essential amino acids obtained via ingesting dietary protein. Both phenylalanine and tyrosine however can

be obtained through endogenous protein turnover. Bodyweight has therefore been monitored in the dietary restriction studies shown here, with no significant changes in bodyweight observed in the restricted groups compared to the control in Figure 5.3C, Figure 5.4C and Figure 5.5C. The increased tyrosine level associated with nitisinone treatment could potentially be preventing weight loss in the dietary restriction groups here due to the tyrosine pool taking longer to deplete. One group of BALB/c *Hgd*$^{-/-}$ mice (n=6) were therefore fed the tyrosine/phenylalanine free diet, with no phenylalanine supplementation in the water, in the absence of nitisinone treatment. Tyrosine pathway metabolites were measured in the blood and body weight recorded.

Figure 5.6A shows the time points at which blood samples were taken. At 3 and 6 days of complete dietary restriction of tyrosine and phenylalanine (Figure 5.6B), plasma tyrosine levels (mean ±SEM) were reduced from 77.3 ±5.0 µmol/L pre-diet to 24.7 ±3.2 µmol/L and 24.2 ±2.8 µmol/L, respectively. This reduction was highly significant at both 3 and 6 days (one-way ANOVA, Tukey post-hoc; $p<0.001$). Phenylalanine, HGA, HPPA and HPLA were all significantly reduced at 3 and 6 days of dietary restriction compared to pre-diet levels.

Bodyweight was closely monitored. Figure 5.6C shows after 3 and 6 days of dietary restriction, that the mean change in body weight from day 0 was -5.7% and -6.3% respectively. To determine whether this change in body weight was consistent with normal weight fluctuations or due to dietary restriction, and to see if nitisinone had any affect, it was compared against both the control and tyrosine/phenylalanine free groups from Figure 5.4, at 3 days of restriction. Figure 5.7 shows that the reduction in body weight in the tyrosine/phenylalanine free group without nitisinone was significantly different to the control group ($p=0.026$) and the tyrosine/phenylalanine group with nitisinone ($p=0.034$).

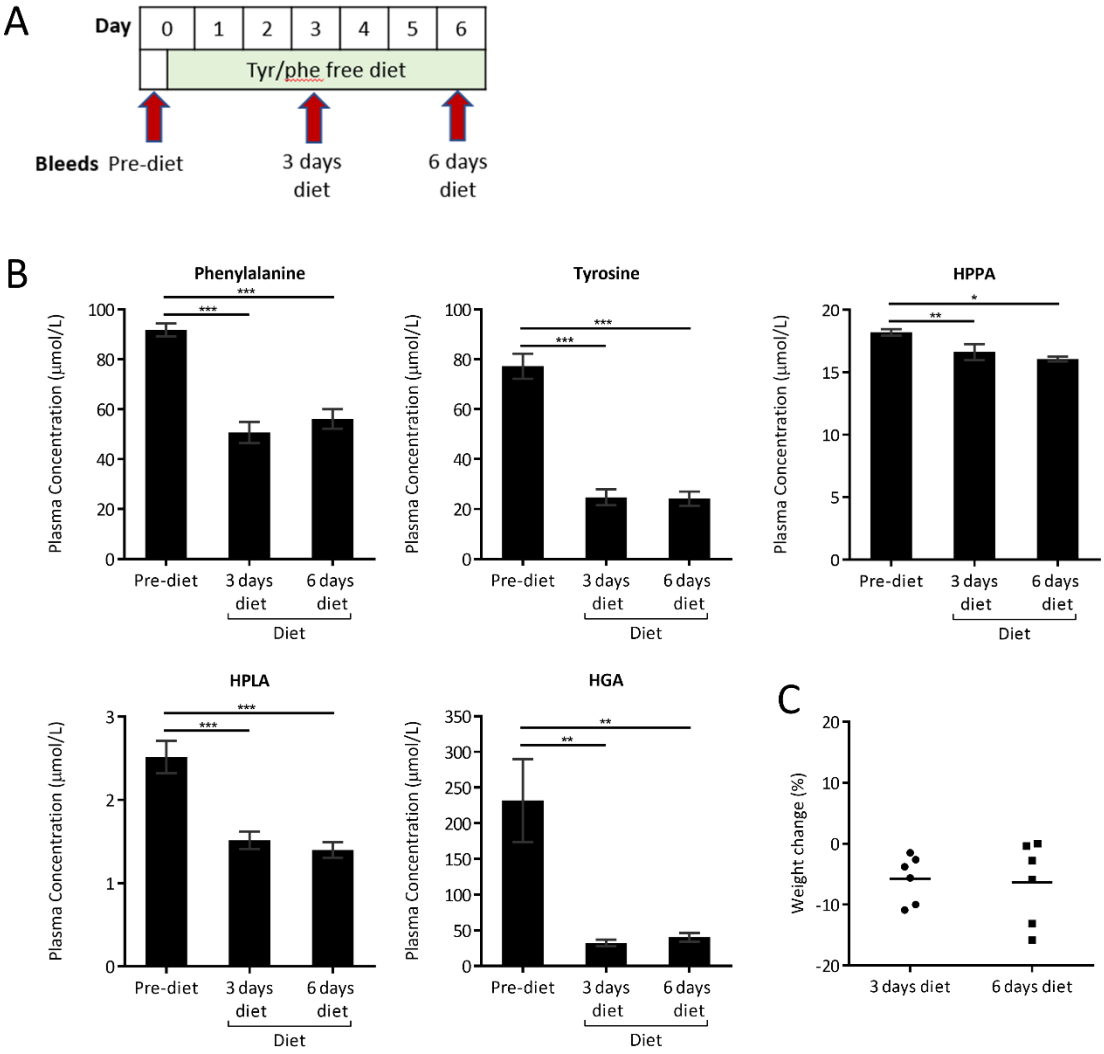

Figure 5.6. Dietary restriction of tyrosine and phenylalanine in BALB/c *Hgd*$^{-/-}$ AKU mice in the absence of nitisinone and phenylalanine supplementation.

A shows when blood samples were taken and when diet conditions were altered. B shows the plasma metabolite levels pre-dietary restriction (n=6; 2 males, 4 females; mean age [range] = 25.7 [23.6-26.7] weeks) and then after 3 and 6 days (n=6) of diet restriction of both tyrosine and phenylalanine. C shows the change in bodyweight of individual mice in each group from day 0 (start of dietary restriction) and day 3 and day 6 (after 3 and 6 days of dietary restriction). HGA = homogentisic acid. HPPA = 4-hydroxyphenylpyruvic acid. HPLA = 4-hydroxyphenyllactic acid. Error bars represent SEM. One-way ANOVA (Tukey post-hoc) significance: p<0.05 *, p<0.01 **, p<0.001 ***.

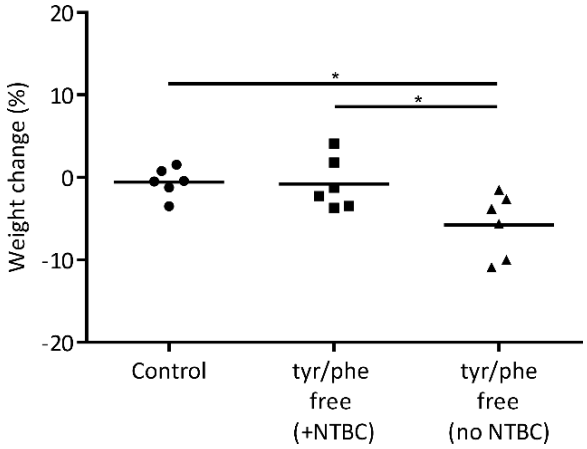

Figure 5.7. Changes in body weight of tyrosine/phenylalanine restricted BALB/c *Hgd*$^{-/-}$ AKU mice in the presence/absence of nitisinone at 3 days.
Control (n=6) and tyr/phe free (+NTBC) (n=6) body weight taken from the tyrosine/phenylalanine restriction study in Figure 5.4, at 3 days of restriction. Tyr/phe free (no NTBC) (n=6) body weight taken from the tyrosine/phenylalanine restriction study in Figure 5.6, at 3 days of restriction. One-way ANOVA (Tukey post-hoc) significance: p<0.05 *, p<0.01 **, p<0.001 ***.

5.2.7 Food and water consumption during dietary restriction

A consideration throughout the dietary restriction studies was the food and water intake of the mice. Supplementation levels were based on assumptions of food and water intake for the background strain as mentioned above in the experiment design (section 5.2.1.1). It's possible that due to differences in the normal mouse diet and the custom restricted diets, such as the consistency of the diet, and potentially taste, the mice may have consumed more or less food. The same is applicable to the drinking water supplemented with nitisinone and phenylalanine; it may have had an altered taste.

The nutritional content of the custom diets is matched to the control normal diet, with a normal level of protein and calories, but specifically deficient in tyrosine and phenylalanine. Another consideration is whether or not the mice consumed more food due to potential amino acid deficiency from the restricted diets. In an attempt to investigate whether food and water consumption was affected by the restricted diets and water supplementation, a study was designed to measure food and water intake of mice subjected to the dietary conditions in Figure 5.3, the first tyrosine/phenylalanine free diet study.

Food and water consumption were measured for 4 male BALB/c *Hgd*$^{-/-}$ mice (aged 53.4-53.7 weeks), who were individually housed in an Oxylet*Pro* System Physiocage (Panlab, Harvard Apparatus, UK), equipped with food and water dispensers designed to accurately record food and water consumption via weight transducer technology. The mice were provided with standard cage enrichment of red dome house, clear tunnel and cage bedding). According to

the scheme in Figure 5.8A, the mice were fed a normal diet in week 1, then received nitisinone in the drinking water at 4 mg/L during week 2, then were switched to the tyrosine/phenylalanine free diet with phenylalanine supplementation (5 mg/ml, n=1; 2.5 mg/ml, n=1; 1.25 mg/ml, n=1) in the drinking water, whilst still on nitisinone, during week 3. One mouse remained on the normal diet and nitisinone throughout week 3 as a control.

Food and water intake monitoring was found to be extremely difficult to monitor. Food intake (Figure 5.8B) was at first consistent during weeks 1 and 2, with mean (±SEM) consumption of the normal diet found to be 4.2 ±1.1 g (all 4 mice). During week 3, the control mouse consumed 4.0 ±0.3 g of food, consistent with weeks 1 and 2. Measuring consumption of the tyrosine/phenylalanine free diet however was not straightforward. The diet was very crumbly and the crumb tray was often overflowed. Vast amounts of the diet were also found on the floor of the cage, as both small pellets and crumbled almost to a powder, either due to its crumbliness or due to the mouse bringing the food into the cage. Attempts were made to gather all the food to calculate the amount eaten by the mouse. The values shown from day 14 onwards however are very unlikely to be a true representation of the amount of food consumed, due to the extreme variation and difficulty recording the intake.

Water intake (Figure 5.8C) was similarly unreliable. The water bottles were found to drip, overflowing the drip tray beneath. This explains the huge variation seen over the first week in water intake. After this, attempts were made to catch water overflowing from the drip tray in a small container, in addition to pipetting up any liquid not caught, although water spilled during each 24-hour period may have evaporated before recordings were made. The variability of water intake measurements was minimised slightly after day 7, however, the measurements obtained were still deemed unreliable. The degree of dripping/leaking appeared to be variable between the cages. In addition, small pieces of food and cage bedding were often found at the water spout or in the drip tray, due to activity of the mouse, absorbing water, again making it difficult to get an accurate reading.

Body weight was monitored over the duration of the food and water intake study (Figure 5.8D). One mouse did not finish the study (tyr/phe free diet + 1.25 mg/ml phe) due to weight loss. It's unlikely however that this mouse lost weight due to dietary restriction; in the tyrosine/phenylalanine dietary restriction study shown in Figure 5.3, on which this study was based, no weight loss was seen after 14 days of restriction. The mouse, which was also 53-weeks old, had only been on a restricted diet for 4 days, therefore it's likely that another

unknown factor caused its weight loss. The other 3 mice all showed a gradual increase in body weight over the 3-week period.

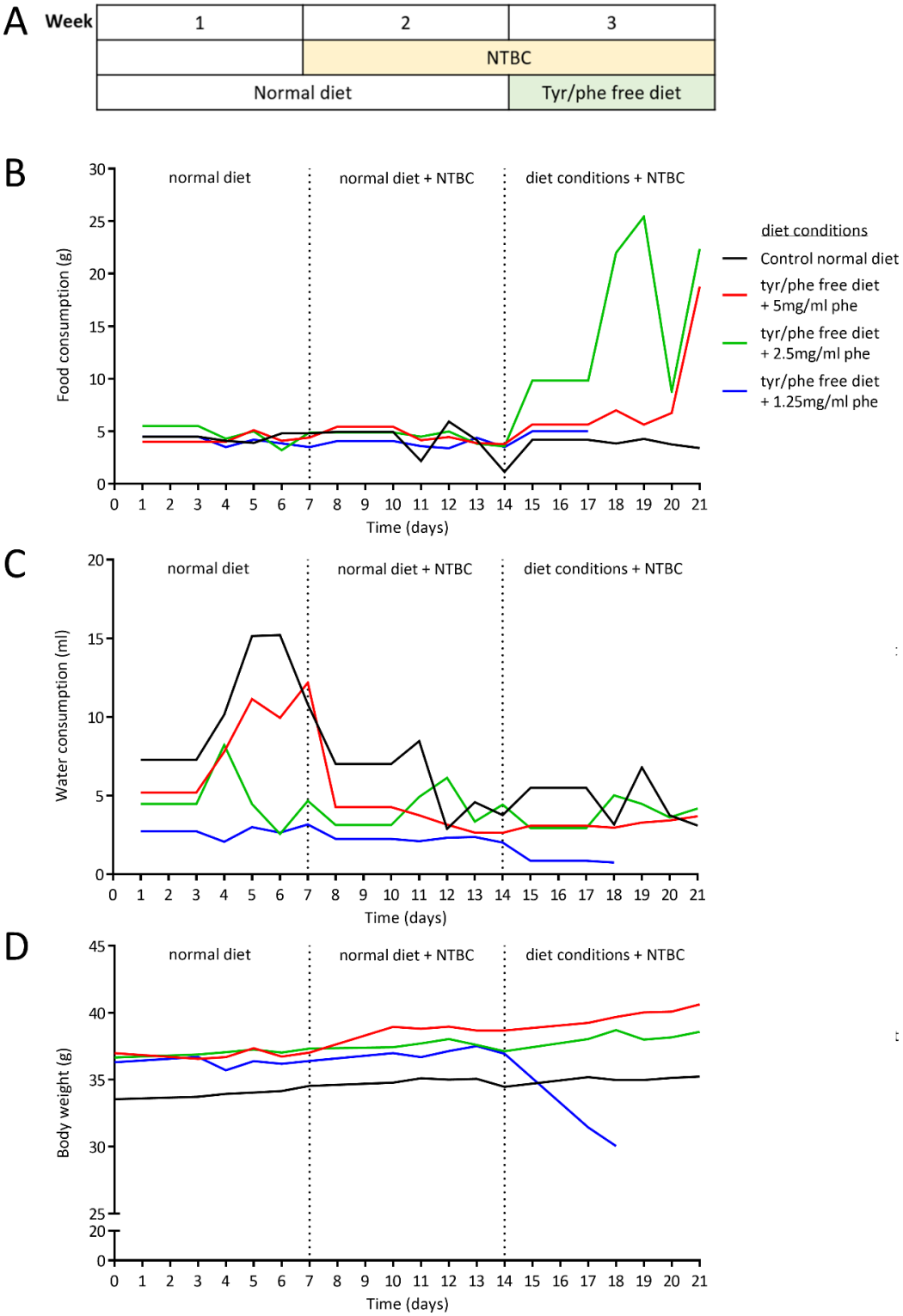

Figure 5.8. Food and water intake of BALB/c *Hgd*$^{-/-}$ AKU mice subjected to altered dietary conditions and nitisinone.

A shows when diet conditions were altered. Phenylalanine was supplemented into the drinking water (5 mg/ml, n=1; 2.5 mg/ml, n=1; 1.25 mg/ml, n=1) of mice fed the tyrosine/phenylalanine free diet. One mouse remained on the normal diet with NTBC during week 3. B shows food consumption, C shows water consumption and D shows

body weight throughout altered diet conditions and addition of nitisinone. All mice (n=4) aged 53.6 weeks, male. NTBC = nitisinone.

5.2.8 Dietary restriction in AKU patients attending the National Alkaptonuria Centre

NAC patients receive off-licence treatment of 2 mg nitisinone daily, dietary advice from a specialist dietician and have serum tyrosine monitored at yearly visits (Milan et al. 2017). The NAC aims to achieve tyrosine <500 µmol/L. Tyrosine thresholds of 500-700 µmol/L and 700-900 µmol/L are used as guidelines for reducing dietary protein consumption to 0.9 g and 0.8 g protein/kg bodyweight/day, respectively. Patients with tyrosine >700 µmol/L are more closely monitored with additional blood sampling if required. Fasting blood samples were taken in the morning. An observational study of 10 anonymised AKU patients attending the NAC with tyrosine levels >700 µmol/L are reported in Figure 5.9. All patients received advice to reduce dietary protein intake to a recommended minimum level of 0.75 g protein/kg bodyweight/day, to reduce circulating tyrosine whilst meeting minimum nutritional requirements. A TYR cooler® (Vitaflo, UK) protein substitute, free in tyrosine/phenylalanine, drink was used by 7/10 patients. TYR cooler dosage was determined by the dietician for each individual; protein removed from the diet, below the recommended minimum, was exchanged for the equivalent amount of protein in the cooler. These patients had been attending the NAC for a mean of 36.5 months [range 29-48] at the initial tyrosine concentration, with a mean age of 56 years [range 29-71]. The gender of patients was 5 males, 5 females. 8 were white British, 1 was Indian and 1 was Pakistani.

Average estimated protein intake from 7-day food diaries in all AKU patients attending the NAC was 1.0 g protein/kg bodyweight/day at baseline visit 1 [293] before any intervention, which is comparable with the general population (National Diet & Nutrition Survey, 2016, Gateway Number 2016248). In an attempt to lower circulating tyrosine with nitisinone, dietary protein intake is restricted to a recommended minimum level of 0.75 g protein/kg bodyweight/day (Scientific Advisory Committee on Nutrition, 2017/Committee on Medical Aspects of Food Policy, 1991), with additional metabolic requirements provided by prescribed tyrosine/phenylalanine-free amino acid supplements in some patients.

Overall, significant reductions in serum tyrosine (Figure 5.9) were seen in the 10 NAC patients observed (p=0.002; two-tailed Wilcoxon's signed rank test), with 4 patients reducing serum tyrosine <700 µmol/L. Three patients (Figure 5.9, dashed lines) reduced serum tyrosine (mean[range]) by 22[18-30]% by advised protein restriction alone; the other 7 patients required a combination of reduced protein intake with tyrosine/phenylalanine-free supplements to achieve a 33[8-62]% reduction. The initial tyrosine value for patients using

amino acid supplements was with dietary restriction alone, with subsequent values using a combination of reduced protein intake and amino acid supplementation. Across all 10 patients and all sample time points, phenylalanine (mean[range]) was 57[38-108] µmol/L.

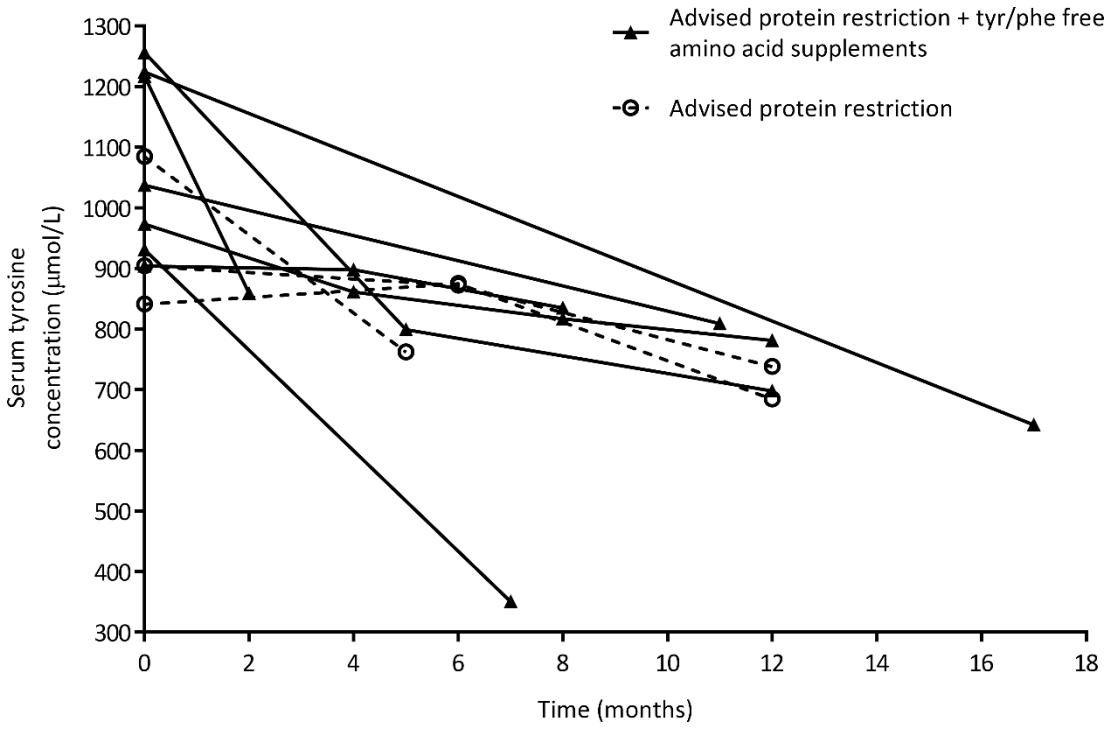

Figure 5.9. Serum tyrosine from 10 AKU patients receiving nitisinone attending the National Alkaptonuria Centre.
All 10 patients had tyrosine >700 µmol/L. Both dietary advice (restriction of dietary protein to a recommended minimum level of 0.75 g protein/kg bodyweight) (n=3) and dietary advice in combination with tyrosine/phenylalanine free amino acid supplements (n=7) reduced serum tyrosine. Initial tyrosine concentrations in the group using amino acid supplements were measured after dietary advice alone, with subsequent tyrosine concentrations measured after a combination of dietary advice and amino acid supplement use. Data provided by Shirley Judd and Professor Lakshminarayan Ranganath.

5.3 Enzymatic breakdown of tyrosine

Ammonia-lyases are a non-mammalian enzyme family that can deaminate amino acids. Of particular interest here are phenylalanine ammonia lyase (PAL) and tyrosine ammonia lyase (TAL). PAL converts L-phenylalanine into trans-cinnamic acid and ammonia. TAL converts L-tyrosine into p-coumaric acid and ammonia. Reported in the literature are PAL and TAL enzymes that can degrade both tyrosine and phenylalanine, usually named after the substrate that they exhibit greater specificity towards. Although PAL activity is initially demonstrated here in this series of preliminary experiments, TAL was the main focus due to

its greater specificity towards tyrosine. In the context of nitisinone-induced tyrosinaemia, a specific tyrosine-degrading enzyme would be more useful than a phenylalanine-specific enzyme.

5.3.1 Phenylalanine ammonia lyase

PAL was initially investigated *in vitro* as it was available to buy commercially as a Grade I, buffered aqueous glycerol solution of PAL from *Rhodotorula glutinis* (part of the pink yeast genus), whereas TAL was not available to purchase.

The first *in vitro* experiment, shown in Figure 5.10, demonstrates the ability of both 0.01U and 0.1U of *R. glutinis* PAL to degrade phenylalanine and tyrosine *in vitro* (in 50 mM Tris-HCl buffer, pH 8.5, 30°C; conditions used by Xue et al. [294]) within 24 hours, at starting substrate concentrations of 10, 50 and 100 µmol/L. By 24 hours, PAL was able to degrade tyrosine and phenylalanine at all starting substrate concentrations, with 0.1U PAL breaking down the substrates faster than 0.01U PAL. It was difficult to tell if PAL was more efficient at breaking down phenylalanine over tyrosine. In this particular experiment, the substrates were not measured at time 0 making it difficult to judge if the difference in tyrosine and phenylalanine concentration at the first time point of 1.8 minutes was due to faster phenylalanine degradation or due to variation in starting substrate concentration. With reference to the 100 µmol/L condition, with 0.1U and 0.01U PAL, both phenylalanine and tyrosine were degraded by 4 hours and 24 hours respectively.

A second *in vitro* experiment was then carried out using 0.1U of PAL at starting phenylalanine and tyrosine concentrations of 100 and 500 µmol/L (Figure 5.11); both substrates were fully degraded by PAL by 4 hours from 100 µmol/L and 8 hours from 500 µmol/L. Again, at 100 µmol/L starting substrate concentration, there was a slight difference in substrate concentration making it difficult to tell whether PAL was more efficient at breaking down tyrosine or phenylalanine. At 500 µmol/L starting substrate concentration, the starting concentrations of tyrosine and phenylalanine incubated with PAL were comparable, and the rate of breakdown observed was almost identical, with variations in tyrosine likely due to pipetting error. The differences in starting concentration of phenylalanine and tyrosine may have been due to differences in solubility (if not fully dissolved, the concentration will be affected), or may have been due to error (e.g. weighing, pipetting) when preparing the stock solutions. Although the experiments in Figure 5.10 and Figure 5.11 could have been repeated with more accurate starting substrate concentrations, it was not deemed necessary as it was

clear that PAL is able to break down tyrosine and phenylalanine effectively *in vitro*, and due to subsequent work focussing on TAL.

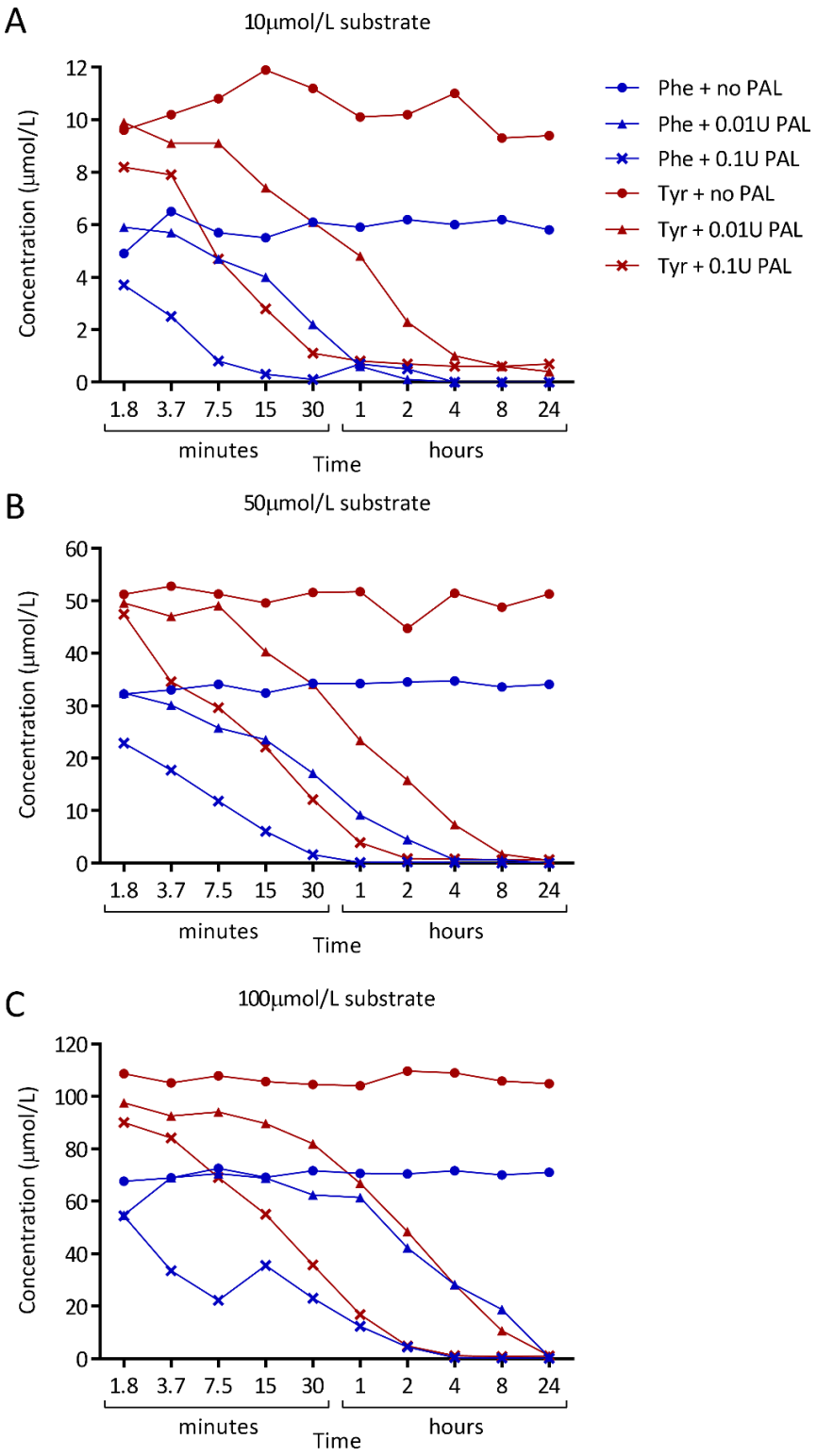

Figure 5.10. PAL-mediated degradation of phenylalanine and tyrosine *in vitro*.
Both 0.01U and 0.1U of PAL enzyme degraded phenylalanine and tyrosine at starting substrate concentrations of 10 µmol/L (A), 50 µmol/L (B) and 100 µmol/L (C). PAL, phenylalanine ammonia lyase. Phe, phenylalanine. Tyr, tyrosine. Assay carried out by Dr Craig Keenan.

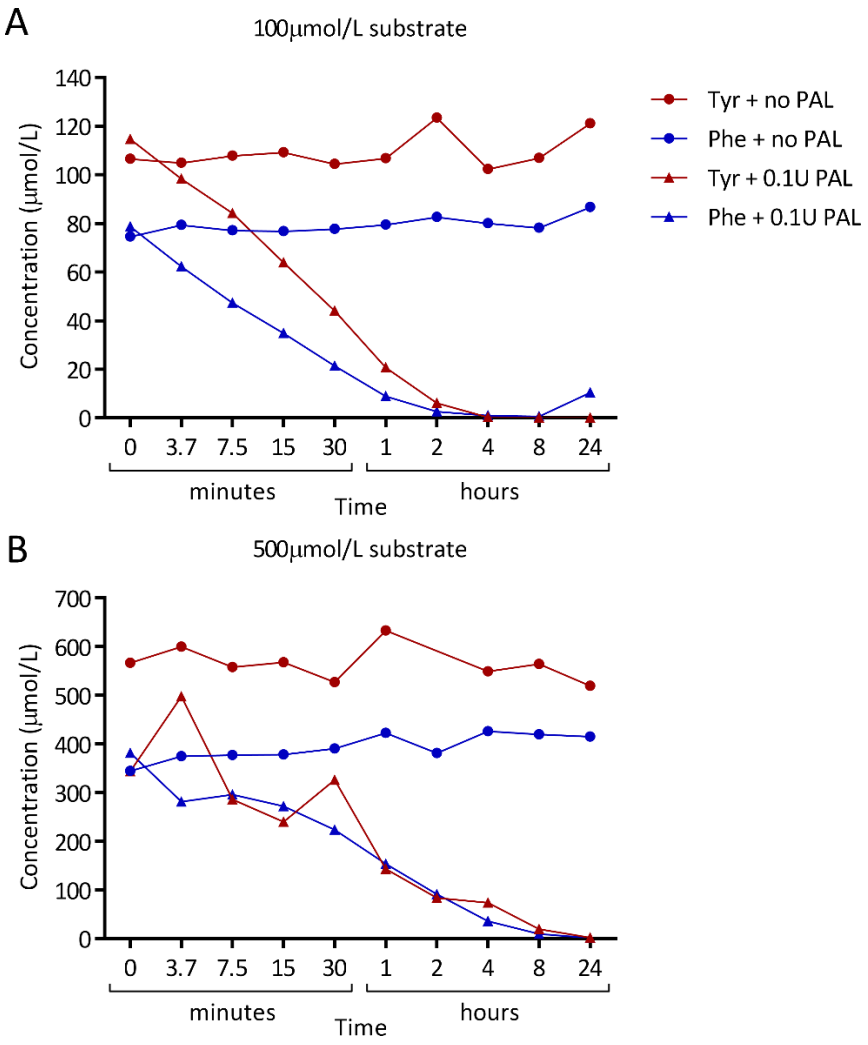

Figure 5.11. PAL-mediated degradation of phenylalanine and tyrosine at higher concentrations *in vitro*. 0.1U of PAL enzyme degraded phenylalanine and tyrosine at starting substrate concentrations of 100 µmol/L (A) and 500 µmol/L (B). PAL, phenylalanine ammonia lyase. Phe, phenylalanine. Tyr, tyrosine.

5.3.2 Tyrosine ammonia lyase

5.3.2.1 Expression, purification and *in vitro* TAL experiments

Initially, a TAL enzyme based on the sequence from *Rhodobacter capsulatus* was custom synthesized and purchased from the Protein Expression Facility at the University of Manchester (UoM, UK). An *in vitro* experiment was performed to test the tyrosine degrading ability of this enzyme. Following this, it was decided that the expression and purification of this enzyme would be performed in-house, using the same expression vector and protocols.

5.3.2.1.1 pETDuet:Tal vector

The *R. capsulatus* TAL sequence was codon optimised for bacterial protein expression and integrated into an expression vector called pETDuet-1, and referred to as pETDuet:Tal. The modified sequence of *R. capsulatus* TAL is shown in Figure 5.12. In order to integrate the TAL sequence into the pETDuet-1 expression vector, 5' BamHI and 3' XhoI restriction enzyme binding sites were added. Two stop codons (TAA) were also added before the XhoI restriction enzyme sequence to terminate translation of the TAL sequence. In order to allow purification of the expressed TAL protein, a histidine·tag (an amino acid motif that has at least 6 histidine residues) present in the expression vector was used that fuses to the N-terminus of the inserted TAL sequence, therefore the protein was expressed as an N-terminal His-TEV-linker fusion protein. The insertion of a tobacco etch virus (TEV) protease cleavage site upstream of the TAL sequence, but downstream of the His·tag, can allow cleavage of the fusion protein from the tag to obtain purified TAL protein, although this step was not used for the in-house purification of TAL. Webcutter 2.0 software shows no predicted cleavage sites for TEV in the TAL gene.

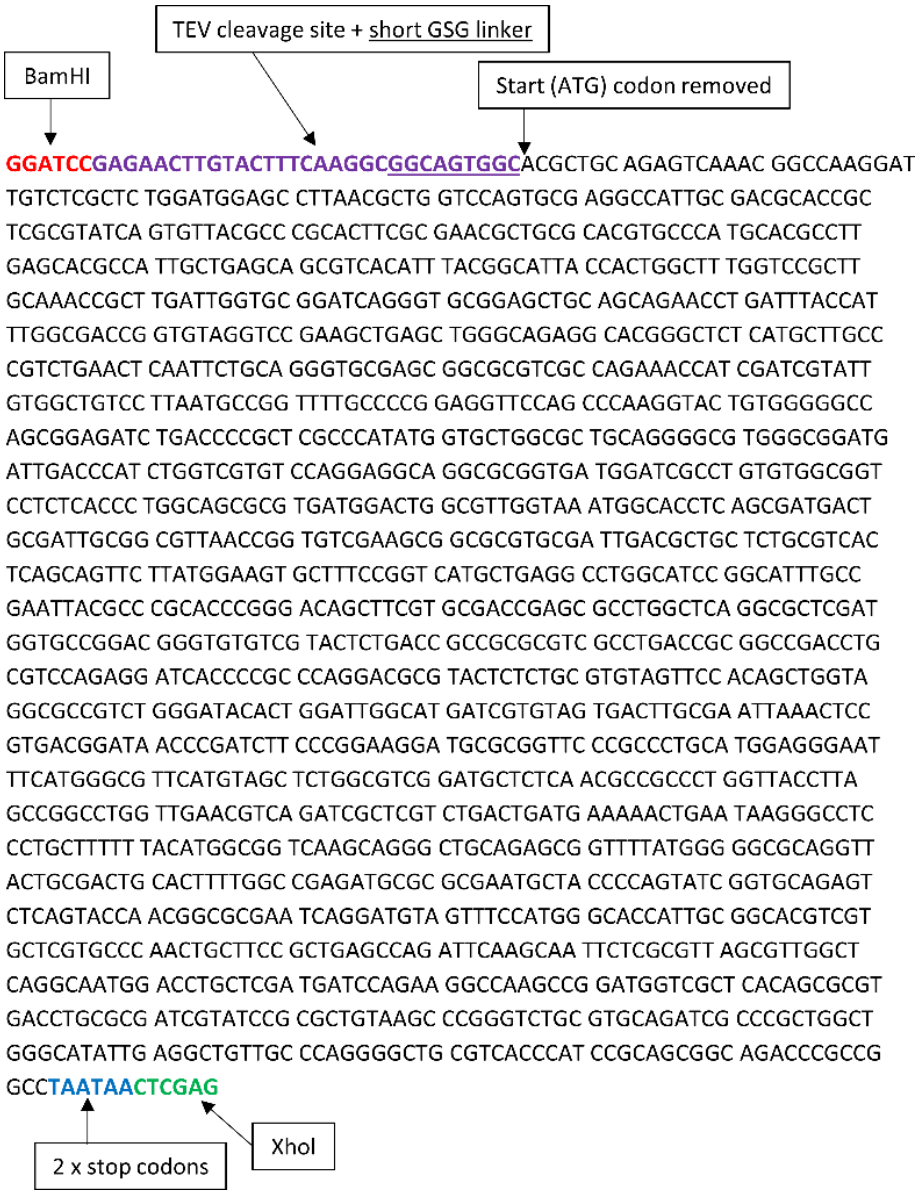

Figure 5.12. Codon optimised *Rhodobacter capsulatus* TAL sequence.
From left to right, N-terminus to C-terminus. Added sequences: 5' BamHI and 3' XhoI restriction enzyme binding sites, two stop codons (TAA) and a tobacco etch virus (TEV) protease cleavage site with a glycine-serine-glycine (GSG) linker sequence. Start codon removed. The protein will be expressed as an N-terminal His-TEV-linker fusion protein. Sequence has also been codon optimised with synonymous mutations to bias codons towards those preferred by the expression bacteria.

The pETDuet-1 vector is a plasmid designed for the co-expression of two genes as it contains two multiple cloning sites, however it was used here for the expression of the single TAL gene. The TAL gene was cloned into the pETDuet-1 vector (see Figure 5.13) to be expressed under the control of the bacteriophage T7 transcription and regulatory system, to be transformed into *E. coli* JM109(DE3) which contain the T7 RNA polymerase gene, for high level protein expression. The multiple cloning site used has a T7 promoter, lac operon and ribosome binding site for expression of the target gene. The T7 promoter can be acted upon

by T7 RNA polymerase to drive high level expression of the target gene. The lac operon (lacO) which is just downstream of the T7 promoter, can be repressed by the lacI protein (gene is part of the pETDuet-1 vector) which binds to the lacO to block transcription by T7 RNA polymerase, to stop leaky expression. Addition of IPTG causes dissociation of the lacI repressor on the lacO, allowing initiation of T7 RNA polymerase transcription and target gene expression. IPTG is therefore used to control the expression of the target gene within the JM109(DE3) bacteria.

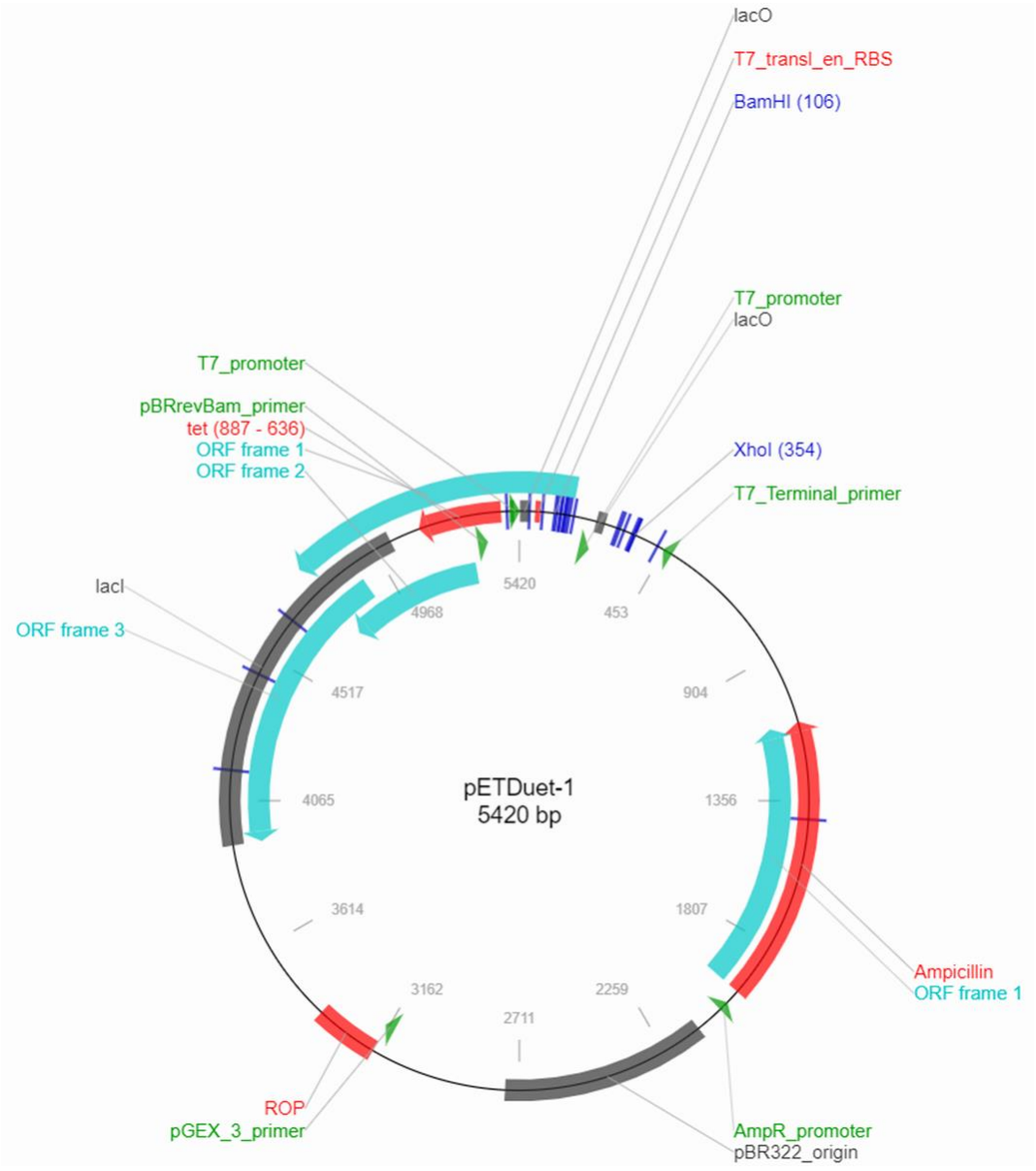

Figure 5.13. pETDuet-1 vector used for bacterial expression of TAL.
Key features are the presence of the T7 promotor, lac operon (lacO), the lacI gene, ampicillin resistance gene, the restriction enzyme binding sites BamHI and XhoI that are to be used to integrate the modified TAL sequence and the His·tag (83-100). Another 21 enzyme restriction sites are present but have not been labelled. ORF, open reading frame. ROP, regulator of origin of plasmid. Vector map from addgene (https://www.addgene.org/vector-database/2659/).

5.3.2.1.2 Preliminary *in vitro* experiment

The first experiment was conducted using the TAL enzyme supplied by The Protein Expression Facility, UoM. This TAL protein was supplied in 25 mM Tris-HCl (pH 7.5), 150 mM NaCl and 10% glycerol. Tyrosine (100 µmol/L) was incubated with 2, 0.2- and 0.02-mM TAL protein in 50 mM Tris-HCl, pH 8.5 at 37°C and at 2 mM in PBS over 24 hours, see Figure 5.14. Tyrosine (100 µmol/L) was fully degraded by the 2- and 0.2-mM TAL enzyme by 4 hours and 24 hours respectively, and was partially degraded by 0.02 mM TAL to approximately 80 µmol/L at 24 hours. Interestingly, 2 mM of TAL enzyme in PBS was not as efficient at degrading tyrosine as the same concentration of TAL in Tris-HCl buffer, reaching approximately 40 µmol/L by 24 hours in PBS. Having confirmed that this TAL enzyme from *R. capsulatus* was able to breakdown tyrosine, TAL was then expressed and purified in house.

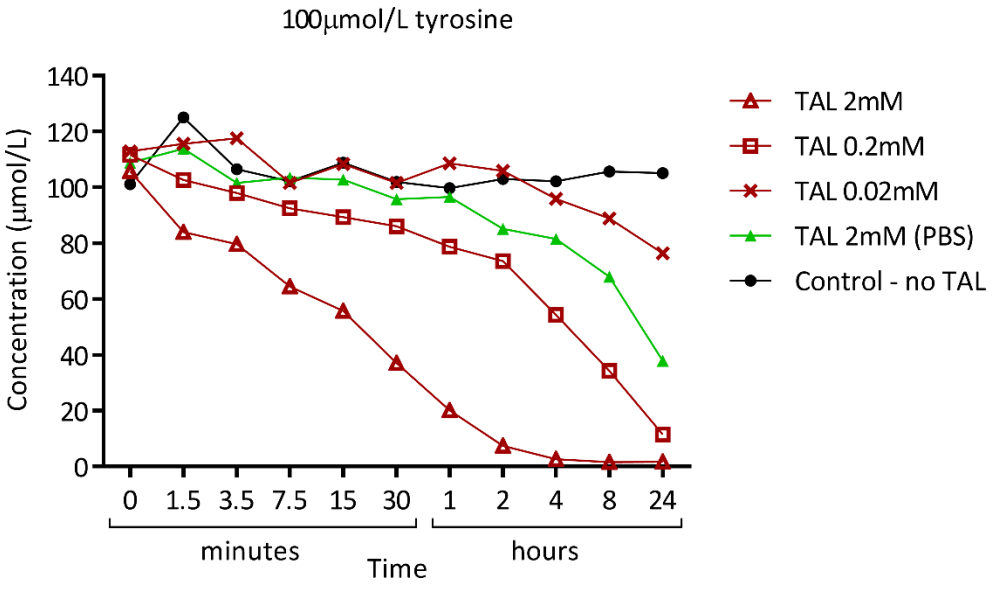

Figure 5.14. Preliminary assay of tyrosine degradation by TAL.
TAL enzyme was incubated with a starting tyrosine concentration of 100 µmol/L at 37°C at various concentrations; 2, 0.2 and 0.02 mM in 50 mM Tris-HCl and at 2 mM in PBS. The control contained no TAL enzyme. TAL, tyrosine ammonia lyase. Assay carried out by Dr Peter Wilson.

5.3.2.1.3 Expression and purification of TAL

In order to express the TAL enzyme in house, the pETDuet:Tal expression vector was obtained from the Protein Expression Facility (UoM, UK). Chemically competent JM109(DE3) bacteria were then transformed with the pETDuet:Tal vector. The procedure for transforming the bacteria and inducing the expression of TAL protein can be found in section 2.6.2.1. Once grown, the TAL protein was harvested and purified, see section 2.6.2.2 for details.

Samples from each step of the purification process were kept for analysis of TAL protein by SDS-PAGE gel stained with Coomassie Blue to visualise protein bands. The predicted molecular weight for the TAL protein is 55.6 kDa. With reference to Figure 5.15, the cell lysate contains all of the proteins expressed by the bacteria (including TAL), and then the soluble fraction contains only the proteins released into the supernatant after clarification. The soluble fraction contained the TAL protein as expected, which was then retained in the purification column with the Ni-NTA beads; the first flow through (FT) and subsequent 2 washes did not contain the TAL protein. The final elute (E) and desalted elute (DS) both contain only one protein band at the expected molecular weight expected for the TAL protein.

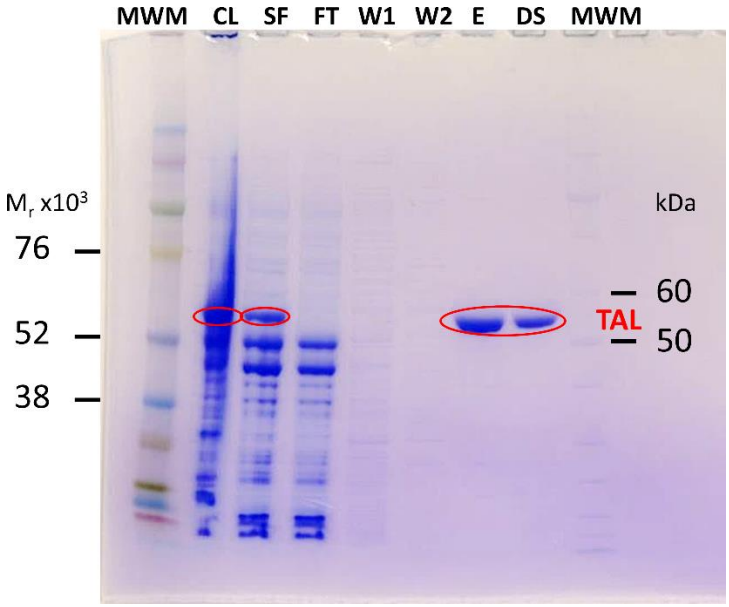

Figure 5.15. TAL purification stages.
6.5 µl samples from each step of the TAL purification procedure was analysed on 4-12% SDS PAGE gel, that was stained with Coomassie Blue. Two different molecular weight markers (MWM) were used: a full range Rainbow MWM on the left, a Novex Sharp unstained protein standard on the right. Abbreviations: CL, cell lysate; SF, soluble fraction; FT, flow through; W1 & W2, wash 1 & 2; E, elute; DS desalted fraction. TAL expression and purification and gel carried out by Dr Peter Wilson.

Three purifications of the TAL protein were carried out from the same culture that was split into 4 equal aliquots. The 1st TAL protein sample was purified according to the methods, using a frozen bacterial pellet re-suspended into lysis buffer as described in section 2.6.2.2. The 2nd TAL protein sample was purified in the same way as the 1st, with an increased sonication of the cell lysate from an amplitude of 6 microns to 24 microns in an attempt to release more TAL protein that was likely to be trapped within inclusion bodies. The 3rd TAL protein sample

was purified using a slightly different method to the 1st and 2nd; a lysozyme extraction was used instead of sonication (sonication is a harsh method of purification that could affect the enzyme's activity), to see if the method of purification affected the activity of TAL; see section 2.6.2.2 (purification of TAL, step 2a). Once lysed and clarified, the 3rd TAL was purified using the same methods as the 1st and 2nd.

In order to quantify the amount of TAL protein purified, a BCA protein assay kit and protocol was followed using colorimetric protein detection and quantification of the purple reaction product (see section 2.6.2.2.2). Briefly, albumin protein standards were used to generate and a standard curve of 562 nm absorbance against known protein concentration and the curve used to determine the concentration of the purified TAL protein. The estimated concentration of TAL protein obtained from each purification is shown in Table 5.2. The increased sonication amplitude during the bacterial cell lysis steps of the 2nd TAL purification increased the amount of TAL protein obtained compared to the 1st purification. Using the lysozyme extraction method resulted in 3.4- to 5-fold less TAL protein obtained from the 3rd TAL purification compared to the 1st and 2nd purifications respectively.

Table 5.2. Estimated concentration of TAL protein, quantified using a BCA protein assay kit.

Purified TAL	**Estimated protein concentration (mg/ml)**
1st TAL (lysis buffer extraction with sonication)	0.415
2nd TAL (lysis buffer extraction with increased sonication)	0.61
3rd TAL (lysozyme extraction, no sonication)	0.122
BCA assay carried out by Dr Peter Wilson.	

The insoluble fraction (cell pellet frozen after bacteria cell lysis) from the 1st TAL purification was tested for TAL activity as it was likely that some TAL was trapped within inclusion bodies. The cell pellet was re-suspended in 1 ml of elution buffer B which was the final buffer used to elute the TAL protein from the desalting column. 200 µl of this sample was used in a 1 ml reaction and referred to as insoluble fraction.

5.3.2.1.4 TAL *in vitro* experiments

The first *in vitro* TAL experiment was performed to test the tyrosine-degrading ability of the TAL enzyme expressed and purified in house. With reference to Figure 5.16, 2 mM TAL from

the 1st (lysis buffer/sonication) and 2nd (lysis buffer/increased sonication) purification, and 1 mM TAL from the 3rd purification (lysozyme/no sonication) were incubated with 100 µmol/L tyrosine in 25 mM Tris-HCl at pH 8.5 over 24 hours at 37°C. Activity of TAL within the insoluble fraction (200 µl used; 1 ml reaction volume) from the purification was also tested. All the TAL enzymes tested (1st – 3rd) were able to breakdown tyrosine; the 1st and 2nd TAL had broken all tyrosine down by 4 hours, with the 3rd breaking tyrosine down at a slower rate, with tyrosine broken down by 8 - 24 hours. The 3rd TAL enzyme however was at 1 mM instead of 2 mM due to the lower protein concentration obtained during the purification limiting the amount TAL protein, which was more dilute, that could be added to the 1 ml reaction volume. A comparison in activity is therefore difficult. At both 30 minutes and 1 hour, the 1st TAL had broken down 1.3-fold more tyrosine than the 3rd TAL and 1.2-fold more at 2 hours, suggesting that the 3rd TAL enzyme was more active than the 1st & 2nd (which were almost identical), as the fold-change was <2, which was the TAL concentration difference. The increased sonication amplitude of the 2nd TAL over the 1st TAL did not appear to affect the activity of the enzyme. The ability of the insoluble fraction to breakdown tyrosine confirmed that the insoluble fraction still contained active TAL enzyme, trapped within inclusion bodies (highly aggregated protein).

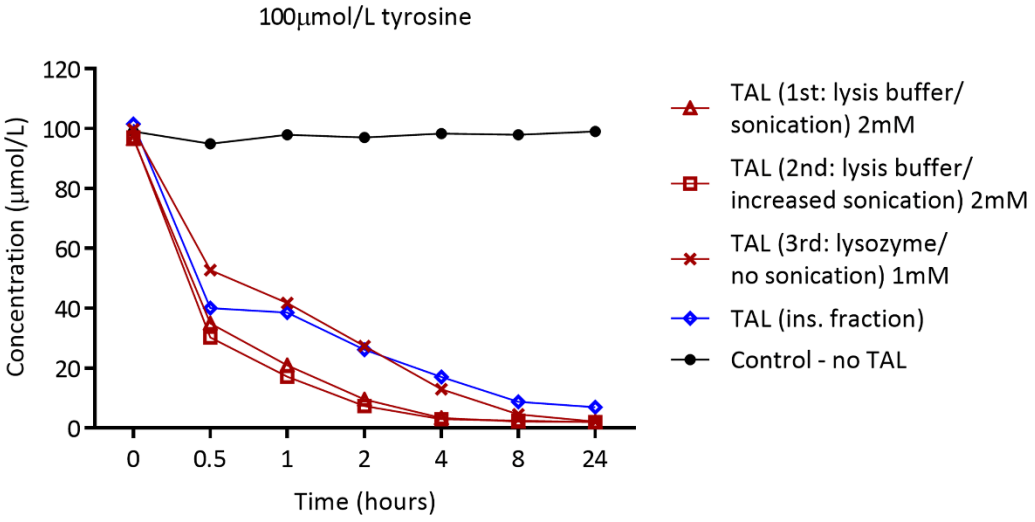

Figure 5.16. *In vitro* degradation of tyrosine by TAL.
2 mM of TAL enzyme from the 1st and 2nd purification, and 1 mM of the 3rd purification was incubated with 100 µmol/L tyrosine in 25 mM Tris-HCl (pH 8.5) over 24 hours at 37°C. TAL activity was also tested for the insoluble fraction from the purification. The control contained no TAL enzyme. TAL, tyrosine ammonia lyase. Assay carried out and samples collected by Dr Peter Wilson.

In order to test the activity of TAL at breaking down tyrosine at different pH's, the reaction mixture was made up using Tris-HCl at pH 1.5, 4.5 and 8.5 (8.5 was used previously), with tyrosine at 100 µmol/L. 2 mM TAL from the 2nd purification was used for this experiment, alongside the same insoluble fraction stock and volume used in Figure 5.16. With reference to Figure 5.17, neither TAL nor the insoluble fraction was able to breakdown tyrosine at pH 1.5 or 4.5. TAL at pH 8.5 was able to breakdown tyrosine by 4 hours, as was observed in the previous experiment.

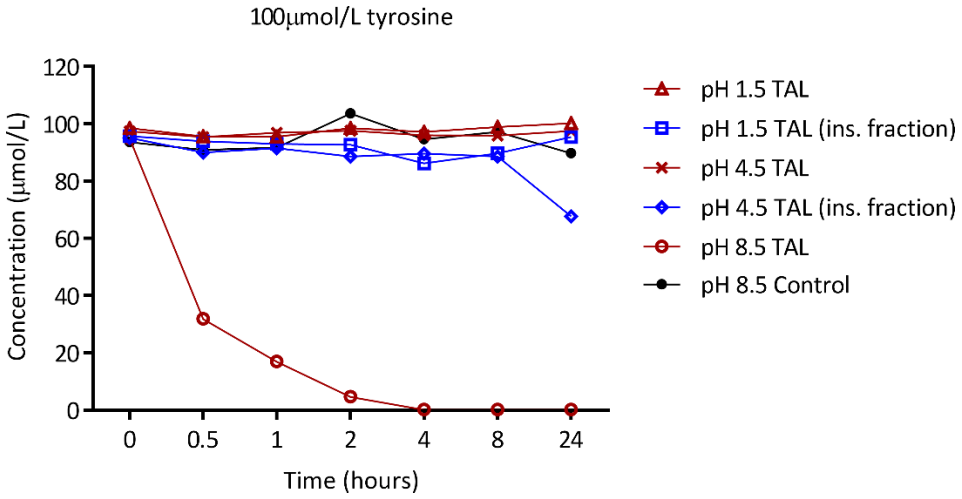

Figure 5.17. *In vitro* degradation of tyrosine by TAL at different pH's.
2 mM of TAL enzyme from the 2nd purification was incubated with 100 µmol/L tyrosine in 25 mM Tris-HCl over 24 hours at 37°C at pH 1.5, 4.5 and 8.5. The insoluble fraction (same stock and amount used in Figure 5.16), was tested in 25 mM Tris-HCl at pH 1.5 and 4.5. The control contained no TAL enzyme. TAL, tyrosine ammonia lyase. Assay carried out and samples collected by Dr Peter Wilson.

5.4 Discussion

The treatment of AKU with the HGA-lowering drug nitisinone has proven to be an effective treatment in AKU patients by lowering HGA [117]. However, data from clinical trial [52] and off-label prescription use at the NAC [53] clearly demonstrate the associated elevated tyrosine in patient's plasma. Although tolerated by many individuals, tyrosinaemia can cause eye and skin keratopathy in a minority of patients requiring a lower dose or cessation of nitisinone, or a strict low protein diet, to resolve symptoms. Low-dose nitisinone, ranging from 0.5-2 mg daily, has caused eye complications in 5 reported AKU patients to date [40,127,129,130].

Attempting to restrict tyrosine and phenylalanine intake from the diet, whilst still taking nitisinone to keep HGA low, is the most logical approach to combat elevated tyrosine. A protein restricted diet however proves very difficult to maintain and often causes

keratopathy to return when not adhered to [130]. Therefore, finding an alternative strategy to reduce dietary uptake of tyrosine and/or phenylalanine would allow nitisinone-treated patients to consume a normal protein diet. Before such strategies are implemented, the findings reported here showed that reducing dietary tyrosine/phenylalanine is effective at reducing tyrosine in AKU mice, with evidence that lowering protein intake in patients is also achievable, therefore establishing a proof-of-principle in targeting dietary tyrosine/phenylalanine in AKU patients who are on nitisinone.

Tyrosine threshold recommendations with nitisinone treatment, which are often arbitrary, vary in the literature. In HT-1 children <12 years, the recommended tyrosine level is 200-400 µmol/L, with concentrations after this age allowed to rise, with eye complications experienced >800 µmol/L [132]. Another HT-1 review of 22 centres treating patients aged 0-24 years found maximum acceptable tyrosine levels to be 200-800 µmol/L, with 400 µmol/L determined to be a safe and feasible target [145]. A report of an adult AKU patient who experienced eye keratopathy whilst receiving low-dose nitisinone (0.5-1.5 mg daily) suggests a target tyrosine of <600 µmol/L [129], whilst a more recent NAC publication suggests <500 µmol/L is acceptable [117]. NAC tyrosine thresholds are designed to fit a dietetic care plan that aims to reduce serum tyrosine in order to prevent symptomatic keratopathy, with systematic removal of dietary protein, whilst taking into account compliance difficulties experienced in patients.

5.4.1 Effect of nitisinone

It is clear from reported data in human patients, and the data presented here in mice, that nitisinone is very effective at inhibiting 4-HPPD and reducing circulating HGA. This metabolic block however causes upstream effects in the tyrosine metabolism pathway. In AKU mice treated with nitisinone here, plasma HGA was lowered, with significant elevations in plasma tyrosine, phenylalanine (although not to the extent of tyrosine), HPPA and HPLA. The most concerning change is the substantial increase in circulating tyrosine, due to ocular and skin keratopathy risks, in addition to concerns about neural cognition due to tyrosine being a precursor to some neurotransmitters. Although mice do not experience keratopathy of the eye for unknown reasons when rats and other laboratory animals experience corneal lesions with nitisinone-induced tyrosinaemia, the tyrosine measured in the eyes of mice on nitisinone (Figure 5.2) was clearly elevated compared to controls, agreeing with previous

published work on nitisinone-induced tyrosinaemia [120–122] in experimental animals, that shows the tyrosine elevation occurs not just in the plasma, but also the eye.

Lock et al. reported that tyrosine within the aqueous humour of mice treated with nitisinone was approximately 2,200 µmol/L, with a plasma level of approximately 1200 µmol/L [121]. Here, tyrosine within the whole eye homogenate of nitisinone-treated AKU mice was about 1,100 µmol/L with a plasma tyrosine of about 600 µmol/L. The relationship/fold-change between plasma and ocular tyrosine reported by Lock et al. is the same as reported here, with ocular tyrosine being 2-fold greater than that of the plasma. The concentrations here however may not truly represent the concentration of tyrosine in the eye, as matrix-matched calibrators were not used to quantitate the tyrosine in the eye (calibrators with a serum matrix were used, the samples were in a methanol/water matrix) which could affect the concentration obtained, in addition to homogenate being of the whole eye, rather than sampling the aqueous humour directly which is situated in the small anterior cavity within the anterior and posterior chambers of the eye between the iris and cornea. Ocular lesions are thought to occur due to a build-up of tyrosine within the eye, which reaches saturation in aqueous solutions at about 4,000 µmol/L at body temperature [295], where it then precipitates as needle-shaped tyrosine crystals that damage cell membranes [296]. In rats where corneal lesions are observed, ocular tyrosine increases to 3500-4000 µmol/L with nitisinone treatment [120], which is close to the reported solubility, and is much higher than the ocular tyrosine in mice with nitisinone treatment.

Although the main focus of elevated tyrosine is towards eye keratopathy and potential neurocognitive affects, it's not known how increased tyrosine in the plasma affects other tissues. Recent data from Khedr et al. investigated the distribution of tyrosine within nitisinone-treated AKU mice compared to untreated AKU and WT control mice, showing that tyrosine was increased in all the tissues investigated; 6.5-fold in bone from the femur, 7.8-fold in the brain, 8.8-fold in the heart, 7.4-fold in the kidney, 4.7-fold in the liver and 6.0-fold in the quadriceps muscle [297]. This has been described by the authors as "tyrosinosis" as elevated tyrosine is not limited to the circulation, but extended to tissues, and is likely to be elevated in all tissues. Additional experimental data was collected by Khedr et al. in human AKU patients and healthy volunteers, who were injected with isotopically-labelled tyrosine and phenylalanine; the tracer and tracee ratios demonstrated that tyrosine decay was almost halted with nitisinone treatment, with phenylalanine being unaffected, with the extracellular tyrosine pool estimated to be 5-fold higher in nitisinone-treated AKU patients, and the intracellular pool estimated to be 3-fold greater, than controls.

In addition to tyrosine elevation, substantial increases in both HPPA and HPLA have been observed in mice and humans. In the tyrosine tracer study in humans, HPLA was not detected in both AKU individuals and healthy controls in the absence of nitisinone; this suggests that the conversion of HPPA to HPLA does not usually occur in untreated AKU patients, but does occur with nitisinone treatment and the blocking of the tyrosine pathway [297]. Another recent paper has quantified the flux of tyrosine metabolites during nitisinone treatment in human AKU patients using SONIA-1 trial data, and also documents the significant increases in tyrosine, HPPA and HPLA, suggesting that these large increases reflect the tyrosine metabolite pool that would have been directed towards pigment formation in the absence of nitisinone [298]. These metabolite increases were also observed here in mice, however the effect of elevated HPPA or HPLA is unknown.

Further metabolomic analysis of urine and serum in both human AKU patients and AKU mice has also revealed other changes in the metabolome that occur with nitisinone treatment; these significantly altered metabolites indicate alterations to tyrosine, tryptophan, purine and TCA cycle metabolism [218,299]. Metabolomic data investigating both urine and serum in humans and mice also demonstrates many other metabolite differences in the untreated-AKU metabolic state and also with nitisinone treatment; these include the presence of HGA biotransformation products that exist in AKU, which are then reduced with nitisinone-treatment, in addition to changes in tyrosine, purine and TCA cycle metabolites in the AKU disease state [231]. It is clear from these evaluations that many changes in tyrosine metabolism occur not only with nitisinone, but also in the AKU metabolic state, however the effects of these changes remain unknown.

5.4.2 Tyrosine/phenylalanine dietary restriction

The tyrosine/phenylalanine free diet study here in mice (Figure 5.3) clearly showed a dose-responsive reduction in plasma tyrosine, with all groups reaching <400 µmol/L, which is below the threshold used by the NAC in human patients. The least restricted group (5 mg/ml phenylalanine) reduced tyrosine to 389 µmol/L at 3 days, achieved with approximately 68% phenylalanine/no tyrosine. Furthermore, in human AKU patients observed at the NAC, it was shown that human patients can reduce serum tyrosine with dietary intervention after advice from a specialist dietician (Figure 5.9). Tyrosine was significantly lowered either by a low protein diet alone or in combination with prescribed tyrosine/phenylalanine free amino acid supplementation. Although only 4 of these 10 patients achieved tyrosine <700 µmol/L,

tyrosine was greatly reduced in some patients, notably from 1,084 µmol/L to 762 µmol/L, and from 1,217 µmol/L to 859 µmol/L. Of the 4 patients that reduced tyrosine below 700 µmol/L, only 1 patient achieved this with dietary advice alone; the other 3 patients used tyrosine/phenylalanine-free amino acid supplementation. Prior to nitisinone, most adult AKU patients will have consumed a normal protein diet throughout their life, therefore adaption to dietary changes can be difficult, especially in the absence of tyrosine-related keratopathy where no benefit is perceived.

The NAC patient data was not collected as a controlled trial, but as an observational study where patients are only advised to restrict their protein intake, therefore strict monitoring of compliance and protein intake was not carried out. After specialist advice, patients were responsible for restricting dietary protein in their daily lives, with guidance from the dietician if needed. Progress with dietary compliance is a long-term iterative process, since achieving long-term, sustained behaviour change in adults is a recognised national dilemma. Dietetic intervention is therefore on going in NAC patients. Compliance is the most likely reason that only 1/10 NAC patients achieved <500 µmol/L tyrosine and is why mice were used for the restriction experiments reported here. The diets of mice are easy to control, in addition to eliminating other confounding factors such as lifestyle, exercise, mobility and disease severity differences. The mouse data provides evidence that dietary restriction of tyrosine/phenylalanine can effectively reduce nitisinone-induced tyrosinaemia, providing the rationale to carry out a controlled trial in human AKU patients, where lower tyrosine levels than those observed here would be expected.

In mice, the dose response observed due to phenylalanine supplementation, in the absence of tyrosine (Figure 5.5), suggests that tyrosine derived from phenylalanine is important to target. However, phenylalanine-only restriction did not effectively lower tyrosine, even in the completely phenylalanine free group, suggesting that targeting removal of dietary phenylalanine alone is ineffective at reducing nitisinone-induced tyrosinaemia. This is an important consideration as emerging phenylalanine-lowering strategies for the metabolic disease PKU may have been beneficial for nitisinone-induced tyrosinaemia if phenylalanine restriction alone had proven effective. Such strategies include enzymatic phenylalanine degradation by exogenous phenylalanine ammonia lyase enzyme (detailed in section 1.2.6.4.3), diets supplemented with naturally occurring glycomacropeptide (GMP) protein that is naturally low in phenylalanine instead of synthetic amino acid foods, and genetically modified probiotics that target phenylalanine-degradation in the intestine [300,301].

Moreover, due to phenylalanine being an essential amino acid, its restriction alone could lead to inadequate protein turnover, with the balance of catabolism/anabolism disrupted, causing a loss of lean mass [302]. Although not significantly different to the control group in the phenylalanine-only restriction study, there was a significant body weight reduction in the phenylalanine free and 0.625 mg/ml groups compared to the 2.5 mg/ml group (Figure 5.5) at 7 days. This weight loss was seen in the presence of tyrosine, suggesting that phenylalanine restriction could lead to catabolism, therefore targeting tyrosine would be more desirable. At 14 days of restriction, no significant weight changes were seen in Figure 5.3 in which tyrosine was absent and phenylalanine was partially present. The presence of nitisinone however did appear to affect weight of the mice; the comparison of weight change (Figure 5.7) between the tyrosine and phenylalanine free groups from Figure 5.4 and Figure 5.5 at 7 days showed that the untreated mice lost significantly more weight than the nitisinone-treated group. This is most likely due to the increase in the tyrosine pool in the circulation and tissues, as described above by Khedr et al. [297], perhaps protecting mice from muscle catabolism as it would take longer to deplete the highly elevated tyrosine pool than it would in mice that do not have tyrosinaemia.

It is essential to balance lowering protein intake in order to lower circulating tyrosine, with maintaining a healthy weight and muscle mass, since catabolism itself provides residual tyrosine. A recent publication documenting the nutritional status of AKU patients attending the NAC at their baseline visit suggested that AKU patients, who have a lower muscle mass and higher body fat composition, are experiencing a protein/energy dilemma, with a reduced protein intake that is consistently at the minimum end of the reference range, that is not compensated for by fat, carbohydrates or other food groups, leading to an energy deficit that can cause catabolism to occur [293]. The report also highlighted the complex nature of dietary intervention in AKU patients, who have decreased mobility as the disease progresses, where reduced muscle functionality leads to muscle atrophy, and therefore a further reduced basal metabolic rate, combined with periods of high metabolic demand such as joint replacement surgery that alters physical activity and impacts on muscle and fat reserves. During yearly routine NAC visits, anthropometric data such as such as grip, mid-upper arm circumference and bioimpedance data such as lean mass and fat mass is collected to provide sequential evidence of body composition trends to minimise risk of catabolism, and are considered during patient monitoring. These parameters were not investigated in the AKU patients presented in the observational study presented here, as less than half of the tyrosine concentrations were measured at a routine NAC visit where such anthropometric data is

collected. These parameters are however worthy of investigation in both mice and humans (this data is already being collected at the NAC) in future studies. Attempts were made to record food and water intake in a subset of mice subjected to dietary restriction, using the experimental conditions of the first tyrosine/phenylalanine restriction study. If dietary restriction had caused the mice to become deficient in tyrosine and/or phenylalanine, it is possible that they could reach a catabolic state where muscle breakdown releases tyrosine/phenylalanine. At the same time, food intake may also have increased in an attempt to consume more dietary protein and amino acids. In the studies here, increased food intake of the restricted diets would not increase the pool of the potentially deficient tyrosine and/or phenylalanine amino acids, but instead would increase calorie intake. Increased calorie intake above the calorific needs of the mouse would increase fat mass, potentially contributing to an overall increase in bodyweight, possibly concealing muscle catabolism. The cage system that was available to use for studying food/water intake however was not suitable, despite having an accuracy of 0.02 g for food intake and 0.01 g for water intake. The diet was crumbly, the water bottles dripped water to such an extent that the drip tray overflowed and the behaviour of the mice regarding the movement of food into the cage prevented adequate recordings of intake, and the results were therefore dismissed. In the future, factors such as lean mass and grip strength to assess muscle function could be investigated to indicate more clearly the anabolic/catabolic state of the mice.

In addition to decreased tyrosine, other metabolic improvements were seen with dietary restriction in mice. HGA, which is lowered with nitisinone treatment, was then significantly lowered in the restricted groups compared to the control in the tyrosine/phenylalanine free studies. Both HPPA and HPLA, which were increased with nitisinone, were also significantly reduced compared to the control with restriction. Although it is not known what effect elevated HPPA and HPLA has, reducing them back towards normal physiological levels would be desirable. Although only elevating 1.5-fold in mice with nitisinone, phenylalanine in mice was significantly reduced after 3 days in the first tyrosine/phenylalanine restriction study compared to the controls, but this was not maintained to 14 days suggesting normal phenylalanine levels with no weight loss observed. In human NAC patients, phenylalanine levels were within the normal reference range at all-time points during the observation period. Overall, it would appear that reducing tyrosine in nitisinone-induced tyrosinaemia also reduces other upstream, off-target metabolic effects of nitisinone such as reducing HPPA and HPLA, therefore it's very likely that reducing tyrosine may also normalise other metabolic affects that have been identified by metabolomics analysis as described above [218,231,299].

Metabolomic evaluation of the plasma samples collected in the dietary restriction studies here was not performed, but would have been beneficial and should be considered in future studies.

5.4.3 Tyrosine ammonia lyase

Tyrosine degradation via the non-mammalian TAL enzyme was investigated here *in vitro*. This enzyme has the potential to be applied to AKU patients, in addition to HT-1 patients, with elevated tyrosine as a consequence of nitisinone treatment. The dietary studies in nitisinone-treated AKU mice have shown the proof-of-concept that reducing the uptake of dietary tyrosine/phenylalanine can reduce plasma tyrosine levels. TAL could be taken orally after or with a normal protein meal, in order to deplete tyrosine in the gastrointestinal tract, by converting it to coumaric acid, leaving less tyrosine available for absorption into the circulation.

This scenario of tyrosine degradation by an exogenous enzyme however is not a new concept. Phenylalanine breakdown by the administration of PAL, another ammonia lyase enzyme, has been greatly studied as an enzyme substitution therapy for PKU. A modified form of PAL has recently been approved for the treatment of PKU by the Food and Drug Administration and the European Medicine's Agency. The research conducted with phenylalanine/PAL, described in section 1.2.6.4.3, highlights many challenges and issues which should be considered before developing a TAL therapeutic, due to the synonymous nature of tyrosine/TAL, and its application to metabolic disease. Although the licensed form of PAL is an injectable form (subcutaneous administration), which may not be considered the most suitable form or the desirable form that a TAL enzyme would take for nitisinone-treated AKU patients, aspects of the journey from the discovery of PAL to its use in human clinical trials will be applicable to the potential development of the TAL enzyme, which will undoubtedly experience similar challenges.

Presented here was a series of *in vitro* experiments that show the ability of the *Rhodobacter capsulatus* TAL (RcTAL) enzyme to breakdown tyrosine. Due to TAL not being available to buy commercially, it was necessary to either request a custom synthesis or express a TAL enzyme in the laboratory. In order to do this, a gene sequence for TAL was required. After a literature search, it was decided that a TAL sequence from *Rhodobacter capsulatus*, a purple photosynthetic bacterium, would be used. Kyndt et al. expressed the RcTAL enzyme using an *E. coli* expression system [154], and calculated the catalytic efficiency with tyrosine and

phenylalanine, and compared these values with already reported catalytic efficiencies of two other PAL/TAL enzymes expressed in *E. coli* from *Zea mays* (maize) [303] and *Petroselinum crispum* (parsley) [304]. The RcTAL enzyme had a 150-fold greater catalytic efficiency with tyrosine as a substrate than phenylalanine. The enzyme from *Z. mays* had similar reported catalytic efficiency with tyrosine and phenylalanine as substrates, however this was 375-fold lower than RcTAL with tyrosine. The enzyme from *P. crispum* exhibited very low catalytic efficiency with tyrosine as a substrate and was much more efficient as a PAL enzyme degrading phenylalanine. An enzyme with more TAL activity over PAL activity was desirable. A later publication by Xue et al. in 2007 compared the kinetic properties of two TAL enzymes expressed in their laboratory from *Rhodobacter sphaeroides* (a purple photosynthetic bacterium) and *R. capsulatus* [294], which were the only reported PAL/TAL enzymes that prefer tyrosine as a substrate than phenylalanine. With tyrosine as a substrate, RcTAL had a greater catalytic efficiency compared with *R. sphaeroides* and was therefore chosen for the work here.

The expression and purification of the RcTAL enzyme in house however was only the first, and relatively minor, challenge to address in the application of TAL to nitisinone-induced tyrosinaemia as an enzyme therapy. Our capabilities and resources in the further development of TAL was limited, with more sophisticated techniques needed to develop it further.

A TAL enzyme therapy would ideally be oral, as nitisinone is currently the best treatment option for AKU and would be a lifelong therapy until curative therapies such as enzyme/gene therapy are successful in restoring long-term enzyme activity. Injectable therapeutics are not very patient friendly, especially if daily administration is required; the PAL/pegvaliase administration in the final phase III PKU clinical trial was administered daily via subcutaneous injection. In addition to the practicality of injecting a therapeutic daily, repeat injection of a non-mammalian protein will almost certainly cause an immune response [305], as was described with the injection of PAL into PKU animals and patients, leading to neutralisation of the therapeutic effect [166,181]. Even with PEGylation, which is designed to decrease immunogenicity and increase the half-life by preventing rapid degradation of a therapeutic protein [306], antibodies to the PEGylated PAL protein were still produced in the PKU clinical trials [190,191], with adverse events such as injection site reactions, hypersensitivity and even anaphylaxis reported. The FDA/EMA approved form of PAL/pegvaliase (PALYNZIQ®) that is administered subcutaneously has allergy warnings including severe anaphylaxis (https://www.biomarin.com/products/palynziq/ [accessed 05.02.2020]).

The National PKU Alliance conducted a survey in 2016 to assess current health status and interest in new treatments, with PKU individuals reporting a desire for new treatments that reduce their blood phenylalanine levels whilst allowing intake of natural protein to increase, with reduced or discontinued intake of medical foods, with a preference for oral administration, and reported a general dislike for injectable therapeutics [307]. In addition to PKU, other patient groups also report a preference for oral therapeutics over injectable/intravenous methods, such as in type II diabetes [308], rheumatoid arthritis [309] and cancer [310,311]. Injecting a TAL enzyme daily would not have been an attractive therapy for reducing/preventing nitisinone-induced tyrosinaemia in the absence of a protein restricted diet in AKU patients and was therefore not considered further here. Although not a preferred route of administration, PKU patients in the pegvaliase trials reportedly consumed more natural protein in their diets and also consumed less medical food [191], which would be a desirable outcome with the application of a TAL enzyme to nitisinone-treated AKU patients. The efficacy of PAL/pegvaliase on phenylalanine levels however was not assessed in the absence of dietary management.

Development of TAL for oral administration in nitisinone-treated AKU patients would therefore be the target of future research; oral PAL administration for the phenylalanine degradation in PKU was only partially explored. As highlighted early on in PAL research, the main challenge of orally dosing TAL would be in preventing proteolytic degradation of the protein by digestive enzymes [161,162]. The first proteolytic attack for an orally administered protein would be from pepsin released by the stomach, an endopeptidase which preferentially prefers hydrolysing links with aromatic amino acids, responsible for 15% protein digestion [312]. Once the contents of the stomach is released into the duodenum, it mixes with bile and pancreatic secretions, with the latter being rich in digestive enzymes [313]. The main proteolytic pancreatic enzymes are trypsin, chymotrypsin, lipase, carboxypeptidase A and B and elastase. Approximately 50% ingested protein is digested in the duodenum, hydrolysed into amino acids and peptides 2-4 amino acids in length [314,315]. Most amino acids are then absorbed by the duodenum, jejunum and proximal ileum therefore TAL would need to not only survive proteolytic digestion, but also be active immediately in the intestine to prevent tyrosine absorption into the bloodstream via the enterocytes of the intestinal epithelium. The enterocytes also have peptidases situated in the brush border that are present to break down di- and tri-peptides, although this can also occur intracellularly, as di- and tri-peptides are taken up faster than free amino acids.

Following successful protease protection, TAL enzyme activity in the gastrointestinal environment would then be crucial for efficient tyrosine breakdown. Due to the secretion of acidic gastric fluid, the pH of the stomach in healthy individuals in a fasting state is approximately 1.0-2.5, increasing to 6.6 in the jejunum and 7.4 in the ileum [316]. The acidic pH of the stomach may be an issue for the TAL enzyme, which was shown here to be inactive at pH 1.5 and pH 4.5 *in vitro*. The insoluble fraction containing TAL within un-lysed *E. coli* bacteria also showed no activity at pH 1.5 and 4.5. A PAL enzyme was previously shown to retain activity at pH 8.5 after a 10 minute exposure to a broad pH range of 4-12 *in vitro*, with the authors suggesting that the enzyme may have enough pH tolerance to remain active after transit through the stomach [185]. The TAL enzyme here was tested separately, and not sequentially at low pH followed by pH 8.5, therefore it's not known if the enzyme was just inactive at lower pH's with further activity possible at pH 8.5, or denatured and permanently inactivated [317]. A TAL enzyme however would potentially be given orally with/after a meal, during which the pH of the stomach contents has been shown to increase from fasting levels of pH 1.0-1.5 to pH 5-7, taking up to 3 hours to return to pre-meal levels in humans [318]. It was shown that gastric pH remains high, decreasing at a slow rate until 50-60% of the contents has emptied. This study also found that a liquid meal resulted in a pH of 5.5 at 50% gastric emptying, and pH 4.6 for a solid meal. Consuming TAL with food may therefore offer some protection due to the rise in gastric pH. Once in the duodenum, the acidic gastric contents is mixed with pancreatic juice that is highly alkaline at pH 8.0-9.5 with a high bicarbonate content [313]. The pancreatic and intestinal digestive enzymes require a neutral or slightly alkaline pH to function therefore the acidity of the stomach contents must be neutralised. The pH within the duodenum and intestine (6.6 in the jejunum as mentioned above in the fasting state) is therefore likely to be favourable towards the alkaline optimum of TAL, with RcTAL shown to be active at pH 8.5 here *in vitro*, with further testing at more pH levels with decimal increments needed to assess the pH optimum further. The optimum pH has been reported for a few PAL/TAL enzymes, with optimum pH's of 8.0-8.5 in *Zea mays* TAL [303], 8.5-9.0 in *Rhodobacter spaeroides* TAL [150] and 8.0-9.0 in *Rhodotorula glutinis* PAL [174].

In vivo TAL experiments with nitisinone-treated AKU mice were not carried out in this thesis, with more *in vitro* work required before pursuing mouse studies, investigating factors such as catalytic efficiency and survival in acidic and protease-rich environments, with modifications/protection techniques likely needed to improve these characteristics. A few protection strategies were investigated in PAL in the literature. The retention of PAL within *E. coli* was shown to offer protease protection *in vitro* and *in vivo* in PKU mice [180]. The

insoluble fraction of the TAL protein expression and purification was tested here *in vitro*, and was shown to breakdown tyrosine with the standard assay conditions at pH 8.5, but did not breakdown tyrosine at pH 4.5. Whether or not TAL within the insoluble fraction or the expression *E. coli* would preserve activity after transit through the stomach is unknown. The effect of proteases on the TAL expressed here was not investigated. An online tool however can be used to predict potential cleavage sites by proteases or chemicals (ExPASy PeptideCutter: https://web.expasy.org/peptide_cutter/). For the RcTAL amino acid sequence, the main digestive proteases are predicted to cleave RcTAL in numerous positions, with pepsin at pH 1.3 predicted to cleave at 111 positions, pepsin at pH >2 at 123 positions, chymotrypsin at 118 positions and trypsin at 42 positions, see Appendix section 8.2, Table 8.1 for all results. The likelihood of TAL being cleaved by proteases is therefore very high. Protease inhibitors, as used by Sarkissian et al. with PAL [180], could be used in conjunction with TAL, however it would be more ideal to find strategies that improve protease resistance without affecting normal digestion of food which could affect nutrition, in addition to the role that proteases play in freeing tyrosine from protein peptides, which is needed in order for TAL to metabolise tyrosine. More sophisticated methods could be used to introduce protease resistance, such as mutagenesis of protease cleavage sites in the TAL sequence, as was investigated in RtPAL, where mutating primary trypsin and chymotrypsin cleavage sites lead to intact PAL protein after incubation with proteases [181]. Encapsulating the enzyme to protect it from proteases/pH environment is another strategy that could be used. The early PAL work encapsulated the PAL enzyme in a semi-permeable gel capsule [160] and then later PAL was immobilised into semi-permeable "artificial cells" designed to allow the passage of small molecules such as amino acids, but protect the contents from enzymes [172]. Despite immobilised PAL not being as active as the free form, it was still able to reduce phenylalanine significantly when dosed orally in experimental HPA animals, but the effect was not reproduced in PKU mice [177].

The encapsulation of TAL would need to provide protection in the stomach, but then allow either tyrosine entry and subsequent degradation within the capsule or the release of the enzyme into the intestinal environment for tyrosine degradation. Many sophisticated techniques now exist and are researched intensively for the gastric protection of proteins for oral administration. Enzyme replacement therapies are used for diseases with lack of intestinal enzymes, such as the lack of lactase in lactose intolerance and lack of pancreatic enzymes such as proteases, lipase and amylase in exocrine pancreatic deficiency. Delivery of these absent enzymes requires gastric protection followed by enzyme activity in the

intestine. For example, the incorporation of lactase enzyme into a hydrogel, made from food-grade materials, co-loaded with a buffer was shown to protect the acid-sensitive lactase enzyme from acid deactivation after exposure to gastric conditions *in vitro*, with only a small shift in pH from 7.2 to 6.6 within the hydrogel [319]. Other recent encapsulation techniques for lactase have included microcapsules formed with gelatin/gum arabic [320], spray congealed lipid micro-particles [321], polysaccharide gel beads [322] and aqueous gelatin/maltodextrin microgels [323]. A review in 2010 reported that pancreatic enzyme replacement preparations available from pharmaceutical companies are usually enteric-coated capsules containing mini-microspheres, pellets or micro-tables <2mm in size, designed to mix with gastric contents, coated with pH-sensitive and acid-resistant polymers that release the contents at pH 5.0-5.5 to prevent acid denaturation of the enzyme in the stomach [324].

These approaches for the gastric protection of other intestinal enzymes would likely be applicable to TAL. A collaborative effort would undoubtedly be needed in order to identify the most suitable method of encapsulation followed by testing in an animal model and then human patients. A review by McClements in 2018 highlighted the range of food grade colloidal-systems (the even distribution of particles within a solution) that can be designed to encapsulate, retain, protect and deliver bioactive proteins to the intestine, that includes microemulsions, emulsions, nanoemulsions, solid lipid nanoparticle, liposomes and microgels [325]. The review also highlights the complex nature of protein encapsulation, with the need to consider factors regarding protein characteristics such as molecular weight, conformation, electrical properties, polarity, solubility and stability; particle characteristics such as composition, size, shape, loading of protein, retention/release properties; and end product requirements such as appearance, product form such as small beverage, gummy-type product or solid tablet, dose, storage and ingredient selection.

In addition to the protection of TAL from proteases and low pH, maximising catalytic efficiency would also be desirable. TAL was shown to degrade tyrosine *in vitro* here, however its catalytic efficiency was not investigated, and it is not known how much of the enzyme would need to be ingested to metabolise a sufficient amount of tyrosine to prevent tyrosinaemia. A more efficient enzyme would require less protein to be incorporated into a therapeutic formulation, which ideally needs to be small. Once the most suitable TAL enzyme has been selected, genetic/protein-engineering technology could then be used to alter the amino acid sequence to improve catalytic efficiency, in addition to other features such as protease resistance, pH stability and solubility. Due to the enormous amount of different sequences that could be created by mutagenesis, it can be necessary to identify 'hotspots'

within an enzyme where mutations are likely to be beneficial using high-throughput screening, followed by individual amino acid optimization [326]. Directed evolution of enzymes is one of the most powerful techniques in protein engineering, and involves repeated rounds of random mutagenesis of the gene of interest, expression of the mutated protein and screening or selection of desirable properties [327]. Further to this, researchers have now begun to use models of protein sequence-function relationships combined with multivariate statistical analysis to guide the evolutionary process. For example, a company called Codexis with expertise in protein engineering have developed an algorithm to assign mutations to be either beneficial, neutral or deleterious on enzyme function before being incorporated into the sequence [328,329].

Watt et al. in 2006 identified a single active site residue responsible for substrate selection in PALs/TALs; replacing His89 with Phe in TAL completely switches the substrate specificity from tyrosine to phenylalanine, converting it to an active PAL [150]. A corresponding mutation in PAL causes the enzyme to lose phenylalanine specificity and gain tyrosine specificity. Not only could TAL be engineered to have a greater substrate specificity towards tyrosine, it could also be engineered to have phenylalanine activity, or a combination of both. The dietary restriction studies here in mice demonstrated that phenylalanine restriction alone would not be effective at reducing nitisinone-induced tyrosinaemia, therefore an enzyme with just PAL activity would not be useful. A TAL enzyme with phenylalanine activity could be beneficial, as the dietary studies showed that phenylalanine reduction with no tyrosine elicited a dose-responsive reduction in plasma tyrosine. The TAL enzyme expressed here was not tested against phenylalanine *in vitro*, and should be included in future assays. Whether a specific TAL or a combined TAL/PAL approach would be better for reducing tyrosinaemia would need further investigation.

The development of TAL clearly has a long way to go in order to be a therapeutic for nitisinone-induced tyrosinaemia in AKU patients. The safety of a new therapy is also crucial to assess. Coumaric acid, produced by TAL deaminating tyrosine, would not be expected to cause adverse effects as it is already consumed naturally in the diet in many fruits, vegetables, cereals and red wines, and has been shown to be antioxidant [330,331], antimicrobial [332] anti-inflammatory and immunosuppressive [333]. The antioxidant and anti-inflammatory properties could be beneficial for the osteoarthropathy manifestations of AKU, with oxidative stress recently shown to occur in an AKU cell model [334]. Ammonia production is also a potential negative affect of TAL. No side effects however were noted with the application of PAL in PKU which also forms ammonia as a by-product. Ammonia is naturally generated in

the body from amino acids obtained from dietary protein and catabolism of glutamine, in addition to other reactions, with around 1000 mmol produced a day in adult humans [335,336]. Due to the high toxicity of ammonia, mechanisms have evolved such as the urea cycle that are designed to metabolise and clear excess ammonia, therefore it's likely that any ammonia produced by TAL would be cleared efficiently.

5.4.4 Future of nitisinone-induced tyrosinaemia in AKU

Nitisinone is a lifelong treatment for AKU and is associated with hyper-tyrosinaemia. Removal of tyrosine/phenylalanine, but not phenylalanine alone, from the diet of mice is effective at reducing circulating tyrosine. Protein restriction coupled with tyrosine/phenylalanine-free amino acid supplementation was able to reduce tyrosine levels in patients observed at the NAC, although these reductions were greater in mice, most likely owing to patient compliance. A controlled dietary restriction trial in AKU patients would likely see results similar to the mouse data shown here. The mouse dietary restriction data suggests that strategies reducing tyrosine uptake from the intestine, such as degradation of tyrosine by an exogenous enzyme or a tyrosine-specific binder that prevents uptake into the circulation, that allow a normal protein diet to be consumed, could be investigated not only for nitisinone-treated AKU patients, but also for nitisinone-treated HT-1 patients. Ideally, a strategy to reduce nitisinone-induced tyrosinaemia would be an oral therapy since other routes such as injectable or intravenous administration would not be desirable or patient friendly. The potential application of tyrosine ammonia lyase could be a promising oral tyrosine-lowering therapy, but needs further investigation and collaborative effort.

6 General conclusion

Over 100 years on from the identification of AKU as the world's first described genetic disease, no cure for this ultra-rare condition exists. The low incidence and relatively normal lifespan of AKU sufferers perhaps drew away the attention of the scientific and research community. It was not until the 1990's that the *HGD* gene was identified and cloned, the first human mutations were described and an AKU mouse model discovered as a result of an ENU mutagenesis programme. In recent years, our knowledge of AKU pathophysiology has greatly increased with advancements in our understanding of disease pathology and progression, genetic characterisation of mutations and the introduction of nitisinone as a disease-modifying therapy. The success of nitisinone-treatment in AKU was built upon pre-clinical studies using the ENU BALB/c *Hgd*$^{-/-}$ AKU mouse model, which was able to show not only the progression of initial pigmentation within individual chondrocytes of articular cartilage, but also demonstrated the ability of nitisinone to lower HGA and prevent/halt ochronosis. Here in this thesis, a new mouse model of AKU was generated and phenotyped, providing some new information and experimental findings that would not have been possible in the existing ENU AKU model.

Although both the newer targeted *Hgd tm1a -/-* and the ENU mutagenesis BALB/c *Hgd*$^{-/-}$ AKU models can continue to be used for future research as the metabolic and ochronotic phenotypes were comparable, the knockout-first model is considered superior as it is specifically targeted to the *Hgd* gene, it has an endogenous *LacZ* reporter gene that can be used to localise *Hgd* gene expression and can be manipulated to obtain the conditional *Hgd tm1d* allele to conduct both tissue specific and inducible *Hgd* deletion.

Despite the advancement in our knowledge of AKU and the introduction of a pharmacological therapy, the process of ochronotic pigmentation still remains somewhat of a mystery. The composition of ochronotic pigment and the mechanism of deposition is still unknown. The AKU research community need to continue to explore ochronotic pathophysiology, even with the introduction of nitisinone, in order to understand more about the damage and processes involved, as many patients will already have a level of ochronosis that could one day be reversed, cleared or prevented by other means. The phenotyping of the new targeted *Hgd tm1a -/-* AKU mouse has provided the most thorough evaluation of tissue ochronosis in mice to date, showing that across a variety of musculoskeletal and other tissues that pigmentation is present only within calcified cartilage in mice, and may be accelerated in areas of greater physiological stress/load. AKU mouse models are likely to play a role in future ochronosis research, however they are limited to the early stages of human ochronotic pigment deposition. This *Hgd tm1a -/-* AKU mouse model, along with heterozygous *Hgd tm1a* mice,

has also provided in-depth metabolic phenotyping that includes both urine and plasma HGA and other tyrosine pathway metabolites that had not all previously been reported in AKU mice, with the *tm1a* model also being used by others for untargeted metabolomic profiling experiments extending beyond the tyrosine pathway, investigating nitisinone and the AKU disease state on the wider metabolome for example.

Nitisinone has proven to be an effective drug therapy for human AKU patients throughout the DevelopAKUre trials and its use at the NAC, however like many other drugs, it is not a perfect therapy. As a consequence of the metabolic block that nitisinone introduces to the tyrosine metabolic pathway, AKU patients treated with nitisinone are required to restrict dietary protein intake in order to lower circulating tyrosine levels. Although most, if not all, patients would trade the debilitating manifestations of AKU osteoarthropathy for nitisinone with a restricted protein diet, most of these adult AKU patients find it difficult to adhere to a restricted diet. The impact of finding a strategy to combat nitisinone-induced tyrosinaemia will not only allow adult patients to consume a normal diet without potentially damaging keratopathy, but could allow nitisinone administration to children by removing the risk of neurocognitive deficits that could be associated with increased tyrosine. The dietary restriction work presented here demonstrates the feasibility of targeting removal of dietary tyrosine/phenylalanine via an oral therapeutic that would prevent intestinal tyrosine absorption, whilst demonstrating the ineffectiveness of phenylalanine-only dietary restriction. Using an exogenous enzyme such as TAL was explored *in vitro* and is deemed plausible, with further investigation and collaborative effort required for successful application to AKU, and potentially HT-1 patients, treated with nitisinone.

Currently, nitisinone is the only disease-modifying treatment option available for AKU. Single gene diseases however have the possibility of being cured in the future by gene therapy. With the continuous development and advancement in molecular biology technology and knowledge, gene therapy may soon no longer be a concept, but a reality. The new targeted and conditional AKU mouse model was used here to determine the location and level of *Hgd* mRNA required to rescue AKU. In adult mice, *Hgd* expression has been precisely localised to the cytoplasm of hepatocytes and the cytoplasm of proximal convoluted tubule cells in the kidney cortex, in addition to low level expression in developing male germ cells located within the testis and epididymis, all confirmed with mRNA expression data. Initiation of *Hgd* expression in the developing liver and kidney was also determined using the *LacZ* reporter gene. MxCre recombinase was then used to specifically delete *Hgd* in the liver of the conditional *Hgd tm1d* (fl/fl) *MxCre* mouse model, leaving kidney *Hgd* expression intact. These

experiments revealed firstly that kidney *Hgd* expression is unable to metabolise a sufficient amount of HGA to reduce the circulating HGA load that ultimately leads to ochronotic pigmentation and joint disease. The liver has therefore been established as the target organ for future gene/enzyme replacement therapy in AKU. The *Hgd tm1d (fl/fl) MxCre* model was then used in a dose response experiment to determine the minimum range of liver *Hgd* mRNA required to reduce circulating HGA, which is critical prerequisite information required for the development of a gene therapy. It was also demonstrated using isotopically-labelled HGA and the presence of a downstream-labelled metabolite that HGA could be taken up from the circulation by hepatocytes to be metabolised, establishing that HGA formed by uncorrected cells in a post-gene therapy scenario will likely be metabolised by corrected cells; an important concept for the success of gene therapy. This work using the conditional mouse model of AKU has provided insights and perspectives, that could not have been achieved in human patients, that will hopefully pave the way for future work that ultimately leads to the development of a successful gene therapy for this iconic, ultra-rare disease.

7 References

1. Ferreira, C. R. & van Karnebeek, C. D. M. Inborn errors of metabolism. in *Handbook of Clinical Neurology* vol. 162 449–481 (Elsevier B.V., 2019).

2. Vernon, H. J. Inborn errors of metabolism: advances in diagnosis and therapy. *JAMA Pediatr.* **169**, 778–782 (2015).

3. Das, S. K. Inborn errors of metabolism: challenges and management. *Indian J. Clin. Biochem.* **28**, 311–313 (2013).

4. La Du, B. N., Zannoni, V. G., Laster, L. & Seegmiller, J. E. The nature of the defect in tyrosine metabolism in alcaptonuria. *J. Biol. Chem.* **230**, 250–261 (1958).

5. Stenn, F., Milgram, J., Lee, S., Weigand, R. & Veis, A. Biochemical identification of homogentisic acid pigment in an ochronotic egyptian mummy. *Science (80-.).* **197**, 566–568 (1977).

6. Lee, S. L. & Stenn, F. F. Characterization of mummy bone ochronotic pigment. *JAMA J. Am. Med. Assoc.* **240**, 136 (1978).

7. Scribonius, G. *De inspectione urinarum*. (1584).

8. O'Brien, W. M., La Du, B. N. & Bunim, J. J. Biochemical, pathologic and clinical aspects of alcaptonuria, ochronosis and ochronotic arthropathy. *Am. J. Med.* **34**, 813–838 (1963).

9. Boedeker, C. Ueber das alcapton; ein neuer beitrag zur frage: welche stoffe des hams kannen kupferreduction bewirken? *Ztschr. rat. med.* 130 (1859).

10. Virchow, R. L. Rudolph Virchow on ochronosis.1866. *Arthritis Rheum.* **9**, 66–71 (1866).

11. Kirk, R. New acid found in human urine which darkens with alkalies (alcaptonuria). *J. Anat. Physiol.* **23**, 69–80 (1888).

12. Wolkow, M. & Baumann, E. Ueber das wesen der alkaptonurie. *Physiol. Chemie* **15**, 22–285 (1891).

13. Albrecht, A. Ueber ochronose. *Ztschr. Heilk* **23**, 366 (1954).

14. Osler, W. Ochronosis: the pigmentaion of cartilages, sclerotics, and skin in alkaptonuria. *Lancet* **163**, 10–11 (1904).

15. Watson, J. D. & Crick, F. H. C. Molecular structure of nucleic acids: a structure for deoxyribose nucleic acid. *Nature* **171**, 737–738 (1953).

16. Garrod, A. E. The incidence of alkaptonuria: a study in chemical individuality. *Lancet* **160**, 1616–1620 (1902).

17. Garrod, A. E. & Hele, T. S. The uniformity of the homogentisic acid excretion in alkaptonuria. *J. Physiol.* **33**, 198–205 (1905).

18. Garrod, A. The Croonian lectures on inborn errors of metabolism. *Lancet* **172**, 1–7 (1908).

19. Neubauer, O. Über den abbau der aminosäuren im gesunden und kranken organismus. *Dtsch. Arch. Klin. Med.* **95**, 211–256 (1909).

20. Phornphutkul, C. *et al.* Natural history of alkaptonuria. *N. Engl. J. Med.* **347**, 2111–2121 (2002).

21. Milch, R. A. Studies of alcaptonuria: inheritance of 47 cases in eight highly inter-related dominican kindreds. *Am. J. Hum. Genet.* **12**, 76–85 (1960).

22. Zatková, A. *et al.* High frequency of alkaptonuria in Slovakia: evidence for the appearance of multiple mutations in HGO involving different mutational hot spots. *Am. J. Hum. Genet.* **67**, 1333–1339 (2000).

23. Goicoechea De Jorge, E. *et al.* Alkaptonuria in the Dominican Republic: identification of the founder AKU mutation and further evidence of mutation hot spots in the HGO gene. *J. Med. Genet.* **39**, e40 (2002).

24. Al-sbou, M., Mwafi, N. & Lubad, M. A. Identification of forty cases with alkaptonuria in one village in Jordan. *Rheumatol. Int.* **32**, 3737–3740 (2012).

25. Al-sbou, M. & Mwafi, N. Nine cases of alkaptonuria in one family in southern Jordan. *Rheumatol. Int.* **32**, 621–625 (2012).

26. Islam, M. M., Ababneh, F. M. & Khan, M. H. R. Consanguineous marriage in Jordan: an update. *J. Biosoc. Sci.* **50**, 573–578 (2018).

27. Moss, A. & Schoenheimer, R. The conversion of phenylalanine to tyrosine in normal rats. *J. Biol. Chem.* **135**, 415–429 (1940).

28. Ranganath, L. R., Jarvis, J. C., Gallagher, J. A. & Ranganath, L. R. Recent advances in management of alkaptonuria (invited review; best practice article). *J Clin Pathol* **66**, 367–373 (2013).

29. Verma, S. Early detection of alkaptonuria. *Indian J. Dermatol. Venereol. Leprol.* **71**, 189–191 (2005).

30. Thalagahage, K. N. H., Jayaweera, J. A. A. S., Kumbukgolla, W. W. & Senavirathne, I. Detection of alkaptonuria in a 1-week-old infant. *BMJ Case Rep.* **2015**, bcr2014208505 (2015).

31. Peker, E., Yonden, Z. & Sogut, S. From darkening urine to early diagnosis of alkaptonuria. *Indian J. Dermatol. Venereol. Leprol.* **74**, 700 (2008).

32. Tokuhara, Y. *et al.* Absorbance measurements of oxidation of homogentisic acid accelerated by the addition of alkaline solution with sodium hypochlorite pentahydrate. *Sci. Rep.* **8**, 11364 (2018).

33. Milch, R. A., Titus, E. D. & Loo, T. L. Atmospheric oxidation of homogentisic acid: spectrophotometric studies. *Science* **126**, 209–210 (1957).

34. Consden, R., Forbes, H. A. W., Glynn, L. E. & Stanier, W. M. Observations on the oxidation of homogentisic acid in urine. *Biochem. J.* **50**, 274–278 (1951).

35. Tokuhara, Y. *et al.* Detection of novel visible-light region absorbance peaks in the urine after alkalization in patients with alkaptonuria. *PLoS One* **9**, e86606 (2014).

36. Barbas, C., García, A., de Miguel, L. & Simó, C. Evaluation of filter paper collection of urine samples for detection and measurement of organic acidurias by capillary electrophoresis. *J. Chromatogr. B* **780**, 73–82 (2002).

37. Öztekin, N., Balta, G. S. & Cansever, M. Ş. Determination of homogentisic acid in urine for diagnosis of alcaptonuria: capillary electrophoretic method optimization using experimental design. *Biomed. Chromatogr.* **32**, e4216 (2018).

38. Jacomelli, G., Micheli, V., Bernardini, G., Millucci, L. & Santucci, A. Quick diagnosis of alkaptonuria by homogentisic acid determination in urine paper spots. *JIMD Rep.* **31**, 51–56 (2016).

39. Lustberg, T. J., Schulman, J. D. & Seegmiller, J. E. The preparation and identification of various adducts of oxidized homogentisic acid and the development of a new sensitive colorimetric assay for homogentisic acid. *Clin. Chim. Acta* **35**, 325–333 (1971).

40. Introne, W. J. *et al.* A 3-year randomized therapeutic trial of nitisinone in alkaptonuria. *Mol. Genet. Metab.* **103**, 307–314 (2011).

41. Oláh, A. V. *et al.* Urinary homogentisic acid in alkaptonuric and healthy children. *Clin. Chem. Lab. Med.* **41**, 356–359 (2003).

42. Bory, C., Boulieu, R., Chantin, C. & Mathieu, M. Homogentisic acid determined in biological fluids by HPLC. *Clin. Chem.* **35**, 321–322 (1989).

43. Mannoni, A. *et al.* Alkaptonuria, ochronosis, and ochronotic arthropathy. *Semin. Arthritis Rheum.* **33**, 239–248 (2004).

44. Al-Sarayreh, S. A. *et al.* Measurements of homogentisic acid levels in alkaptonuria patients using an optimized and validated gas chromatography method/mass spectrometry. *Jordan J. Biol. Sci.* **7**, 195–198 (2014).

45. Suzuki, Y., Oda, K., Yoshikawa, Y., Maeda, T. & Suzuki, T. A novel therapeutic trial of homogentisic aciduria in a murine model of alkaptonuria. *J. Hum. Genet.* **44**, 79–84 (1999).

46. Hughes, A. T. *et al.* Urine homogentisic acid and tyrosine: simultaneous analysis by liquid chromatography tandem mass spectrometry. *J. Chromatogr. B* **963**, 106–112 (2014).

47. Hughes, A. T. *et al.* Serum markers in alkaptonuria: simultaneous analysis of homogentisic acid, tyrosine and nitisinone by liquid chromatography tandem mass spectrometry. *Ann. Clin. Biochem.* **52**, 597–605 (2015).

48. Bory, C., Boulieu, R., Chantin, C. & Mathieu, M. Diagnosis of alcaptonuria: rapid analysis of homogentisic acid by HPLC. *Clin. Chim. Acta.* **189**, 7–11 (1990).

49. Deutsch, J. C. & Santhosh-Kumar, C. R. Quantitation of homogentisic acid in normal human plasma. *J. Chromatogr. B Biomed. Sci. Appl.* **677**, 147–151 (1996).

50. Davison, A. S., Milan, A. M., Hughes, A. T., Dutton, J. J. & Ranganath, L. R. Serum concentrations and urinary excretion of homogentisic acid and tyrosine in normal subjects. *Clin. Chem. Lab. Med.* **53**, e81-3 (2015).

51. Wolff, F. *et al.* Renal and prostate stones composition in alkaptonuria: a case report. *Clin. Nephrol.* **84**, 339–342 (2015).

52. Ranganath, L. R. *et al.* Suitability of nitisinone in alkaptonuria 1 (SONIA 1): an international, multicentre, randomised, open-label, no-treatment controlled, parallel-group, dose-response study to investigate the effect of once daily nitisinone

on 24-h urinary homogentisic acid. *Ann. Rheum. Dis.* **1**, 1–6 (2014).

53. Milan, A. M. *et al.* The effect of nitisinone on homogentisic acid and tyrosine: a two-year survey of patients attending the National Alkaptonuria Centre, Liverpool. *Ann. Clin. Biochem.* **54**, 323–330 (2017).

54. Gaines, J. J. & Pai, G. Cardiovascular ochronosis. *Arch. Pathol. Lab. Med.* **111**, 991–994 (1987).

55. Helliwell, T. R., Gallagher, J. A. & Ranganath, L. Alkaptonuria - a review of surgical and autopsy pathology. *Histopathology* **53**, 503–512 (2008).

56. Karimzadeh, H., Mohtasham, N., Karimifar, M., Salesi, M. & Bonakdar, Z. S. A case of ochronosis with gout and monckeberg arteries. *Rheumatol. Int.* **29**, 1507–1510 (2009).

57. Taylor, A. M. *et al.* The role of calcified cartilage and subchondral bone in the initiation and progression of ochronotic arthropathy in alkaptonuria. *Arthritis Rheum.* **63**, 3887–3896 (2011).

58. Lichtenstein, L. & Kaplan, L. Hereditary ochronosis; pathologic changes observed in two necropsied cases. *Am. J. Pathol.* **30**, 99–125 (1953).

59. Galdston, M., Steele, J. M. & Dobriner, K. Alcaptonuria and ochronosis. *Am. J. Med.* **13**, 432–452 (1952).

60. Fisher, A. A. & Davis, M. W. Alkaptonuric ochronosis with aortic valve and joint replacements and femoral fracture: a case report and literature review. *Clin. Med. Res.* **2**, 209–215 (2004).

61. Özmanevra, R., Güran, O., Karatosun, V. & Günal, I. Total knee arthroplasty in ochronosis: a case report and critical review of the literature. *Jt. Dis. Relat. Surg.* **24**, 169–172 (2013).

62. Cebesoy, O. *et al.* Total hip replacement for an ochronotic patient: a technical trick. *Am. J. Case Rep.* **15**, 27–30 (2014).

63. Harun, M. *et al.* A rare cause of arthropathy: an ochronotic patient with black joints. *Int. J. Surg. Case Rep.* **5**, 554–557 (2014).

64. Ventura-Ríos, L. *et al.* Ochronotic arthropathy as a paradigm of metabolically induced degenerative joint disease. A case-based review. *Clin. Rheumatol.* **35**, 1389–1395

(2016).

65. Manoj Kumar, R. V & Rajasekaran, S. Spontaneous tendon ruptures in alkaptonuria. *J. Bone Joint Surg. Br.* **85**, 883–886 (2003).

66. Parambil, J. G., Daniels, C. E., Zehr, K. J. & Utz, J. P. Alkaptonuria diagnosed by flexible bronchoscopy. *Chest* **128**, 3678–3680 (2005).

67. Gaines, J. J. The pathology of alkaptonuric ochronosis. *Hum. Pathol.* **20**, 40–46 (1989).

68. Hall, M. G., Wilks, M. F., Provan, W. M., Eksborg, S. & Lumholtz, B. Pharmacokinetics and pharmacodynamics of NTBC (2-(2-nitro-4-fluoromethylbenzoyl)-1,3-cyclohexanedione) and mesotrione, inhibitors of 4-hydroxyphenyl pyruvate dioxygenase (HPPD) following a single dose to healthy male volunteers. *Br. J. Clin. Pharmacol.* **52**, 169–177 (2001).

69. Wauthy, P., Seghers, V., Mathonet, P. & Deuvaert, F. E. Cardiac ochronosis: not so benign. *Eur. J. Cardio-Thoracic Surg.* **35**, 732–733 (2009).

70. Gottschalk, B. H., Blankenstein, J. & Guo, L. Ochronosis of mitral valve and coronary arteries. *Ann. Thorac. Surg.* **106**, e19–e20 (2018).

71. Wilke, A., Dapunt, O. & Steverding, D. Bluish-black pigmentation of the sclera and the aortic valve in a patient with alkaptonuric ochronosis. *Herz* **35**, 41–41 (2010).

72. Concistrè, G. *et al.* Black aorta in a patient with alkaptonuria (ochronosis). *J. Cardiovasc. Med. (Hagerstown).* **12**, 444–445 (2011).

73. Hannoush, H. *et al.* Aortic stenosis and vascular calcifications in alkaptonuria. *Mol. Genet. Metab.* **105**, 198–202 (2012).

74. Sridhar, F. K., Mukha, R. P., Kumar, S. & Kekre, N. S. Lower urinary tract symptoms and prostatic calculi: a rare presentation of alkaptonuria. *Indian J. Urol.* **28**, 219–221 (2012).

75. Strimer, R. M. & Morin, L. J. Renal, vesical, and prostatic calculi associated with ochronosis. *Urology* **10**, 42–43 (1977).

76. Sutor, D. J., Wooley, S. E. & Krízek, V. The composition of calculi from patients with alcaptonuria. *Br. J. Urol.* **42**, 386–388 (1970).

77. Sutor, D. J. & Wooley, S. E. The crystalline composition of prostatic calculi. *Br. J. Urol.*

46, 533–535 (1974).

78. Taylor, A. M. *et al.* Ultrastructural examination of tissue in a patient with alkaptonuric arthropathy reveals a distinct pattern of binding of ochronotic pigment. *Rheumatology* **49**, 1412–1414 (2010).

79. Gallagher, J. A., Dillon, J. P., Sireau, N., Timmis, O. & Ranganath, L. R. Alkaptonuria: an example of a "fundamental disease"—a rare disease with important lessons for more common disorders. *Semin. Cell Dev. Biol.* **52**, 53–57 (2016).

80. Chow, W. Y., Taylor, A. M., Reid, D. G., Gallagher, J. A. & Duer, M. J. Collagen atomic scale molecular disorder in ochronotic cartilage from an alkaptonuria patient, observed by solid state NMR. *J. Inherit. Metab. Dis.* **34**, 1137–1140 (2011).

81. Tinti, L. *et al.* Development of an in vitro model to investigate joint ochronosis in alkaptonuria. *Rheumatology* **50**, 271–277 (2011).

82. Zannoni, V. G., Lomtevas, N. & Goldfinger, S. Oxidation of homogentisic acid to ochronotic pigment in connective tissue. *Biochim. Biophys. Acta - Gen. Subj.* **177**, 94–105 (1969).

83. Ranganath, L., Norman, B. & Gallagher, J. Ochronotic pigmentation is caused by homogentisic acid and is the key event in alkaptonuria leading to the destructive consequences of the disease – a review. *J. Inherit. Metab. Dis.* **42**, 776–792 (2019).

84. Titus, G. P. *et al.* Crystal structure of human homogentisate dioxygenase. *Nat. Struct. Biol.* **7**, 542–546 (2000).

85. Pollak, M. R. *et al.* Homozygosity mapping of the gene for alkaptonuria to chromosome 3q2. **5**, 201–204 (1993).

86. Montagutelli, X. *et al.* AKU, a mutation of the mouse homologous to human alkaptonuria, maps to chromosome 16. *Genomics* **19**, 9–11 (1994).

87. Janocha, S. *et al.* The human gene for alkaptonuria (AKU) maps to chromosome 3q. *Genomics* **19**, 5–8 (1994).

88. Schmidt, S. R., Muller, C. R. & Kress, W. Murine liver homogentisate 1,2-dioxygenase. Purification to homogeneity and novel biochemical properties. *Eur. J. Biochem.* **228**, 425–430 (1995).

89. Fernández-Cañón, J. M. & Peñalva, M. A. Molecular characterization of a gene

encoding a homogentisate dioxygenase from Aspergillus nidulans and identification of its human and plant homologues. *J. Biol. Chem.* **270**, 21199–21205 (1995).

90. Fernández-Cañón, J. *et al.* The molecular basis of alkaptonuria. *Nat. Genet.* **14**, 19–24 (1996).

91. Granadino, B., de Bernabé, D. B.-V., Fernández-Cañón, J. M., Peñalva, M. A. & de Córdoba, S. R. The human homogentisate 1,2-dioxygenase (HGO) gene. *Genomics* **43**, 115–122 (1997).

92. Zatkova, A. An update on molecular genetics of alkaptonuria (AKU). *J. Inherit. Metab. Dis.* **34**, 1127–1136 (2011).

93. Ascher, D. B. *et al.* Homogentisate 1,2-dioxygenase (HGD) gene variants, their analysis and genotype–phenotype correlations in the largest cohort of patients with AKU. *Eur. J. Hum. Genet.* **27**, 888–902 (2019).

94. Rodriguez, J. M. *et al.* Structural and functional analysis of mutations in alkaptonuria. *Hum. Mol. Genet.* **9**, 2341–2350 (2000).

95. Zatkova, A. *et al.* Identification of 11 novel homogentisate 1,2 dioxygenase variants in alkaptonuria patients and establishment of a novel LOVD-based HGD mutation database. *JIMD Rep.* **4**, 55–65 (2012).

96. Beltrán-Valero de Bernabé, D., Jimenez, F. J., Aquaron, R. & Rodríguez de Córdoba, S. Analysis of alkaptonuria (AKU) mutations and polymorphisms reveals that the CCC sequence motif is a mutational hot spot in the homogentisate 1,2 dioxygenase gene (HGO). *Am. J. Hum. Genet.* **64**, 1316–1322 (1999).

97. Nemethova, M. *et al.* Twelve novel HGD gene variants identified in 99 alkaptonuria patients: focus on 'black bone disease' in Italy. *Eur. J. Hum. Genet.* **24**, 66–72 (2016).

98. Zannoni, V. G., Seegmiller, J. E. & La Du, B. N. Nature of the defect in alcaptonuria. *Nature* **193**, 952–953 (1962).

99. Bernardini, G. *et al.* Homogentisate 1,2 dioxygenase is expressed in brain: implications in alkaptonuria. *J. Inherit. Metab. Dis.* **38**, 807–814 (2015).

100. Laschi, M. *et al.* Homogentisate 1,2 dioxygenase is expressed in human osteoarticular cells: implications in alkaptonuria. *J. Cell. Physiol.* **227**, 3254–3257 (2012).

101. Wolff, J. A. *et al.* Effects of ascorbic acid in alkaptonuria: alterations in benzoquinone

acetic acid and an ontogenic effect in infancy. *Pediatr. Res.* **26**, 140–144 (1989).

102. De Haas, V. *et al.* The success of dietary protein restriction in alkaptonuria patients is age-dependent. *J. Inherit. Metab. Dis.* **21**, 791–798 (1998).

103. Kobak, A. C., Oder, G., Kobak, Ş., Argin, M. & Inal, V. Ochronotic arthropathy: disappearance of alkaptonuria after liver transplantation for hepatitis B-related cirrhosis. *J. Clin. Rheumatol.* **11**, 323–325 (2005).

104. Introne, W. J. *et al.* Exacerbation of the ochronosis of alkaptonuria due to renal insufficiency and improvement after renal transplantation. *Mol. Genet. Metab.* **77**, 136–142 (2002).

105. Cox, T. F. & Ranganath, L. A quantitative assessment of alkaptonuria. *J. Inherit. Metab. Dis.* **34**, 1153–1162 (2011).

106. Langford, B. *et al.* Alkaptonuria severity score index revisited: analysing the AKUSSI and its subcomponent features. *JIMD Rep.* **41**, 53–62 (2018).

107. Schulz, A., Ort, O., Beyer, P. & Kleinig, H. SC-0051, a 2-benzoyl-cyclohexane-1,3-dione bleaching herbicide, is a potent inhibitor of the enzyme p-hydroxyphenylpyruvate dioxygenase. *FEBS Lett.* **318**, 162–166 (1993).

108. Lindstedt, S., Holme, E., Lock, E. A., Hjalmarson, O. & Strandvik, B. Treatment of hereditary tyrosinaemia type I by inhibition of 4-hydroxyphenylpyruvate dioxygenase. *Lancet* **340**, 813–817 (1992).

109. Ellis, M. K. *et al.* Inhibition of 4-hydroxyphenylpyruvate dioxygenase by 2-(2-nitro-4-trifluoromethylbenzoyl)-cyclohexane-1,3-dione and 2-(2-chloro-4-methanesulfonylbenzoyl)-cyclohexane-1,3-dione. *Toxicol. Appl. Pharmacol.* **133**, 12–19 (1995).

110. Ashorn, M., Pitkanen, S., Salo, M. K. & Heikinheimo, M. Current strategies for the treatment of hereditary tyrosinemia type I. *Pediatr. Drugs* **8**, 47–54 (2006).

111. Holme, E. & Lindstedt, S. Nontransplant treatment of tyrosinemia. *Clin. Liver Dis.* **4**, 805–814 (2000).

112. Holme, E. & Lindstedt, S. Tyrosinaemia type I and NTBC (2-(2-nitro-4-trifluoromethylbenzoyl)-1,3-cyclohexanedione). *J. Inherit. Metab. Dis.* **21**, 507–517 (1998).

113. Anikster, Y., Nyhan, W. L. & Gahl, W. A. NTBC and alkaptonuria. *Am. J. Hum. Genet.* **63**, 920–921 (1998).

114. Suwannarat, P. *et al.* Use of nitisinone in patients with alkaptonuria. *Metabolism* **54**, 719–728 (2005).

115. Preston, A. J. *et al.* Ochronotic osteoarthropathy in a mouse model of alkaptonuria, and its inhibition by nitisinone. *Ann. Rheum. Dis.* **73**, 284–289 (2014).

116. Keenan, C. M. *et al.* Nitisinone arrests but does not reverse ochronosis in alkaptonuric mice. *JIMD Rep.* **24**, 45–50 (2015).

117. Ranganath, L. R. *et al.* Nitisinone arrests ochronosis and decreases rate of progression of alkaptonuria: evaluation of the effect of nitisinone in the United Kingdom National Alkaptonuria Centre. *Mol. Genet. Metab.* **125**, 127–134 (2018).

118. Olsson, B. *et al.* Relationship between serum concentrations of nitisinone and its effect on homogentisic acid and tyrosine in patients with alkaptonuria. *JIMD Rep.* **24**, 21–27 (2015).

119. Cox, T. *et al.* Subclinical ochronosis features in alkaptonuria: a cross-sectional study. *BMJ Innov.* **5**, 82–91 (2019).

120. Lock, E. A. *et al.* Tissue distribution of 2-(2-nitro-4-trifluoromethylbenzoyl)cyclohexane-1,3-dione (NTBC): effect on enzymes involved in tyrosine catabolism and relevance to ocular toxicity in the rat. *Toxicol. Appl. Pharmacol.* **141**, 439–447 (1996).

121. Lock, E. A. *et al.* Tissue distribution of 2-(2-nitro-4-trifluoromethylbenzoyl)-cyclohexane-1,3-dione (NTBC) and its effect on enzymes involved in tyrosine catabolism in the mouse. *Toxicology* **144**, 179–187 (2000).

122. Lock, E. A., Gaskin, P., Ellis, M., Provan, W. M. & Smith, L. L. Tyrosinemia produced by 2-(2-nitro-4-trifluoromethylbenzoyl)-cyclohexane-1,3-dione (NTBC) in experimental animals and its relationship to corneal injury. *Toxicol. Appl. Pharmacol.* **215**, 9–16 (2006).

123. Masurel-Paulet, A. *et al.* NTBC treatment in tyrosinaemia type I: long-term outcome in french patients. *J. Inherit. Metab. Dis.* **31**, 81–87 (2008).

124. Meissner, T. *et al.* Richner–Hanhart syndrome detected by expanded newborn

screening. *Pediatr. Dermatol.* **25**, 378–380 (2008).

125. Lock, E., Ranganath, L. R. & Timmis, O. The role of nitisinone in tyrosine pathway disorders. *Curr. Rheumatol. Rep.* **16**, 457 (2014).

126. Macsai, M. S. *et al.* Tyrosinemia type II: nine cases of ocular signs and symptoms. *Am. J. Ophthalmol.* **132**, 522–527 (2001).

127. Stewart, R. M. K., Briggs, M. C., Jarvis, J. C., Gallagher, J. A. & Ranganath, L. Reversible keratopathy due to hypertyrosinaemia following intermittent low-dose nitisinone in alkaptonuria: a case report. *JIMD Rep.* **17**, 1–6 (2014).

128. Gertsman, I., Barshop, B. A., Panyard-Davis, J., Gangoiti, J. A. & Nyhan, W. L. Metabolic effects of increasing doses of nitisinone in the treatment of alkaptonuria. *JIMD Rep.* **24**, 13–20 (2015).

129. White, A. & Tchan, M. C. Nitisinone-induced keratopathy in alkaptonuria: a challenging diagnosis despite clinical suspicion. *JIMD Rep.* **40**, 7–9 (2018).

130. Khedr, M. *et al.* Asymptomatic corneal keratopathy secondary to hypertyrosinaemia following low dose nitisinone and a literature review of tyrosine keratopathy in alkaptonuria. *JIMD Rep.* **40**, 31–37 (2018).

131. Gissen, P., Preece, M. A., Willshaw, H. A. & McKiernan, P. J. Ophthalmic follow-up of patients with tyrosinaemia type I on NTBC. *J. Inherit. Metab. Dis.* **26**, 13–16 (2003).

132. De Laet, C. *et al.* Recommendations for the management of tyrosinaemia type 1. *Orphanet J. Rare Dis.* **8**, 8 (2013).

133. Davison, A. S. *et al.* Assessment of the effect of once daily nitisinone therapy on 24-h urinary metadrenalines and 5-hydroxyindole acetic acid excretion in patients with alkaptonuria after 4 weeks of treatment. *JIMD Rep.* **41**, 1–10 (2018).

134. Davison, A. S. *et al.* Clinical and biochemical assessment of depressive symptoms in patients with alkaptonuria before and after two years of treatment with nitisinone. *Mol. Genet. Metab.* **125**, 135–143 (2018).

135. van Ginkel, W. G. *et al.* Neurocognitive outcome in tyrosinemia type 1 patients compared to healthy controls. *Orphanet J. Rare Dis.* **11**, 87 (2016).

136. McKiernan, P. J., Preece, M. A. & Chakrapani, A. Outcome of children with hereditary tyrosinaemia following newborn screening. *Arch. Dis. Child.* **100**, 738–741 (2015).

137. De Laet, C. *et al.* Neuropsychological outcome of NTBC-treated patients with tyrosinaemia type 1. *Dev. Med. Child Neurol.* **53**, 962–964 (2011).

138. Thimm, E. *et al.* Neurocognitive outcome in patients with hypertyrosinemia type I after long-term treatment with NTBC. *J. Inherit. Metab. Dis.* **35**, 263–268 (2012).

139. Bendadi, F. *et al.* Impaired cognitive functioning in patients with tyrosinemia type I receiving nitisinone. *J. Pediatr.* **164**, 398–401 (2014).

140. Scott, C. R. The genetic tyrosinemias. *Am. J. Med. Genet. Part C Semin. Med. Genet.* **142C**, 121–126 (2006).

141. Goldsmith, L. A. *et al.* Tyrosinemia with plantar and palmar keratosis and keratitis. *J. Pediatr.* **83**, 798–805 (1973).

142. Heylen, E. *et al.* Tyrosinemia Type III detected via neonatal screening: management and outcome. *Mol. Genet. Metab.* **107**, 605–607 (2012).

143. Ellaway, C. J. *et al.* Outcome of tyrosinaemia type III. *J. Inherit. Metab. Dis.* **24**, 824–832 (2001).

144. Hillgartner, M. A. *et al.* Tyrosinemia type I and not treatment with NTBC causes slower learning and altered behavior in mice. *J. Inherit. Metab. Dis.* **39**, 673–682 (2016).

145. Mayorandan, S. *et al.* Cross-sectional study of 168 patients with hepatorenal tyrosinaemia and implications for clinical practice. *Orphanet J. Rare Dis.* **9**, 107 (2014).

146. van Spronsen, F. J., van Rijn, M., Meyer, U. & Das, A. M. Dietary considerations in tyrosinemia type I. in *Advances in experimental medicine and biology* (ed. R, T.) vol. 959 197–204 (Springer, Cham, 2017).

147. Acosta, P. B. & Matalon, K. M. Nutrition management of patients with inherited disorders of aromatic amino acid metabolism. in *Nutrition management of patients with inherited metabolic disorders* (ed. Acosta, P. B.) 119–174 (Jones and Bartlett Publishers, 2010).

148. Parmeggiani, F., Weise, N. J., Ahmed, S. T. & Turner, N. J. Synthetic and therapeutic applications of ammonia-lyases and aminomutases. *Chem. Rev.* **118**, 73–118 (2018).

149. Schwede, T. F., Rétey, J. & Schulz, G. E. Crystal structure of histidine ammonia-lyase revealing a novel polypeptide modification as the catalytic electrophile. *Biochemistry* **38**, 5355–5361 (1999).

150. Watts, K. T., Mijts, B. N., Lee, P. C., Manning, A. J. & Schmidt-Dannert, C. Discovery of a substrate selectivity switch in tyrosine ammonia-lyase, a member of the aromatic amino acid lyase family. *Chem. Biol.* **13**, 1317–1326 (2006).

151. Koukol, J. & Conn, E. E. The metabolism of aromatic compounds in higher plans. IV. Purification and properties of the phenylalanine deaminase of Hordeum vulgare. *J. Biol. Chem.* **236**, 2692–2698 (1961).

152. Cusanovich, M. A. & Meyer, T. E. Photoactive yellow protein: a prototypic PAS domain sensory protein and development of a common signaling mechanism. *Biochemistry* **42**, 4759–4770 (2003).

153. Berner, M. *et al.* Genes and enzymes involved in caffeic acid biosynthesis in the actinomycete Saccharothrix espanaensis. *J. Bacteriol.* **188**, 2666–2673 (2006).

154. Kyndt, J. A., Meyer, T. E., Cusanovich, M. A. & Van Beeumen, J. J. Characterization of a bacterial tyrosine ammonia lyase, a biosynthetic enzyme for the photoactive yellow protein. *FEBS Lett.* **512**, 240–244 (2002).

155. Williams, R. A., Mamotte, C. D. S. & Burnett, J. R. Phenylketonuria: an inborn error of phenylalanine metabolism. *Clin. Biochem. Rev.* **29**, 31–41 (2008).

156. Ten Hoedt, A. E. *et al.* High phenylalanine levels directly affect mood and sustained attention in adults with phenylketonuria: a randomised, double-blind, placebo-controlled, crossover trial. *J. Inherit. Metab. Dis.* **34**, 165–171 (2011).

157. Bilder, D. A. *et al.* Systematic review and meta-analysis of neuropsychiatric symptoms and executive functioning in adults with henylketonuria. *Dev. Neuropsychol.* **41**, 245–260 (2016).

158. MacDonald, A., Gokmen-Ozel, H., van Rijn, M. & Burgard, P. The reality of dietary compliance in the management of phenylketonuria. *J. Inherit. Metab. Dis.* **33**, 665–670 (2010).

159. Burnett, J. R. Sapropterin dihydrochloride (Kuvan/Phenoptin), an orally active synthetic form of BH4 for the treatment of phenylketonuria. *IDrugs* **10**, 805–813 (2007).

160. Hoskins, J. A. *et al.* Enzymatic control of phenylalanine intake in phenylketonuria. *Lancet* **1**, 392–394 (1980).

161. Gilbert, H. J. & Jack, G. W. The effect of proteinases on phenylalanine ammonia-lyase from the yeast Rhodotorula glutinis. *Biochem. J.* **199**, 715–723 (1981).

162. Gilbert, H. J. & Tully, M. Protection of phenylalanine ammonia-lyase from proteolytic attack. *Biochem. Biophys. Res. Commun.* **131**, 557–563 (1985).

163. Ogata, K., Uchiyama, K. & Yamada, H. Metabolism of aromatic amino acid in microorganisms: Part 1. Formation of cinnamic acid from phenylalanine. *Agric. Biol. Chem.* **31**, 200–206 (1967).

164. Hoskins, J. A. & Gray, J. Phenylalanine ammonia lyase in the management of phenylketonuria: the relationship between ingested cinnamate and urinary hippurate in humans. *Res. Commun. Chem. Pathol. Pharmacol.* **35**, 275–282 (1982).

165. Hoskins, J. A., Holliday, S. B. & Greenway, A. M. The metabolism of cinnamic acid by healthy and phenylketonuric adults: a kinetic study. *Biol. Mass Spectrom.* **11**, 296–300 (1984).

166. Fritz, R. R., Hodgins, D. S. & Abell, C. W. Phenylalanine ammonia-lyase. Induction and purification from yeast and clearance in mammals. *J. Biol. Chem.* **251**, 4646–4650 (1976).

167. Ambrus, C. M. *et al.* Extracorporeal enzyme reactors for depletion of phenylalanine in phenylketonuria. *Ann. Intern. Med.* **106**, 531–537 (1987).

168. Pedersen, H., Horvath, C. & Ambrus, C. M. Preparation of immobilized L-phenylalanine ammonia-lyase in tubular form for depletion of L-phenylalanine. *Res. Commun. Chem. Pathol. Pharmacol.* **20**, 559–569 (1978).

169. Kalghatgi, K., Horváth, C. & Ambrus, C. M. Multitubular reactors with immobilized L-phenylalanine ammonia-lyase for use in extracorporeal shunts. *Res. Commun. Chem. Pathol. Pharmacol.* **27**, 551–561 (1980).

170. Ambrus, C. M. *et al.* In vivo safety of hollow fiber enzyme-reactors with immobilized phenylalanine ammonia-lyase in a large animal model for phenylketonuria. *J. Pharmacol. Exp. Ther.* **224**, 598–602 (1983).

171. Chang, T. M. S. Semipermeable microcapsules. *Science (80-.).* **146**, 524–525 (1964).

172. Bourget, L. & Chang, T. M. Artificial cell-microencapsulated phenylalanine ammonia-lyase. *Appl. Biochem. Biotechnol.* **10**, 57–59 (1984).

173. Bourget, L. & Chang, T. M. S. Phenylalanine ammonia-lyase immobilized in semipermeable microcapsules for enzyme replacement in phenylketonuria. *FEBS Lett.* **180**, 5–8 (1985).

174. Bourget, L. & Chang, T. M. S. Phenylalanine ammonia-lyase immobilized in microcapsules for the depletion of phenylalanine in plasma in phenylketonuric rat model. *Biochim. Biophys. Acta - Gen. Subj.* **883**, 432–438 (1986).

175. Bourget, L. & Chang, T. M. S. Effects of oral administration of artificial cells immobilized phenylalanine ammonia-lyase on intestinal amino acids of phenylketonuric rats. *Biomater. Artif. Cells Artif. Organs* **17**, 161–181 (1989).

176. Shedlovsky, A., McDonald, J. D., Symula, D. & Dove, W. F. Mouse models of human phenylketonuria. *Genetics* **134**, 1205–1210 (1993).

177. Safos, S., Eng, B. & Chang, T. M. S. Enzyme replacement therapy in enu2 phenylketonuric mice using oral microencapsulated phenylalanine ammonia-lyase: a preliminary report. *Artif. Cells, Blood Substitutes, Biotechnol.* **23**, 681–692 (1995).

178. Gilbert, H. J., Clarke, I. N., Gibson, R. K., Stephenson, J. R. & Tully, M. Molecular cloning of the phenylalanine ammonia lyase gene from Rhodosporidium toruloides in Escherichia coli K-12. *J. Bacteriol.* **161**, 314–320 (1985).

179. Orum, H. & Rasmussen, O. F. Expression in E. coli of the gene encoding phenylalanine ammonia-lyase from Rhodosporidium toruloides. *Appl. Microbiol. Biotechnol.* **36**, 745–747 (1992).

180. Sarkissian, C. N. *et al.* A different approach to treatment of phenylketonuria: phenylalanine degradation with recombinant phenylalanine ammonia lyase. *Proc. Natl. Acad. Sci. U. S. A.* **96**, 2339–2344 (1999).

181. Wang, L. *et al.* Structure-based chemical modification strategy for enzyme replacement treatment of phenylketonuria. *Mol. Genet. Metab.* **86**, 134–140 (2005).

182. Gámez, A. *et al.* Development of pegylated forms of recombinant Rhodosporidium toruloides phenylalanine ammonia-lyase for the treatment of classical phenylketonuria. *Mol. Ther.* **11**, 986–989 (2005).

183. Gámez, A. *et al.* Structure-based epitope and PEGylation sites mapping of phenylalanine ammonia-lyase for enzyme substitution treatment of phenylketonuria. *Mol. Genet. Metab.* **91**, 325–334 (2007).

184. Sarkissian, C. N. *et al.* Preclinical evaluation of multiple species of PEGylated recombinant phenylalanine ammonia lyase for the treatment of phenylketonuria. *Proc. Natl. Acad. Sci. U. S. A.* **105**, 20894–20899 (2008).

185. Wang, L. *et al.* Structural and biochemical characterization of the therapeutic Anabaena variabilis phenylalanine ammonia lyase. *J. Mol. Biol.* **380**, 623–635 (2008).

186. Tyssandier, V. *et al.* Processing of vegetable-borne carotenoids in the human stomach and duodenum. *Am. J. Physiol. - Gastrointest. Liver Physiol.* **284**, G913-23 (2003).

187. Longo, N. *et al.* Single-dose, subcutaneous recombinant phenylalanine ammonia lyase conjugated with polyethylene glycol in adult patients with phenylketonuria: an open-label, multicentre, phase 1 dose-escalation trial. *Lancet* **384**, 37–44 (2014).

188. Thomas, J. A. *et al.* Evaluation of multiple dosing regimens in phase 2 studies of rAvPAL-PEG (BMN 165, Pegvaliase) for control of blood phenylalanine levels in adults with phenylketonuria. *Mol. Genet. Metab.* **114**, 364–365 (2015).

189. Zori, R. *et al.* Induction, titration, and maintenance dosing regimen in a phase 2 study of pegvaliase for control of blood phenylalanine in adults with phenylketonuria. *Mol. Genet. Metab.* **125**, 217–227 (2018).

190. Longo, N. *et al.* Long-term safety and efficacy of pegvaliase for the treatment of phenylketonuria in adults: combined phase 2 outcomes through PAL-003 extension study. *Orphanet J. Rare Dis.* **13**, 108 (2018).

191. Thomas, J. *et al.* Pegvaliase for the treatment of phenylketonuria: results of a long-term phase 3 clinical trial program (PRISM). *Mol. Genet. Metab.* **124**, 27–38 (2018).

192. Harding, C. O. *et al.* Pegvaliase for the treatment of phenylketonuria: a pivotal, double-blind randomized discontinuation Phase 3 clinical trial. *Mol. Genet. Metab.* **124**, 20–26 (2018).

193. Harding, C. O. Gene and cell therapy for inborn errors of metabolism. in *Inherited Metabolic Diseases* 155–171 (Springer Berlin Heidelberg, 2017). doi:10.1007/978-3-662-49410-3_22.

194. Brunetti-Pierri, N. Gene therapy for inborn errors of liver metabolism: progress towards clinical applications. *Ital. J. Pediatr.* **34**, 2 (2008).

195. Hardouin, S. N. & Nagy, A. Mouse models for human disease. *Clin. Genet.* **57**, 237–244

(2000).

196. Justice, M. J., Siracusa, L. D. & Stewart, A. F. Technical approaches for mouse models of human disease. *Dis. Model. Mech.* **4**, 305–310 (2011).

197. Russell, W. L. *et al.* Specific-locus test shows ethylnitrosourea to be the most potent mutagen in the mouse. *Proc. Natl. Acad. Sci. U. S. A.* **76**, 5818–5819 (1979).

198. Justice, M. J., Noveroske, J. K., Weber, J. S., Zheng, B. & Bradley, A. Mouse ENU mutagenesis. *Hum. Mol. Genet.* **8**, 1955–1963 (1999).

199. Hitotsumachi, S., Carpenter, D. A. & Russel, W. L. Dose-repetition increases the mutagenic effectiveness of N-ethyl-N-nitrosourea in mouse spermatogonia. *Proc. Natl. Acad. Sci. U. S. A.* **82**, 6619–6621 (1985).

200. Soriano, P. Gene targeting in ES cells. *Annu. Rev. Neurosci.* **18**, 1–18 (1995).

201. Waterston, R. H. *et al.* Initial sequencing and comparative analysis of the mouse genome. *Nature* **420**, 520–562 (2002).

202. Lander, E. S. *et al.* Initial sequencing and analysis of the human genome. *Nature* **409**, 860–921 (2001).

203. Nadeau, J. H. *et al.* Sequence interpretation. Functional annotation of mouse genome sequences. *Science* **291**, 1251–1255 (2001).

204. Gurumurthy, C. B. & Kent Lloyd, K. C. Generating mouse models for biomedical research: technological advances. *DMM Dis. Model. Mech.* **12**, dmm029462 (2019).

205. Sternberg, N. & Hamilton, D. Bacteriophage P1 site-specific recombination. I. Recombination between loxP sites. *J. Mol. Biol.* **150**, 467–486 (1981).

206. Sauer, B. & Henderson, N. Site-specific DNA recombination in mammalian cells by the Cre recombinase of bacteriophage P1. *Proc. Natl. Acad. Sci. U. S. A.* **85**, 5166–5170 (1988).

207. Sadowski, P. D. The Flp recombinase of the 2-microns plasmid of Saccharomyces cerevisiae. *Prog. Nucleic Acid Res. Mol. Biol.* **51**, 53–91 (1995).

208. Missirlis, P. I., Smailus, D. E. & Holt, R. A. A high-throughput screen identifying sequence and promiscuity characteristics of the loxP spacer region in Cre-mediated recombination. *BMC Genomics* **7**, 73 (2006).

209. Andrews, B. J., Proteau, G. A., Beatty, L. G. & Sadowski, P. D. The FLP recombinase of the 2μ circle DNA of yeast: interaction with its target sequences. *Cell* **40**, 795–803 (1985).

210. Metzger, D. & Chambon, P. Site- and time-specific gene targeting in the mouse. *Methods* **24**, 71–80 (2001).

211. Skarnes, W. C. *et al.* A conditional knockout resource for the genome-wide study of mouse gene function. *Nature* **474**, 337–342 (2011).

212. Bradley, A. *et al.* The mammalian gene function resource: the international knockout mouse consortium. *Mamm. Genome* **23**, 580–586 (2012).

213. Fire, A. *et al.* Potent and specific genetic interference by double-stranded RNA in caenorhabditis elegans. *Nature* **391**, 806–811 (1998).

214. Tiscornia, G., Singer, O., Ikawa, M. & Verma, I. M. A general method for gene knockdown in mice by using lentiviral vectors expressing small interfering RNA. *Proc. Natl. Acad. Sci. U. S. A.* **100**, 1844–1848 (2003).

215. Wang, H. X. *et al.* CRISPR/Cas9-based genome editing for disease modeling and therapy: challenges and opportunities for nonviral delivery. *Chem. Rev.* **117**, 9874–9906 (2017).

216. Brouns, S. J. J. *et al.* Small CRISPR RNAs guide antiviral defense in prokaryotes. *Cancer Epidemiol. Biomarkers Prev.* **2**, 531–535 (1993).

217. Davison, A. S. *et al.* Serum amino acid profiling in patients with alkaptonuria before and after treatment with nitisinone. *JIMD Rep.* **41**, 109–117 (2018).

218. Norman, B. P. *et al.* A comprehensive LC-QTOF-MS metabolic phenotyping strategy: application to alkaptonuria. *Clin. Chem.* **65**, 530–539 (2019).

219. Lewis, J. Alcaptonuria in a rabbit. *J. Biol. Chem.* 659–661 (1926).

220. Watkins, S., Benley, H. & Shulman, N. *2nd Conference on experimental medicinine and surgery in primates, New York, NY, September 1969*. *Medical Primatology 1970* (Karger, 1970).

221. Keeling, M. E., McClure, H. M. & Kibler, R. F. Alkaptonuria in an orangutan (Pongo pygmaeus). *Am. J. Phys. Anthropol.* **38**, 435–438 (1973).

222. Johnson, E. H. & Miller, R. L. Alkaptonuria in a cynomolgus monkey (Macaca fascicularis). *J. Med. Primatol.* **22**, 428–430 (1993).

223. Moran, T. J. & Yunis, E. J. Studies on ochronosis. 2. Effects of injection of homogentisic acid and ochronotic pigment in experimental animals. *Am. J. Pathol.* **40**, 359–369 (1962).

224. Blivaiss, B. B., Rosenberg, E. F., Kutuzov, H. & Stoner, R. Experimental ochronosis. Induction in rats by long-term feeding with L-tyrosine. *Arch. Pathol.* **82**, 45–53 (1966).

225. Ericsson, A. C., Crim, M. J. & Franklin, C. L. A brief history of animal modeling. *Mo. Med.* **110**, 201–205 (2013).

226. Schmidt, S. R. *et al.* Cloning of the homogentisate 1,2-dioxygenase gene, the key enzyme of alkaptonuria in mouse. *Mamm. Genome* **8**, 168–171 (1997).

227. Manning, K., Fernandez-Canon, J. M., Montagutelli, X. & Grompe, M. Identification of the mutation in the alkaptonuria mouse model. *Hum. Mutat.* **13**, 171–171 (1999).

228. Kress, W., Schmidt, S. R., Halliger-Keller, B., Montagutelli, X. & Müller, C. R. The genetic defect of the alkaptonuric mouse (aku). *Mamm. Genome* **10**, 68–70 (1999).

229. Taylor, A. M. *et al.* Ochronosis in a murine model of alkaptonuria is synonymous to that in the human condition. *Osteoarthr. Cartil.* **20**, 880–886 (2012).

230. Davison, A. S. *et al.* Assessing the effect of nitisinone induced hypertyrosinaemia on monoamine neurotransmitters in brain tissue from a murine model of alkaptonuria using mass spectrometry imaging. *Metabolomics* **15**, 68 (2019).

231. Norman, B. P. *et al.* Studies in alkaptonuria reveal new roles beyond drug clearance for phase I and II biotransformations in tyrosine metabolism. *bioRxiv* Pre-print (2020) doi:10.1101/2020.04.16.044347.

232. Keenan, C. M. *et al.* Concentric lamellae – novel microanatomical structures in the articular calcified cartilage of mice. *Sci. Rep.* **9**, 11188 (2019).

233. Hughes, J. H. *et al.* Dietary restriction of tyrosine and phenylalanine lowers tyrosinaemia associated with nitisinone therapy of alkaptonuria. *J. Inherit. Metab. Dis.* **43**, 259–268 (2019).

234. Krechowec, S. O. *et al.* Postnatal changes in the expression pattern of the imprinted signalling protein XLαs underlie the changing phenotype of deficient mice. *PLoS One*

7, e29753 (2012).

235. Kranz, A. *et al.* An improved Flp deleter mouse in C57Bl/6 based on Flpo recombinase. *Genesis* **48**, 512–520 (2010).

236. Kühn, R., Schwenk, F., Aguet, M. & Rajewsky, K. Inducible gene targeting in mice. *Science* **269**, 1427–1429 (1995).

237. Moriya, K. *et al.* A fibronectin-independent mechanism of collagen fibrillogenesis in adult liver remodeling. *Gastroenterology* **140**, 1653–1663 (2011).

238. Sakai, T. *et al.* Plasma fibronectin supports neuronal survival and reduces brain injury following transient focal cerebral ischemia but is not essential for skin-wound healing and hemostasis. *Nat. Med.* **7**, 324–330 (2001).

239. Keenan, C. M. Identification of ochronosis, its inhibition by nitisinone, and the use of surgical and chemical interventions in murine models of alkaptonuria. (University of Liverpool, 2015).

240. Burgess-Brown, N. A. *et al.* Codon optimization can improve expression of human genes in Escherichia coli: a multi-gene study. *Protein Expr. Purif.* **59**, 94–102 (2008).

241. Collins, F. S. & Rossant, J. A mouse for all reasons. *Cell* **128**, 9–13 (2007).

242. Glasson, S. S., Chambers, M. G., Van Den Berg, W. B. & Little, C. B. The OARSI histopathology initiative – recommendations for histological assessments of osteoarthritis in the mouse. *Osteoarthr. Cartil.* **18**, S17–S23 (2010).

243. Hughes, J. H. *et al.* Conditional targeting in mice reveals that hepatic homogentisate 1,2-dioxygenase activity is essential in reducing circulating homogentisic acid and for effective therapy in the genetic disease alkaptonuria. *Hum. Mol. Genet.* **28**, 3928–3939 (2019).

244. Kalliokoski, O. *et al.* Mice do not habituate to metabolism cage housing - a three week study of male BALB/c mice. *PLoS One* **8**, e58460 (2013).

245. Hademenos, G. J. & Massoud, T. F. Biophysical mechanisms of stroke. *Stroke* **28**, 2067–2077 (1997).

246. Staines, K. A., Poulet, B., Wentworth, D. N. & Pitsillides, A. A. The STR/ort mouse model of spontaneous osteoarthritis – an update. *Osteoarthr. Cartil.* **25**, 802–808 (2017).

247. Van der Kraan, P. M., Vitters, E. L., Van de Putte, L. B. A. & Van den Berg, W. B. Development of osteoarthritic lesions in mice by 'metabolic' and 'mechanical' alterations in the knee joints. *Am. J. Pathol.* **135**, 1001–1014 (1989).

248. Kamekura, S. *et al.* Osteoarthritis development in novel experimental mouse models induced by knee joint instability. *Osteoarthr. Cartil.* **13**, 632–641 (2005).

249. Glasson, S. S., Blanchet, T. J. & Morris, E. A. The surgical destabilization of the medial meniscus (DMM) model of osteoarthritis in the 129/SvEv mouse. *Osteoarthr. Cartil.* **15**, 1061–1069 (2007).

250. Poulet, B., Hamilton, R. W., Shefelbine, S. & Pitsillides, A. A. Characterizing a novel and adjustable noninvasive murine joint loading model. *Arthritis Rheum.* **63**, 137–147 (2011).

251. Christiansen, B. A. *et al.* Non-invasive mouse models of post-traumatic osteoarthritis. *Osteoarthr. Cartil.* **23**, 1627–1638 (2015).

252. Fang, H. *et al.* Early changes of articular cartilage and subchondral bone in the DMM mouse model of osteoarthritis. *Sci. Rep.* **8**, 2855 (2018).

253. Rojkind, M., Giambrone, M.-A. & Biempica, L. Collagen types in normal and cirrhotic liver. *Gastroenterology* **76**, 710–719 (1979).

254. Gelse, K., Poschi, E. & Aigner, T. Collagens—structure, function, and biosynthesis. *Adv. Drug Deliv. Rev.* **55**, 1531–1546 (2003).

255. Frank, C. B. Ligament structure, physiology and function. *J. Musculoskelet. Neuronal Interact.* **4**, 199–201 (2004).

256. Franchi, M., Trirè, A., Quaranta, M., Orsini, E. & Ottani, V. Collagen structure of tendon relates to function. *Sci. World J.* **7**, 404–420 (2007).

257. Mjaatvedt, C. H., Kern, C. B., Norris, R. A., Fairey, S. & Cave, C. L. Normal distribution of melanocytes in the mouse heart. *Anat. Rec. Part A Discov. Mol. Cell. Evol. Biol.* **285A**, 748–757 (2005).

258. Dutta, S. & Sengupta, P. Men and mice: relating their ages. *Life Sci.* **152**, 244–248 (2016).

259. Levine, M. New concepts in the biology and biochemistry of ascorbic acid. *N. Engl. J. Med.* **314**, 892–902 (1986).

260. Vilboux, T. *et al.* Mutation spectrum of homogentisic acid oxidase (HGD) in alkaptonuria. *Hum. Mutat.* **30**, 1611–1619 (2009).

261. Aizarani, N. *et al.* A human liver cell atlas reveals heterogeneity and epithelial progenitors. *Nature* **572**, 199–204 (2019).

262. Snyder, J. M., Hagan, C. E., Bolon, B. & Keene, C. D. Nervous System. in *Comparative Anatomy and Histology* 403–444 (Academic Press, 2018).

263. Kopp, H. G., Hooper, A. T., Shmelkov, S. V. & Rafii, S. β-galactosidase staining on bone marrow. The osteoclast pitfall. *Histol. Histopathol.* **22**, 971–976 (2007).

264. Katschinski, D. M. *et al.* Targeted disruption of the mouse PAS domain serine/threonine kinase PASKIN. *Mol. Cell. Biol.* **23**, 6780–6789 (2003).

265. Nishimura, H. & L'Hernault, S. W. Spermatogenesis. *Curr. Biol.* **27**, R988–R994 (2017).

266. West, D. B. *et al.* A lacZ reporter gene expression atlas for 313 adult KOMP mutant mouse lines. *Genome Res.* **25**, 598–607 (2015).

267. Hess, R. A. & De Franca, L. R. Spermatogenesis and cycle of the seminiferous epithelium. in *Molecular Mechanisms in Spermatogenesis. Advances in Experimental Medicine and Biology* (ed. Cheng, C. Y.) vol. 636 1–15 (Springer, 2008).

268. Sharma, R. & Agarwal, A. Spermatogenesis: an overview. in *Sperm Chromatin* (eds. Zini, A. & Agarwal, A.) 19–44 (Springer, 2011). doi:10.1007/978-1-4419-6857-9_2.

269. Cooper, T. G. Cytoplasmic droplets: the good, the bad or just confusing? *Hum. Reprod.* **20**, 9–11 (2005).

270. Cooper, T. G. The epididymis, cytoplasmic droplets and male fertility. *Asian J. Androl.* **13**, 130–138 (2011).

271. Yuan, S., Zheng, H., Zheng, Z. & Yan, W. Proteomic analyses reveal a role of cytoplasmic droplets as an energy source during epididymal sperm maturation. *PLoS One* **8**, e77466 (2013).

272. Lichter-Konecki, U., Hipke, C. M. & Konecki, D. S. Human phenylalanine hydroxylase gene expression in kidney and other nonhepatic tissues. *Mol. Genet. Metab.* **67**, 308–316 (1999).

273. Stanley, J. C., Fisher, M. J. & Pogson, C. I. The metabolism of L-phenylalanine and L-

tyrosine by liver cells isolated from adrenalectomized rats and from streptozotocin-diabetic rats. *Biochem. J.* **228**, 249–255 (1985).

274. Kida, K. *et al.* Hepatic tyrosine aminotransferase in tyrosinaemia type II. *J. Inherit. Metab. Dis.* **5**, 229–230 (1982).

275. Goldsmith, L. A., Thorpe, J. & Roe, C. R. Hepatic enzymes of tyrosine metabolism in tyrosinemia II. *J. Invest. Dermatol.* **73**, 530–532 (1979).

276. Ruppert, S. *et al.* Deficiency of an enzyme of tyrosine metabolism underlies altered gene expression in newborn liver of lethal albino mice. *Genes Dev.* **6**, 1430–1443 (1992).

277. Endo, F., Katoh, H., Yamamoto, S. & Matsuda, I. A murine model for type III tyrosinemia: lack of immunologically detectable 4-hydroxyphenylpyruvic acid dioxygenase enzyme protein in a novel mouse strain with hypertyrosinemia. *Am. J. Hum. Genet.* **48**, 704–709 (1991).

278. Grompe, M. *et al.* Loss of fumarylacetoacetate hydrolase is responsible for the neonatal hepatic dysfunction phenotype of lethal albino mice. *Genes Dev.* **7**, 2298–2307 (1993).

279. Hargrove, J. L. & Mackin, R. B. Organ specificity of glucocorticoid-sensitive tyrosine aminotransferase. Separation from aspartate aminotransferase isoenzymes. *J. Biol. Chem.* **259**, 386–393 (1984).

280. Endo, F. *et al.* Primary structure deduced from complementary DNA sequence and expression in cultured cells of mammalian 4-hydroxyphenylpyruvic acid dioxygenase. Evidence that the enzyme is a homodimer of identical subunits homologous to rat liver-specific alloantigen F. *J. Biol. Chem.* **267**, 24235–24240 (1992).

281. Fellman, J. H., Fujita, T. S. & Roth, E. S. Assay, properties and tissue distribution of p-hydroxyphenylpyruvate hydroxylase. *BBA - Enzymol.* **284**, 90–100 (1972).

282. Roche, P. A., Moorehead, T. J. & Hamilton, G. A. Purification and properties of hog liver 4-hydroxyphenylpyruvate dioxygenase. *Arch. Biochem. Biophys.* **216**, 62–73 (1982).

283. Li, L. *et al.* Fumarylacetoacetate hydrolase knock-out rabbit model for hereditary tyrosinemia type 1. *J. Biol. Chem.* **292**, 4755–4763 (2017).

284. Labelle, Y., Phaneuf, D. & Tanguay, R. M. Cloning and expression analysis of a cDNA encoding fumarylacetoacetate hydrolase: post-transcriptional modulation in rat liver and kidney. *Gene* **104**, 197–202 (1991).

285. McDonald, D. J. *et al.* The phenylketonuria mouse model: a meeting review. *Mol. Genet. Metab.* **76**, 256–261 (2002).

286. Crawford, L. W., Foley, J. F. & Elmore, S. A. Histology atlas of the developing mouse hepatobiliary system with emphasis on embryonic days 9.5-18.5. *Toxicol. Pathol.* **38**, 872–906 (2010).

287. Sasaki, K. & Sonoda, Y. Histometrical and three-dimensional analyses of liver hematopoiesis in the mouse embryo. *Arch. Histol. Cytol.* **63**, 137–146 (2000).

288. Yin, H. *et al.* Genome editing with Cas9 in adult mice corrects a disease mutation and phenotype. *Nat. Biotechnol.* **32**, 551–553 (2014).

289. Takemura, T. *et al.* Conditional knockout of heparin-binding epidermal growth factor-like growth factor in the liver accelerates carbon tetrachloride-induced liver injury in mice. *Hepatol. Res.* **43**, 384–393 (2013).

290. Ranganath, L. *et al.* Homogentisic acid is not only eliminated by glomerular filtration and tubular secretion but also produced in the kidney in alkaptonuria. *J. Inherit. Metab. Dis.* Online ahead of print (2019) doi:10.1002/jimd.12181.

291. Espana-Agusti, J. *et al.* Generation and characterisation of a Pax8-CreERT2 transgenic line and a Slc22a6-CreERT2 knock-in line for inducible and specific genetic manipulation of renal tubular epithelial cells. *PLoS One* **11**, 1–15 (2016).

292. Bachmanov, A. A., Reed, D. R., Beauchamp, G. K. & Tordoff, M. G. Food intake, water intake, and drinking spout side preference of 28 mouse strains. *Behav. Genet.* **32**, 435–443 (2002).

293. Judd, S. *et al.* The nutritional status of people with alkaptonuria: an exploratory analysis suggests a protein/energy dilemma. *JIMD Rep.* Online ahead of print (2020) doi:10.1002/jmd2.12084.

294. Xue, Z., McCluskey, M., Cantera, K., Sariaslani, F. S. & Huang, L. Identification, characterization and functional expression of a tyrosine ammonia-lyase and its mutants from the photosynthetic bacterium Rhodobacter sphaeroides. *J. Ind. Microbiol. Biotechnol.* **34**, 599–604 (2007).

295. Dunn, M. S., Ross, F. J. & Read, L. S. The solubility of the amino acids in water. *J. Biol. Chem.* **103**, 579–595 (1933).

296. Gipson, I. K., Burns, R. P. & Wolfe-Lande, J. D. Crystals in corneal epithelial lesions of tyrosine-fed rats. *Invest. Ophthalmol.* **14**, 937–941 (1975).

297. Khedr, M. *et al.* Nitisinone causes acquired tyrosinosis in alkaptonuria. *J. Inherit. Metab. Dis.* Online ahead of print (2020) doi:10.1002/jimd.12229.

298. Milan, A. M. *et al.* Quantification of the flux of tyrosine pathway metabolites during nitisinone treatment of alkaptonuria. *Sci. Reports 2019 91* **9**, 10024 (2019).

299. Davison, A. S. *et al.* Evaluation of the serum metabolome of patients with alkaptonuria before and after two years of treatment with nitisinone using LC-QTOF-MS. *JIMD Rep.* **48**, 67–74 (2019).

300. Al Hafid, N. & Christodoulou, J. Phenylketonuria: a review of current and future treatments. *Transl. Pediatr.* **4**, 304–17 (2015).

301. Bell, S. M. *et al.* Formulation and PEGylation optimization of the therapeutic PEGylated phenylalanine ammonia lyase for the treatment of phenylketonuria. *PLoS One* **12**, e0173269 (2017).

302. Yannicelli, S. Protein requirements in inherited metabolic diseases. in *Nutrition Management of Inherited Metabolic Diseases. Lessons from Metabolic University.* (eds. Bernstein, L. E., Rohr, F. & Helm, J. R.) 63–73 (Springer International Publishing Switzerland, 2015). doi:8.

303. Rösler, J., Krekel, F., Amrhein, N. & Schmid, J. Maize phenylalanine ammonia-lyase has tyrosine ammonia-lyase activity. *Plant Physiol.* **113**, 175–179 (1997).

304. Appert, C., Logemann, E., Hahlbrock, K., Schmid, J. & Amrhein, N. Structural and catalytic properties of the four phenylalanine ammonia-lyase isoenzymes from parsley (Petroselinum crispum Nym.). *Eur. J. Biochem.* **225**, 491–499 (1994).

305. De Groot, A. S. & Scott, D. W. Immunogenicity of protein therapeutics. *Trends Immunol.* **28**, 482–490 (2007).

306. Veronese, F. M. & Mero, A. The impact of PEGylation on biological therapies. *BioDrugs* **22**, 315–329 (2008).

307. Brown, C. S. & Lichter-Konecki, U. Phenylketonuria (PKU): a problem solved? *Mol.*

Genet. Metab. Reports **6**, 8–12 (2016).

308. DiBonaventura, M. *et al.* Multinational internet-based survey of patient preference for newer oral or injectable type 2 diabetes medication. *Patient Prefer. Adherence* **4**, 397 (2010).

309. Barclay, N., Tarallo, M., Hendrikx, T. & Marett, S. Patient preference for oral versus injectable and intravenous methods of treatment for rheumatoid arthritis. *Value Heal.* **16**, A568 (2013).

310. Fallowfield, L. *et al.* Patients' preference for administration of endocrine treatments by injection or tablets: results from a study of women with breast cancer. *Ann. Oncol.* **17**, 205–210 (2005).

311. Eek, D. *et al.* Patient-reported preferences for oral versus intravenous administration for the treatment of cancer: a review of the literature. *Patient Prefer. Adherence* **10**, 1609–1621 (2016).

312. Smith, M. E. & Morton, D. G. The stomach: basic functions. in *The Digestive System* 39–50 (Churchill Livingstone, 2010). doi:10.1016/B978-0-7020-3367-4.00003-7.

313. Smith, M. E. & Morton, D. G. Pancreas: exocrine functions. in *The Digestive System* 71–84 (Elsevier, 2010). doi:10.1016/B978-0-7020-3367-4.00005-0.

314. Smith, M. E. & Morton, D. G. Digestion and absorption. in *The Digestive System* 129–152 (Elsevier, 2010). doi:10.1016/B978-0-7020-3367-4.00008-6.

315. Antalis, T. M., Shea-Donohue, T., Vogel, S. N., Sears, C. & Fasano, A. Mechanisms of disease: protease functions in intestinal mucosal pathobiology. *Nat. Clin. Pract. Gastroenterol. Hepatol.* **4**, 393–402 (2007).

316. Evans, D. F. *et al.* Measurement of gastrointestinal pH profiles in normal ambulant human subjects. *Gut* **29**, 1035–1041 (1988).

317. Fink, A. L., Calciano, L. J., Goto, Y., Kurotsu, T. & Falleros, D. R. Classification of acid denaturation of proteins: intermediates and unfolded states. *Biochemistry* **33**, 12504–12511 (1994).

318. Sams, L., Paume, J., Giallo, J. & Carrière, F. Relevant pH and lipase for in vitro models of gastric digestion. *Food Funct.* **7**, 30–45 (2016).

319. Zhang, Z., Zhang, R. & McClements, D. J. Lactase (β-galactosidase) encapsulation in

hydrogel beads with controlled internal pH microenvironments: impact of bead characteristics on enzyme activity. *Food Hydrocoll.* **67**, 85–93 (2017).

320. Souza, C. J. F., Comunian, T. A., Kasemodel, M. G. C. & Favaro-Trindade, C. S. Microencapsulation of lactase by W/O/W emulsion followed by complex coacervation: effects of enzyme source, addition of potassium and core to shell ratio on encapsulation efficiency, stability and kinetics of release. *Food Res. Int.* **121**, 754–764 (2019).

321. Bertoni, S., Albertini, B., Dolci, L. S. & Passerini, N. Spray congealed lipid microparticles for the local delivery of β-galactosidase to the small intestine. *Eur. J. Pharm. Biopharm.* **132**, 1–10 (2018).

322. Yang, Z. *et al.* Highly efficient production of soluble proteins from insoluble inclusion bodies by a two-step-denaturing and refolding method. *PLoS One* **6**, e22981 (2011).

323. Beldengrün, Y. *et al.* Gelatin/maltodextrin water-in-water (W/W) emulsions for the preparation of cross-linked enzyme-loaded microgels. *Langmuir* **34**, 9731–9743 (2018).

324. Sikkens, E. C. M., Cahen, D. L., Kuipers, E. J. & Bruno, M. J. Pancreatic enzyme replacement therapy in chronic pancreatitis. *Best Pract. Res. Clin. Gastroenterol.* **24**, 337–347 (2010).

325. McClements, D. J. Encapsulation, protection, and delivery of bioactive proteins and peptides using nanoparticle and microparticle systems: a review. *Adv. Colloid Interface Sci.* **253**, 1–22 (2018).

326. van der Meer, J.-Y., Biewenga, L. & Poelarends, G. J. The generation and exploitation of protein mutability landscapes for enzyme engineering. *ChemBioChem* **17**, 1792–1799 (2016).

327. Turner, N. J. Directed evolution drives the next generation of biocatalysts. *Nat. Chem. Biol.* **5**, 567–573 (2009).

328. Fox, R. J. & Huisman, G. W. Enzyme optimization: moving from blind evolution to statistical exploration of sequence-function space. *Trends Biotechnol.* **26**, 132–138 (2008).

329. Fox, R. J. *et al.* Improving catalytic function by ProSAR-driven enzyme evolution. *Nat. Biotechnol.* **25**, 338–344 (2007).

330. Kiliç, I. & Yeşiloğlu, Y. Spectroscopic studies on the antioxidant activity of p-coumaric acid. *Spectrochim. Acta - Part A Mol. Biomol. Spectrosc.* **115**, 719–724 (2013).

331. Zang, L. Y. *et al.* Effect of antioxidant protection by p-coumaric acid on low-density lipoprotein cholesterol oxidation. *Am. J. Physiol. Cell Physiol.* **279**, C954-60 (2000).

332. Lou, Z. *et al.* p-Coumaric acid kills bacteria through dual damage mechanisms. *Food Control* **25**, 550–554 (2012).

333. Pragasam, S. J., Venkatesan, V. & Rasool, M. Immunomodulatory and anti-inflammatory effect of p-coumaric acid, a common dietary polyphenol on experimental inflammation in rats. *Inflammation* **36**, 169–176 (2013).

334. Schiavone, M. L. *et al.* Homogentisic acid affects human osteoblastic functionality by oxidative stress and alteration of the Wnt/β-catenin signaling pathway. *J. Cell. Physiol.* Online ahead of print (2020) doi:10.1002/jcp.29575.

335. Walker, V. Ammonia metabolism and hyperammonemic disorders. *Adv. Clin. Chem.* **67**, 73–150 (2014).

336. Dimski, D. S. Ammonia metabolism and the urea cycle: function and clinical implications. *J. Vet. Intern. Med.* **8**, 73–78 (1994).

8 Appendix

8.1 Alignment of HGD across different species

Figure 8.1 shows the gene/protein tree alignment of HGD across different species, generated from the Ensembl gene tree tool. The *HGD* gene is highly conserved gene.

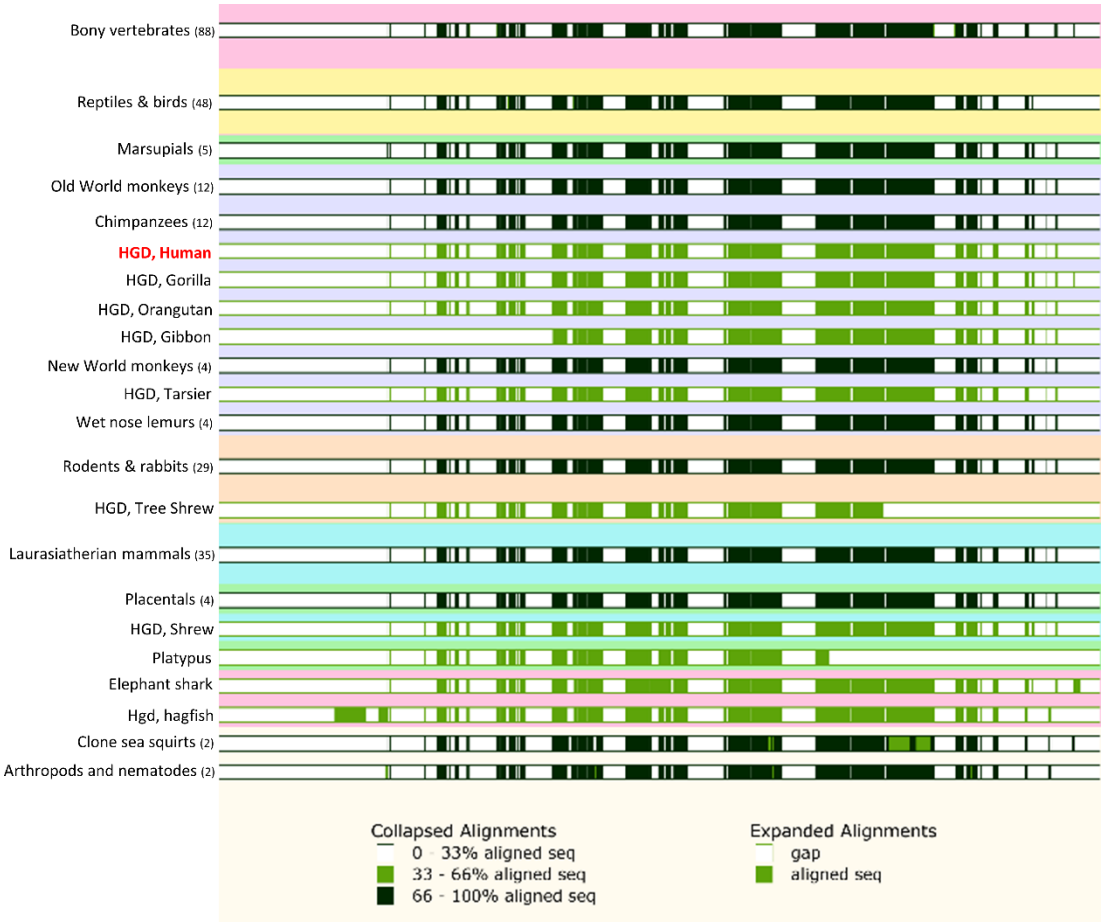

Figure 8.1. Gene/protein alignment of HGD between different species.
Across most species, the *HGD* gene is very well conserved. Number in brackets after species group represents the number of HGD homologs within the group. Image adapted the Ensemble gene tree tool (https://www.ensembl.org/index.html).

8.1.1 Alignment of human and mouse HGD nucleotide sequences

To show how conserved the *HGD* gene is between humans and mice, the NCBI BLAST tool was used to align the nucleotide sequences (CCDS; consensus CDS sequence) and calculate how identical they are. The CCDS sequences for human *HGD* was NCBI gene ID 3081 and mouse *Hgd* was NCBI gene ID 15233. Both the mouse and human sequences contain 1338 nt, with 88.42% of nucleotides being identical (1183/1338 nt identical). The sequence below shows a dot (·) where the nucleotide is identical, and then red letter where the mouse nucleotide differs from the human nucleotide.

```
Human  1     ATGGCTGAGTTAAAGTACATTTCTGGATTTGGGAATGAGTGTTCTTCAGAGGATCCTCGC  60
Mouse  1     .....A.....................................G.................  60

Human  61    TGCCCAGGTTCCCTGCCAGAAGGACAGAATAATCCTCAGGTCTGCCCCTACAATCTCTAT  120
Mouse  61    ..T.............CA................................C.....C  120

Human  121   GCTGAGCAGCTCTCAGGATCGGCTTTCACTTGTCCACGGAGCACCAATAAGAGAAGCTGG  180
Mouse  121   ............G.....A..C................A...................  180

Human  181   CTGTATAGGATTCTACCTTCAGTTTCTCACAAGCCCTTTGAATCCATTGACGAAGGCCAA  240
Mouse  181   ............T.................A........G.....C...C.......T  240

Human  241   GTCACTCACAACTGGGATGAAGTTGATCCTGATCCTAACCAGCTTAGATGGAAACCATTT  300
Mouse  241   .......................GC.................A...............  300

Human  301   GAGATTCCAAAAGCATCTCAGAAGAAAGTAGACTTTGTGAGTGGCCTGCATACCTTGTGT  360
Mouse  301   ............G...G.........G.............TT..T.C.....A...  360

Human  361   GGAGCTGGAGACATAAAGTCTAACAATGGGCTTGCTATCCACATTTTCCTCTGCAATACC  420
Mouse  361   .....A........C...........C..C......G.G........T..G..T..CT..  420

Human  421   TCCATGGAGAACAGATGCTTTTACAATTCAGATGGGGACTTCTTGATTGTTCCGCAGAAA  480
Mouse  421   ............G...........C...........T...C..........C......  480

Human  481   GGGAACCTTCTCATTTACACCGAGTTTGGCAAGATGCTTGTACAGCCCAATGAGATCTGC  540
Mouse  481   .....A.............................TCCC.G...........A......  540

Human  541   GTCATTCAGAGAGGAATGCGGTTCAGCATAGATGTCTTTGAGGAGACCAGGGGCTACATC  600
Mouse  541   ....................A......G.C.............................  600

Human  601   TTGGAGGTCTATGGTGTCCACTTTGAGTTACCTGACCTTGGACCAATTGGGGCCAATGGC  660
Mouse  601   C.....................................G.....C..C..A..A......  660

Human  661   TTGGCCAATCCTCGTGATTTCTTGATACCCATTGCCTGGTATGAGGATCGCCAAGTACCA  720
Mouse  661   ............A...........T...G............A.....T.G...G...  720

Human  721   GGTGGTTACACGGTCATTAATAAATACCAGGGCAAGCTGTTTGCTGCCAAACAGGATGTC  780
Mouse  721   ...........T..G..........T...................TG............  780

Human  781   TCCCCGTTCAATGTTGTGGCCTGGCACGGGAATTATACACCCTACAAGTACAACCTGAAG  840
Mouse  781   ..T..A........C...........T..A..C..C...................AG..  840

Human  841   AATTTCATGGTTATCAACTCAGTGGCCTTTGACCATGCAGACCCATCCATTTTCACAGTA  900
Mouse  841   ..C........C.....TG.G..A.............G..T..T...........C..G  900

Human  901   TTGACTGCTAAGTCTGTCCGCCCTGGAGTGGCCATTGCTGATTTTGTCATCTTCCCACCT  960
Mouse  901   C.......C..A..CC....A.....G.....T........C.................  960

Human  961   CGATGGGGGGTTGCTGATAAGACCTTCAGGCCTCCTTATTACCATAGGAACTGCATGAGT  1020
Mouse  961   ..G.....A.....A.....A........A.............C..............  1020

Human  1021  GAGTTCATGGGACTCATCCGAGGTCACTATGAGGCAAAGCAAGGTGGGTTCCTGCCAGGG  1080
Mouse  1021  ...........C......AA............................A...........  1080

Human  1081  GGAGGGAGTCTACACAGCACAATGACCCCCCATGGACCTGATGCTGACTGCTTTGAGAAG  1140
Mouse  1081  ..C..C..C..G.....TG.C........T..C..C..C.....A...........A...  1140

Human  1141  GCCAGCAAGGTCAAGCTGGCACCTGAGAGGATTGCCGATGGCACCATGGCATTTATGTTT  1200
Mouse  1141  ..........C...A..C.AG..A........A..T..C...........G.........  1200

Human  1201  GAATCATCTTTAAGTCTGGCGGTCACAAAGTGGGGACTCAAGGCCTCCAGGTGTTTGGAT  1260
Mouse  1201  .....T..C......T..........C..............A...GT..C.........  1260

Human  1261  GAGAACTACCACAAGTGCTGGGAGCCACTCAAGAGCCACTTCACTCCCAACTCCAGGAAC  1320
Mouse  1261  .........T....A..T........T...CG...........C.....T.......G.  1320

Human  1321  CCAGCAGAACCTAATTGA  1338
Mouse  1321  ..GA....G.....G...  1338
```

8.2 Predicted cleavage sites in *Rhodobacter capsulatus* TAL amino acid sequence

The potential cleavage of the RcTAL amino acid sequence by proteases/chemicals was predicted using an online tool called ExPASy PeptideCutter, with the results shown in Table 8.1 (https://web.expasy.org/peptide_cutter/ [accessed 06.02.2020).

Table 8.1. Potential protease and chemical cleavage sites in RcTAL.

Name of enzyme	No. of cleavages	Positions of cleavage sites
Arg-C proteinase	41	30 32 40 42 45 49 58 73 105 111 129 167 169 176 186 197 222 229 253 260 264 274 277 283 284 291 304 322 376 380 420 449 450 452 490 493 495 497 504 507 521
Asp-N endopeptidase	27	9 14 77 127 152 171 184 197 224 269 288 293 298 314 317 320 332 360 382 438 473 476 477 490 493 505 527
Asp-N endopeptidase + N-terminal Glu	49	9 14 23 40 50 55 77 81 102 124 127 140 152 171 178 184 197 218 224 235 242 250 262 269 288 292 293 298 314 317 320 326 332 338 360 374 382 383 417 438 473 476 477 479 490 493 505 513 527
BNPS-Skatole	5	101 245 314 319 485
CNBr	12	1 108 160 170 184 209 235 352 406 419 443 473
Chymotrypsin-high specificity (C-term to [FYW], not before P)	14	61 67 89 101 138 245 249 301 314 319 351 393 405 485
Chymotrypsin-low specificity (C-term to [FYWML], not before P)	104	1 3 12 14 18 20 29 39 47 50 52 59 61 67 70 74 83 87 89 90 91 99 101 107 108 109 112 116 134 138 154 157 160 162 164 170 184 187 192 194 200 202 209 215 228 230 234 235 238 241 245 249 252 259 265 269 279 285 290 301 303 309 314 317 319 328 346 347 351 352 355 358 363 367 370 373 381 386 393 394 395 401 405 406 415 416 419 431 443 455 458 465 467 469 473 475 476 485 487 492 503 509 512 520
Clostripain	41	30 32 40 42 45 49 58 73 105 111 129 167 169 176 186 197 222 229 253 260 264 274 277 283 284 291 304 322 376 380 420 449 450 452 490 493 495 497 504 507 521
Formic acid	27	10 15 78 128 153 172 185 198 225 270 289 294 299 315 318 321 333 361 383 439 474 477 478 491 494 506 528
Glutamyl endopeptidase	22	24 41 51 56 82 103 125 141 179 219 236 243 251 263 293 327 339 375 384 418 480 514
Hydroxylamine	2	204 434
Iodosobenzoic acid	5	101 245 314 319 485
LysC	4	9 98 385 388
LysN	4	8 97 384 387
NTCB (2-nitro-5-thiocyanobenzoic acid)	7	10 22 42 187 275 325 340
Pepsin (pH1.3)	111	2 3 12 13 14 17 18 19 20 39 50 66 69 74 82 83 86 87 90 91 99 106 108 109 112 115 116 133 134 137 153 156 162 163 164 187 191 193 194 200 201 202 214 215 227 228 233 234 237 238 249 251 258 259 265 268 269 278 289 302 303 309 316 317 327 328 337 346 350 351 358 362 363 366 367 369 370 372 373 381 385 386 393 394 400 401

		404 405 414 415 416 430 431 456 457 464 465 466 467 468 469 474 475 476 486 487 491 503 508 519 520
Pepsin (pH>2)	123	2 3 12 13 14 17 18 19 20 39 50 66 69 74 82 83 86 87 88 89 90 91 99 101 106 108 109 112 115 116 133 134 137 153 156 162 163 164 187 191 193 194 200 201 202 214 215 227 228 233 234 237 238 244 249 251 258 259 265 268 269 278 289 300 301 302 303 309 313 314 316 317 318 319 327 328 337 346 350 351 358 362 363 366 367 369 370 372 373 381 385 386 393 394 400 401 404 405 414 415 416 430 431 456 457 464 465 466 467 468 469 474 475 476 484 485 486 487 491 503 508 519 520
Proline-endopeptidase [*]	7	247 254 256 292 296 508 523
Proteinase K	286	2 3 7 8 12 13 14 17 18 19 20 21 24 25 26 27 28 33 35 36 38 39 41 44 46 48 50 51 53 54 55 56 60 61 63 64 65 67 70 71 74 75 77 81 82 83 87 88 89 91 92 93 95 99 101 102 103 104 106 107 109 110 112 115 116 119 122 125 126 127 130 131 132 133 134 136 138 139 141 142 144 147 148 150 154 155 157 158 161 162 163 164 171 177 179 180 182 183 187 192 193 194 195 196 200 201 202 203 206 208 210 211 212 213 214 215 216 218 219 220 221 223 224 226 227 228 232 233 234 236 237 238 242 243 244 245 248 249 250 251 252 259 261 262 263 265 266 268 269 272 275 278 279 280 281 282 285 286 287 288 290 293 297 300 301 303 305 306 309 310 312 313 314 316 317 319 323 324 325 327 328 331 332 336 337 339 342 343 345 346 351 354 356 357 358 359 362 363 365 366 367 368 369 370 371 373 374 375 378 379 381 382 384 386 390 392 393 394 399 401 405 408 410 411 412 413 414 415 416 417 418 421 423 424 426 428 431 433 436 440 441 445 446 447 448 451 453 455 456 458 461 463 464 465 466 467 468 469 470 472 475 476 480 483 485 487 488 489 492 496 498 499 503 505 509 510 513 514 515 516 517 520 525 526 527 531
Staphylococcal peptidase I	22	24 41 51 56 82 103 125 141 179 219 236 243 251 263 293 327 339 375 384 418 480 514
Thermolysin	211	2 7 11 12 13 16 17 19 20 25 26 32 34 37 38 43 45 47 49 52 53 54 59 62 66 69 70 73 74 76 80 86 87 90 91 94 98 101 105 106 107 108 109 111 114 115 118 121 126 129 130 131 132 133 135 137 143 147 149 156 157 159 160 161 162 163 169 170 176 181 182 183 186 191 193 194 195 199 200 201 202 207 208 210 211 212 213 214 217 220 222 223 226 227 231 232 233 234 237 241 247 248 249 258 260 264 265 267 268 271 274 278 280 281 284 286 287 296 302 304 308 309 311 312 316 322 323 330 335 341 344 345 350 351 353 355 356 357 358 362 364 365 366 367 369 370 372 373 377 378 380 385 391 392 393 398 400 404 405 407 409 411 413 414 415 416 420 422 425 427 430 435 440 442 445 446 447 450 452 454 457 460 462 463 464 465 466 467 468 469 471 472 475 482 486 488 495 497 498 502 504 508 509 512 515 516 519 524 525 526 530
Thrombin	1	167
Trypsin	42	9 30 32 40 42 45 49 58 73 98 105 111 129 167 169 176 186 197 222 229 260 264 274 277 283 284 304 322 376 380 385 388 420 449 450 452 490 493 495 497 504 521
These enzymes do not cut: Caspase 1, 2, 3, 4, 5, 6, 7, 8, 9, 10, Enterokinase, Factor Xa, Granzyme B, Tobacco etch virus protease		

9 Publications

9.1 Published articles

Hughes, J. H., Bou-Gharios, G., Ranganath, L. R., & Gallagher, J. A. The contribution of mouse models in the rare disease alkaptonuria. *Drug Discov. Today Dis. Models* (2019) doi:10.1016/j.ddmod.2019.10.005

Hughes, J. H., Liu, K., Plagge, A., Wilson, P. J. M., Sutherland, H., Norman, B. P., Hughes, A. T., Keenan, C. M., Milan, A. M., Sakai, T., Ranganath, L. R., Gallagher, J. A.* & Bou-Gharios, G.* Conditional targeting in mice reveals that hepatic homogentisate 1,2-dioxygenase activity is essential in reducing circulating homogentisic acid and for effective therapy in the genetic disease alkaptonuria. *Hum. Mol. Genet.* **28**, 3928-3939 (2019)

Hughes, J. H., Wilson, P. J. M., Sutherland, H., Judd, S., Hughes, A. T., Milan, A. M., Jarvis, J. C., Bou-Gharios, G., Ranganath, L. R., & Gallagher, J. A. Dietary restriction of tyrosine and phenylalanine lowers tyrosinemia associated with nitisinone therapy of alkaptonuria. *J. Inherit. Metab. Dis.* **43**, 259-268 (2019)

Hughes, J.H.*, Keenan, C. M.*, Sutherland, H., Edwards, H. R., Jarvis, J. C., Bou-Gharios, G. & Gallagher, J. A. Anatomical distribution of ochronotic pigment in alkaptonuric mice is associated with calcified cartilage chondrocytes at osteochondral interfaces. *Calcif. Tissue Int.* [accepted 28.09.2020]

* denotes joint authorship

9.2 Manuscripts in preparation

Wilson, P. J. M., Ranganath, L. R., Bou-Gharios, G., Gallagher, J. A & Hughes, J. H. Expression of tyrosine pathway enzymes in mice demonstrates that homogentisate 1,2-dioxygenase deficiency in the liver is responsible for homogentisic acid-derived ochronotic pigmentation. *Manuscript submitted.*